SEGREGATION EFFECTS DURING SOLIDIFICATION IN WEIGHTLESS MELTS

FINAL REPORT

(Reporting Period: January 1, 1972, to June 29, 1973)

RE-458

by

Chou Li

Research Department
Grumman Aerospace Corporation
Bethpage, New York 11714

Prepared under Contract NAS8-27891

for the

National Aeronautics and Space Administration
George C. Marshall Space Flight Center
Marshall Space Flight Center, Alabama 35812

June 1973

Copy No.

SEGREGATION EFFECTS DURING SOLIDIFICATION IN WEIGHTLESS MELTS

FINAL REPORT

(Reporting Period: January 1, 1972, to June 29, 1973)

RE-458

by

Chou Li

Research Department
Grumman Aerospace Corporation
Bethpage, New York 11714

Prepared under Contract NAS8-27891

for the

National Aeronautics and Space Administration
George C. Marshall Space Flight Center
Marshall Space Flight Center, Alabama 35812

June 1973

Approved by: Charles E. Mack, Jr.
Charles E. Mack, Jr.
Director of Research

This report was prepared by Grumman Aerospace Corporation. Part of the work described was supported under Contract NAS8-2791 for the George C. Marshall Space Flight Center of the National Aeronautics and Space Administration.

ACKNOWLEDGEMENT

The principal investigator wishes to thank Dr. R. S. Snyder and Mr. R. C. Ruff of Marshall Space Flight Center for directing and monitoring this contract. He also wishes to thank Dr. J. L. Muhkeejee, and Messers. K. P. Gupta and C. H. Lin of the New York State University at Stony Brook, New York (SUNY), for their participation in working on this contract. Mr. M. Gershinsky of Grumman Data Systems developed the numerical computer program summarized in Part III of this final report. Stimulating and challenging discussions were had with Drs. J. Bredt and M. Johnston of NASA; with Profs. F. F. Y. Wang and H. H. Herman of SUNY; and also with Drs. J. T. Yen, T. T. Kassal, and A. L. Loeffler, Jr., at Grumman. He is also grateful to the Grumman management for their wise counsel and encouragement.

CONTENTS

CONTENTS (Con't)

CONTENTS (Con't)

CONTENTS (Con't)

ILLUSTRATIONS

ILLUSTRATIONS (Con't)

ILLUSTRATIONS (Con't)

TABLES

GENERAL INTRODUCTION AND SUMMARY

This final report discusses the work accomplished over the past four years on segregation effects. The past year, this program was partially supported under NASA contract NAS 8-27891, "Segregation Effects During Solidification in Weightless Melts." The contract covered the period from January 1, 1972 to December 31, 1972.

Two types of melt segregation effects were studied: evaporative segregation, or segregation due to surface evaporation; and freezing segregation, or segregation due to liquid-solid phase transformation.

These segregation effects are closely related. In fact, evaporative segregation always precedes freezing segregation to some degree and must often be studied prior to performing meaningful solidification experiments. This is particularly true since evaporation may cause the melt composition, at least at the critical surface regions or layers to be affected manyfold within seconds so that the surface region or layer melting point and other thermophysical properties, nucleation characteristics, base for undercooling, and critical velocity to avoid constitutional supercooling, may be completely unexpected.

An important objective was, therefore, to develop the necessary "normal evaporation equations" for predicting the compositional changes within specified times at temperature and to correlate these equations with actual experimental data collected from the literature. An evaporative congruent temperature (or equi-evaporative temperature) was then defined and listed for various binary or ternary alloys. The application of this unique temperature in explaining, predicting, or planning "anomalous" evaporative or constitutional melting (on cooling) or solidification (on heating) experiments were discussed. We then computed the reactive jetting forces due to surface evaporation and, in particular, showed that these forces can be very substantial on a differentially heated sample and may completely destroy the unique zero-gravity environment in space manufacturing. In addition, these jetting forces may initiate surface deformation and vibration or other fluid disturbances, and may even produce new types of important convection currents probably never anticipated. These studies also showed which sample materials

are preferable and which to avoid, and what impurities are effective as stabilizing influences. The relation between normal evaporation and normal freezing was then considered. Finally, applications of evaporation to space manufacturing concerning material loss and dimensional control, compositional changes, evaporative purification, surface cooling, materials standards, and freezing data interpretation were briefly described.

In the area of segregation due to solidification, we started with an explanation of the normal freezing process and its successful use in the semiconductor industry. Various constitutional diagrams demonstrated the desirability of using non-constant segregation coefficient techniques in metallurgical studies. We then stated the basic normal freezing differential equation, together with its solutions for cases where the liquidus and solidus are quadratic, cubic, high-degree polynomial, and exponential functions of the melt temperature. The meaning of constant segregation coefficient was discussed, together with the associated errors due to curvatures of the liquidus and solidus lines and the best value of constant segregation coefficient for a given solidification experiment. Numerical methods for computing the normal freezing behavior were then given. Finally and as an example, the steady state solidification of the Ni-Sn system under conditions of limited liquid diffusion and non-constant segregation coefficients was described.

The report ends with some suggestions for future work.

PART I

EVAPORATIVE SEGREGATION

Section 1. INTRODUCTION

In normal evaporation, we assume that the evaporating alloy is always homogeneous in composition, that the vapor is instantly removed, and that the alloy follows Raoult's law (Dushman 1962). Such conditions exist or are approached in an induction-stirred, melt-in-vacuum, or liquid drop-in-space.

We deal here mainly with the normal evaporation of binary alloys. In particular, we study the evaporative segregation patterns, i.e., the type and degree of enrichment or depletion of solute in the evaporating source at different evaporation temperatures and times.

Normal evaporation is important in space melting and solidification for the following reasons:

- Significant evaporation of alloy components always occurs at high temperatures in space vacuum environments
- High-temperature evaporation of alloys is generally a neglected area of systematic research. Yet, unless the complete evaporative segregation behavior is understood and analyzed, solidification and its related segregation effects may not be properly studied because of ill-defined initial conditions. Before the liquid alloy can be controllably solidified or even melted, there is invariably some surface evaporation to cause changes in composition, freezing temperature, supercooling characteristics, nucleation and growth morphology conditions, and the like
- Controlled space evaporation probably most closely meets the requirements of normal evaporation. We may thus be able to obtain material purity or evaporation standards, thermal properties, or even basic thermodynamic properties such as heat of evaporation, activity coefficients, sticking

coefficients, etc., that are difficult or impossible to obtain on earth

- Normal evaporation is a much simpler process than normal freezing, since the former does not involve such complicated phenomena as nucleation, phase transformation, and constitutional or nonconstitutional supercooling. Thus in normal evaporation we may, for specific geometries or alloy systems, ideally isolate and investigate such other phenomena as heat conduction or radiation, liquid or solid diffusion, fluid dynamics, and convection currents. Exact knowledge of these phenomena is necessary to understand solidification

- Evaporation causes surface cooling due to the heat of evaporation. This evaporative cooling effect is particularly important in low-melting materials

- Different rates of evaporation at various surface regions give rise to unbalanced forces and momenta that may produce erratic or unwanted accelerations, surface distortions and vibrations, exceedingly large "equivalent gravities", and possibly new types of powerful convection currents in zero-gravity conditions, as will be discussed later

- Evaporation may cause the surface composition of certain unwanted or unsuspected impurities to be increased a thousandfold or millionfold within seconds so that the layer's melting point and other thermophysical properties, nucleation characteristics, base for undercooling, and critical velocity to avoid constitutional supercooling, may be completely unexpected. In fact, anomalous "constitutional" or evaporative melting on cooling, or solidification on heating, is possible because of surface evaporation

Section 2. DIFFERENTIAL EQUATION OF NORMAL EVAPORATION

Zinsmeister (1964) and Li (1966) gave the exact equation for the normal evaporation of binary alloys. This equation, relating the concentration m of the solute in the evaporating alloy at time t, when the mole fraction of the alloy remaining is F, is

$$F = \frac{N}{N_o} = \left(\frac{m}{m_o}\right)^{\frac{V}{U-V}} \left(\frac{1-m_o}{1-m}\right)^{\frac{U}{U-V}} \tag{1}$$

where N and N_o are, respectively, the number of moles of both solvent and solute at evaporating times t = t and t = 0; m_o is the initial molar concentration of the evaporating alloy; and U and V are, respectively, the evaporation rate of pure solute and solvent.

The evaporation rates in $mol/m^2/sec$ for pure solute and solvent are

$$U = K\, 10^{A_u - B_u/T} (M_u T)^{-\frac{1}{2}} \tag{2}$$

and

$$V = K\, 10^{A_v - B_v/T} (M_v T)^{-\frac{1}{2}} \tag{3}$$

where $K = 5.833 \times 10^{-9}\ \alpha$, $\alpha = 1$ for most metals (Dushman 1962); M_u and M_v are, respectively, the molecular weights of the solute and solvent atoms; T is the evaporating temperature in degrees Kelvin; and A_u and B_u or A_v and B_v are evaporating constants for the solute or solvent. Table 1-1 gives the values of the constants A and B for 51 different elements, as given by Dushman (1962). Data on the melting point and density of these elements were obtained from Smithell (1967).

TABLE 1-1 EVAPORATING CONSTANTS FOR 51 CHEMICAL ELEMENTS

Element	A	B/1000	At. Wt	Melting Pt K	Density
Ag	11.85	14.27	107.9	1234	10.5
Al	11.79	15.94	26.98	933.3	2.7
Au	11.89	17.58	197.0	1336	19.3
B	13.07	29.62	10.82	2300	2.34
Ba	10.70	8.76	137.4	977.1	3.5
Be	12.01	16.47	9.013	1556	1.848
Bi	11.18	9.53	209.0	544.1	9.8
C	15.73	40.03	12.01	3973	2.25
Ca	11.22	8.94	40.08	1123	1.54
Cb	14.37	40.40	92.91	2688	8.57
Cd	11.56	5.72	112.4	594.1	8.64
Ce	13.74	20.10	140.1	1077	6.75
Co	12.70	21.11	58.94	1765	8.9
Cr	12.94	20.00	52.01	2176	7.1
Cs	9.91	3.80	132.9	301.8	1.87
Cu	11.96	16.98	63.54	1356	8.96
Fe	12.44	19.97	55.85	1812	7.87
Ga	11.41	13.84	69.72	302.8	5.91
Ge	11.71	18.03	72.60	1210	5.32
In	11.23	12.48	114.8	429.7	7.3
Ir	13.07	31.23	192.2	2716	22.4
K	10.28	4.48	39.10	336.3	.86
La	11.60	20.85	138.9	1103	6.19
Li	10.99	8.07	6.94	459.7	.534
Mg	11.64	7.65	24.32	924	1.74
Mn	12.14	13.74	54.94	1517	7.4
Mo	11.64	30.85	95.95	2883	10.2
Na	10.72	5.49	22.99	371	.97
Ni	12.75	20.96	58.71	1726	8.9
Os	13.59	37.00	190.2	2970	22.5
Pb	10.77	9.71	207.2	600.6	11.68
Pd	11.78	19.71	106.7	1825	12.
Pt	12.53	27.28	195.1	2045	21.45
Rb	10.11	4.08	85.48	312.1	1.53
Rh	12.94	27.72	102.9	2239	12.4
Ru	13.50	33.80	101.1	2700	12.2
Sb	11.15	8.63	243.5	903.7	6.68
Sc	11.94	18.57	44.96	1673	2.99
Si	12.72	21.30	28.09	1685	2.34

TABLE 1-1 EVAPORATING CONSTANTS FOR 51 CHEMICAL ELEMENTS (Continued)

Element	A	B/1000	At. Wt	Melting Pt K	Density
Sn	10.88	14.87	118.7	505	7.3
Sr	10.71	7.83	87.63	1033	2.6
Ta	13.04	40.21	180.9	3270	16.6
Th	12.52	28.44	232.0	1968	11.85
Ti	12.50	23.23	47.90	1941	4.5
Tl	11.07	8.96	204.4	576.8	11.85
U	11.59	23.31	238.1	1406	19.97
V	13.07	25.72	50.95	2290	6.1
W	12.40	40.68	183.9	3653	19.3
Y	12.43	21.97	88.91	1773	4.47
Zn	11.63	6.56	65.38	692.6	7.14
Zr	12.33	30.26	91.22	2130	6.49

Differentiating Eq (1) yields

$$dm = \frac{(U-V)m(1-m)}{[mU+(1-m)V]N}\, dN \tag{4}$$

but

$$dN = -[mU+(1-m)V]\, A\, dt \tag{5}$$

where A is the evaporating area of the alloy, assumed constant here.

Substituting Eq (5) into Eq (4) results in

$$dt = Gm^{\alpha}(1-m)^{\beta}dm \tag{6}$$

where

$$G = -\frac{N_o(1-m_o)^{\alpha+2}}{A(U-V)m_o^{\alpha+1}} \tag{7}$$

$$\alpha = (2V-U)/U-V) \tag{8}$$

$$\beta = (V-2U)/(U-V) \tag{9}$$

2.1 EVAPORATING RATES AND EVAPORATIVE SEGREGATION COEFFICIENT

The evaporating rates of elements, being exponential functions of the evaporating temperature as shown in Eq (2) and (3), are strongly temperature-dependent. At the melting point of nickel, i.e., 1726K, these rates vary from 1.30×10^{-15}, 1.05×10^{-14} 1.25×10^{-13}, 1.68×10^{-12}, and 2.76×10^{-13} $Kg/m^2/sec$ respectively, for W, Ta, Cb, C, and Os to 26,200, 8270, 7670, 7240, 4250, 2330, and 1120 $Kg/m^2/sec$ for Cd, Cu, Zn, Rb, K, Na, and Mg. The molar evaporating rates vary from 7.11×10^{-15}, 5.57×10^{-14}, 1.35×10^{-12}, 1.45×10^{-11}, and 1.40×10^{-14} $moles/m^2/sec$ respectively for W, Ta, Cb, Os, and C to 2.34×10^{5}, 1.31×10^{5}, 1.17×10^{5}, 1.09×10^{5}, 1.00×10^{5}, 8.5×10^{4} $moles/m^2/sec$ for Cd, Cu, Zn, K, Na, and Rb. The evaporating rates can also be expressed in terms of the velocity of interfacial movement in m/sec, i.e., from 6.74×10^{-16}, 6.31×10^{-15}, 1.36×10^{-13}, 1.23×10^{-12}, and 7.45×10^{-12} respectively for W, Ta, Cb, Os, and C to 4.96×10^{6}, 4.72×10^{6}, 3.03×10^{6}, 2.40×10^{6}, 1.07×10^{6}, 9.25×10^{5} for K, Rb, Cd, Na, Zn, and Cu. For the solvent nickel in nickel alloys, the evaporating rates at 1726K are 4.35×10^{-4} $Kg/m^2/sec$, 7.42×10^{-3} $moles/m^2/sec$, and 4.89×10^{-8} m/sec (or 489 A/sec). Note that the evaporating rates of the various solute elements in nickel generally vary by many orders of magnitude.

When the solute concentration in the evaporating alloy is m mole fraction, the solute concentration of the vapor is $mU/[mU+(1-m)V]$, where V and U are, as defined previously, the molar evaporating rates of the solvent and solute, respectively. The evaporative segregation coefficient k_v is, therefore,

$$k_v = U/[mU+(1-m)V]$$

which varies with m and U and V and, hence, the evaporating temperature T.

Since U and V are generally widely different, we have the following two usual cases:

- $U \gg V$: $k_v = 1/m$, i.e., the evaporative segregation coefficient depends only on m, but not on T.
- For the more important case of $U \gg V$, in which the solute may be concentrated manyfold on the surface,

$$k_v = \frac{U}{(1-m)V}$$

If, in addition to $U \ll V$, m is small, i.e., $m \ll 1$, $k_v = U/V$ = constant at a given T.

Thus, for small, particularly trace, amount of low-evaporative impurities or solutes in nickel alloys evaporating at 1724K, the evaporating segregation coefficient $k_v = U/V$ can be as small as 1.38×10^{-12}, 1.29×10^{-11}, 2.78×10^{-10}, 2.51×10^{-9}, and 1.53×10^{-8} for W, Ta, Cb, Os, and C, respectively.

For highly evaporative impurities (relative to nickel), the evaporative segregation coefficient at 1726K is

$$k_v = 1/m \text{ for } U \gg V$$

which can be very large for small values of m. Thus, if $m = 10^{-6}$ or 10^{-9}, the instantaneous evaporative segregation coefficient is 10^6 or 10^9. Since $U \gg V$, m is rapidly decreasing. Hence, the evaporative segregation coefficient may rapidly decrease by many orders of magnitude within a single experimental run, even for the same impurity, when $U \gg V$.

2.2 SPECIAL CASE SOLUTIONS OF THE NORMAL EVAPORATION EQUATION

Equations (6) - (9) enable us to determine the evaporating time, t, for an evaporating alloy to reach a specific solute concentration, m. Unfortunately, these equations are not exactly solvable in the general case. All of the following special and important cases, (except Case V), however, are solvable in closed forms.

Case I: The solute is much more evaporative than the solvent, i.e., $U \gg V$; or $\alpha = -1$ and $\beta = -2$. In this case

$$dt_1 = \frac{G_1 dm}{m(1-m)^2} \tag{10}$$

where

$$G_1 = -\frac{N_o(1-m_o)}{AU}$$

and the evaporating time is:

$$t_1 = G_1 \left[\ell n \frac{(1-m_o)m}{m_o(1-m)} + \frac{m-m_o}{(1-m_o)(1-m)} \right] \tag{11}$$

In terms of the initial and final weight fractions of the solute in the evaporating alloy, w_o and w respectively, the evaporating time can be shown to be:

$$t_1 = G_1 \left[\ell n \frac{(1-W_o)W}{W_o(1-W)} + \frac{W-W_o}{(1-W)(1-W_o)} \cdot \frac{M_U}{M_U} \right] \tag{11a}$$

For given m_o and evaporating temperature T or evaporating rate U, the evaporation constant G_1 is proportional to N_o/A. For a dilute evaporating alloy in spherical form of diameter d, density ρ, and weight W, G_1 is proportional to $d\rho/W$. Hence, for dilute alloys and given initial and final conditions, the evaporating time is directly proportional to the diameter d of the evaporating source.

When $m \simeq m_o$, the second term in the bracket in Eq. 11 (or 11a) may be nearly 0. The evaporation time for this first case, t_1, is then a logarithmic function of m (or w), as has been experimentally observed (see e.g., Tefelske and Chang 1972).

Also, when $m \simeq m_o \simeq 0$,

$$t_1 \simeq \frac{N_o}{AU} \ell n \frac{m_o}{m} \tag{12}$$

When, however, $m \simeq m_o \simeq \frac{1}{2}$, the logarithmic term in Eq 11 or 11a may be small. The evaporating time t_1 is then approximately linearly related to the final solute concentration (m or w) in the source.

Case II: The solvent is much more evaporative than the solute, i.e., $V \gg U$; or $\alpha = -2$ and $\beta = -1$. In this case

$$dt_2 = \frac{G_2 dm}{(1-m)m^2} \tag{13}$$

where

$$G_2 = \frac{m_o N_o}{AV}$$

and

$$t_2 = G_2 \left[\ell n \frac{(1-m_o)m}{m_o(1-m)} + \frac{m-m_o}{m_o m} \right] \tag{14}$$

In terms of weight fractions

$$t_2 = G_2 \left[\ell n \frac{(1-W_o)W}{W_o(1-W)} + \frac{W-W_o}{W_o W} \frac{Mu}{Mv} \right] \tag{14a}$$

For the initial stages of evaporation, i.e., $m \simeq m_o$, t_2 also becomes a logarithmic function of m, as has been observed. On the other hand, when $m \simeq m_o \simeq 0$, t_2 may be approximately linearly related to $1/m$.

Case III: $\alpha = (2V-U)/(U-V) = 0$, i.e., $U = 2V$ and $\beta = -3$

$$t_3 = G_3 \left[(1-m)^{-2} - (1-m_o)^{-2} \right], \tag{15}$$

where

$$G_3 = -\frac{N_o(1-m_o)^2}{2AVm_o}$$

Case IV: $\beta = (V-2U)/(U-V) = 0$, i.e., $V = 2U$ and $\alpha = -3$. In this case

$$t_4 = G_4 \left(m^{-2} - m_o^{-2} \right) \tag{16}$$

where

$$G_4 = -\frac{N_o m_o^2}{2AU(1-m_o)}$$

Equations (15) and (16) show that under some conditions, the evaporating time, t, is better represented by linear functions of $(1-m)^{-2}$ or m^{-2} than by logarithmic functions of m.

Case V: For relatively dilute alloys, i.e., m and $\beta m \ll 1$, the following solution by series expansion can be obtained from Eq (6):

$$dt_5 = Gm^{\alpha}\left[1 - \beta m + \frac{(\beta m)^2}{2!} + \ldots + (-1)^i \frac{(\beta m)^i}{i!} + \ldots\right] dm \tag{17}$$

and

$$t_5 = G\left[\frac{m^{\alpha+1} - m_o^{\alpha+1}}{\alpha+1} - \frac{m^{\alpha+2} - m_o^{\alpha+2}}{\alpha+2}\beta + \ldots + (-1)\frac{m^{\alpha+i+1} - m_o^{\alpha+i+1}}{(\alpha+i+1)i!}\beta^i \ldots\right] \tag{18}$$

For computer calculations, it is desirable to know the ratio of the i^{th} term to the $(i-1)^{th}$ term. Thus,

$$-\frac{T_i}{T_{i-1}} = \frac{\beta(\alpha+1)\left(m^{\alpha+i+1} - m_o^{\alpha+i+1}\right)}{i\,(\alpha+i+1)\left(m^{\alpha+i} - m_o^{\alpha+i}\right)} \tag{19}$$

which is generally less than $\beta m/i$ or $\beta m_o/i$.

Because $\beta m \ll 1$ and i constantly increases with each additional term, this series converges rapidly unless β is very large, i.e., unless U = V, which leads to Case VI.

Case VI: The solute and solvent are evaporating at equal rates, i.e., U = V. In this case, we would expect

$$m = m_o \quad \text{for all } t \ . \tag{20}$$

There is, then, no evaporative segregation, i.e., there is neither solute enrichment nor depletion in the evaporating source.

For any pair of solvent and solute, there is a unique temperature, T_s, at which U = V and, hence, the alloy concentration remains stable or constant. From Eq (2) and (3),

$$T_s = \frac{B_u - B_v}{A_u - A_v - 0.5 \log(M_u/M_v)} \tag{21}$$

This unique "equi-evaporative, or evaporative congruent, temperature" T_s has some important implications and applications, as will be shown.

Case VII: With extremely dilute alloys, i.e., $m \simeq m_o \simeq 0$, we have (Li, 1966)

$$F = N/N_o = (m/m_o)^{\alpha+1} \tag{22}$$

Hence,

$$t_7 = \frac{N_o}{AV}\left[1 - (m/m_o)^{\alpha+1}\right] \tag{23}$$

2.3 EXAMPLES OF COMPUTATION

A generalized computer program has been written to analyze the evaporative segregation pattern (i.e., type and degree), based on the equations given above, on various potential aerospace materials suitable for space experiments. Computations have been made that give the maximum allowable time (often less than a minute or second) for space experiments without material loss or compositional changes of a specified amount for various solute elements in nickel, iron, or other alloys.

2.3.1 Nickel Alloys

Several nickel alloys have been selected for the M512 Skylab experiments. As an example of the use of the various derived equations, the evaporation behavior of an alloy containing 8% by weight of Al in Ni at the melting point of pure Ni (i.e., 1726K) is computed. Here, the solute element (Al) is comparatively highly evaporative relative to the solvent (Ni). Equation (11) therefore applies, and the time, t_1, to reach a final solute concentration m from a specified initial concentration m_o is directly proportional to N_oA/U (in the G_1 constant). Table 1-2 gives the times to reach various final Al concentrations for one mole (5.367×10^{-2} Kg) of the 8% Al in Ni alloy ($m_o = 0.159$) evaporating at 1726K (the melting point of Ni) from its (supposedly constant) 10^{-3} m^2 surface.

TABLE 1-2 NORMAL EVAPORATION OF 8% BY WEIGHT ALUMINUM IN NICKEL AT 1726K

Evaporation Time, Sec	Final Solute Concentration		Alloy Remaining	
	Weight Fraction	Mole Fraction	Weight, Kg	Mole
0.	0.080	0.1591	5.366×10^{-3}	1.0000
28.3	0.078	0.1555	5.353×10^{-3}	0.9955
57.1	0.076	0.1518	5.341×10^{-3}	0.9910
86.5	0.074	0.1481	5.328×10^{-3}	0.9865
117	0.072	0.1444	5.315×10^{-3}	0.9820
147	0.070	0.1407	5.303×10^{-3}	0.9775
179	0.068	0.1370	5.290×10^{-3}	0.9731
211	0.066	0.1333	5.2×10^{-3}	0.9686
244	0.064	0.1295	5.2×10^{-3}	0.9642
277	0.062	0.1258	5.25×10^{-3}	0.9598
312	0.060	0.1220	5.240×10^{-3}	0.9554
347	0.058	0.1182	5.227×10^{-3}	0.9510
384	0.056	0.1143	5.214×10^{-3}	0.9467
421	0.054	0.1105	5.202×10^{-3}	0.9423
460	0.052	0.1066	5.189×10^{-3}	0.9379
500	0.050	0.1028	5.177×10^{-3}	0.9336
542	0.048	0.0989	5.164×10^{-3}	0.9292
584	0.046	0.0950	5.152×10^{-3}	0.9249
629	0.044	0.0910	5.139×10^{-3}	0.9206
675	0.042	0.0871	5.126×10^{-3}	0.9163
723	0.040	0.0831	5.114×10^{-3}	0.9120
774	0.038	0.0792	5.101×10^{-3}	0.9076
827	0.036	0.0752	5.088×10^{-3}	0.9033
882	0.034	0.0711	5.075×10^{-3}	0.8990
940	0.032	0.0671	5.062×10^{-3}	0.8947
1000	0.030	0.0631	5.049×10^{-3}	0.8904
1070	0.028	0.0590	5.036×10^{-3}	0.8860
1130	0.026	0.0549	5.023×10^{-3}	0.8817
1210	0.024	0.0508	5.009×10^{-3}	0.8773
1290	0.022	0.0467	4.996×10^{-3}	0.8729
1380	0.020	0.0425	4.982×10^{-3}	0.8685
1480	0.018	0.0384	4.967×10^{-3}	0.8640
1590	0.016	0.0342	4.953×10^{-3}	0.8594
1710	0.014	0.0300	4.938×10^{-3}	0.8549
1850	0.012	0.0257	4.922×10^{-3}	0.8501
2010	0.010	0.0215	4.905×10^{-3}	0.8453
2210	0.008	0.0172	4.887×10^{-3}	0.8401
2470	0.006	0.0130	4.866×10^{-3}	0.8346
2820	0.004	0.0087	4.841×10^{-3}	0.8284
3430	0.002	0.0043	4.805×10^{-3}	0.8204

Thus, it takes 312 seconds for 5.37×10^{-2} Kg (1 mole) of an 8% Al in Ni to change to 6% in Al concentration ($A = 10^{-3}$ m^2), with a decrease of 1.26×10^{-3} Kg (2.33%) in the weight of the evaporating alloy. The same evaporating Ni-Al alloy takes an additional 411 seconds to change its aluminum concentration to 4% with an additional loss of 4.71% in alloy weight. An additional time of 657 seconds is required for the same alloy to change in aluminum concentration by another 2% (to 2%) with an additional loss of 13.15% in the alloy weight. If the evaporating alloy is spread out as a thin layer with an evaporating area $A = 10^{-2}$ m^2 instead of 10^{-3} m^2, all the evaporating times given in Table 1-2 must be reduced by a factor of 10, in accordance with Eq 11 or 11a.

The alloy evaporating rate is directly proportional to the evaporating area A and generally must, therefore, continuously decrease with shrinking alloy volume, mass, or surface. If the geometric shape of the evaporating alloy sample is fixed and known, the time to reach a certain sample size or deposit composition can be computed by numerical techniques based on Eq 6-9. Molten materials in zero-gravity environments readily assume spherical shapes due to surface tension. An example of such spherical evaporation at the melting point of pure nickel, i.e., 1726K, for a 6.35×10^{-3} m ($\frac{1}{4}$ in.) sphere with a composition containing 8 weight percent of aluminum in nickel is depicted in Figure 1-1. In this figure, curve 1 represents the weight fraction of the remaining evaporating sphere (WFR); curve 2 the diameter of the remaining sphere (DM); curve 3 the weight fraction of aluminum in the remaining sphere (WFA); and curve 4 the weight fraction of aluminum in the vapor (WFV). All four parameters are plotted against the evaporation time in seconds.

Figures 1-2 and 1-3 show the normal evaporation behavior at 1726K of several nickel alloys containing 10% by weight of such highly evaporative solutes as Cd, K, Na, and Rb, these elements being much more volatile than Al. Figure 2 gives the weight fraction remaining in grams upon reaching specified solute concentrations in weight fractions, or weight percentages from the original 10 weight percent and decreasing successively by 0.5%. Figure 3 gives the evaporating times (t_i in Eq 11) to reach the same successive solute concentrations. Again, the evaporating area A is assumed constant at 10^{-3} m^2. It can be seen that all these fast-evaporating elements reach the different final solute concentrations five orders of magnitude faster than Al. Specifically, they take only about

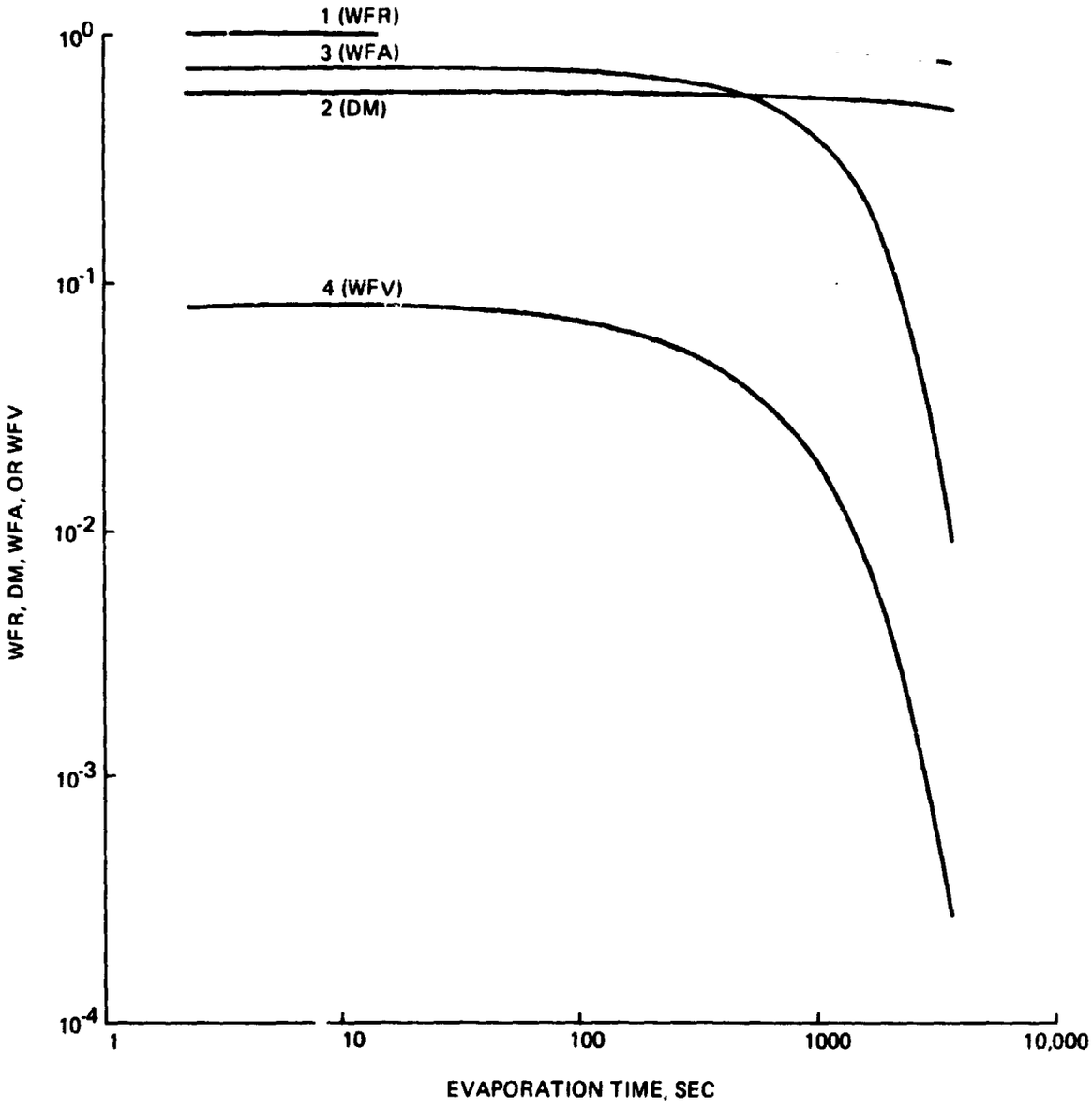

Fig. 1-1 Normal Evaporation at 1726K of a $6x10^{-3}$ m Sphere Containing 8 Weight Percent of Al in Ni

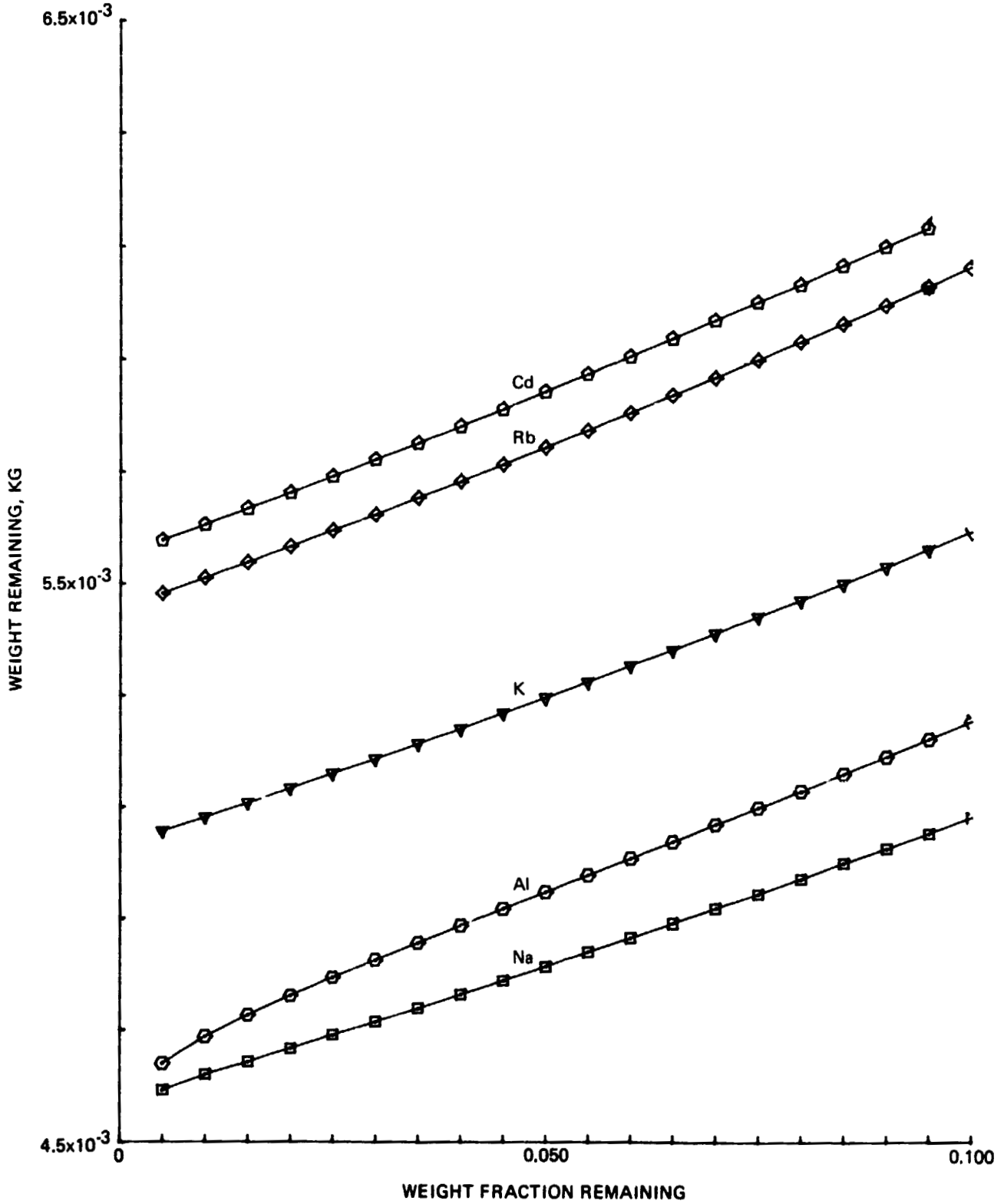

Fig. 1-2 Normal Evaporation of 10 Weight Percent Nickel Alloys at 1726K

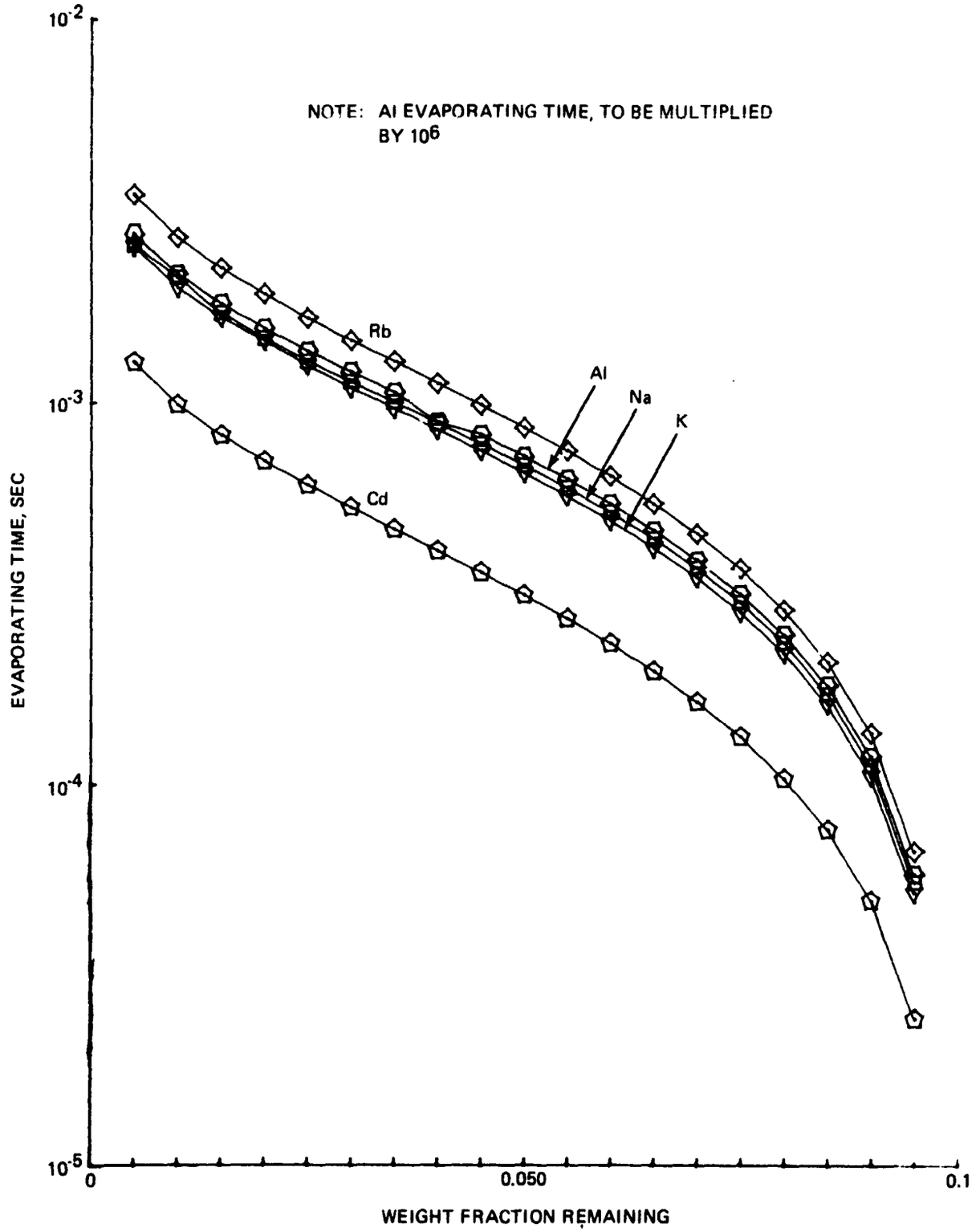

Fig. 1-3 Evaporation Time During Normal Evaporation of 10 Weight Percent Nickel Alloys

500 microseconds, vs 58.3 seconds for Al, for the solute concentration to change from the initial 10 weight percent to 9.5 weight percent. Very small droplets or thin films having large evaporating areas relative to their masses would, therefore, change compositions significantly, so rapidly that the change can never be prevented. The behavior of any subsequent solidification may thus be completely unexpected, and accurate solidification analysis may thus be rendered impossible or meaningless unless the exact thermal history of the alloy is first very accurately measured and an evaporation study then undertaken to determine the magnitude of the surface composition changes in these alloys.

Comprehensive computations have been made for nickel alloys containing initial solute concentrations of from 2 to 10 weight percent (at 2% intervals) of 50 different solute elements evaporated at 1726K, the melting point of nickel. For each solute element, the evaporating times were computed for 0.1% decrements in the solute concentrations until the final concentration of 1% was reached. The final molar and weight fractions of the alloy remaining at the end of each evaporation period were also computed. These computations, designed to furnish a handy reference for future experiment planning, are available on request. In our original proposal, we recommended for study nickel alloys containing 2 or 8 weight percent of tin or aluminum as the specimen materials for our proposed experiment.

2.3.2 Iron Alloys

The evaporation behavior of binary iron alloys containing 20 different solute elements has also been studied. Table 1-3, listing the equi-evaporative temperatures for these 20 different alloy systems, gives the ratios of the solute evaporating rate, U, at 1873K, to that of the solvent iron, V. At 1873K, 10 of these solute elements evaporate faster than the solvent (the three left columns) and 10 slower (the three right columns). Moreover, these ratios vary widely over 18 decades, from 4.41×10^{-12} for the slowest evaporating, W, to 3.76×10^{6} for the fastest evaporating, Cd. Because of this wide variation, and due to the extreme sensitivities of the evaporating surface to unsuspected contaminants, predicted or experimental evaporating results cannot generally be very accurate.

TABLE 1-3 EQUI-EVAPORATIVE TEMPERATURES FOR TWENTY BINARY IRON ALLOYS

Solute	U/V at 1873 K	T_s, K	Solute	U/V at 1873K	T_s, K
Cd	3.765×10^{6}	13,813	W	4.412×10^{-12}	-69,317
Zn	2.065×10^{6}	15,883	C	8.210×10^{-8}	5,556
Mg	9.074×10^{5}	19,383	Mo	1.879×10^{-7}	-11,857
Ca	5.503×10^{4}	9,608	Zr	1.950×10^{-6}	-47,517
Pb	3.333×10^{3}	5,249	B	6.832×10^{-5}	9,783
Mn	1.070×10^{3}	21,013	V	3.804×10^{-3}	8,847
Al	45.65	8,291	Ti	2.254×10^{-2}	34,923
Cu	12.25	5,886	Co	4.362×10^{-1}	4,591
Sn	9.978	2,959	Si	5.238×10^{-1}	3,098
Cr	3.158	58.1	Ni	5.897×10^{-1}	3,309

The equi-evaporative temperatures in iron alloys also vary widely. Binary iron alloys containing Cr, Zr. Mo, and W have no practical equi-evaporative temperatures. One can, therefore, always expect these alloys to change compositions continuously with the evaporating time.

Table 1-4 shows the effect of evaporating temperature on the U/V ratios for four different solute elements Mg, Ca, Mn, and Al. In the range of 1773K to 2173K and beyond, increasing the evaporating temperatures always decreases the U/V ratios. This can also be seen from Table 1-3, as the equi-evaporative temperatures shown for these four binary iron alloys are higher than 1873K, at which temperature the four solute elements evaporate much faster than the solvent iron. Table 1-4 also shows that, for the same temperature variation, the more evaporative the solute element the greater the percentage variation in the U/V ratio. In the case of Mg the U/V ratio decreases by about 20 times from 1773K → 2173K, whereas for Al the same ratio decreases only by less than three times over the same temperature interval.

TABLE 1-4 EFFECT OF SOLUTE ELEMENTS AND EVAPORATING TEMPERATURES ON THE VALUES OF U/V (x 1000) IN IRON ALLOYS

Temp (K)	Solutes			
	Mg	Ca	Mn	Al
1773	2132.0	118.2	1.649	0.06037
1873	907.4	55.03	1.070	0.04565
1973	421.2	27.68	0.7261	0.03552
2073	210.5	14.88	0.5110	0.02831
2173	112.1	8.466	0.3719	0.02304

Figure 1-4 shows the effect of solute elements and evaporating temperature, T, on the evaporating time t, for a given set of initial and final solute concentrations (i.e., m_o = 0.01 and m = 1 ppm). For given m_o and m, the log t versus 1/T curves for these highly evaporative solute elements are approximately linear and have positive slopes. This can be predicted from Eq (11) since, for given m_o and m, log t is linearly related to B/T - 0.5 log T, and 0.5 log T is small relative to B/T within the evaporating temperature range studied. Thus, one can use Fig. 1-4 to determine the value of the elemental evaporating constant B, or heat of evaporation $\Delta H = 4.574\ B$ (Dushman, 1962), for the solute elements by plotting log t versus 1/T and measuring the slope of the resultant, nearly straight lines.

In Fig. 1-5, the log t versus 1/T relationships also appear nearly linear for all the four different initial concentrations (i.e., $m_o = 10^{-1}$, 10^{-2}, 10^{-3}, and 10^{-4}) of Al in Fe. This can also be seen from Eq (11) and (12). All these nearly straight lines have identical slopes, from which the heat of evaporation of pure Al can be evaluated.

Figures 1-6 and 1-7 display the effect on the evaporating time, t, of final solute concentration, m, and either initial concentration m_o (in Fig. 1-6) or solute elements (in Fig. 1-7).

Figure 1-8 indicates that Mg, Ca, and Mn in Fe alloys are so evaporative at

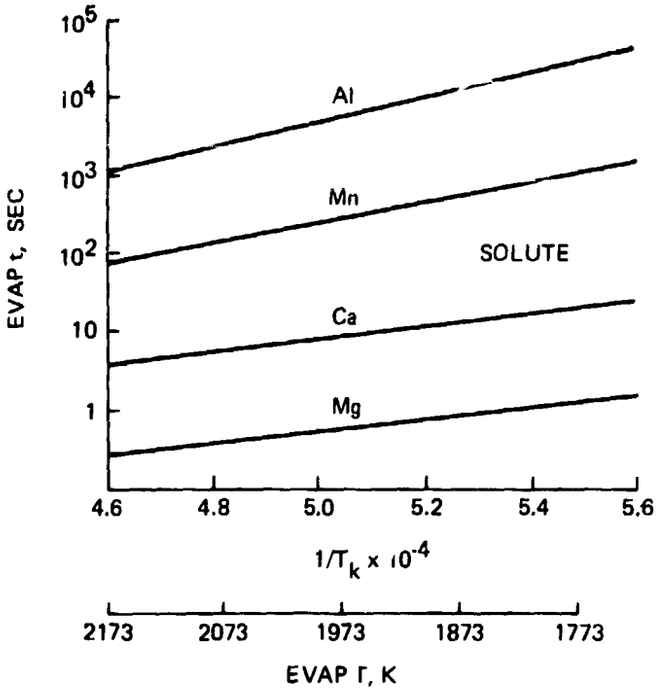

Fig. 1-4 Evaporating Times for Different Dilute Iron Alloys to Change Concentration from $m_o = 0.01$ to m = 1 ppm

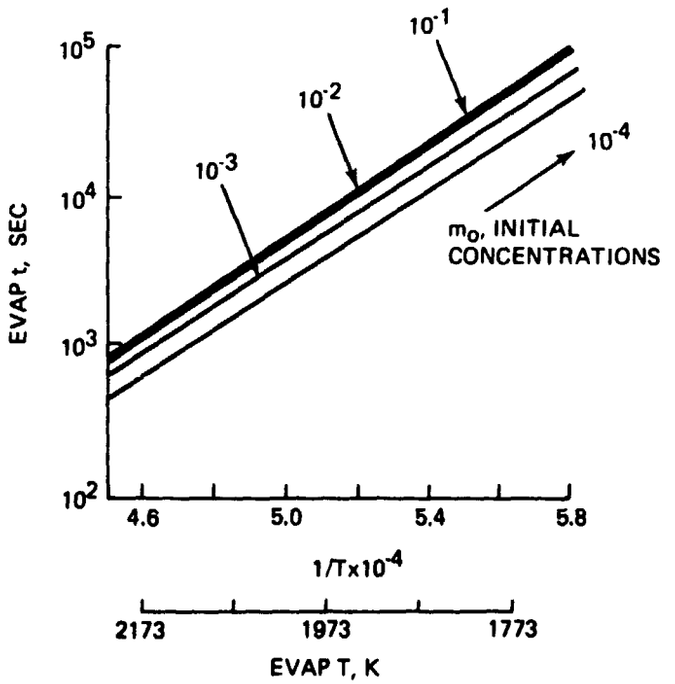

Fig. 1-5 Evaporating Times for Dilute Iron Alloys Containing Al and Starting at Four Different Initial Concentrations, to Reach a Final Concentration of m = 1 ppm

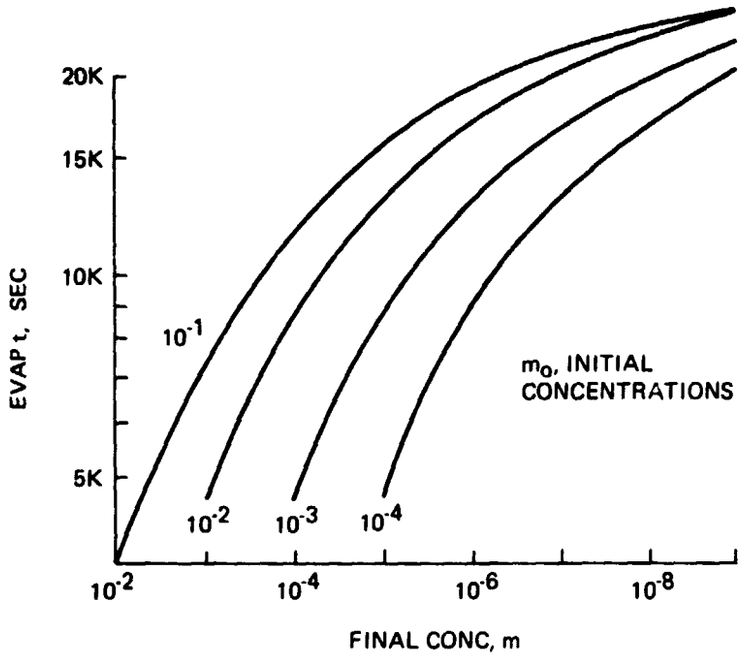

Fig. 1-6 Effect of Initial and Final Solute Concentrations on the Evaporating Times in Dilute Iron Alloys Containing Al at 1873K

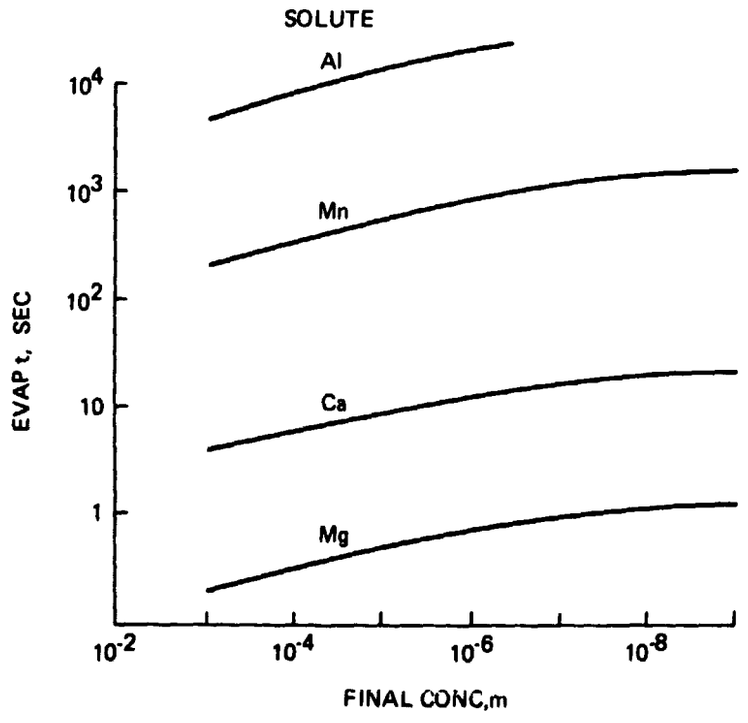

Fig. 1-7 Effect of Solute Elements and Final Concentration on the Evaporating Times in Dilute Iron Alloys at 1873 K

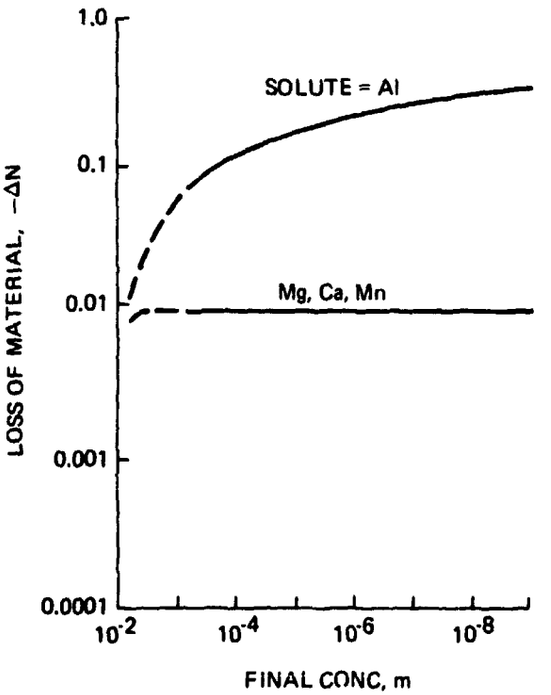

Fig. 1-8 Evaporation Loss of Dilute Iron Alloys at 1573K as a Function of Solute Elements and Final Solute Concentrations

1873K that practically all of these elements are removed by evaporation, without much evaporative loss of the solvent Fe atoms. On the other hand, Al is comparatively less evaporative, and much of the solvent Fe atoms are evaporated off together with Al. To achieve a purification factor of 10^7 (i.e., to $m = 10^{-9}$) from $m_o = 0.01$, for example, the initial evaporating alloy must lose over 30% of its material.

2.4 ACCURACY OF PREDICTED RESULTS

To check the validity of our derived equations for normal evaporation of binary alloys, we searched the current literature. Several sets of alloy evaporation data have been found that are amenable to normal evaporation analysis.

2.4.1 The Fe-Ni and Ni-Cr Systems

An analysis has been made of the data by Obradovic et al. (1969) for Fe-Ni and Ni-Cr alloys evaporated at 1873K for different times under various ambient pressures. In the 80% Ni-20% Cr case, evaporation started with $N_o = 0.7582$ moles of the alloy having an evaporating area $A = 10^{-3}$ m^2. The solute and solvent evaporating rates are, respectively, $U_{Cr} = 3.479 \times 10^{-1}$ and $V_{Ni} = 6.386 \times 10^{-2}$ mol/m^2/sec. In this case the solute, Cr, is comparatively highly evaporative relative to the solvent, Ni. Hence, the evaporating time t_1 given in Eq (11) applies, i.e.,

$$t_1 = G_1 \left[\ell n \frac{(1-m_o)m}{m_o(1-m)} + \frac{m-m_o}{(1-m_o)(1-m)} \right]$$

where $G_1 = -N_o (1-m_o)/AU$, and m_o and m are the initial and final molar solute concentrations in the alloy.

Least-square fits of the Obradovic data give nearly constant values of observed G_1: -1.785, -5.064, and -5.064 ($\times 10^4$ sec) for ambient pressures of 1, 100, and 500 ($\times 10^{-3}$ torr), respectively. The calculated values of G_1, though also nearly constant, are, however, one order of magnitude smaller, indicating surface solute depletion. Similar analysis for the 60% Fe-40% Ni alloy evaporated with $N_o = 0.7478$ moles and $A = 10^{-3}$ m^2 gives $U_{Ni} = 6.386 \times 10^{-2}$ and $V_{Fe} = 1.081 \times 10^{-1}$ mol/m^2/sec. Here, the solvent Fe is much more evaporative than the solute Ni, and Eq (14) applies. The

values of observed evaporating coefficients $G_2 = m_o N_o / AV$ are 2.469, 1.369, and 8.386 (x 10^4 sec) for ambient pressures of 0.133, 13.3, and 66.7 Newtons/m^2, respectively. The calculated G_2's are again nearly constant but also an order of magnitude smaller than the observed G_2's, again indicating solvent depletion (or solute enrichment) at the surface. Details of these analyses are given in Appendix A.

2.4.2 Beryllium Purification

The kinetics of normal evaporation for beryllium have been quantitatively checked with actual results of beryllium purification during vacuum induction melting. Details are given in Appendix B. In these tests by Bunshah and Juntz (1966), beryllium was crucible-free, induction-melted under an ambient pressure of 1.33×10^{-4} Newton/m^2. The actual temperature of the melt was not known, and the exact evaporating rates for the beryllium solvent and various solute elements cannot be computed. However, because all solute elements (i.e., Fe, Cr, Mn, Ni, Si, Al, Mg, Cu, Zn, and Na) and the solvent, Be, were evaporating from the same or common liquid-gas interface of a fixed area for the same length of time, we can compute the values of P, defined as the product of the evaporating time, t, and solvent evaporating rate, V (for $V \gg U$), or solute evaporating rate, U (for $U \gg V$); thus, $P = tV$ or tU. Table 1-5 gives the initial concentrations and final concentrations (in ppm) of the various solutes, together with the value of P, actual surface concentrations, ratio of actual surface to bulk concentrations, and effective times to reach the final concentrations under the assumption that the evaporating temperature was 1523K. The following conclusions can be drawn from Table 5-1:

- The solute elements can be divided into three groups: Fe, Cr, Ni, Si, and Cu evaporate much more slowly than Be; Mg, Zn, and Na evaporate much more rapidly than Be; and Al evaporates at about the same rate as Be
- The computed times to reach the final concentrations under normal evaporation conditions (complete liquid mixing) are fairly constant for the solute elements that evaporate much slower than Be (i.e., Fe, Cr, Ni, Si, and Cu), being about 4×10^4

TABLE 1-5 PURIFICATION KINETICS OF BERYLLIUM DURING CRUCIBLE-FREE VACUUM INDUCTION MELTING

Solute Element	Initial Conc., m_o, ppm Atomic	Final Conc. m, ppm Atomic	Ideal Evap. Rate at 1773 K, U_i, moles m^2 /sec	Time to Reach Final Conc., t_i, secs	$P = t_i U_i$ or $= t_i V_i$ ** moles m^2	Surface Conc., m_s, Atomic	m_s / m_o	Effective Time to Reach Final Conc., t_e, secs	$\frac{t_e, 1673K}{t_e, 1773K}$
Fe	1.55	4.5	2.7885×10^{-2}	2.69×10^{3}	655	1.34×10^{-4}	8.60×10^{1}	2.69×10^{3}	3.49
Cr	0.65	2.1	8.7887×10^{-2}	2.84×10^{3}	690	1.79×10^{-5}	2.75×10^{1}	2.84×10^{3}	3.48
Ni	4.95	7.5	1.5353×10^{-2}	1.39×10^{3}	340	7.82×10^{-4}	1.57×10^{2}	1.40×10^{3}	3.48
Si	4.50	5.0	1.3320×10^{-2}	0.41×10^{3}	100	8.19×10^{-4}	1.82×10^{2}	0.41×10^{3}	3.48
Cu	1.50	1.5	4.2039×10^{-1}	0.13×10^{3}	32	8.66×10^{-6}	5.77	0.13×10^{3}	3.53
Al	6.50	4.0	1.6834	-2.57×10^{3}	-625	9.37×10^{-6}	1.44	-2.57×10^{3}	3.49
Mg	4.0	0.03	5.9444	0.82	4,892	1.63×10^{-10}	4.00×10^{-5}	20.14×10^{3}	3.48
Zn	4.10	0.2	14.5917	0.20	3,020	6.82×10^{-11}	1.66×10^{-5}	12.43×10^{3}	3.48
Na	59.0	8.0	12.1483	0.16	1,998	1.17×10^{-9}	1.00×10^{-5}	8.22×10^{3}	3.49
Average					1,465			5.64×10^{3}	3.48

* for U = V

** for U = V

V_i (Be) 2.4287 moles m^2 sec

T 1772K

Ambient Pressure 1.33×10^{-4} newtons m^2

- The computed times to reach the final concentrations for the highly evaporative Mg, Zn, and Na are also fairly constant, but about four orders of magnitude smaller
- After correction for limited liquid mixing (Appendix B), the effective times to reach the final concentrations are much more constant, even between the groups of solute elements. In particular, the highly evaporative elements Mg, Zn, and Na have their results improved by several orders of magnitude
- Limited liquid diffusion must, therefore, be considered, particularly for the highly evaporative elements
- The surface solute concentrations can be changed by up to six orders of magnitude so that the effective evaporating rates can be similarly changed.

2.5 NORMAL EVAPORATION VS NORMAL FREEZING

Normal evaporation and normal freezing (Pfann 1966) are strikingly similar in many respects. Both deal with idealized transition phenomena between two phases. In normal evaporation, the two phases are either vapor and liquid or vapor and solid. In normal freezing, the two phases are always solid and liquid. In either case, the interface between these two phases moves in accordance with the constraints of mass transfer, heat transfer, and liberation or absorption of the heat of evaporation or fusion. Either phenomenon is idealized under the three assumptions tabulated below.

TABLE 1-6 COMPARISON BETWEEN ASSUMPTIONS IN NORMAL EVAPORATIONS AND NORMAL FREEZING

Normal Evaporation	Normal Freezing
Vapor or solid: complete vapor removal, i.e., $D_v = \infty$	Zero solid diffusion, $D_s = 0$
Liquid: complete liquid mixing, $D_l = \infty$	Complete liquid mixing, $D_l = \infty$
Phase Equilibrium: Raoult's Law	Phase diagram

In practice, complete vapor removal in normal evaporation has the same effect as no solid diffusion in normal freezing. Both assume that the material changed into the vapor phase (in normal evaporation) or solid phase (in normal freezing) is permanently and completely lost, and no longer has anything to do with the remaining material, as far as mass transfer is concerned. Complete liquid mixing is assumed in both cases. From the phase diagram, the freezing segregation coefficient k can be determined; based on Raoult's Law, the evaporative segregation coefficient k_v can be obtained. Both segregation coefficients are generally functions of the solute concentration and phase transition temperature, but can be considered constant under certain special conditions. Specifically, in extremely dilute solutions with limited solidifcation range, k is nearly constant; while if $U \ll V$ and $m \ll 1$, k_v is constant at a given evaporation temperature, as indicated above.

The value of k in normal freezing generally is within the relatively narrow range of 10^{-3} to 10. On the other hand, k_v in normal evaporation of nickel alloys at 1726K varies from 1.38×10^{-12} for W to over 10^{9} for such highly evaporative solute elements as K, Rb, and Cd as shown above. The values of k_v are thus many orders of magnitude wider in range than those of k.

The velocity v of interfacial movement has a much broader range in normal evaporation than in normal freezing. Normally, v varies from 10^{-6} to 10^{-3} m/sec, only three orders of magnitude from maximum to minimum. In normal evaporation of nickel alloys at 1726K, on the other hand, v varies from 6.74×10^{-20} m/sec for W to about 5.0 m/sec for K and Rb. The spread is almost 20 orders of magnitude.

Among the three assumptions (Table 1-6) in normal evaporation or freezing, the one on complete liquid diffusion is most subject to error. Much work has been done to include the effect of limited liquid diffusion in normal freezing. The equations of Tiller et al (1953) consider the initial transient state, the subsequent steady state, and the final stage of solidification, because of solute pile-up in front of the solid-liquid interface due to limited liquid diffusion. These equations are not very accurate for the general case (Pohl, 1954), except when k is nearly zero. Fortunately, for the important case of surface enrichment of trace impurities of a highly non-volatile impurity in solution, the

evaporative segregation coefficient at a given evaporation temperature is $k_v = U/V$, which is indeed close to zero. Hence, Tiller's equation for limited liquid diffusion can be bodily transferred to the normal evaporation study with limited liquid diffusion.

We thus see that with limited liquid diffusion before the steady state is reached, there exists a transient state during which the solute concentration and thermophysical properties of the surface-enriched layer change constantly in a manner that can be, but apparently never has been predicted.

For the special case of $U \ll V$ and $m \ll 1$ involved in space experimentation, it is necessary to know the "characteristic distance" and "decay constant" (across and over which the relative solute concentration changes by a factor of e, as defined by Tiller et al (1953)). Such determinations allow us to see how much unavoidable evaporation affects solidification during a given test period, or indeed to determine if the solidification experiment is meaningful or definitive and not unduly distorted by surface evaporation.

The characteristic distance is, as defined by Tiller et al (1953), D_1/kv, where D_1 is the liquid diffusion coefficient (generally about 10^{-8} m^2/sec). This distance for normal freezing thus covers about seven orders of magnitude, from 10^{-6} to 10.0 m. The characteristic distance for normal evaporation has a much broader range, covering over 41 orders of magnitude and varying from 10^{-18} to 10^{23} m.

The decay constant is, as defined by Tiller et al (1953), D_1/kv^2 and for normal freezing thus covers about 10 orders of magnitude, from 10^{-3} to 10^{7} sec. The decay constant for normal evaporation also has a much broader range, covering over 71 orders of magnitude, from 10^{-28} to 10^{43} sec.

These much greater evaporative segregation effects would almost certainly conceal any minor or subtle zero-gravity effects, especially in the presence of other unknown or uncontrolled effects. Definitive space solidification work should, therefore, be preceded by an evaporative compatibility study of the sample materials and associated impurities. In fact, evaporation is almost certain to be very important or so overwhelming that the effect of zero-gravity or freezing segregation may be masked or even reversed. A freely suspended molten drop in space may, for example, have its surface solute concentration

greatly enriched, even as much as a millionfold by neglected and undetectable trace impurities within a fraction of a second of its deployment. We are then dealing at the critical surface layer with a completely new and unanticipated alloy, e.g., trace impurity indium instead of the original zinc, having entirely different composition, melting point, surface tension, thermophysical properties, latent heat of fusion, undercooling and nucleation characteristics, growth morphology, and the like.

These and similar analyses suggest that the normal evaporation equations presented above work surprisingly well for the several alloy systems studied so far. The equations generally give results accurate to within an order of magnitude of the correct values, perhaps even for highly concentrated solutions (e.g., 20% Cr in Ni or 40% Ni in Fe). Such accuracies are sufficient for many evaporation studies.

In more critical studies, however, refined evaporation analyses may be needed. In particular, the effect of limited diffusion and, hence, surface depletion or enrichment of the solute must often be accounted for. This is true especially for the highly evaporative solutes such as Mg, Zn, and Na in the solvent Be. We already have results that confirm this conclusion. Details of these results will be published in Ref. 8 and elsewhere.

Section 3. ACCELERATIONS DUE TO DIFFERENTIAL EVAPORATION

In any zero-gravity experiment, it is important not to subject the test samples to accelerations due to gravity or other forces. Further, the molten samples should not touch the wall of the test chamber before solidification. Different rates of evaporation at various surface regions of a freely suspended sample do, however, give rise to unbalanced forces and momenta that may produce erratic or unwanted accelerations and undesirable sample impingement onto the test chamber wall. Such differential evaporation may result from solute segregation, nozzle detachment, or temperature gradient. For example, one-sided heating by an electron beam, introduces severe evaporative segregation and very steep temperature gradients. Previous work by Dr. T. Kassal at Grumman Research on water jetting into vacuum indicates that differential evaporation introduces unpredictable movements that are easily observed in motion pictures.

When planning space experiments on material solidification it is, therefore,

desirable to have quantitative answers to the following specific questions:

- What are the jetting forces on samples of different elemental materials under given temperature nonuniformity conditions? What elements are stable (i.e., subjected to small jetting forces) at their melting points, and what elements are unstable?
- What is the effect of sample size and density on jetting forces?
- For a given sample material, what are the critical or undesirable impurities, and what are the desirable or stabilizing impurities?
- What are the equivalent accelerations or gravities on the samples under specified test conditions?
- Starting from rest, how long does it take for a differentially evaporating sample to reach the wall of test chamber of a given size?
- What is the minimum test chamber size or maximum degree of superheating for a given sample material and size?
- How should the sample be heated and released, and with what equipment?

3.1 ANALYSIS OF THE JETTING ACTION

The above questions can be answered by a simple analysis of the jetting action on a differentially heated sphere, such as is shown in Fig. 1-9. The right half of the sphere is assumed to have a surface temperature T_1, which is lower than T_2, the surface temperature of the left half of the sphere. As a result, the vapor pressure p_2 on the left half is greater than that (p_1) on the right half. There is then a net force f which produces an acceleration a. This acceleration causes the sphere (diameter d, density ρ) to travel a distance s to impact the wall of the test chamber or other nearby objects.

The jetting force due to differential evaporation is (see Appendix C)

$$f = \tfrac{1}{2}\left(\frac{\pi}{4}\, d^2\right)(p_2 - p_1) = \left(\frac{\pi}{6}\, d^3 \rho\right) a$$

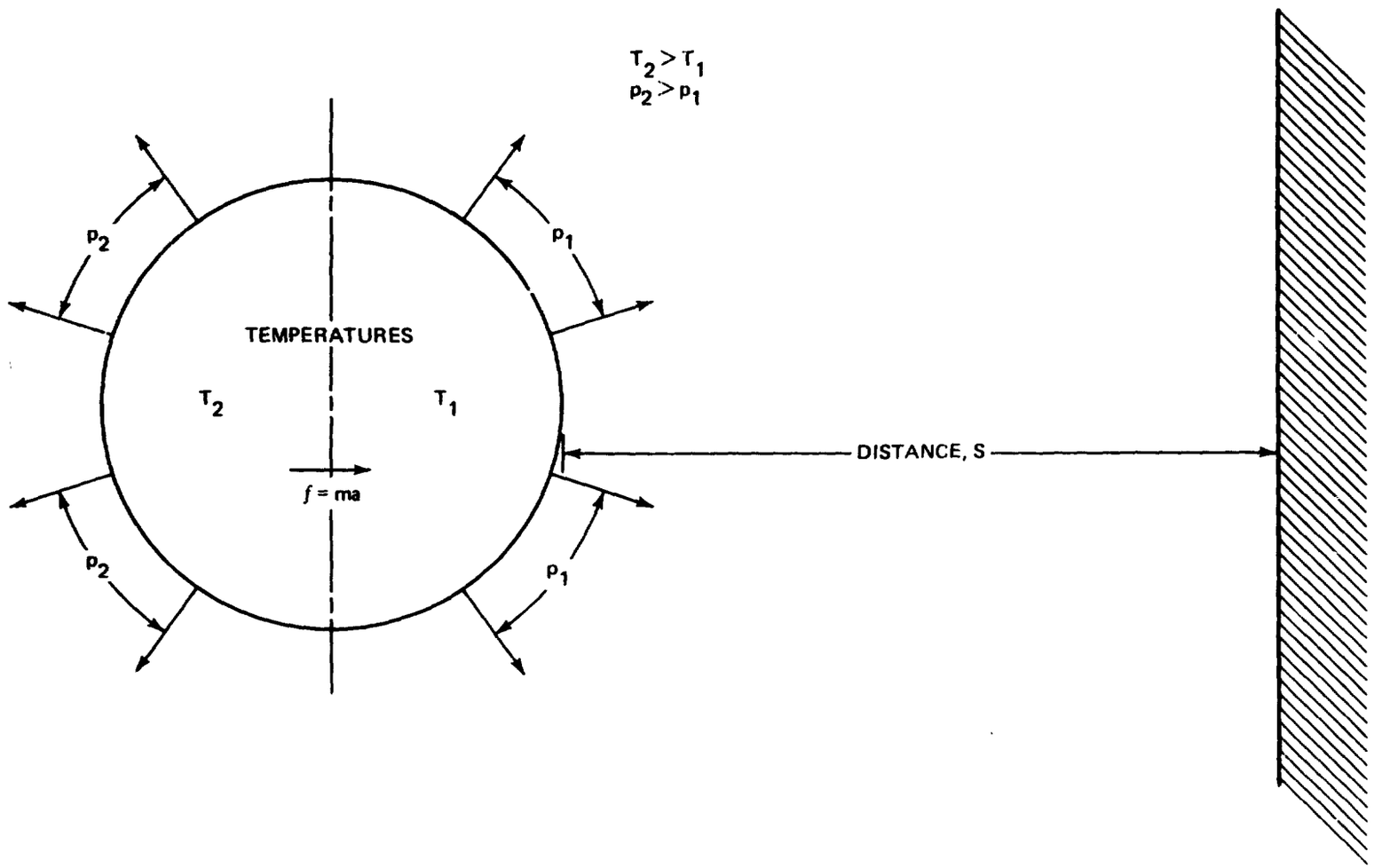

Fig. 1-9 Jetting on a Differentially-Heated Sphere

Hence, the acceleration due to the jetting action is:

$$a = (p_2 - p_1)/4d\rho$$

The equivalent gravity is then a divided by the gravitational constant g = 9.81 m/sec^2,

$$g_e = a/g = a/9.81$$

And the time t for the jetting sample to travel the distance s before impacting the nearby wall or object is

$$t = \sqrt{2s/a} = \sqrt{8ds\rho/3\,(p_2 - p_1)}$$

In the above analysis, we assumed zero initial velocity and acceleration; the equations are easily corrected for nonzero initial velocity and acceleration. The times computed are, therefore, the maximum allowables for performing the experiment or processing. Note that these times are proportional to ρds raised to the one-half power. In addition, they depend even more critically on $\Delta T = T_2 - T_1$ and on the evaporation behavior of the sample material, i.e., on $p_2 - p_1$. This is because the elemental vapor pressures vary by over 38 orders of magnitude at the melting point of nickel (1726K), and because these vapor pressures are highly temperature sensitive, as previously shown.

3.2 COMPUTED JETTING ACTION ON SINGLE ELEMENTS

The 51 metallic elements listed in Table 1-1 have been screened for potential, space-processing sample materials. Here, the sample diameter is fixed at 6×10^{-3} m, while the allowable distance of travel is constant at 0.3 m. Further, half of the spherical surface is assumed to be at T_1, the melting point of the sample material, while the other half is at T_2, being superheated by 5 to 100% of the absolute melting temperature. Computations show that the allowable times at 5% superheating vary widely from tens of milliseconds to over 10^9 years for gallium. Table 1-7 summarizes the data on these highly stable sample materials, as compared to nickel. These results further stress the critical importance of evaporative segregation.

Figures 1-10 through 1-12 show the jetting characteristics of the top four, or most

TABLE 1-7 LIST OF STABLE SAMPLE MATERIALS, AS COMPARED TO NICKEL

Rank	Element	Melting Point, K	Vapor Press. at Melting Point newtons/m^2	Times at Degree of Superheating Indicated, sec				
				5%	10%	20%	50%	100%
1	Ga	302.9	7.04×10^{-34}	1.65×10^{17}	1.68×10^{16}	3.13×10^{14}	4.88×10^{10}	7.60×10^{6}
2	Sn	505.0	3.64×10^{-18}	6.31×10^{9}	1.43×10^{9}	1.09×10^{8}	3.84×10^{5}	1.35×10^{3}
3	In	429.7	2.05×10^{-17}	2.71×10^{9}	6.26×10^{8}	4.96×10^{7}	1.89×10^{5}	7.17×10^{2}
4	La	1099	5.69×10^{-7}	2.73×10^{4}	1.00×10^{4}	1.90×10^{3}	49.8	1.31
5	Bi	544	6.17×10^{-6}	1.14×10^{4}	4.47×10^{3}	9.59×10^{2}	33.3	1.15
6	Pb	600.6	5.35×10^{-5}	4.63×10^{3}	1.92×10^{2}	4.61×10^{2}	20.7	0.930
	Ni	1726	0.540	5.33	2.60	0.870	8.42×10^{-2}	8.20×10^{-3}
	Fe	1812	3.51	2.14	1.09	0.399	4.78×10^{-2}	5.77×10^{-3}

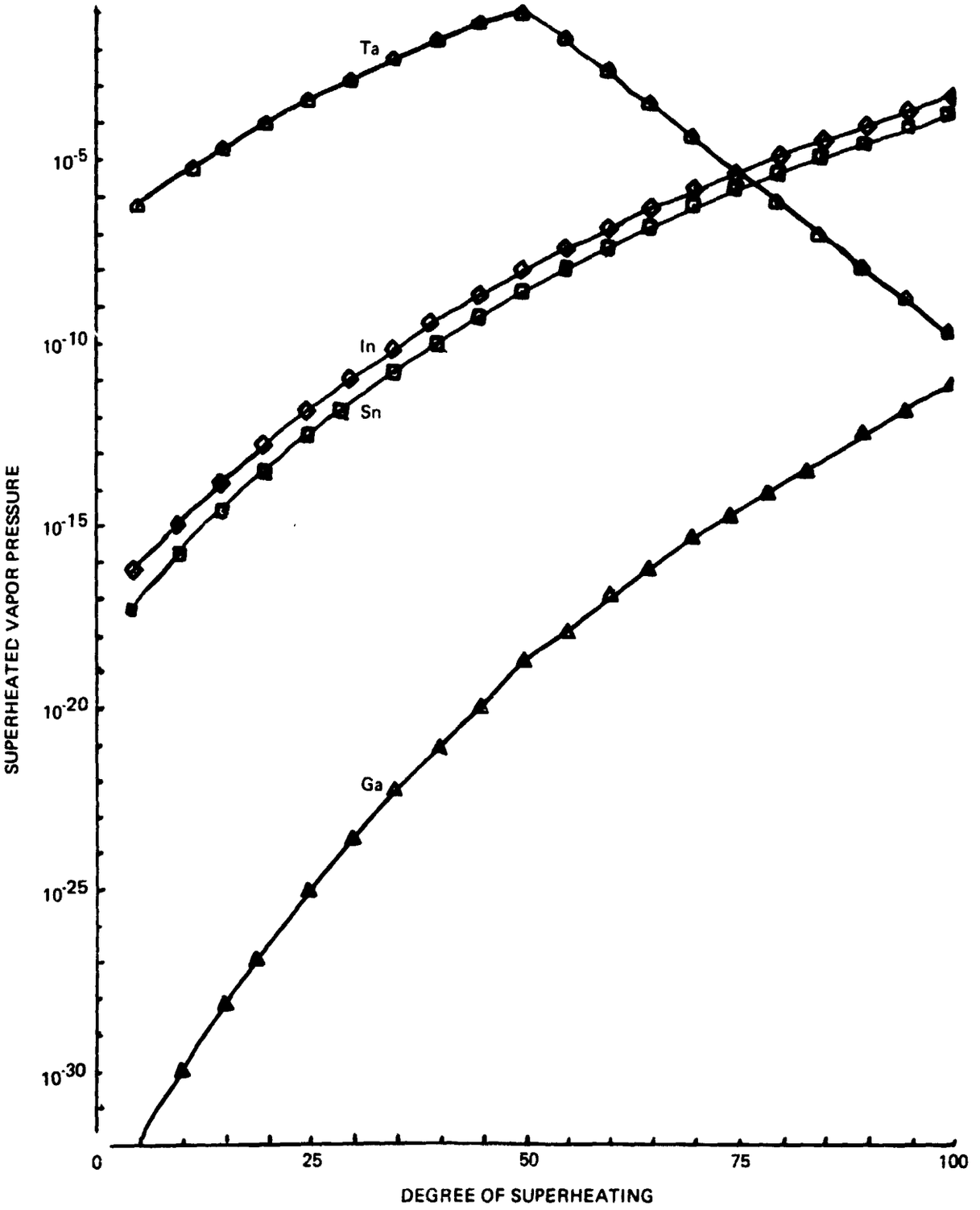

Fig. 1-10 Superheated Vapor Pressure on 6×10^{-3} m Metal Spheres, One Side at the Absolute Melting Point While the Other Side at Specified Degree of Superheating

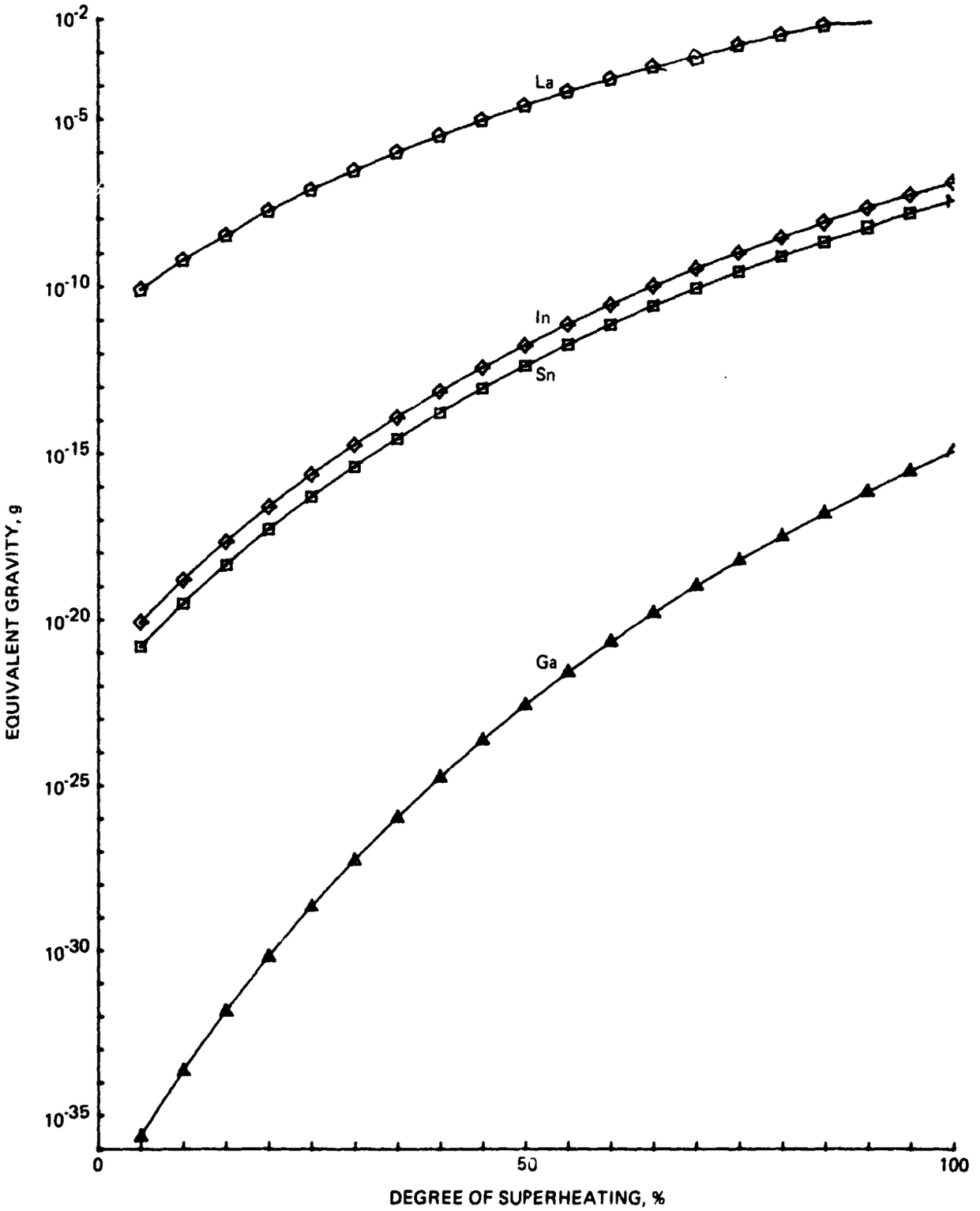

Fig. 1-11 Equivalent Gravity on 6×10^{-3} m Metal Spheres, One Side at the Absolute Melting Point While the Other Side at Specified Degree of Superheating

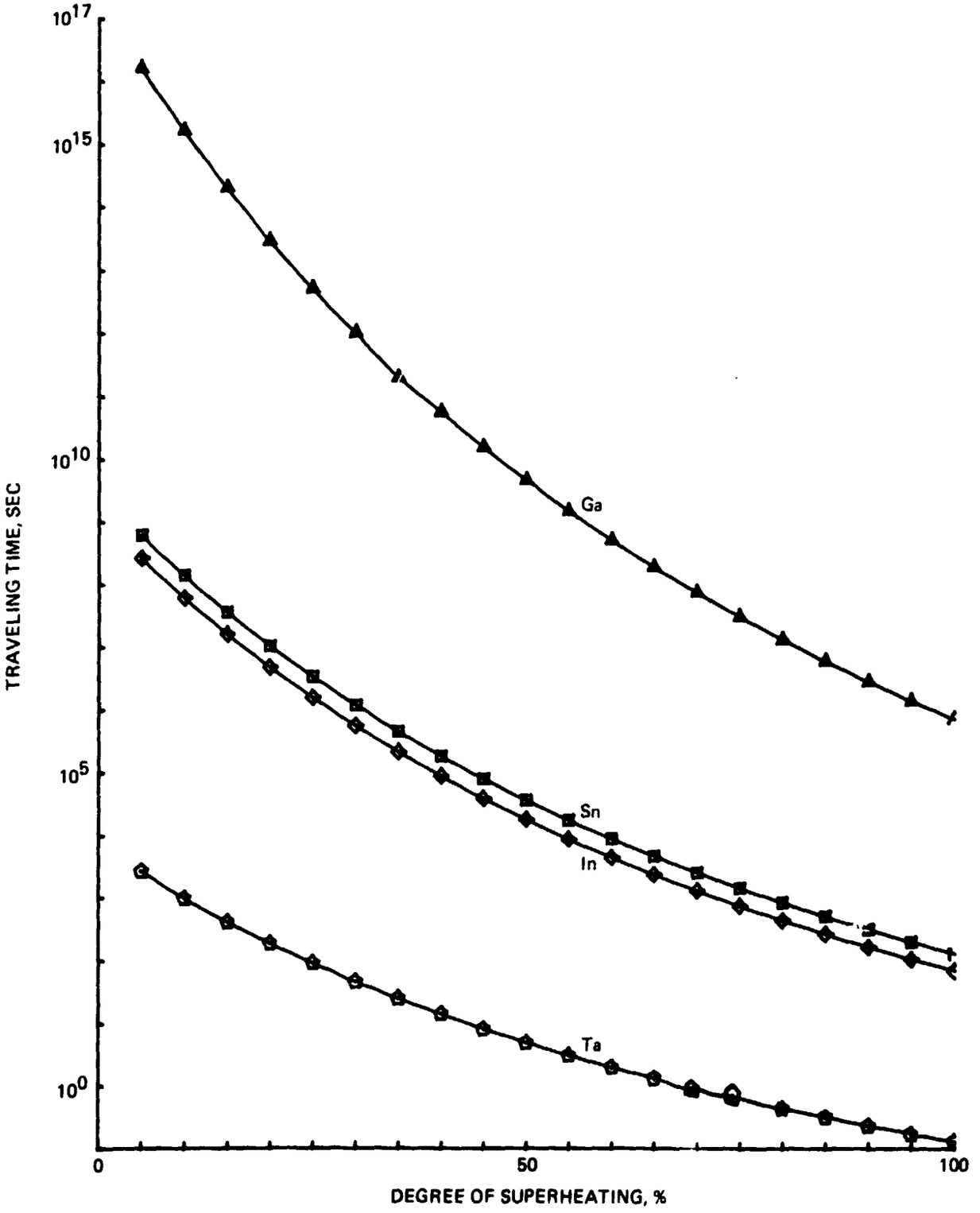

Fig. 1-12 Time to Travel 0.3m for 6×10^{-3}m Metal Spheres, One Side at the Absolute Melting Point While the Other Side at Specified Degree of Superheating

stable elements, i.e., Ga, Sn, In, and La. These figures illustrate the superheated vapor pressure, equivalent gravity, and time to travel 0.30 m, for a 6.0×10^{-3} m molten metal sphere, heated to its melting point on one side but superheated on the other. The amount of superheating varies from 5 to 100% at 5% intervals. Figures 1-13 and 1-14 give similar jetting data, but for nickel and iron samples respectively.

Thus, the unwanted accelerations due to differential evaporation, while completely negligible in many materials, are serious factors to be considered in others, including the specified nickel samples in M512 Skylab experiments. Specifically, it takes only 10 or 20% superheating on one side of a 6×10^{-3} m molten nickel sphere to impact the experimental chamber wall 0.3 m away within three or one seconds, respectively, of its release. Complete solidification in free suspension may, therefore, be very difficult under these conditions.

In other words, nonuniformly heated, 6×10^{-3} m spheres are subjected to equivalent gravities of from 2.26×10^{-39} Kg for gallium to 3.25×10^{-3} Kg for magnesium, if the spheres are superheated by only 5% on one side relative to the other side at its absolute melting point. From this, we anticipate new types of powerful evaporative convection currents to be described later.

Notice that, in both nickel and iron spheres of the specified size, the computed equivalent gravity exceeds the one-g level if one side is superheated by 35 and 26%, respectively, relative to the other side at its absolute melting point. Such evaporation and jetting action is, of course, merely the familiar rocket action. In the performance of some Skylab experiments, however, such differential jetting can have important and serious implications. The 6×10^{-3} m spheres in the M512 sphere-forming experiment, for example, are known to be very unevenly heated by the electron beam from one side, to the point of occasional spitting or explosion, but remain solid on the other side. Such samples may be subjected to very large, unwanted accelerations (and hence equivalent gravities) of unpredictable magnitude, direction, and duration. Unless corrective action is taken, such as changing the sample material, improving the hardware design (now considered too late), or optimized heating procedures, any solidification results may be difficult to interpret in terms of zero-gravity effects.

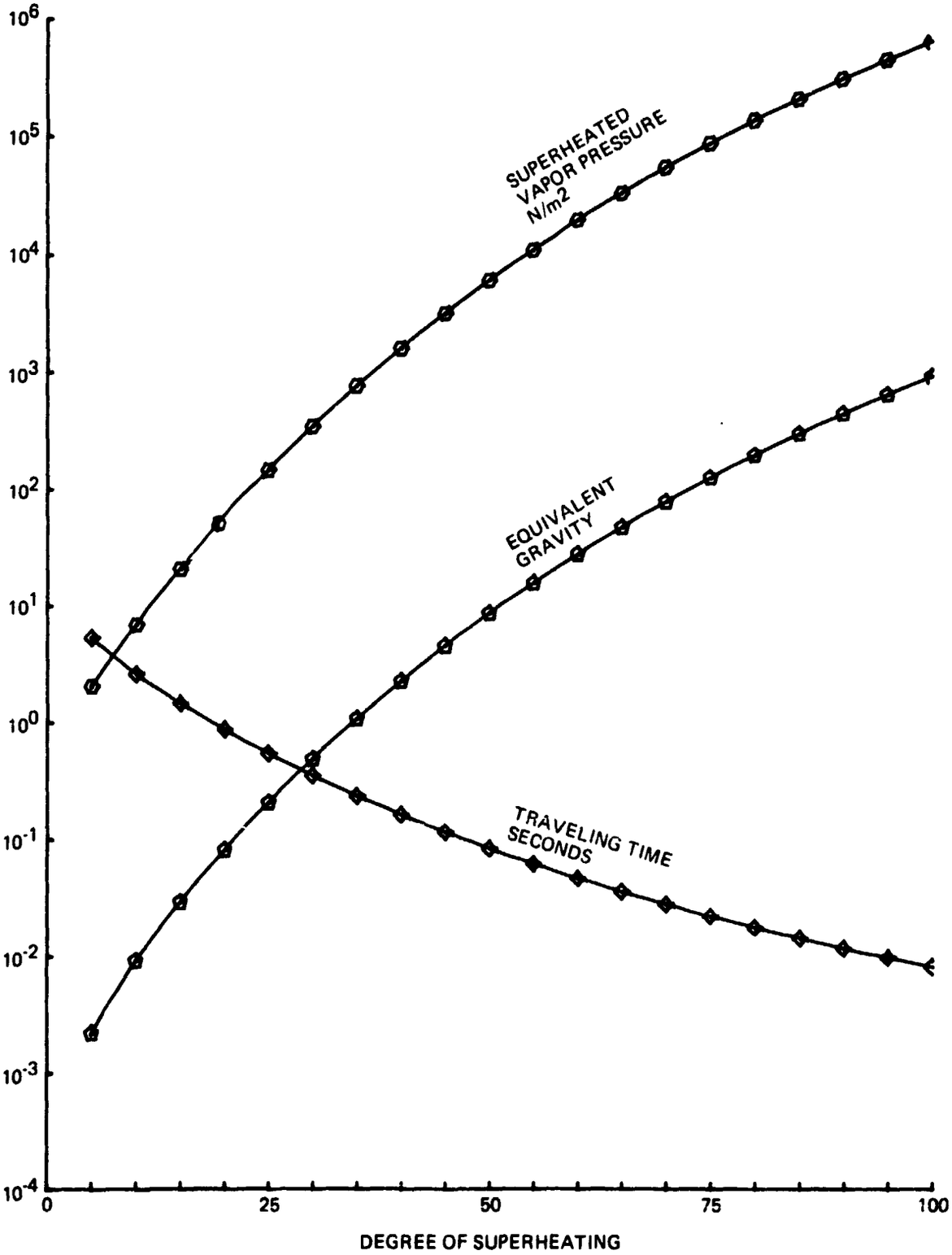

Fig. 1-13 Jetting Action on 6×10^{-3} m Nickel Sphere, One Side at the Absolute Melting Point of 1726K while the Other Side at Specified Degree of Superheating

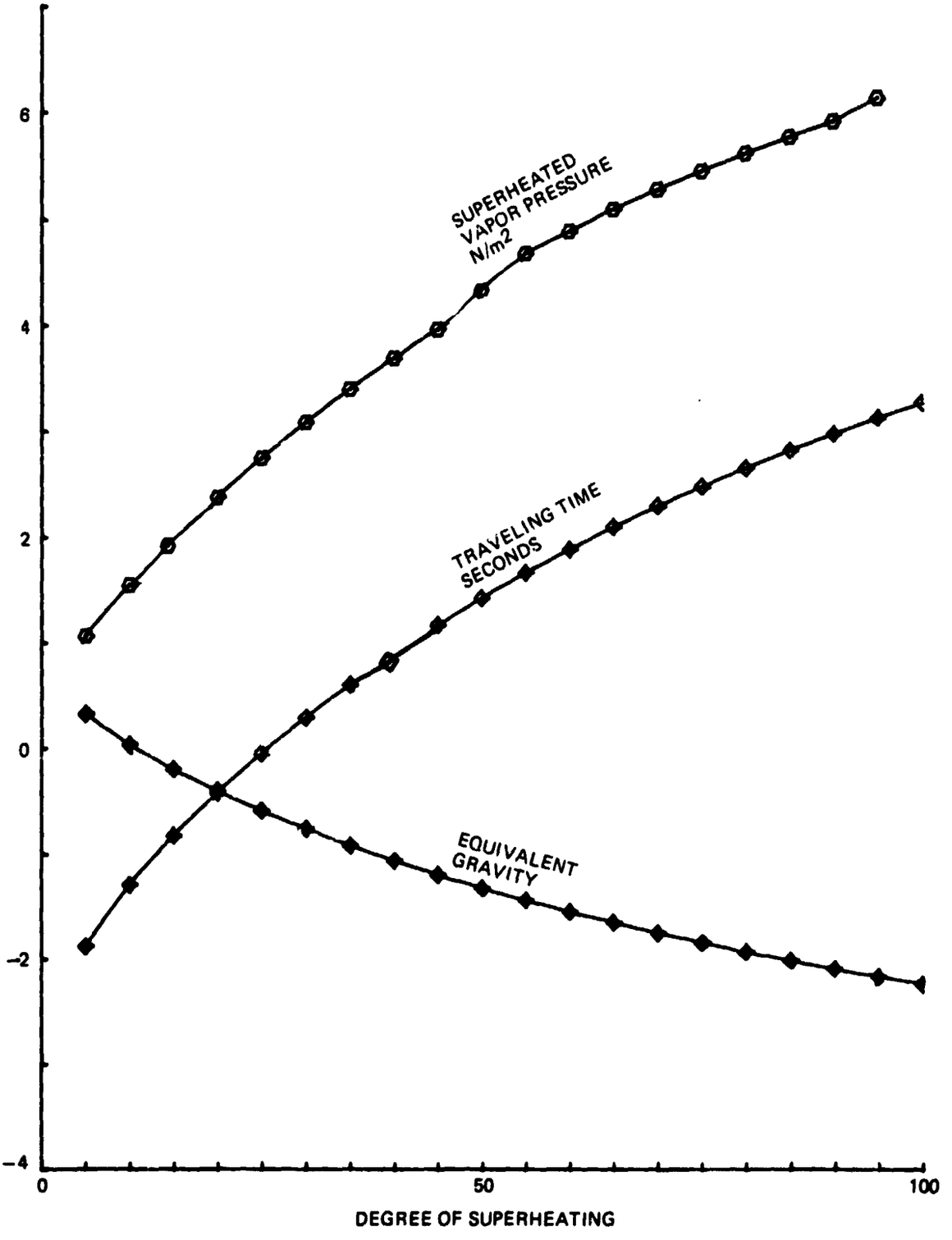

Fig. 1-14 Jetting Action on 6×10^{-3} m Iron Sphere, One Side at the Absolute Melting Point of 1812K while the Other Side at Specified Degree of Superheating

Figures 1-15 and 1-16 display the jetting characteristics on partially superheated, 6×10^{-3} m spheres of highly volatile materials due to differential evaporation. These figures are, respectively, for equivalent gravity and time to travel 0.3 m, for seven different volatile elements at eight different degrees of superheating from 5 to 100%.

3.3 COMPUTED JETTING ACTION OF IMPURITIES IN NICKEL

The undesirable jetting action due to certain evaporating impurities can also be replaced by the desirable stabilizing action of other impurities. Specifically, a 6.0×16^{-3}-m nickel sphere, at its melting point of 1726K, may have its normal jetting action at 5% superheating on one side reduced from 2.15×10^{-3} g to 7.34×10^{-15} g by an enriched surface layer of tungsten, or to 6.75×10^{-14} g by tantalum. These data on the stabilizing impurities on nickel are illustrated in Fig. 1-17.

Figures 1-18 to 1-23 show the stabilizing actions of surface layers of the six most powerful stabilizers in nickel. These stabilizers, as shown in Fig. 1-17, are W, Ta, Cb, Os, C, and Mo. These figures show, as ordinates, the superheated vapor pressure, equivalent gravity, and time to travel 0.3 m, for a 6×10^{-3} m molten nickel sphere. This sphere has a surface layer of the specified stabilizing element and is heated to the melting point of nickel (1726K) on one side but superheated on the other. The amount of superheating in percentage points is plotted as the abscissa.

Figures 1-24 and 1-25 give the jetting characteristics on partially superheated, 6×10^{-3} m nickel spheres, surface-contaminated with powerful agitators or highly volatile elements. These figures are, respectively, for equivalent gravity and time to travel 0.3 m for several volatile elements at different degrees of superheating up to 100%.

If we compare Fig. 1-18 with Fig. 1-24 or 1-25 we see that, on a 6×10^{-3} m nickel sphere superheated above its absolute melting point by 5% on one side, the equivalent gravity varies by 19 orders of magnitude from 4.87×10^{7} for K to 7.34×10^{-15} for W. For the same partially superheated nickel sphere, the time to travel 0.3 m varies by 10 orders of magnitude from 1.84×10^{-4} sec (i.e., 184 μsec) for K to 2.89×10^{6} sec (i.e., 0.92 years) for W surface layer.

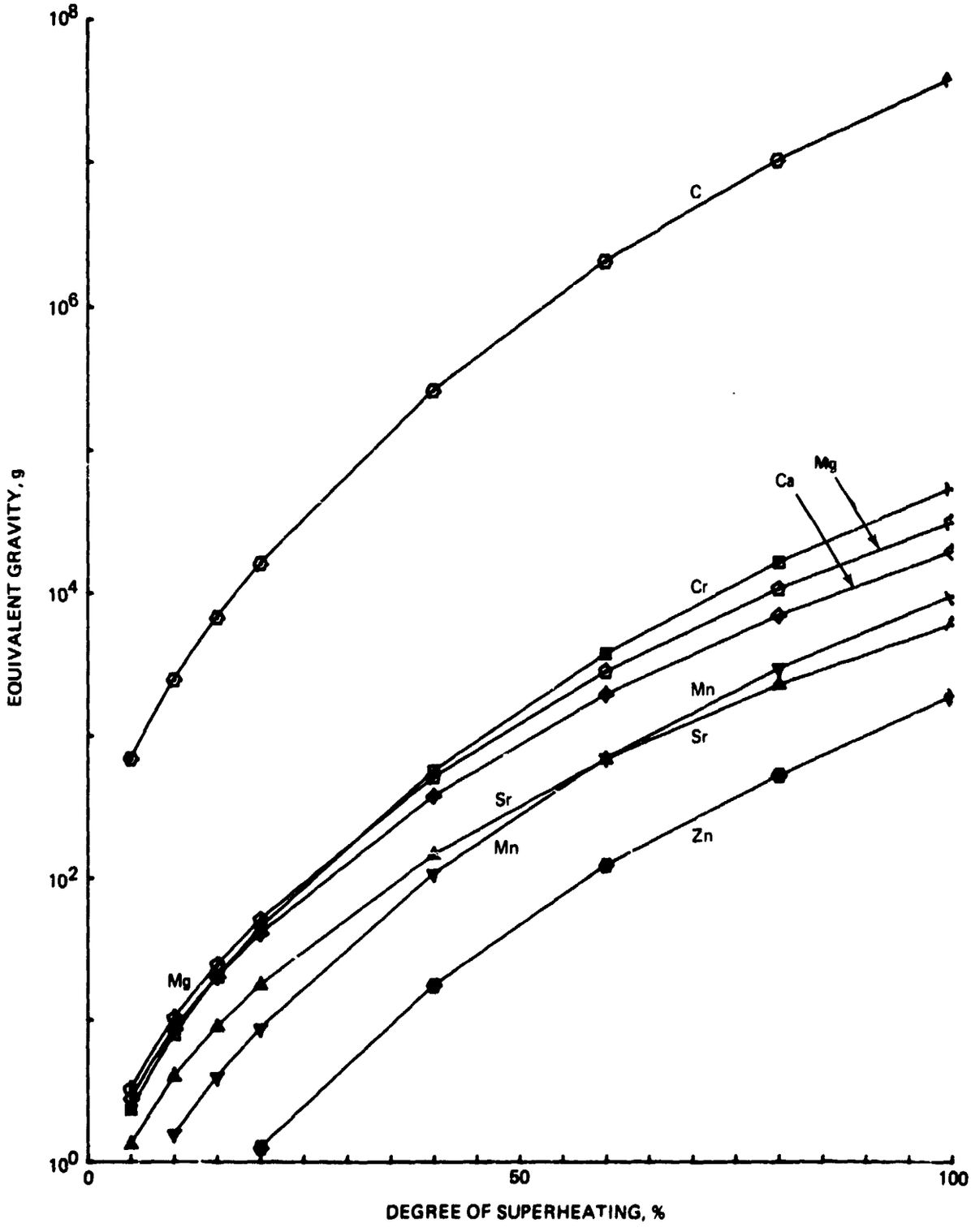

Fig. 1-15 Equivalent Gravity on Partially Superheated, 6×10^{-3} m Sphere of Highly Volatile Material Due to Differential Evaporation and Jetting

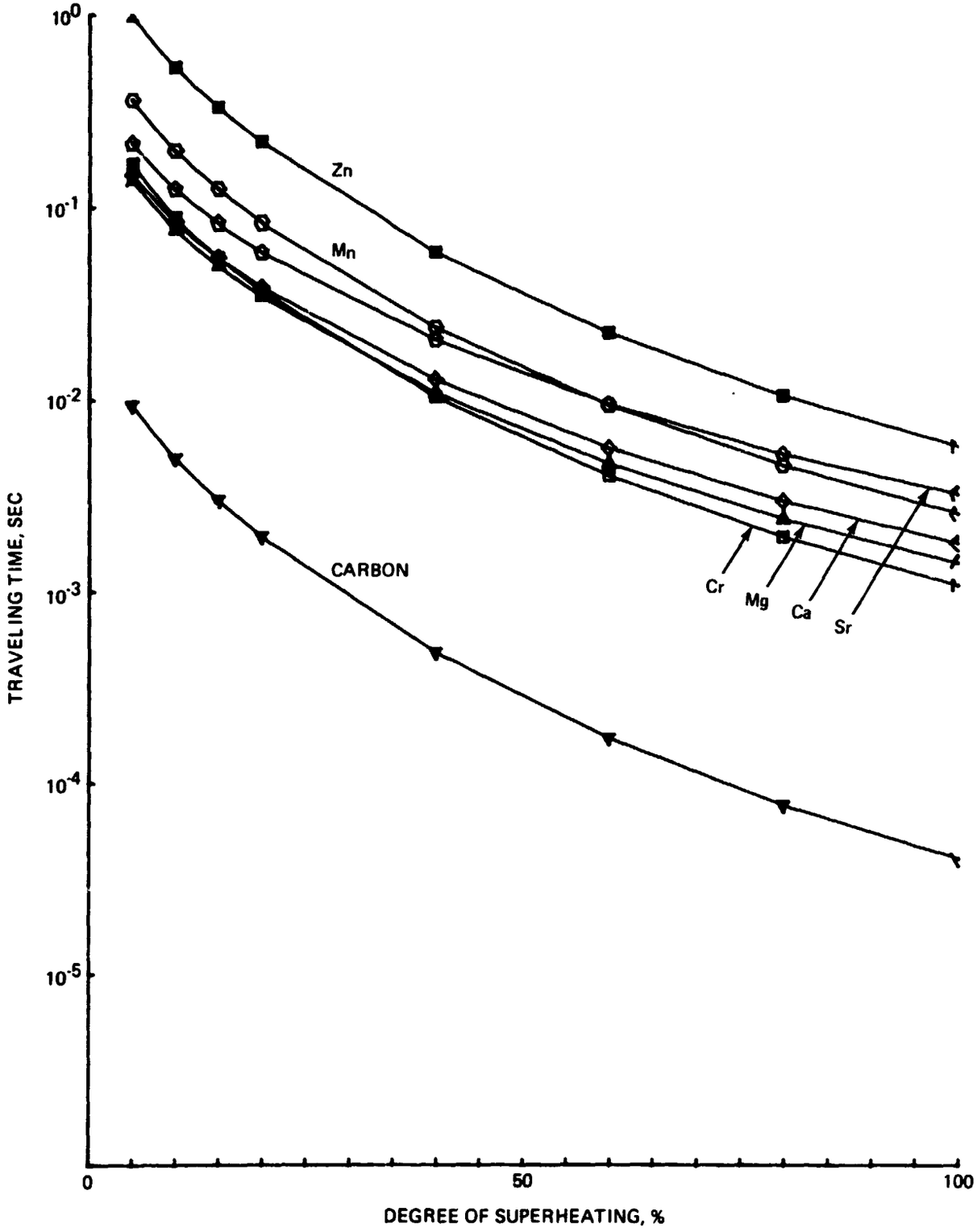

Fig. 1-16 Time for a Partially Superheated, 6×10^{-3} m Sphere of Highly Volatile Material to Travel 0.3m Due to Differential Evaporation and Jetting

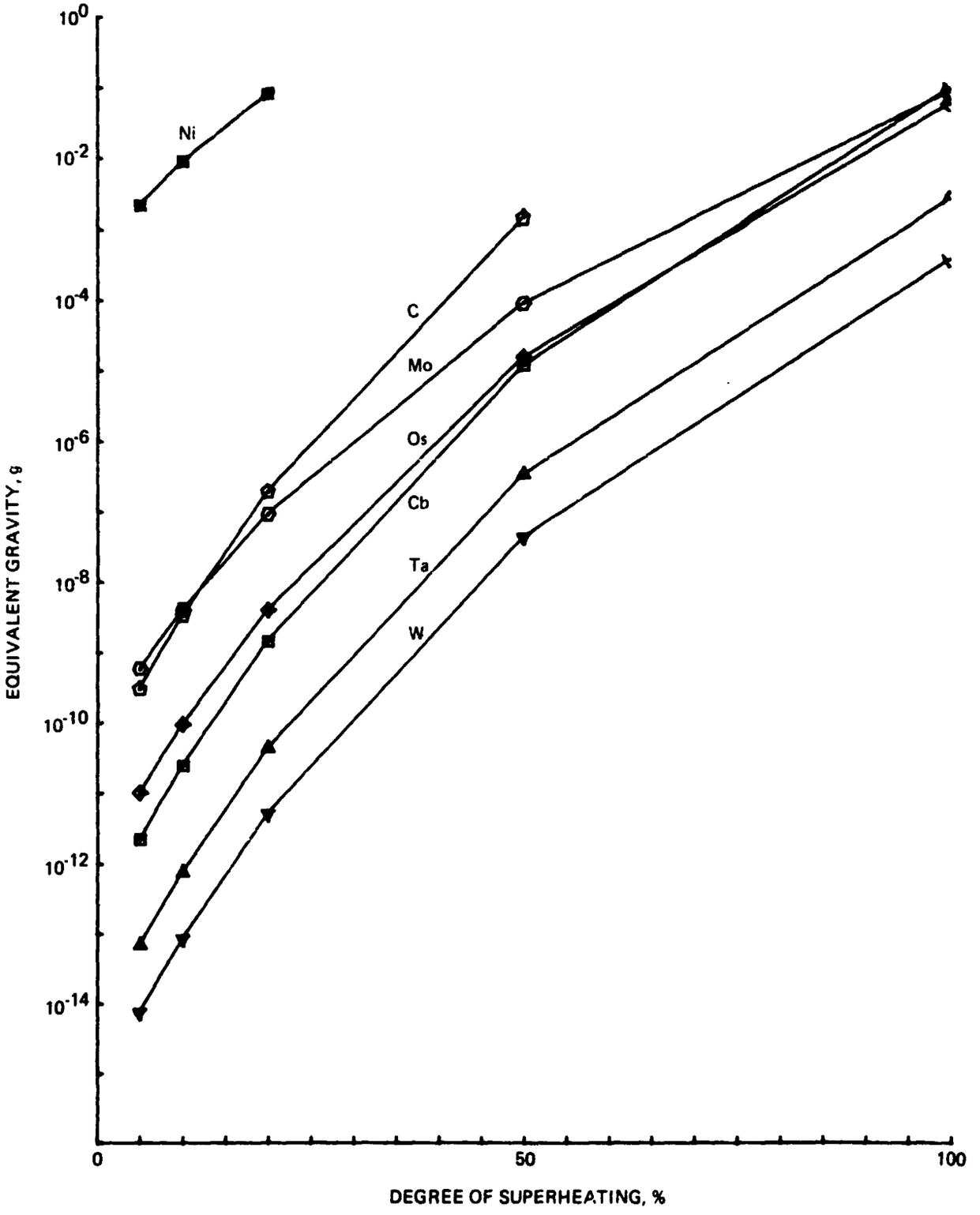

Fig. 1-17 Equivalent Gravity Due to Stabilizing Impurities for Nickel at 1726K, at Specified Degrees of Superheating

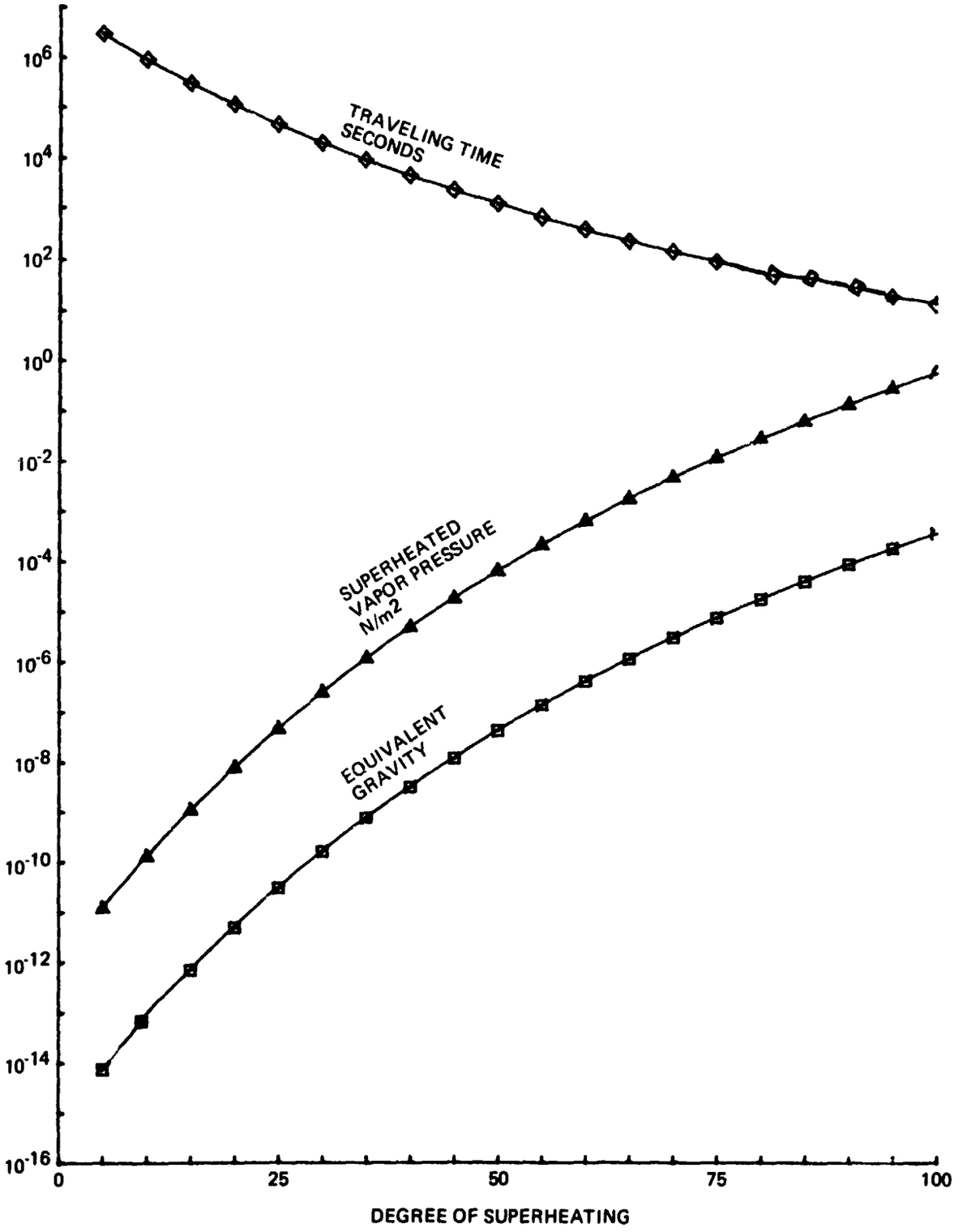

Fig. 1-18 Jetting Action on 6×10^{-3} m Nickel Sphere Containing Surface Layer of W

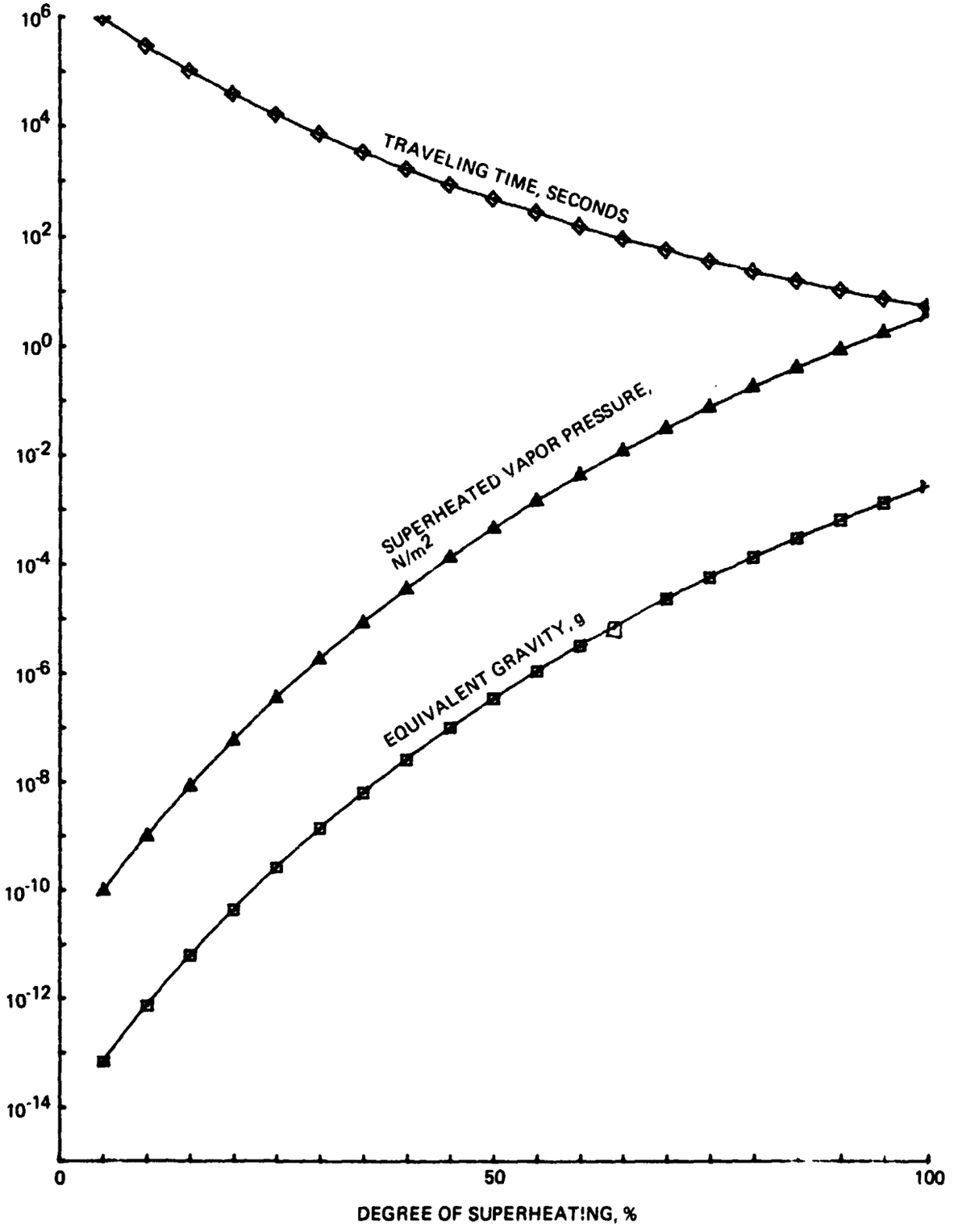

Fig. 1-19 Jetting Action on 6×10^{-3} m Nickel Sphere Containing Surface Layer of Ta

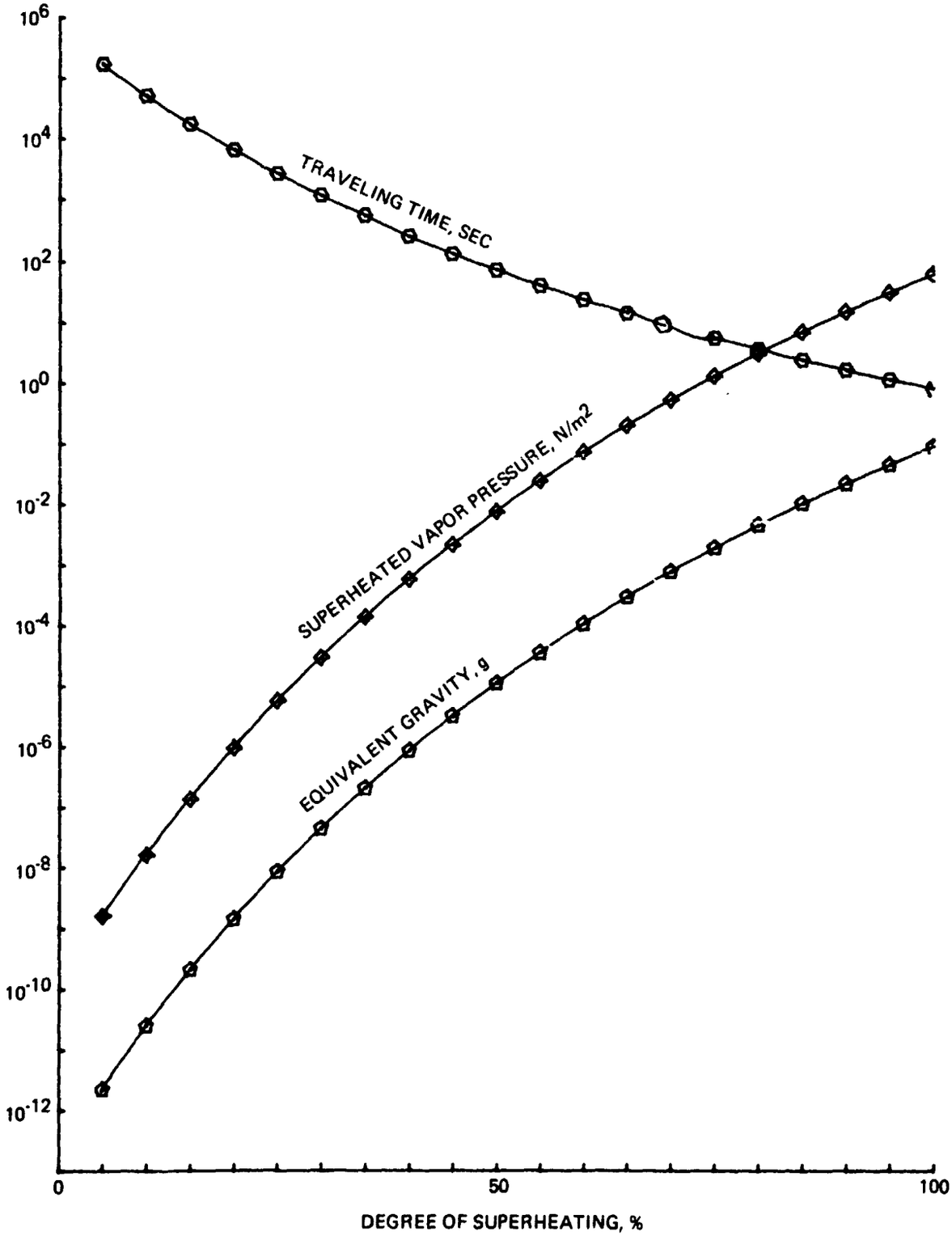

Fig. 1-20 Jetting Action on 6×10^{-3} m Nickel Sphere Containing Surface Layer of Cb

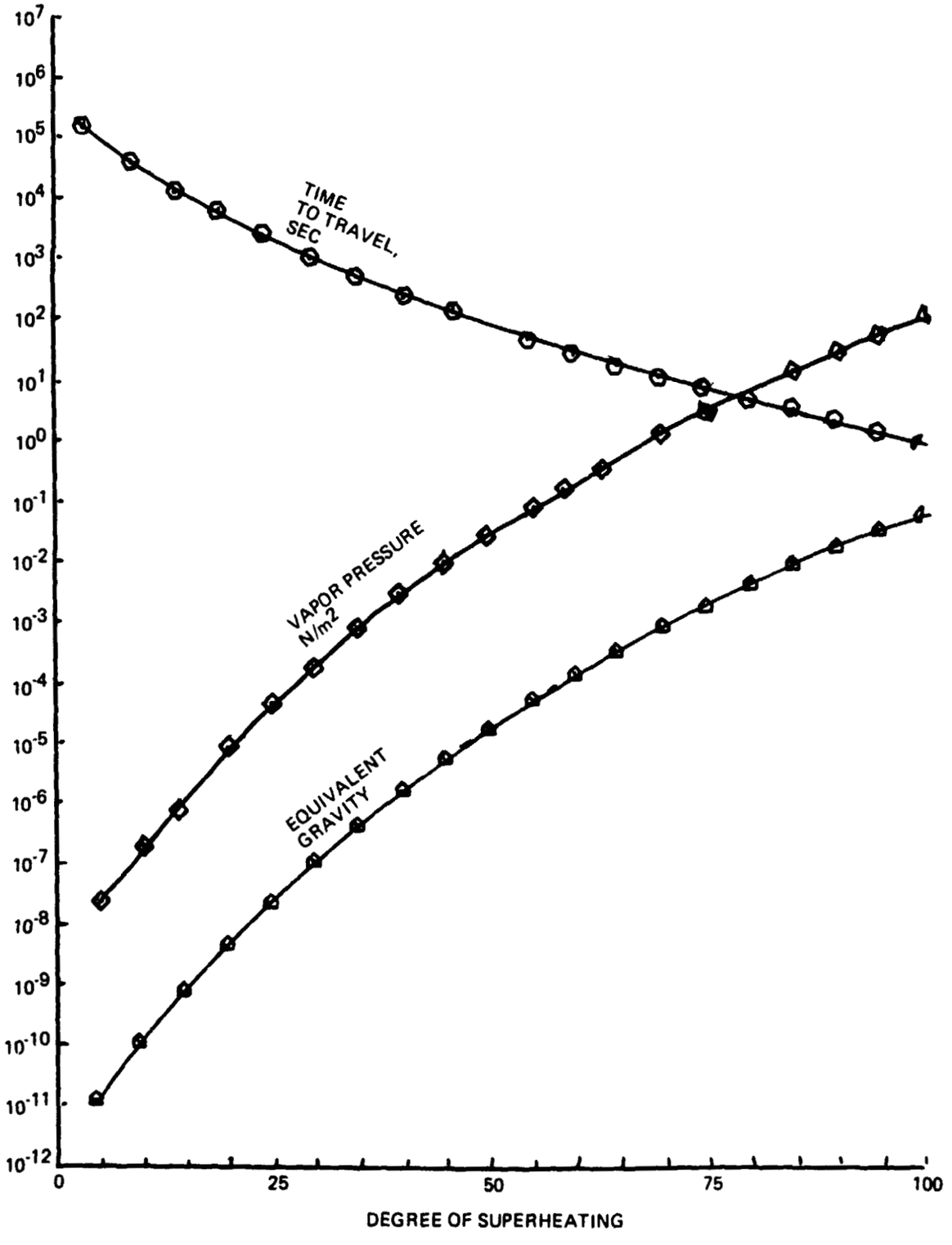

Fig. 1-21 Jetting Action on 6×10^{-3} m Nickel Sphere Containing Surface Layer of Os

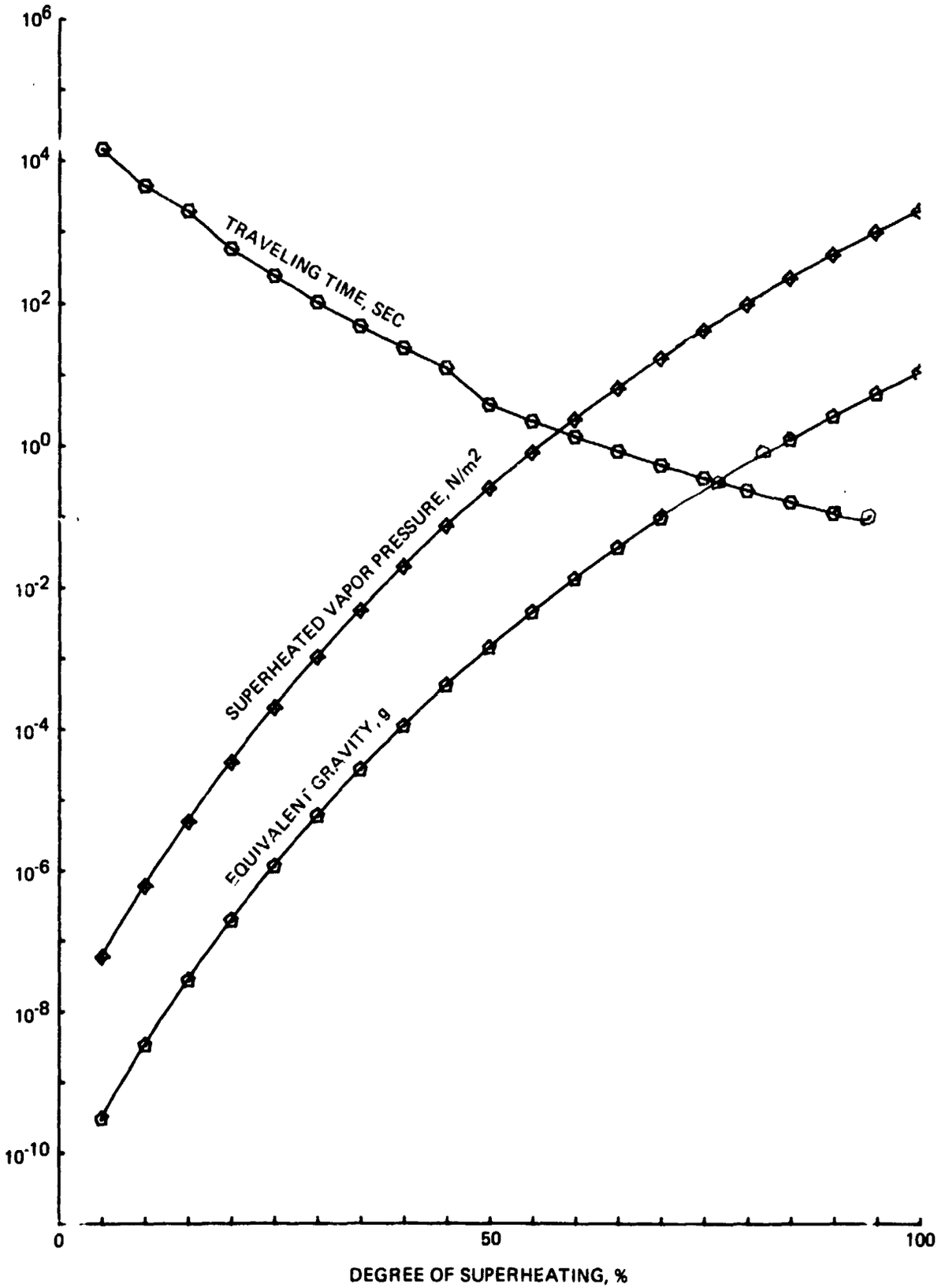

Fig. 1-22 Jetting Action on 6×10^{-3} m Nickel Sphere Containing Surface Layer of C

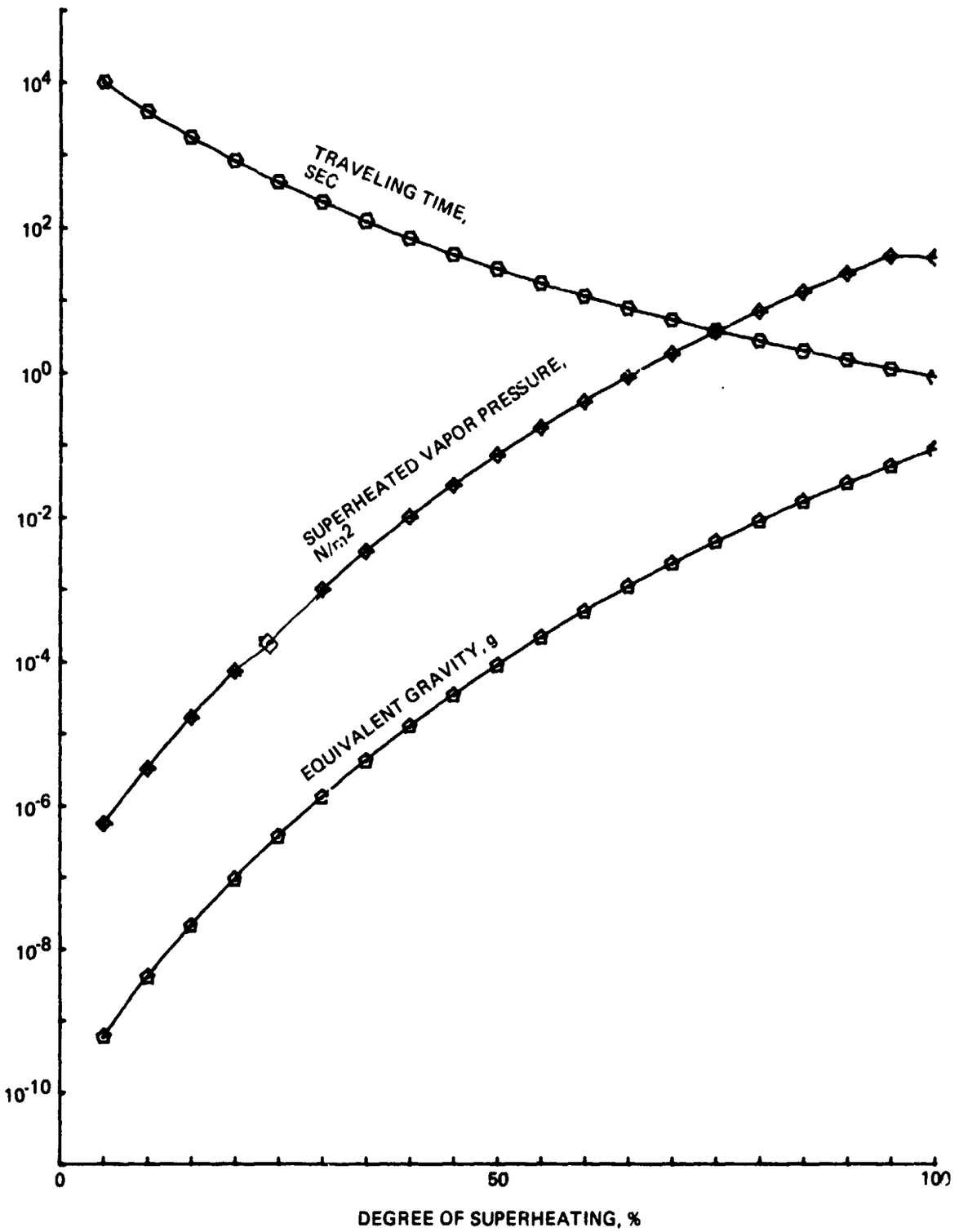

Fig. 1-23 Jetting Action on 6×10^{-3} m Nickel Sphere Containing Surface Layer of Mo

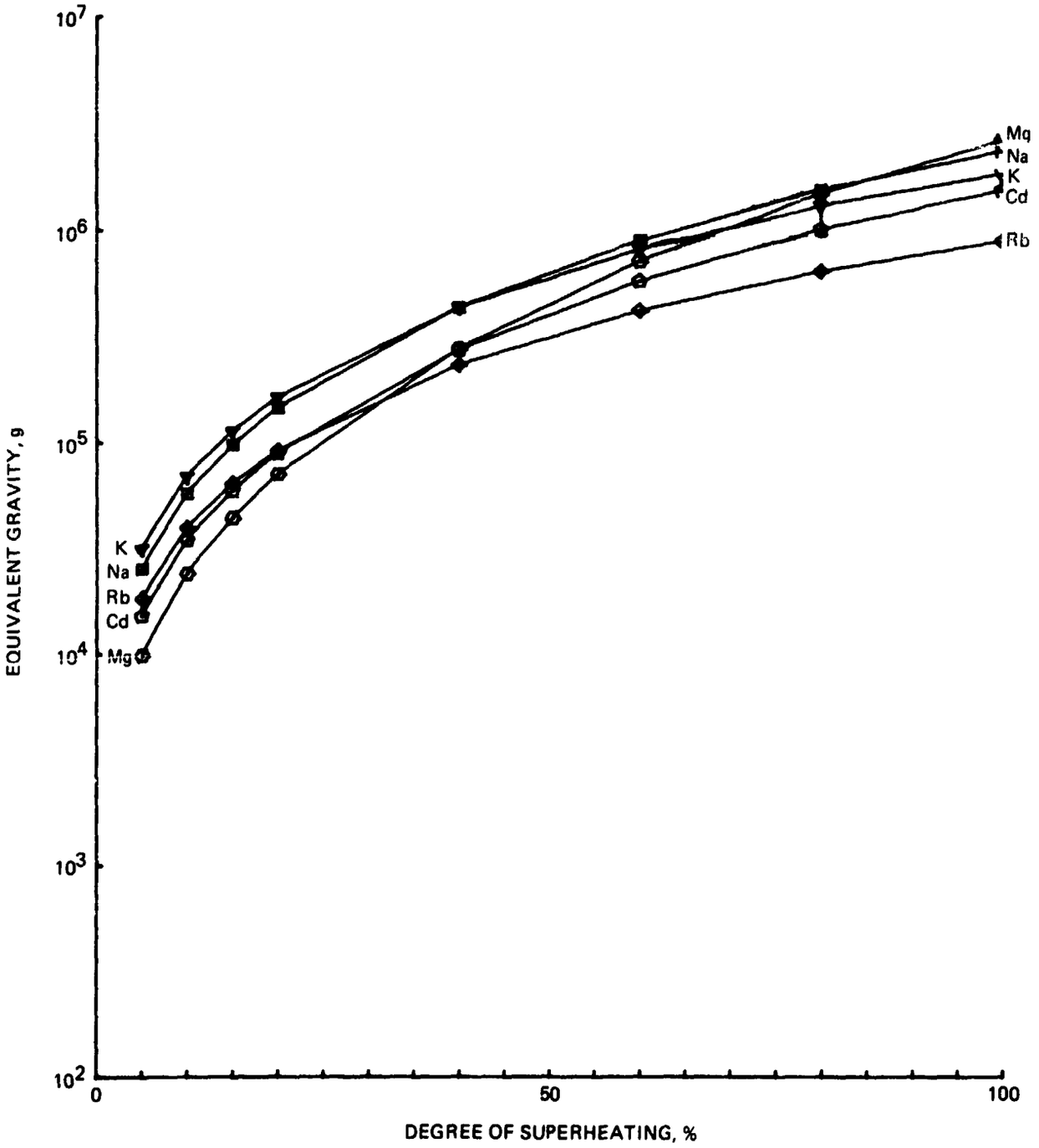

Fig. 1-24 Equivalent Gravity on 6×10^{-3} m Partially Superheated Nickel Sphere with Surface Layer of Highly Volatile Element Due to Differential Evaporation and Jetting (Sheet 1 of 2)

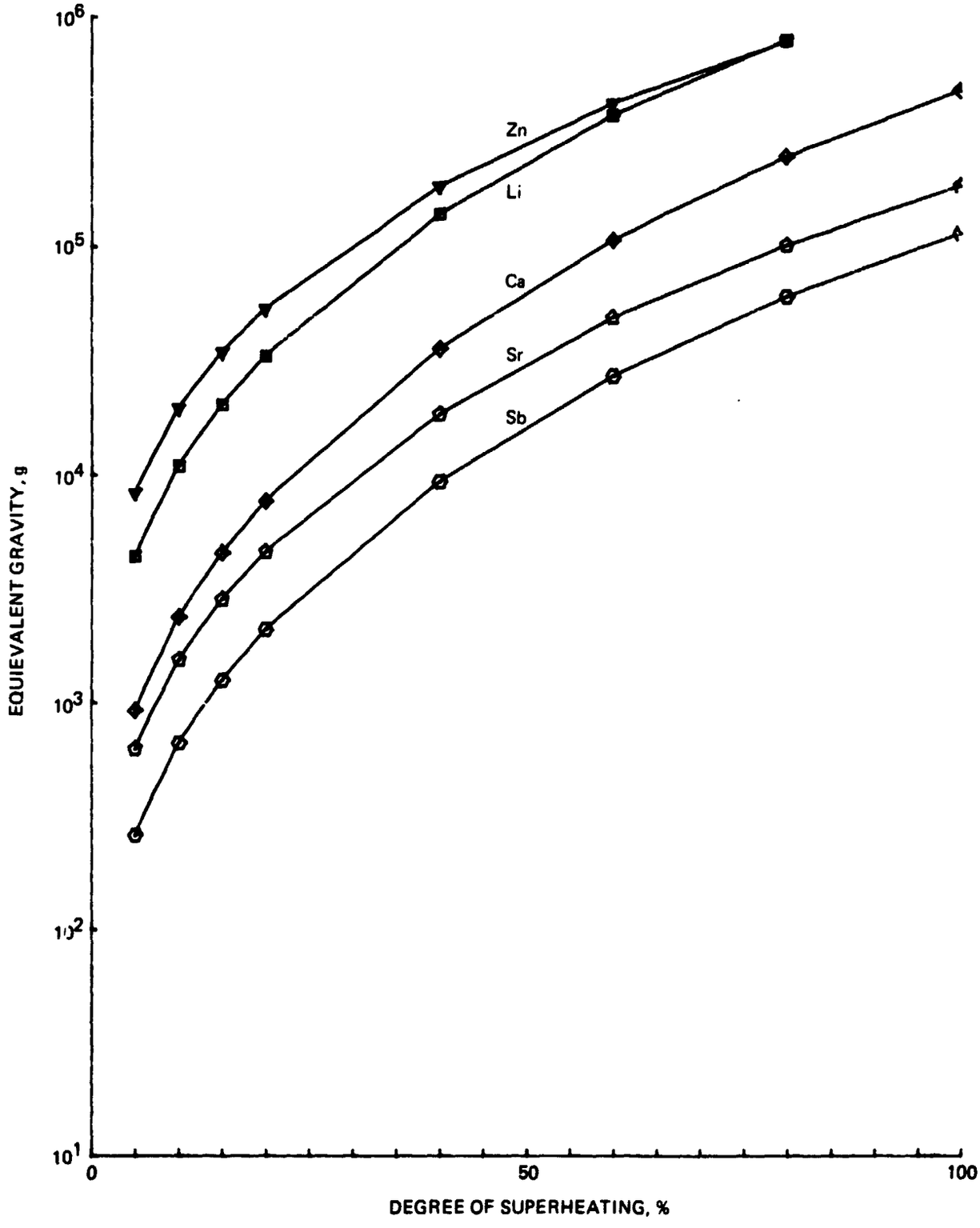

Fig. 1-24 Eqivalent Gravity on 6×10^{-3} m Partially Superheated Nickel Sphere with Surface Layer of Highly Volatile Element Due to Differential Evaporation and Jetting (Sheet 2 of 2)

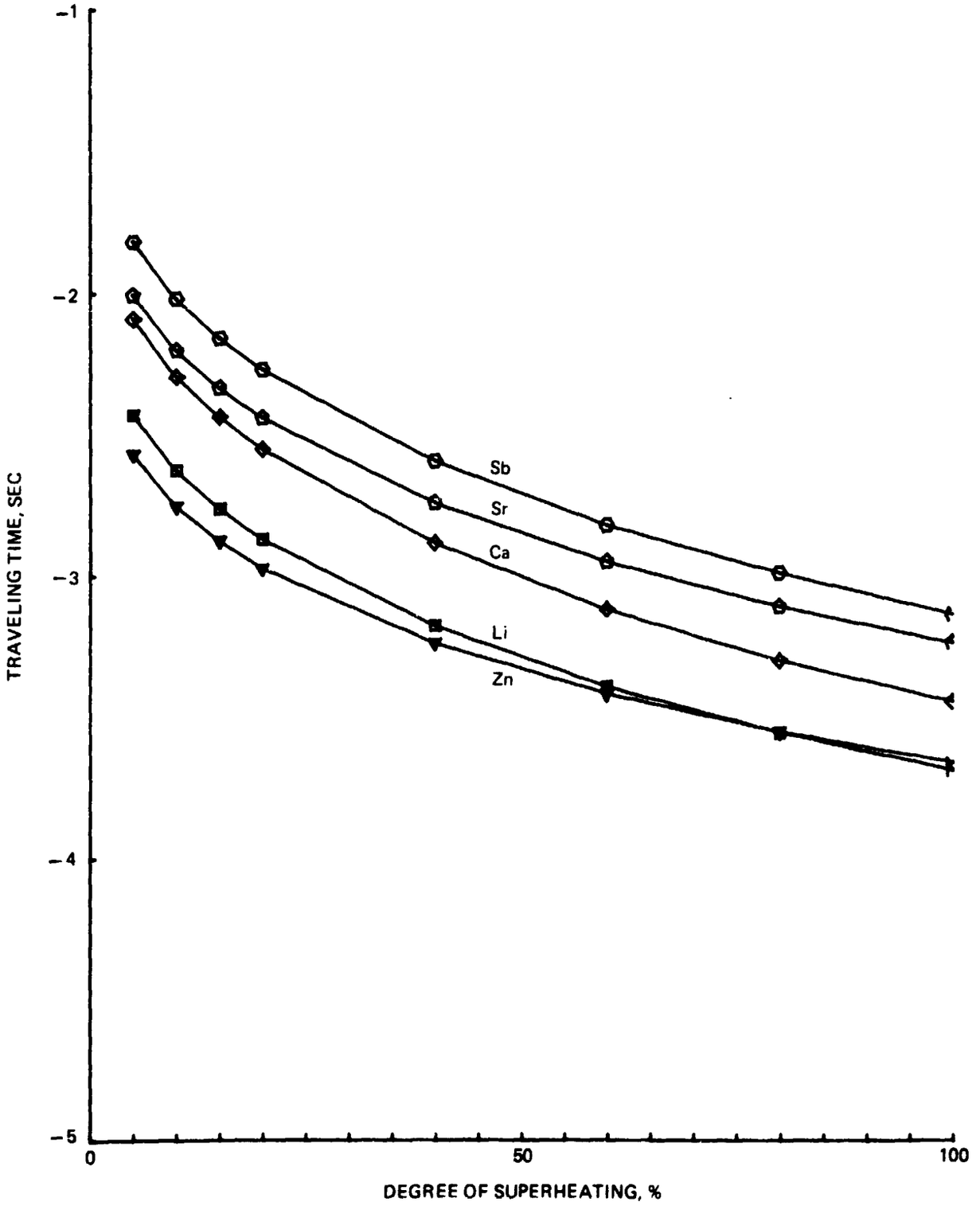

Fig. 1-25 Time to Travel 0.3m for 6×10^{-3} m Partially Superheated Nickel Sphere with Surface Layer of Highly Volatile Element Due to Differential Evaporation and Jetting (Sheet 1 of 2)

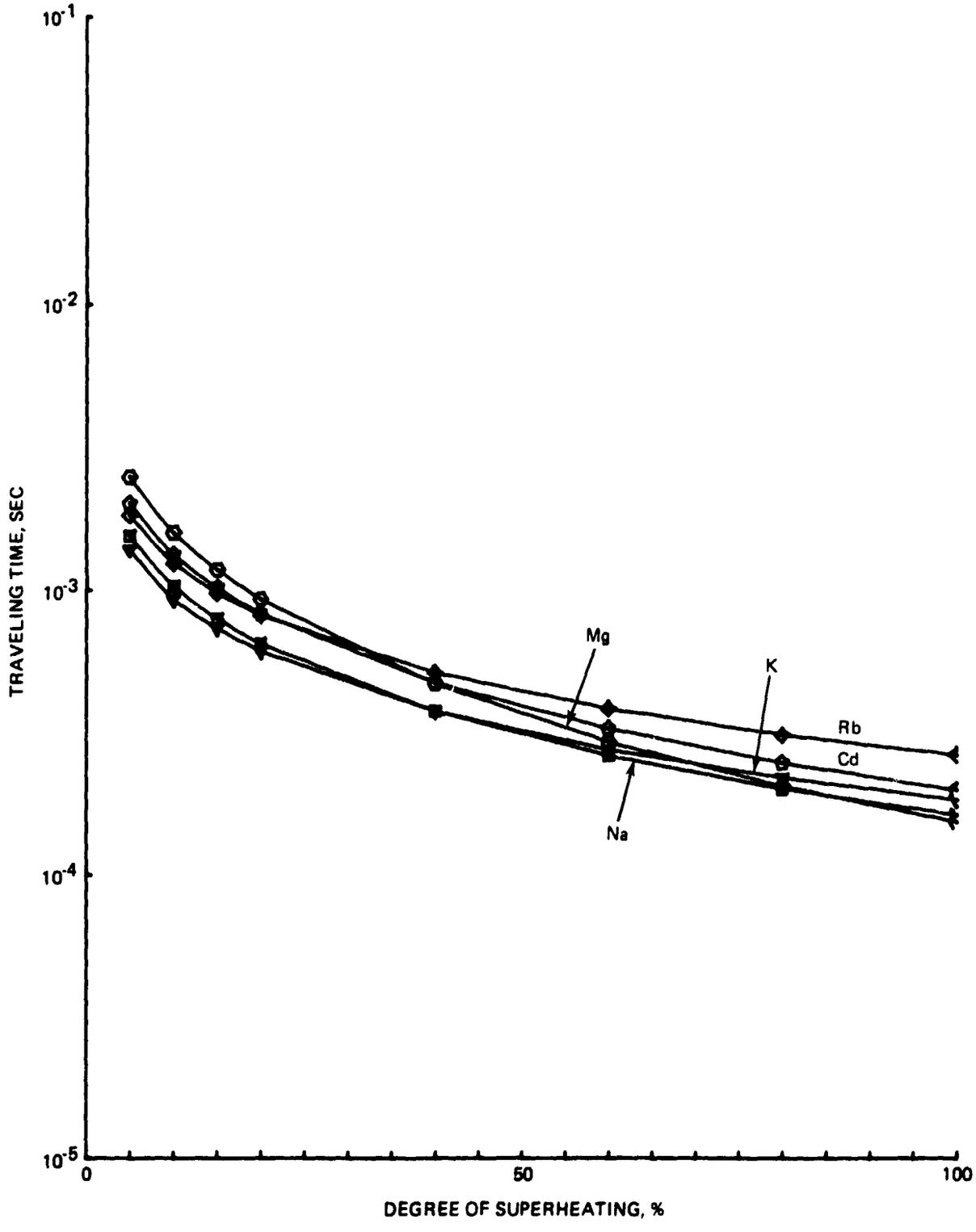

Fig. 1-25 Time to Travel 0.3m for 6×10^{-3} m Partially Superheated Nickel Sphere with Surface Layer of Highly Volatile Element Due to Differential Evaporation and Jetting (Sheet 2 of 2)

3.4 FLUID DISTURBANCES DUE TO JETTING FROM DIFFERENTIAL EVAPORATION

Two of the great advantages of manufacturing in space are zero-gravity conditions and the complete absence of convection currents due to the earth's gravity. With the absence of all convection currents, localized fluid disturbances, temperature differences, concentration variations, and complex heat and mass transfer conditions do not exist. Solidification can, therefore, be more easily controlled, and defect-free crystals are then readily obtained.

However, even in zero gravity, localized or interfacial fluid flow, movement, instability, or other disturbance can still occur due to surface tension gradients resulting from temperature or concentration gradients. This phenomenon, generally called the Marangoni effect or instability (Bikerman 1958, Scriven & Sterling 1960, Sterling & Scriven 1959) manifests itself in such forms as "interfacial engine", instability, twitching, cellular motion, Benard's cells, and tear drop in a wine glass.

Another type of fluid disturbance not previously reported may result from jetting or rocket action due to differential evaporation as described above. A nonuniformly heated liquid drop in space will be non-spherical because both surface tension and jetting action are strongly dependent on temperature. At equilibrium, the internal pressure of the drop is, of course, constant. The varying jetting pressure therefore appears as a variation in the curvature of the drop so that the algebraic sum of the jetting pressure and the internal pressure due to surface tension is constant. Since the jetting pressure and surface tension vary according to entirely different functions of the drop temperature, such constancy can be maintained for only a selected point or ring on the drop surface. The overall shape of the liquid drop must, therefore, be non-spherical.

Under gravity or the equivalent, jetting action may show up as local variations in the fluid level. Figure 1-26(a) shows the heating characteristics of a liquid in a container. The instantaneous profiles for the temperature, evaporation rate, jetting pressure, surface tension, and surface curvature are shown. For a liquid being heated in a container, the sides are at higher temperatures and, hence, have higher evaporating rates and jetting pressure, but generally lower surface tension than the center region.

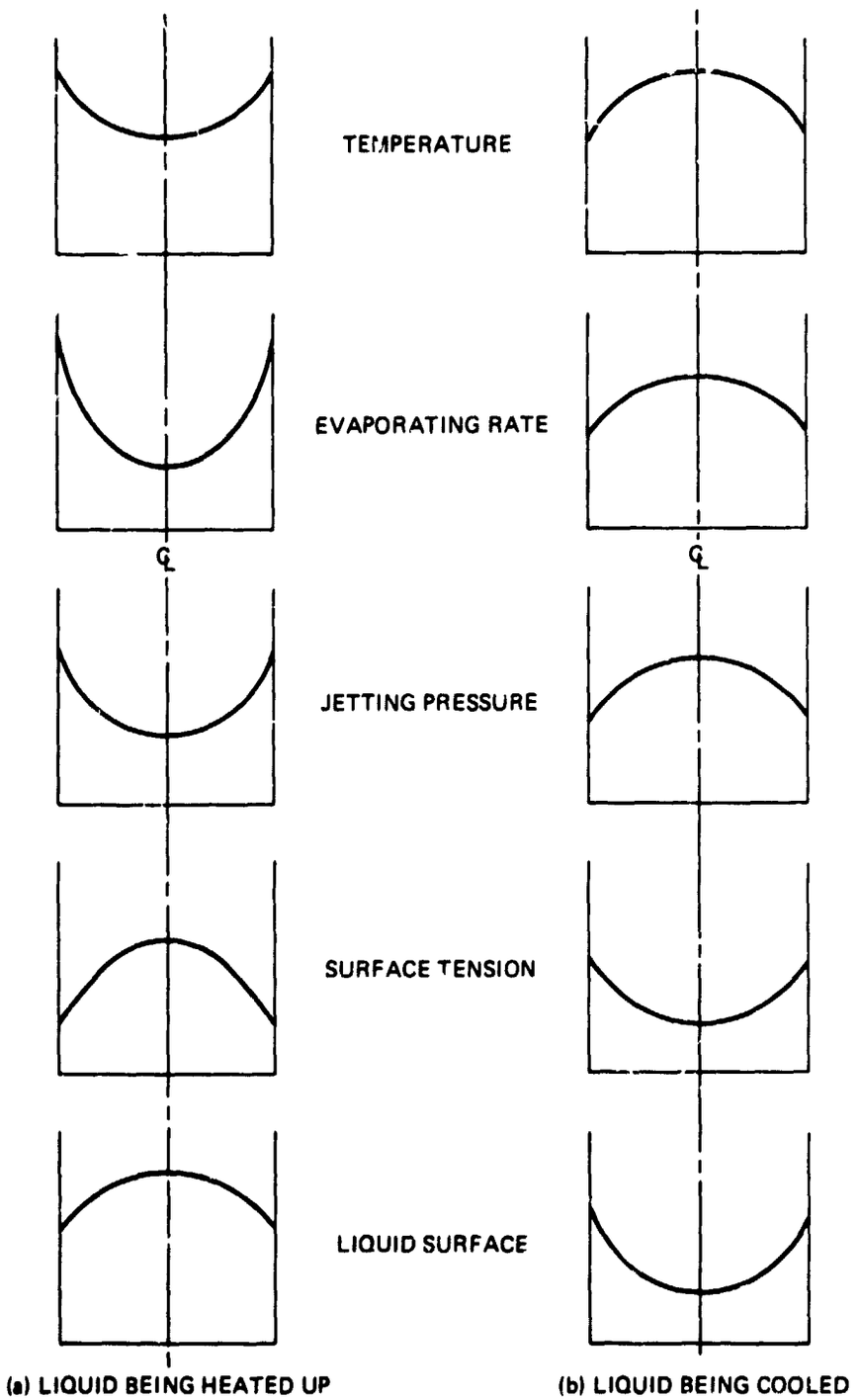

Fig. 1-26 Heating or Cooling Characteristics of Liquid in a Container Under some True or Equivalent Gravity.

The liquid surface must therefore convex upward if the jetting pressure is large. Large jetting pressures are often possible, as shown previously. Note that the effect of lowering surface tension with temperature partly compensates for that of the jetting action; the liquid surface is more planar than if surface tension were absent. Similarly, Fig. 1-26(b) shows the cooling characteristics of the same liquid in the same container.

Jetting action may also introduce a new type of powerful convection current. The surface of liquid drop is usually not clean. Certain spots or regions S on the surface may be contaminated with slow-evaporating material (Fig. 1-27(a)). These spots or regions may be oxidized into relatively non-evaporating oxides. Even under uniform heating conditions, such a drop may be evaporating nonuniformly over its surface. Localized, differential evaporation or jetting forces may then develop to supply the necessary mechanical energy for initiating or maintaining convection currents, as shown in the Figure.

Figure 1-27(b) shows a similar, uniformly heated liquid drop that is surface-contaminated with highly-evaporative material at certain spots or regions S, resulting in higher jetting pressures p_s at S compared to neighboring regions. Such differential jetting forces may, again, initiate powerful convection currents. It has been shown by Prof. Reid of MIT (1971) that even a few atomic layers of selected materials can increase the local evaporating rates by orders of magnitudes for sustained periods of time.

Note that these convection currents, resulting from differential evaporation, are completely different in origin and characteristics from those induced by differential surface tension (Marangoni effect). In fact, the two types of convection currents often have counteracting effects, one tending to compensate for or cancel the other. Also, they differ from gravitational convection currents. Gravitational convection currents are generally very massive, extending deep into the body of the liquid. Convection currents due to differential surface tension, on the other hand, are by nature surface limited. The new convection currents induced by jetting due to differential evaporation extend to a degree intermediate between the other two types of convection currents. Solidification behavior predictions of a specified system based on results on one type of convection current may, therefore, not be valid when applied to other types of convection currents.

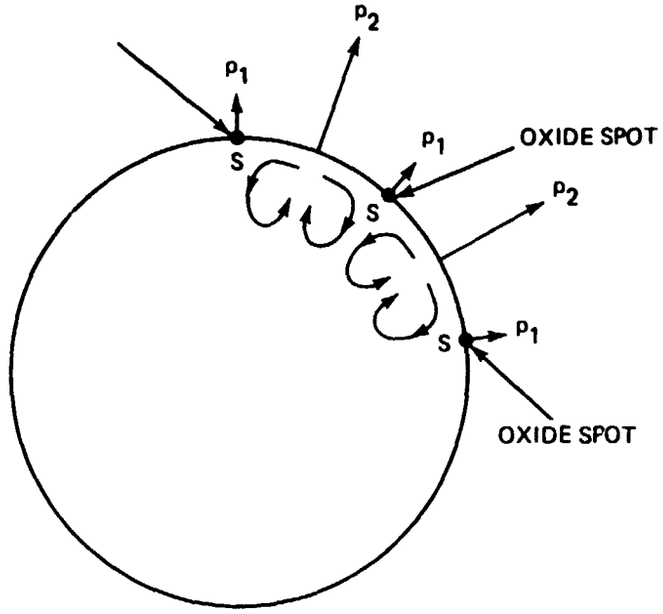

(a) LOCALIZED OXIDE CONTAMINATION

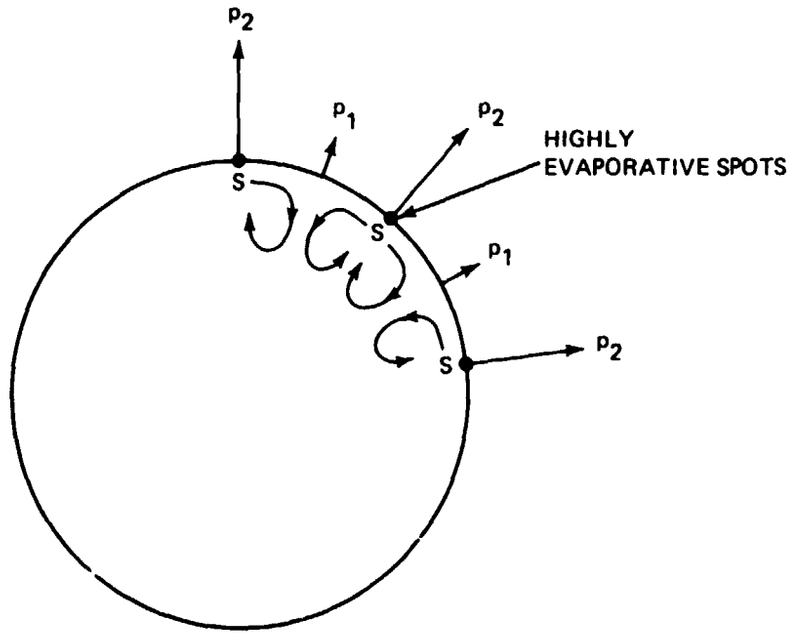

(b) LOCALIZED CONTAMINATION BY HIGHLY VOLATILE MATERIALS

Fig. 1-27 Convection Currents Induced by Differential Evaporation and Jetting

Section 4. EQUI-EVAPORATIVE TEMPERATURES AND THEIR APPLICATIONS

The normal evaporation techniques presented above give results accurate within an order of magnitude of the correct values, at least for the several systems studied. More refined methods, including those accounting for the limited liquid diffusion in the evaporating source, should be considered, as evidenced by the great improvement in the predicted results in the purification of beryllium containing such highly evaporative solutes as Mg, Zn, and Na. During evaporation, not only the solute concentration, but also the shape, size, and evaporating area of the evaporating source may be constantly changing. Figure 1-1 clearly shows the normal evaporation behavior of a 6×10^{-3} m sphere containing 8 weight percent of aluminum in nickel.

In the most general case, we consider steady-state and transient-state evaporation with constant changes in solute concentration, shape, and size of the evaporating source. The liquid diffusion is usually far from complete, and Raoult's Law of ideal solution may not be valid. Not only mass diffusion, but also heat transfer, fluid dynamics, and other related phenomena must be dealt with.

4.1 EQUI-EVAPORATIVE TEMPERATURES IN ALLOY SYSTEMS

The evaporation of alloy samples likely to be met in space processing (zone melting, crystal growth, thin film formation or, in general, controlled solidification and heat treatment) is complicated. Fortunately, for a given solvent and solute there exists a unique equi-evaporative temperature at which the solvent and solute are equally evaporative, i.e., U = V. Hence, at this unique temperature the alloy remains constant in composition, independent of the initial solute concentration and sample shape or size. This temperature, which can be computed from Eq (21), may be non-existent because it is negative or it may be too high or too low to be practical.

However, for many binary or even ternary alloy systems, the equi-evaporative temperatures do exist and are practical. A computer search has been conducted among the 2550 binary combinations (i.e., 51 solvents x 50 solutes) and of 62,475 (i.e., 51 solvents x 50 x 49/2 first and second solutes) ternary combinations, of the 51 metallic elements listed in Table 1-1. By "practical" we mean that the equi-evaporative

temperature is no higher than 200% of the absolute melting point of the solvent. At each such equi-evaporative temperature, the relevant binary phase diagram in Hansen (1958) was consulted to determine the range of solute concentrations for which the alloy is in liquid form.

The results of these computer searches are summarized in Tables 1-8, 1-9, and 1-10. Table 1-8 gives the equi-evaporative temperatures for binary alloy systems containing liquid phases. Table 1-9 lists the same temperatures, but for other binary alloy systems which either contain no liquid phases at these unique temperatures or have ill-defined phase diagrams according to Hansen (1958). Table 1-10 gives the equi-evaporative temperatures for ternary alloy systems. With the exception of alloys of carbon, which generally have ill-defined phase diagrams, all other alloys having practical equi-evaporative temperatures are listed in these tables.

Consider, for example, Table 1-8. The Ag-Ga system has a equi-evaporative temperature of 1245.8K or 972.7^{o}C. This unique temperature is 101% of the absolute melting point of Ag (1233.9 K) but over 411% of the absolute melting point of Ga (302.9 K or 29.81^{o}C. Hence, Ag alloys containing Ga having a "practical" equi-evaporative temperature of 1246K are listed in Table 1-8; but Ga alloys containing Ag have an "impractically" high equi-evaporative temperature (also at 1246K) and are not listed.

TABLE 1-8 EQUI-EVAPORATIVE TEMPERATURES FOR TWO-COMPONENT SYSTEMS CONTAINING LIQUID PHASES

Solvent	Melting Point, K	Solute Ts°, C	% Melting Point	Liquid Concentration Range	Page No. in Hansen's
Ag	960.8	Ga 1246	101	0-1.00	
Al	660.0	Sn 868.7	94	> .26	135
		Be 1257	124	< .13	73
Au	1063.	Ce 1310	99	.03-.16, .30-.32, .37-.38, > .72	194
		Cr 1807	136	< .89	196
Be	1284.0	Al 1157	75	>.87	73
Cd	321.0	Na 464.3	79	> .95	429
		K 1180	199	0-1.00	422
Mn	1244	In 1178	78	< .56	850
Na	97.8	Cd 464	126	< .05	429
Sn	231.9	Al 868.7	173	> .26	135

TABLE 1-9 EQUI-EVAPORATIVE TEMPERATURES FOR OTHER TWO-COMPONENT SYSTEMS

Solvent	Melting Point, K	Solute and TsK
Au	1336	Sc 2670
B	2573	La 4333; Rh 3069; Pt 2003; Th 970.7; V 2933
Ba	983.1	Tl 704.8
Be	1557	Ga 2519; In 2994; Sn 946.8
Ca	1116	Sb_2 671.3; Sr 1633
Cb	2741	Mo 3489; Os 3634; Zr 4980
Cd	594.1	Cs 1139; Rb 1179
Ce	1077	Au 1310; Cu 1940; Ge 1097; Sc 985.0; Sn 1852
Co	1765	Au 3293; Ge 2975; Pd 1335; Si 1050; Sn 3164
Cr	2173	Al 4030; Au 1807; Cu 2951; Ga 3865; Ge 1513; In 3996; Pb 4166; Sc 1477; Sn 2291
Fe	1809	Au 2902; Ge 2465; Ni 3309; Pd 324.8; Sc 3091; Si 3099; Sn 2959
Ge	1210	Ce 1097; Cr 1513; Sc 1617
Ir	2716	Mo 297.1; Ru 4513; Th 4722; U 5188; Zr 1678
La	1193	Si 306.7; Ti 2104; Y 1208
Li	453.1	Sr 288.9
Mg	923.1	Cs 1834
Mn	1517	Pb 2430
Mo	2893	Cb 3489; IR 297.1; Os 3414; Ru 1596
Ni	1726	Au 3110; Fe 3309; Ge 2798; Pd 1137; Sc 3178; Si 2614; Sn 3111
Os	3318	Cb 3634; Mo 3414; Zr 6125
Pd	1825	Co 1335; Fe 324.7; Ni 1137; Si 10470; Y 3277
Pt	2042	B 2003; Ru 801.5; U 4038
Rh	2233	B 3069; Pt 801.5; U 2878
Ru	2583	Ir 4513; Mo 1596; Th 4619; V 5005; Zr 3085
Sb	903.6	Ca 671.3
Sc	1811	Au 2670; Ce 985.0; Cr 1477; Fe 3091; Ge 1617; Ni 3178; Si 3095; Sn 2912
Si	1685	Au 2969; Co 1010; Fe 3099; Ge 2689; La 306.7; Ni 2614; Pd 1293; Sc 2095; Sn 2987
Sn	505.0	Be 946.8
Sr	1043	Ca 1633; Li 288.9
Th	2027	B 970.7
Ti	1940	La 2104
Tl	576.1	Ba 704.8
U	1403	V 1328
V	2193	La 2885; Pd 4143; U 1328
Y	1793	La 1208; Pd 3277
Zr	2133	Ir 1678; Ru 3084

TABLE 1-10 EQUI-EVAPORATIVE TEMPERATURES FOR THREE-COMPONENT SYSTEMS

Solvent	Melting Point, K	Solute	Ts, K	Liquid Concentration Range
Cd	321.0	K	1180	0-1.00
		Rb	1179	
Si	1412.0	Sc	3095	
		Fe	3099	
Ni	1453.0	Au	3010	
		Sn	3011	

4.2 SIGNIFICANCE OF THE EQUI-EVAPORATIVE TEMPERATURE

The binary or ternary alloy systems presented in Tables 1-8 through 1-10 are ideal, at their respective unique temperatures, for the study of heat transfer, sphere detachment, deformation and oscillation, bubble formation and movement inside the liquid, and the like, since their solute concentration is constant regardless of the initial concentration and sample shape or size. In addition, by changing the initial solute concentration we can isolate and study the effect on these phenomena of such concentration-related properties as surface tension. In all such experiments, the solute concentration will remain constant throughout the entire sample during the experiment. There is no concentration nonuniformity and no surface concentration gradient. The initial, boundary, intermediate, and final conditions of the sample composition are completely defined, known, and stable.

At these unique temperatures, we can accurately determine the equilibrium liquid and solid solute concentrations for use, for example, as reference points on conventional phase diagrams. These solute concentrations can be obtained with an accuracy completely independent of the sample shape and size, and even independent of the heating rate if the sample is equilibrated at the equi-evaporative temperature. The

resultant sample will display a sharp solid-liquid interface. There will be a completely uniform liquid composition, and a completely uniform but different composition in the solid. No concentration gradients exist in either the liquid or the solid. Any portion, large or small, of the liquid or solid is perfectly representative of the same phase and resolution of the analytic instrument or technique becomes immaterial. We can, therefore, determine these concentrations by Auger, electron probing, spectroanalysis, chemical analysis, etc., with almost the same precision. This is true even if the alloy contains one or more highly volatile components. The segregation coefficient k at this unique temperature can, therefore, also be accurately determined.

We can also propose the following unique, isothermal solidification experiment. A liquid alloy sphere containing 0.75 mole fraction of tin in aluminum is evaporated at slightly below the equi-evaporative temperature, say at 863K. The solvent aluminum now evaporates more slowly than solute tin. This condition results in a solute enrichment in the remaining liquid. Upon reaching 0.74 mole fraction of tin, the alloy solidifies according to the phase diagram. The solidification proceeds from the surface, but remains at the constant temperature of 863K. The evaporating time can be calculated by means of our normal evaporation equations presented in a previous section of this report, after the shape and size of the evaporating sphere are specified. By controlling the evaporation temperature one can control the rate of solute enrichment which, together with mass diffusion constraints, allows us to control the rate of solidification. When the evaporation or isothermal solidification temperature is very close to the equi-evaporative temperature of 868.7K, one gets a true picture of solute segregation due to solidification rather than the combined effects of solidification and unknown amount of evaporation, as is almost always the case in current studies. Further, in space, where surface tension is important but gravitational convection is negligible, one can start with a homogeneous sphere and freeze it isothermally from the spherical surface at a rate so slow that unique cellular and granular structures can be obtained. In addition, one can locally control the temperature of the molten sphere by means of a heated or cooled sting, or by means of concentrated electron or optical energy, so as to initiate single crystal growth in the manner of Walter and Snyder (1971).

Section 5. CONSTITUTIONAL MELTING AND SOLIDIFICATION DUE TO EVAPORATION

Consider aluminum and tin. Al melts at 933.3K and Sn at 505.0K (see Table 1-1). This binary system has a equi-evaporative temperature of 868.7K (Table 1-8), which lies between the melting points of the two components. At this unique temperature T_s (line AB in Fig. 1-28), both elements are evaporating at exactly the same rate and no compositional change takes place. At a temperature $T > T_s$, Al evaporates faster than Sn, and (surface) depletion of Al and enrichment of Sn occur. At a $T < T_s$, the reverse is true and Al enrichment and Sn depletion occur.

According to the Al-Sn phase diagram (Hansen 1958), the binary alloy is liquid if it contains more than 0.36 mole fraction of Sn at T_s (point D). Let us select a liquid composition below line AB and somewhat to the right of point D, e.g., 0.265 mole fraction of Sn at 868.1K (point G). Since at 868.1K Al is evaporating slower than Sn, the alloy composition will constantly increase in Al, and must move isothermally toward the left or Al-rich side. Upon reaching the liquidus on the Al-rich side of the phase diagram, i.e., point H, the alloy solidifies, first on the surface but progressively toward the center of the sample because of mass diffusion. We thus achieve a new isothermal solidification of non-eutectic, binary alloy, because of surface constitutional or compositional changes through evaporation. Note that isothermal solidification of alloys (not pure metals) can only occur at the eutectic temperature. Our constitutional solidification experiment, is, however, not limited to the eutectic composition.

If point G is sufficiently below line AB, we can heat up the molten sample G below the line AB to achieve Al enrichment and, hence, solidification on heating.

Similarly, the solid composition M can be constitutionally melted at a constant temperature (along line MN) or at a decreasing temperature (along line MP).

All four constitutional phase change phenomena, i.e., isothermal melting (path 1), melting on cooling (path 2), isothermal solidification (path 3), and solidification on heating (path 4), of non-eutectic, binary (ternary, or other multi-component) alloy systems appear to have never been reported. Yet these phenomena may well occur in space experimentation. In fact, these "anomalies" may greatly confuse the experimenter

PATH 1 CONSTITUTIONAL MELTING AT CONSTANT TEMPERATURE
PATH 2 CONSTITUTIONAL MELTING ON DECREASING TEMPERATURE
PATH 3 CONSTITUTIONAL SOLIDIFICATION AT CONSTANT TEMPERATURE
PATH 4 CONSTITUTIONAL SOLIDIFICATION ON INCREASING TEMPERATURE

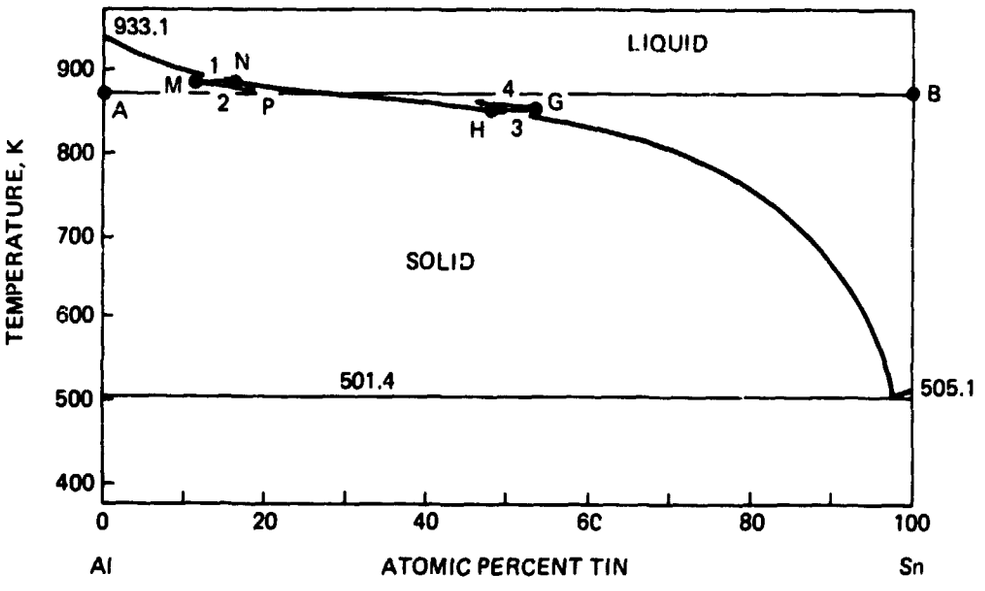

Fig. 1-28 Constitutional Melting and Solidification of Al-Sn Alloys

if an evaporation analysis is not first performed for the particular alloy system within the temperature range of the experiment.

For Au-Ce alloys, Table 1-8 gives equi-evaporative temperature as T_s = 1310K (line AB in Fig. 1-29), which is intermediate between the melting points of the two components. At a temperature $T < T_s$ Ce evaporates slower than Au, while at a temperature $T > T_s$ Ce evaporates faster than Au.

An interesting point about the Au-Ce system is that, at $T = T_s$, the alloy is liquid within the following several ranges of Ce atomic concentration: 0.03-0.16, 0.30-0.32, 0.37-0.38, and 0.72 (Hansen 1958).

An alloy starting at point F and isothermally heated at 1323K will be initially liquid. The alloy will, however, lose more Ce than Au at this temperature, and its composition will therefore move along line EF toward the Au-rich side. Solid crystals of CeAu will separate out on the surface when the composition reaches point G. Continued heating at the temperature of 1323K will cause more intensified surface depletion of Ce, i.e., the alloy composition will further shift toward the left, on the surface, through evaporative segregation, but inside the sample through solid and liquid diffusions. Eventually, the alloy will have four solid phases representing, in order, the compositions CeAu, $CeAu_2$, $CeAu_3$, and nearly pure Au. The compositions of the phase boundaries can be read off Fig. 1-29 at the intersection points of line EF with the several liquidus lines. If the sample is in the form of a freely suspended drop or sphere in space, it will have seven, alternately liquid and solid, concentric spherical shells. Such a structure is novel and unique, but may be used to determine solid and liquid diffusivities and phase boundaries. Since Au has a density of 19.3, compared to 6.75 of Ce, we may use this composite structure to study convection currents or other fluid movements due to gravity in spherical shell geometries.

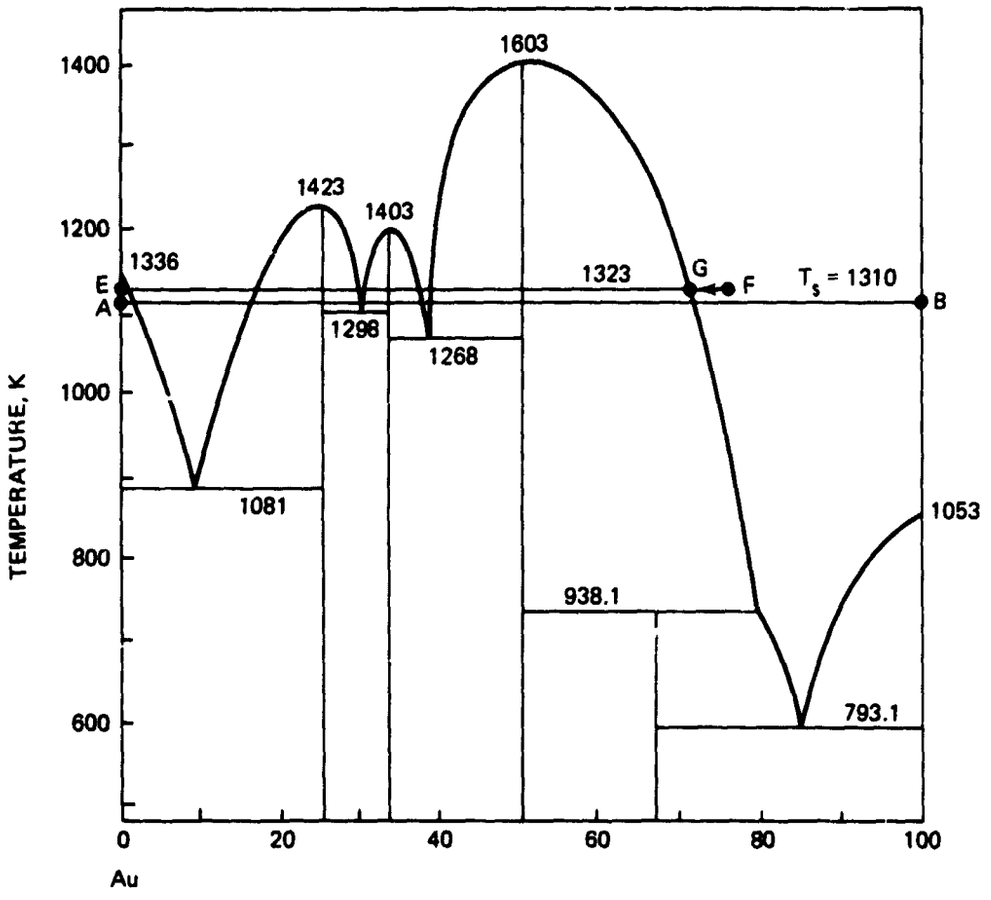

Fig. 1-29 Evaporation, Constitutional Melting, and Solidification Experiment on Au-Ce Alloys

Section 6. APPLICATIONS OF EVAPORATION TO SPACE MANUFACTURING

In summary, surface evaporation of materials has the following important applications or effects relative to space manufacturing of materials.

6.1 MATERIAL LOSSES

Data have been presented to show, for example, how the solute Al in a uniformly heated, 6.0×10^{-3}-m sphere containing 8 percent by weight of Al in Ni evaporates. The losses of material, mostly Al at, and the times to reach, various weight fractions and surface concentrations are given. The preferential evaporation of Al makes it difficult to control sample weight, size, and composition. The Al vapor coats the vacuum chamber walls and, more seriously, the nearby samples in the Skylab experiments. Worst of all, the electron beam source for heating these samples may be contaminated to the point of erratic electron emision and loss of control. As a result of these disadvantages, which were partly confirmed by actual simulation runs, the Al-Ni alloy was dropped as a sample material for the M512 experiment.

6.2 EVAPORATIVE PURIFICATION

Evaporative purification would benefit the following processes: floating zone melting; single crystal growth; thin film growth; and preparation of materials standards. As shown, we presented quantitative data on the purification of nickel alloys with aluminum as a solute. We further described, in some detail, the evaporative purification behaviors of nickel-iron and nickel-chromium alloys. The purification of beryllium containing nine impurities in the ppm range was separately treated. Three reports have been published on these data and the necessary predictive equations, and submitted for outside publication. A paper on evaporation prepared under the contract was also presented at the AACG at Princeton University in July, 1972.

Not fully appreciated, it appears, is the fact that evaporative purification is relative, in terms of speeds and results. It is also a two-edged sword. Thus, while with some elements evaporating faster than the solvent we have evaporative purification, with other elements evaporating slower than the solvent we have evaporative (surface) contamination or enrichment. A freely suspended molten drop in space may, for

example, have its surface solute concentration enriched a thousandfold or a millionfold by neglected and undetectable trace impurities within a fraction of a second of its deployment. From there on, evaporative purification may be completely negligible, for any practical length of time. Further, evaporative purification or (surface) contamination can be so fast as to be unavoidable, or so slow as to be practically non-existent.

6.3 "ANOMALOUS" MELTING AND SOLIDIFICATION

Because of evaporative segregation, anomalous "constitutional" or evaporative melting (on cooling) and solidification (on heating) can occur, as shown above. We have, therefore, pointed out that any solidification study, particularly on nucleation, must be preceded by an evaporation compatibility study. We have also suggested unique and definitive solidification experiments that circumvent or minimize the evaporation effects.

6.4 DIFFERENTIAL EVAPORATION AND JETTING ACTION

Different rates of evaporation at various surface regions, such as those resulting from nozzle detachment, temperature gradient, or surface contamination, give rise to unbalanced forces and momenta that may produce erratic or unwanted accelerations. Very large "equi-valent gravities" may be produced. Another effect of such jetting actions may be the formation of powerful convection currents with entirely new characteristics that can not be directly correlated with those of other convection currents.

6.5 SURFACE COOLING

Evaporation requires the absorption of the heat of evaporation. Surface cooling therefore results. For nickel at its melting point of 1726K, the evaporative surface cooling component is about four orders of magnitude smaller than the radiative cooling component and is, therefore, probably negligible. For low-melting materials, particularly those having high heat of evaporation, the evaporative cooling component may be very important. Work by Dr. Thomas T. Kassal of the Grumman Research Department with water or brine streams jetting into vacuum demonstrates the importance of surface cooling in ice formation.

6.6 MATERIALS STANDARDS

Properly controlled evaporation, particularly in space, allows us to obtain material purity or evaporation standards, thermal properties, and even basic thermodynamic constants.

PART II

FREEZING SEGREGATION

This section on freezing segregation represents, in part, a review paper the principal investigator has been asked to prepare for inclusion in "Advances in Materials Science." While this work was not done under NASA support, it is included for the sake of completeness and because of its relevancy.

Section 1. INTRODUCTION

In this section, we will discuss the normal freezing process, and its application to steady-state solidification in the Ni-Sn system.

In the first part of this section, the normal freezing process is described in some detail. The assumptions, its industrial application and importance, the normal freezing differential equation and its solution for the various cases are given. The meaning of the segregation coefficient k is then discussed. The best value of k and the errors involved in assuming constant k for various cases are studied. Finally, numerical computation of the normal freezing process is exemplified.

The formation of spirals or screw dislocations and other defects has always received great attention because these defects make all materials very weak compared to their theoretical potentials. During this contract, new spiral growth observations on barium st ıtium niobates grown under controlled conditions were made. These observations cannot be explained by the classical core-first growth theory (or BCF model) A new mechanism was therefore developed to explain them. We believe that knowledge of the formation mechanism of these and other defects will enable us to control or eliminate them in space manufacturing and other operations. Details of this new mechanism is given in Appendix F.

Steady-state solidification is related to the important process of single crystal growth. In particular, the critical temperature gradient must be accurately determined in order to achieve interfacial planarity and single crystal growth. We used a non-constant k approach to study the steady-state growth of Ni-Sn alloys. Our results show that assuming constant k may introduce intolerable errors in predicting solidification behavior in general and single crystal growth in particular.

Section 2. THE NORMAL FREEZING PROCESS

In normal freezing, we assume that the liquid is completely mixed, that no atomic diffusion occurs in the solid, and that the compositions of the freezing solid and liquid, respectively, follow the solidus and liquidus curves of the constitutional diagram.

Since the liquid is completely mixed, there is, effectively, infinite diffusion in the liquid. The liquid is, therefore, always homogeneous. Solute pile-up in front of the liquid-solid interface is not possible and solute concentration at this interface is, therefore, the minimum possible. The equilibrium solute concentration in the freezing solid is also minimal. Thus, the interface acts as if it were an efficient atomic filter, allowing pure solvent atoms to freeze out together with the minimum amount of solute atoms while keeping the maximum amount of solute atoms in the remaining liquid (for the case where the segregation coefficient is less than 1). Thus, normal freezing is the most efficient purifying or segregating process, as far as separating solute and solvent atoms in the liquid (according to the constitutional diagram) is concerned.

In contrast to infinite liquid diffusion, the solid diffusion is zero during normal freezing. Thus, all the (solvent and solute) atoms stay exactly where they first freeze and remain completely and forever immobilized. Justifications of these assumptions, as well as additional comments and implications, will be more fully described.

Normal freezing is a useful and important ideal limiting case, as is infinitely rapid quench or splat cooling. In the rapid freezing process, time is not allowed for any solid and liquid diffusion, or even equilibration, according to the constitutional diagram. The effective solid and liquid diffusion constants are thus zero. The solute and solvent atoms are instantly frozen, in situ, from the melt; and the constitutional diagram is completely

irrelevant. There is also no solvent purification or solute segregation. In practice, when the characteristics distance d_c, defined as the liquid diffusion constant D_1 divided by the growth rate v, falls appreciably under the resolution limit of the detecting instrument, the frozen material appears to be homogeneous and the freezing process is practically identical to that of an infinitely rapid quench. Since D_1 is generally about 10^{-4} cm^2/sec, a growth rate greater than 10 cm/sec from a severe quench yields a characteristic distance of $d_c = D_1/Kv = 1\,\mu m$. Such a frozen material would thus appear homogeneous under the electron microprobe, which has a resolution of about $1\,\mu m$.

Another useful and limiting freezing process is equilibrium freezing according to the level rule. Here, both the liquid and solid are homogeneous, and the liquid-solid interface is perfectly permeable to the solute and solvent atoms. At all times, the liquid and solid are in equilibrium according to the constitutional diagram, and unique, "equilibrium segregation" results obtained.

Any actual freezing results must fall within these maximum segregation, no segregation, and equilibrium segregation limits. For some alloys systems, the limits between maximum and equilibrium segregation results may be only a few percent apart (Li, 1966). Further, the relative proximity of practical freezing results to either of these limits can often be at least qualitatively predicted by a study of the freezing conditions.

Among the three methods, normal freezing is generally the most important since it gives the maximum solvent purification or solute segregation, the purest possible single crystals, and the most defect-free devices or structures since many defects are often associated with segregated impurities. Also, it is particularly valuable in the preparation of many material specifications which call for precisely these limiting case conditions and require the maximum initial solute content, the maximum defect size of a given type, the maximum grain boundary thickness for grains of a given size, and the like.

Normal freezing often does not represent the true freezing conditions. This is particularly true in dendritic growth when the growth velocity is high and solid diffusion is negligible (normal freezing assumption 2) but liquid diffusion is not complete (normal freezing assumption 1). With single crystal growth, the growth speed is often orders of

magnitude lower, solid diffusion is still negligible, and the liquid diffusion conditions are more nearly normal. In addition, if the melt is mechanically or induction stirred, the melt may be indeed nearly homogeneous and normal freezing conditions are realized.

Even a lack of normality does not detract from the usefulness of the normal freezing methodology. This is partly because actual freezing conditions are more or less normal. The departure from normality can be predicted and actually evaluated, as will be shown. Further, normal freezing gives limiting results which are useful for writing materials specifications. As will be shown, normal freezing conditions give, at each step during the freezing process, the maximum crystal purity possible (for the usual case where $k < 1$). Thus, normal freezing calculations allow us to prescribe the maximum initial impurity concentration to achieve a given minimum degree of purity in the final product, a given thickness of grain or cell boundary thickness, or even given mechanical properties such as creep and ductile-to-brittle transition temperature. In addition, abnormal conditions such as limited liquid diffusion and loss of materials through surface evaporation or chemical reaction can be accounted for, as will be shown.

2.1 NORMAL FREEZING AS USED IN THE SEMICONDUCTOR INDUSTRY

Normal freezing techniques has been successfully used in the semiconductor industry and are indispensible in such areas as material purification, single crystal growth, dopant control, diode formation, and liquid epitaxy. Here, the conditions discussed below are most favorable for the use of these techniques.

The most common germanium and silicon materials are very pure. They generally contain only ppm or ppb of impurities and are, therefore, orders of magnitude purer than most other pure materials. We are thus dealing with extremely dilute, simple or ideal solutions.

There is a critical need for control, at microscopic distances, of absolute depant levels to ppm ($\sim 10^{18}$/cc) or ppb ($\sim 10^{15}$/cc). Even the dopant concentration gradients at these extremely low concentration levels and small distances are critical. In fact, even ppb of wanted or unwanted impurities can radically change the characteristics of the resultant semiconductor devices.

Only a portion, often a small portion, of the solidified material is used; and the solidification range of interest is often exceedingly narrow. In the growth of single crystal of pure germanium containing 100 ppm of antimony in the melt, for example, the growth starts at 1209.10K or 935.98°C ($k_{1209.10K} = 0.276$), and ends at 1208.12K or 935°C ($k_{1208.12K} = 0.276$), and over 98.0% of the melt by weight (representing more than the material of interest) is grown (Li, 1966). The liquidus and solidus curves of interest can be represented by two tiny straight lines extending over solute concentration ranges of only 4,660 and 130 ppm, respectively, over a temperature interval of 1°K. The segregation is constant at 0.276 to within the third decimal place. Again, in the growth of a germanium alloy diode with a 50-micron indium sphere, only the first 0.1-micron linear distance (representing less than 0.5% by weight solidified) is critical in the formation of the pn junction (Li, 1966). Here, the useful solidified portion is extremely small, as is the solidification temperature range of interest. The segregation constant k is, therefore, again constant. Pfann's constant-k, normal freezing equation (Pfann, 1952) thus finds its ideal application.

Most germanium and silicon alloys have extremely low solute, solubility limits in the solid. According to the constitutional diagrams (Hansen, 1958), germanium alloys containing Ag, Al, Au, Cd, Co, Cu, Fe, In, Mg, Mn, Ni, Pb, Sn, Te, Tl, and Zn, and silicon alloys containing Ag, Al, As, Au, Ca, Ce, Co, Cr, Cu, Fe, In, Mg, Mn, Nb, Ni, Pd, Pt, Sb, Sn, Ti, and Zr, have invisible solidus lines. Only germanium alloys containing As, Bi, Ga, and Sb, and silicon alloys containing U, have some visible solidus lines that are very close to the vertical temperature axes.

The segregation coefficients for the above germanium and silicon alloys are very small, being close to zero. Also, the solute material frozen in the solid is negligible, and does not appreciably affect the fraction solidified. It is therefore possible to consider multiple, non-interacting dopants in the same crystal for the determination of the pn junction depth. Extending this approach indiscriminately would be misleading or meaningless. Unfortunately, this has been done.

2.2 EXAMPLES OF CONSTITUTIONAL DIAGRAMS

Figure 2-1 shows several common types of constitutional diagrams that we deal with in solidification studies. Figure 2-1(a) represents a simple eutectic system typified by the Pb-Sn alloys. Here, solid α or Pb crystals are shown to have different concentrations of Sn, reaching their maximum Sn concentration of c_{su} at the eutectic temperature of 456.1K (183^{o}C) as described by the left, or Pb-rich, solidus line. Similarly, solid β or Sn crystals also have different concentrations of Pb, also reaching their maximum Sn concentration of c_{su} at the eutectic temperature, as represented by the right or Sn-rich solidus line. At each melt temperature, the α or β crystals are in equilibrium with only one single melt composition, as determined by the appropriate liquidus line.

Figure 2-1(a) also shows that the four liquidus and solidus lines are far from being straight lines. The liquidus and solidus of the Sn-rich alloys may be approximately represented by quadratic functions of the melt temperature. The liquidus and solidus of the Pb-rich alloys, on the other hand, would probably be more adequately fitted with cubic equations of the melt temperature. The exact degree of such fits should, however, be determined objectively by statistical tests (Anderson and Bancroft 1952).

Figure 2-1(b) shows the complete constitutional diagram for the Au-Ag system. In this system, the Au and Ag are completely miscible, both in the solid and liquid phases. Hence, there is only a single liquidus and a single solidus for the entire system, instead of the two liquidus and solidus lines shown in Fig. 2-1(a). It is immaterial whether we consider Au or Ag as the solvent. It is even arbitrary or artificial to consider the major constituent as the solvent and the minor constituent as the solute, since such a designation depends on whether weight percentages or atomic percentages are used as the classifying criterion. Thus, an alloy containing between 50 to 67 weight percent of Au would be considered as an alloy of Ag in Au if weight percentages are used and, yet, should be considered as an alloy of Au in Ag if atomic percentages are used as the classifying criterion. In many other systems, such as W-C, Ta-C, and W-B, this disparity is even wider and the designation of one component as the solvent or solute is even less meaningful. It would, therefore, be better to identify an alloy of, e.g., 10% of Ag in Au simply as such; or, interchangeably, as an alloy of 90% of Au in Ag.

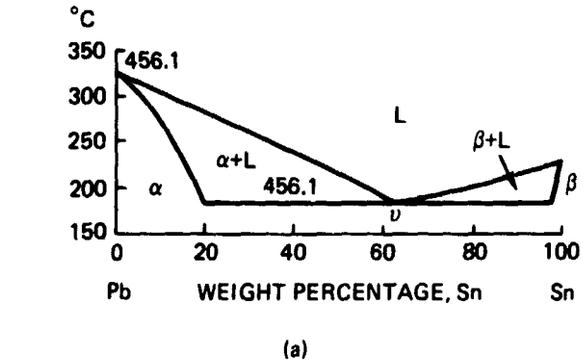

(a)

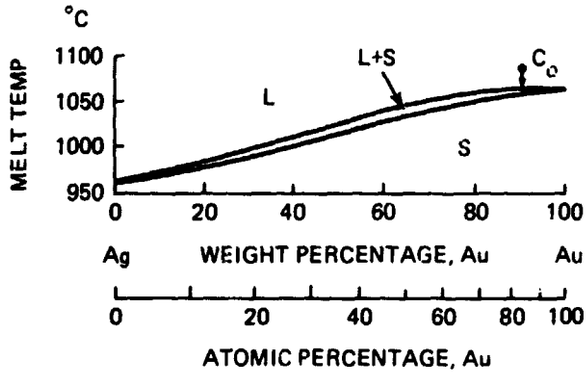

(b)

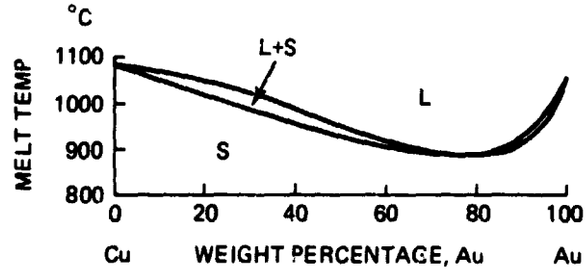

(c)

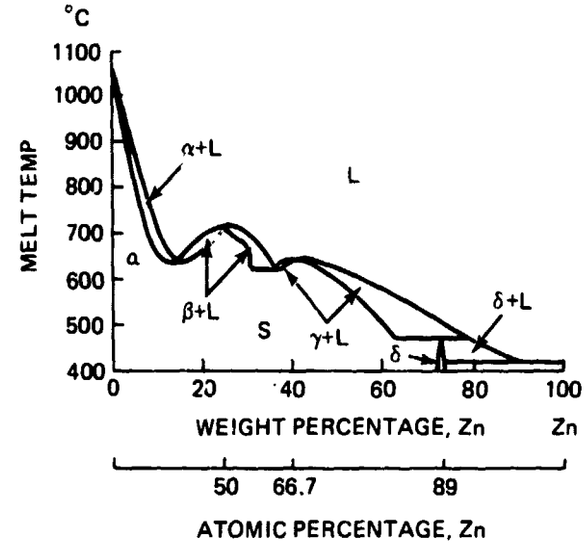

(d)

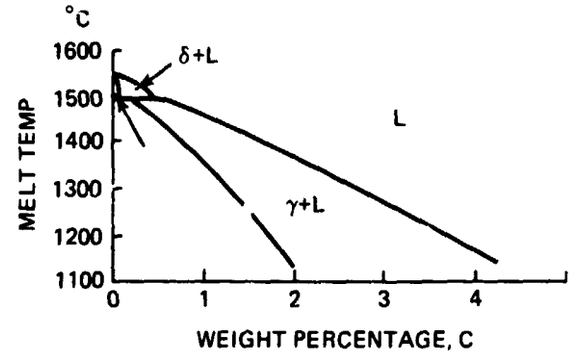

(e)

Fig. 2-1 Some Types of Constitutional Diagrams

A good system of solidification methodology, in particular the normal freezing equation, should be a self-consistent one. It will be shown using this Au-Ag diagram and several other considerations that the constant-k method is not such a system.

Figure 2-1(c) shows the Cu-Au constitutional diagram. This system is characterized by having very large solid solubilities at either terminal region.

Figure 2-1(d) shows the Au-Zn constitutional diagram, revealing the presence of a number of intermetallic compounds, i.e., AuZn, $AuZn_2$, and $AuZn_8$. Further, at the compositions of the first two compounds, the liquidus and solidus reach their peak temperatures. In many such systems involving intermetallic compound formations, the liquidus lines, and even the solidus lines, have horizontal tangents ($k = \infty/\infty$ = indefinite) at their peak temperatures at the most important compositions. This condition has important implications in the determination of the segregation coefficients k, as will be described.

Figure 2-1(e) shows a portion of the Fe-C diagram. An interesting feature is that a peritectic reaction occurs at a T_r of about 1765K (or 1492°C). At this temperature, the solidification process is discontinuous. A small portion of the Fe-C system has two distinct liquidus and two distinct solidus lines, one set above and one set below T_r. The slopes of the two liquidus lines are discontinuous at T_r. Not only are the slopes of the two solidus lines discontinuous, but even the values of the solute concentrations in the solid, i.e., c_s, are discontinuous. Specifically, c_s changes abruptly from 0.10% at slightly above T_r to 0.18% at slightly below T_r. The study of solidification of Fe-C alloys in this portion of the diagram thus requires dividing the solidification process into two regions, one above and one below T_r. In each region, a unique set of liquidus and solidus lines should be used.

2.3 THE NORMAL FREEZING DIFFERENTIAL EQUATION

Let c_l and c_s be functions of a modified melt temperature $T = T_e - T_m$, where T_e is the fixed melting point of the pure solvent and T_m is the variable melt temperature (Fig. 2-2). Thus:

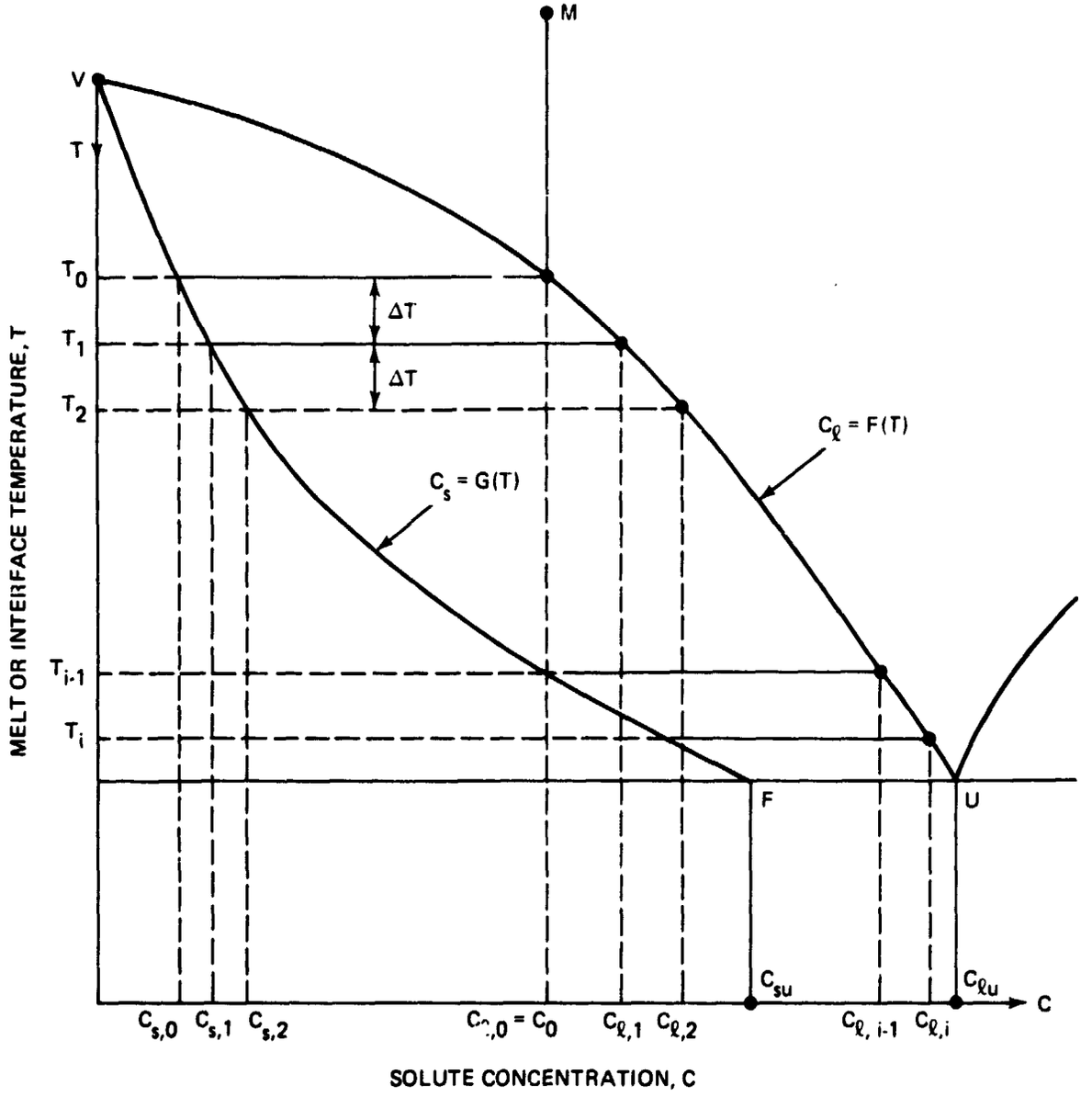

Fig. 2-2 The Normal Freezing Process

$$c_l = L(T)$$

$$c_s = S(T)$$

where L(T) and S(T) are functions of the modified melt temperature, for the solidus and liquidus curves of the constitutional diagram.

At the beginning of normal freezing, time $t = t_o = 0$, the fraction solidified $p = p_o = 0$, $c_l = c_{lo} = c_o$, $T = T_o$, and $k = k_l = S(T_o)/L(T_o)$, where T_o can be determined from $c_o = L(T_o)$. The frozen length is $x = x_o = p_o H = 0$, where H is the total melt or crystal length.

At t = t, the fraction solidified, frozen length, and modified melt temperature are, respectively, p, x = ph, and T. At the end of the next short time interval Δt from t, these values will respectively increase to $p + \Delta p$, $x + \Delta x$, and $T + \Delta T$.

Balancing the amount of solute Q in the remaining melt at time t according to a general procedure previously described (see, e.g., Pfann 1952) gives

$$\Delta Q = -c_s \Delta p = \Delta \left[(1-p)c_l\right] - f_l\,(c_l,\ \Delta t,\ T,\ \ldots) \qquad (24)$$

where f_l represents the loss of solute from causes such as surface evaporation and chemical reaction. This loss may depend on c_l, Δt, T, melt volume, or free surface.

In many cases, $f_l = 0$. If we then take the limit as Δt, Δp, Δx, and ΔT all approach zero, we obtain the following basic differential equation for normal freezing:

$$dp/(1-p) = -d\ \ln(1-p) = \left\{L'(T)/\left[L(T)-S(T)\right]\right\}dT \qquad (25)$$

where L'(T) is the temperature derivative of the liquidus curve L(T).

In the above derivation, c_l and c_s may be in terms of weight fractions. Q then represents the weight of solute in the liquid melt for each one gram of original melt. If, however, c_l and c_s are in terms of atomic fractions, Q then represents the number of moles of solute atoms for each mole of combined solvent and solute atoms in the original melt.

2.3.1 Constant-k Normal Freezing Equation

In a few constitutional diagrams, the liquidus and solidus curves can be approximated by straight lines. When we are dealing with very narrow ranges of freezing temperature, solute concentration, or fraction solidified, such as in the previous examples of growing pure germanium and silicon crystals and of forming germanium alloy diodes, the portions of the generally curved liquidus and solidus lines of interest may be so small that they can be represented by two straight lines. We then have:

$$c_l = aT + e_l$$

$$c_s = fT + e_s$$

where a and f are the slopes of the liquidus and solidus lines, and e_l and e_s are the intercepts of these lines, when extended, on the vertical temperature axis (see Fig. 2-2).

The normal freezing differential equation, Eq (25), then reduces to

$$\frac{dp}{(1-p)} = \frac{a}{(a-f)\,T + (e_l - e_s)}\,dT$$

This equation is easily integrated. When proper initial conditions are included, we obtain the following general, constant-k, normal freezing equation:

$$1 - p = \left[\frac{(a-f)T + (e_l - e_s)}{(a-f)T_o + (e_l - e_s)}\right]^{a/(f-a)} \tag{26}$$

When pure germanium crystal or diode materials are dealt with, only the terminal regions of the constitutional diagrams are used. The two short liquidus and solidus lines then usually both pass through the melting point of pure germanium, and both e_l and e_s are zero. Equation (26) then reduces to the familar, constant-k normal freezing equation:

$$T/T_o = aT/aT_o = c_l/c_o = c_s/kc_o = (1-p)^{(f-a)/a} = (1-p)^{k-1} \tag{27}$$

This equation is so important in materials processing, particularly in the semiconductor industry, that it has been repeatedly derived (Gulliver 1922, Scheuer 1931, Hayes 1939, Luneau 1942, Mathier 1942, Scheil 1942, McFee 1947, and Pfann 1952). An analogous equation, known as Rayleigh's equation, has also been derived and used for "simple" distillations in chemical engineering (Rayleigh 1902).

2.3.2 Accuracy of the Constant-k Normal Freezing Equation

According to Christian (1965), Pfann's equation applied to reasonably dilute solutions, is a useful approximation until some 80% of the liquid has solidified, that is, until $p = 0.80$.

Dowd and Rose (1953) studied the distribution of radioactive indium in germanium, and concluded that the indium concentration obeyed Pfann's equation. On the other hand, Goruw and Jentoft (1967), in evaluating the effectiveness of normal freezing, column crystallization, and zone melting of $n\text{-}C_{14}H_{30}$ in $n\text{-}C_{16}H_{34}$, found that the segregation coefficient is a linear function of the solute concentration in the melt.

Kurgistsev (1967) analyzed the problem of determining k from experimental data and showed that the methods which reduce this problem to that of finding a solution of the equation on the assumption that k is constant lead to erroneous results.

Brody and Flemings (1966) analyzed their data on the Al-Cu system using their semi-theoretical, constant-k normal freezing equation. They emphatically concluded that the constant-k equation gives "accurate" results, although they had to multiply their experimental data by an unfounded factor of three to achieve reasonable fit. Johnston and Tiller (1962) considered the problem of the segregation coefficient k, or effective segregation coefficient k, varying as a function of the interface position (or p), and determined some of the functions required to produce particular solute distributions in the solid. Wilcox (1964) also considered k_e to vary with c_s, and set up the necessary normal freezing and zone melting equations for numerical integration.

c1

Pfann (1958) stated that the linear normal freezing equation, Eq 27, does not describe the complete freezing behavior for the whole length of the ingot. The complete concentration curve, however, can be calculated by Hamming's method (Pfann 1958) by taking the dependence of k on the concentration into account.

2.3.3 Non-constant-k, Normal Freezing Equations

As pointed out above, Eq (27) has been very successfully used to determine gross concentration profiles in the useful crystal, and other solidification behavior, of pure germanium and silicon materials. This is true even when the liquidus and solidus lines are distinctly curved (Li, 1966) due to the unique conditions previously described. In other normal freezing studies related to general metallurgy, however, the entire solidification range must be considered. Such studies include the investigation of the segregation of trace impurities at grain, subgrain, cell, or subcell boundaries; the formation of freezing-in or induced point, line, surface, and massive defects in electronic or structural materials (Li, 1967b); the selection of homogenization, oxidation-precipitation, diffusion-reaction, or other heat-treatments from the calculated distribution of alloying elements in polycrystalline welded or soldered joints; and the magnitude and character of voids or vacancies, and of residual stresses or strains, in castings, caused by variable solid and liquid material densities.

2.3.4 Quadratic Liquidus and Solidus Lines

When the solidus and liquidus can be represented by second-degree functions of the melt temperature $T_m = T_e - T$, i.e.,

$$c_l = aT + bT^2 = a(T_e - T_m) + b(T_e - T_m)^2$$

$$c_s = fT + gT^2 = f(T_e - T_m) + g(T_e - T_m)^2$$

Eq (1) then becomes:

$$-d\ \ln(1-p) = \frac{(a-2bT)\,dT}{(a-f)T + (b-g)T^2}$$

Hence,

$$1-p = (T/T_o)^{l} \left[\frac{(a-f) + (b-g)T}{(a-f) + (b-g)T_o}\right]^2 \qquad (28)$$

where $Q_1 = a/(f-a)$ and $Q_2 = (ab+ag-2bf)/(f-a)(b-g)$, as given by Li (1967a).

Li further showed (1967a) that Eq (28) reduces to Eq (27) only under the restricted conditions of very dilute melts, nearly straight liquidus and solidus lines, and very small solidification ranges. Hence, when one or more of these conditions are not met, the use of Eq 27 in normal freezing studies requires caution.

2.3.5 Cubic Liquidus and Solidus Lines

An examination of binary constitutional diagrams (with $k < 1$) reveals that, of 171 binary diagrams given in the ASM Metals Handbook (1948), 36 (or 21%) have distinctly cubic liquidus and/or solidus lines. It is, therefore, desirable to derive the normal freezing equation for cases with cubic liquidus and solidus lines, i.e., when:

$$c_l = L(T) = aT + bT^2 + dT^3$$

$$c_s = S(T) = fT + gT^2 + hT^3$$

For this case, Eq (25) reduces to (Li, 1968):

$$-d\ln(1-p) = \frac{(a+2bT + 3dT^3)dT}{(a-f)T + (b-g)T^2 + (d-h)T^3} = \frac{Q_1}{T}\,dT + \frac{Q_2}{T+u}\,dT + \frac{Q_3}{T+v}\,dT$$

where

$$u = \left[b-g+\sqrt{(b-g)^2 - 4(a-f)(d-h)}\right]/2(d-h)$$

$$v = \left[b-g-\sqrt{(b-g)^2 - 4(a-f)(d-h)}\right]/2(d-h)$$

$$Q_1 = -a/uv(d-h)$$

$$Q_2 = -\left[uv(3du-2b) + av\right]/uv(d-h)(u-v)$$

$$Q_3 = -\left[uv(2b-3dv) + au\right]/uv(d-h)\ (u-v)$$

and

$$1 - p = (T/T_o)^{Q_1}\left(\frac{T+u}{T_o+u}\right)^{Q_2}\left(\frac{T+v}{T_o+v}\right)^{Q_3} \tag{29}$$

2.3.6 Quartic and Higher Degree Liquidus and Solidus Lines

Here, the liquidus and solidus lines, L(T) and S(T) respectively, can be represented by two polynomials in T such that L(T) - S(T) is an nth degree function, and the degree of L'(T) is less than n. Then, Eq (25) yields (Li, 1968):

$$-d\ln(1-p) = \left\{L'(T)/\left[L(T) - S(T)\right]\right\} dT = \sum_{i=1}^{n} Q_1/(T-T_i)\ dT = \sum_{i=1}^{n} Q_1 d\ \ln(T-T_i)$$

from which

$$1 - p = \prod_{i=1}^{n}\left[(T-T_i)/(T_o-T_i)\right]^{-Q_i} \tag{30}$$

the T_i's are the roots of the polynomial L(T) - S(T), and the Q_i's are the numerators of the various partial fractions for the function $L'(T)/\left[(L(T)-S(T)\right]$.

2.3.7 Ideal Binary Systems

In an ideal solution having an ideal, dilute solid solution in equilibrium with a simple melt solution (Panish and Ilegems 1970), the liquidus curve (in mole fraction) is given, according to Prigogine and Defay (1954), by:

$$c_1 = 1 - \exp\left[(1/T_o - 1/T)\,\Delta H/r\right] = 1 - \exp\,(a+b/T) = 1 - U$$

where ΔH is the molar heat of fusion, T_o is the absolute melting temperature of the pure solvent, T is the absolute melt temperature, $b = -\Delta H/R$, $a = -b/T$, and $U = \exp\,(a+b/T)$.

For an ideal solution in equilibrium with a dilute ideal solution, the segregation coefficient for the dilute component can also be shown to be an exponential function of the reciprocal absolute melt temperature, both theoretically (Hildebrand and Scott 1950;

Thurmond and Struthers 1953) and experimentally (Hall 1957; Orioni and Hall 1958). Thus

$$k = \exp (f' + g'/T)$$

and the equation of the ideal solidus curve is

$$c_s = \exp (a + b/T) \exp (f' + g'/T) = \exp (f + g/T) = V,$$

where f', g', f = a + f', and g = b + g' are constants, and V = exp (f + g/T).

The basic normal freezing, differential equation, Eq (25), then becomes:

$$-d\ln(1-p) = \frac{\exp (a+b/T)\ (-b/T^2)dT}{\exp (a+b/T) - \exp (f+g/T}$$

Hence (Li, 1971),

$$1 - p = \left[\frac{\exp (a+b/T)\ /\exp (f+g/T) - 1}{\exp (a+b/T_o)/\exp (f+g/T_o) - 1}\right]^{b/(g-b)} = \left(\frac{U/V-1}{U_o/V_o-1}\right)^{Q_1} \qquad (31)$$

where $T_o = b/\left[\ln(1-c_o)-a\right]$, $U_o = \exp (a+b/T_o)$, $V_o = \exp (f+g/T_o)$, and $Q_1 = b/(g-b)$.

2.3.8 Ideal Ternary Systems of the Pseudobinary Type

Many ternary liquid solutions are ideal in that the A, B, and C atoms in the solution are solidified into ideal solid solutions of AB-AC with the A atoms on one sublattice and B or C atoms on the other. Such systems can be treated as pseudobinary systems.

In such systems, the mole fraction for the AB compound in the solid is (Panish and Ilegems 1970):

$$c_s^{AB} = (1-V)/(U-V)$$

where U = exp (a+b/T), V = exp (f+g/T), $b = -\Delta H_{AB}/R$, $a = -b/T_{AB}$, $g = -\Delta H_{AC}/R$, $f = -g/T_{AC}$, ΔH_{AB} is the heat of formation of compound AB at its absolute melting point T_{AB}, and ΔH_{AC} is the heat of formation of compound AC at its absolute melting point T_{AC}. The mole fraction of B atoms in the liquid solution is (Panish and Ilegems 1970).

$$c_1^B = U\, c_s^{AB}/2$$

By introducing chemical molar concentrations m^A, m^B, and m^C, we can balance the amount of B or C in the remaining liquid. Thus, by accounting for the amount of B in the liquid, Q_B, Eq (25) becomes (Li, 1972):

$$-d\ln(1-p) = \frac{V[b(1-V) - g(1-U)]}{(1-U)\,(1-V0\,(1-V/U)}\, d(1/T) = \left[\frac{Q_1}{1-U} + \frac{Q_2}{1-V} + \frac{Q_3}{1-V/U}\right] d(1/T)$$

Hence,

$$1 - p = \left[\frac{1-U^{-1}}{1-U_o^{-1}}\right]^{Q_1} \left[\frac{1-V^{-1}}{1-V_o^{-1}}\right]^{Q_2} \left[\frac{1-U/V}{1-U_o/V_o}\right]^{Q_3} \tag{32}$$

where

$$Q_1 = q/(q-1),$$

$$Q_2 = 1/(1-s),$$

$$Q_3 = r/(1-r),$$

$$q = \exp\,(f-ga/b),$$

$$r = \exp\left[(ag-bf)/(g-b)\right]$$

$$s = \exp\left[(bf-ag)/g\right]$$

T_o, the initial freezing temperature, can be determined from the pseudoliquidus line by substituting the initial melt composition $c_{1,o}^{AB}$ for c_1^{AB}.

Complete details of the derivation of Eq (32) and its application to the theoretical computation of the normal freezing behavior of GaAlAs system is given in Appendix D.

2.3.9 Summary of Normal Freezing Equations

The closed-form, normal freezing solutions described above, but expressed in slightly different forms, are given as follows:

- Linear

$$\frac{c_s}{kc_o} = (1-p)^{k-1} \text{ or } 1-p = 1-p_s = \left[\frac{c_\ell}{c_o}\right]^{\frac{1}{k-1}} = 1-\left(\frac{T}{T_o}\right)^{\frac{1}{k-1}} \tag{27}$$

- Quadratic

$$1-p = \left(\frac{T}{T_o}\right)^{Q_1}\left(\frac{a+bT}{a+bT_o}\right)^{Q_2} \tag{28}$$

- Cubic

$$1-p = \left[\frac{T-T_1}{T_o-T_1}\right]^{Q_1}\left[\frac{T-T_2}{T_o-T_2}\right]^{Q_2}\left[\frac{T-T_3}{T_o-T_3}\right]^{Q_3} \tag{29}$$

- General Polynomial

$$1-p = \prod_{i=1}^{n}\left[\frac{T-T_i}{T_o-T_i}\right]^{Q_i} \tag{30}$$

- Simple Binary Solutions

$$1-p = \left[\frac{U/V-1}{U_o/V_o-1}\right] \tag{31}$$

- Pseudobinary

$$1-p = \left[\frac{1-U^{-1}}{1-I_o^{-1}}\right]^{Q_1}\left[\frac{1-V^{-1}}{1-V_o^{-1}}\right]^{Q_2}\left[\frac{1-U/V}{1-U_o/V_o}\right]^{Q_3} \tag{32}$$

2.4 APPLICATIONS OF NORMAL FREEZING EQUATIONS TO SOLIDIFICATION

Application of the various normal freezing equations to solidification problems will now be described, with emphasis placed on the constant-k normal freezing equation (or Pfann's Equation) which is so important in the semiconductor industry. Specifically considered are several methods of fitting straight lines to liquidus and solidus curves; the meaning of the constant segregation coefficient; the best value of a constant segregation coefficient for a given solidification problem; and errors in the use of a constant k when the liquidus and solidus are curved. Next, we will show that the last portion of a freezing melt must be a eutectic having a fixed composition, i.e., the eutectic composition. Finally, we give two useful numerical computation methods, i.e., the Runge Kutta Method and The Finite Difference Method, to treat cases not covered by the various normal freezing equations given above.

2.4.1 Fitting Straight Lines to Liquidus and Solidus Curves

Most liquidus and solidus lines are more or less curved. There are many ways a straight line can be fitted to a curve. The most obvious method is to fit a straight line through the discrete data points (obtained experimentally or from the constitutional diagram) to minimize the sum of square of the residual errors (line 1, Fig. 2-3a). This is the standard, least-square fitting technique (Anderson and Bancroft, 1952). For most solidification work, however, this technique is improper. In the case of pure Ge, Si, or other materials, particularly during single crystal growth, we are mainly interested in the terminal region (around the point E) of the constitutional diagram. Line 1, however, often gives the highest errors in these regions. Further, these fitted lines often cannot be used in the various freezing equations, failing even to meet at point E for zero solute concentrations. These lines are thus physically unsatisfactory and often meaningless. Moreover, line 1 does not give the correct eutectic compositions.

A second fitting method is to pass both straight lines through the melting point of the pure solvent (i.e., point E), while still minimizing the sum of squares of the residual errors (line 2, Fig. 2-3b). Unfortunately, most liquidus and solidus lines have curvatures around point E. If these lines are convex upward, line 2 will consistently underestimate the melt temperature for a given solute concentration, and vice versa. Further, the

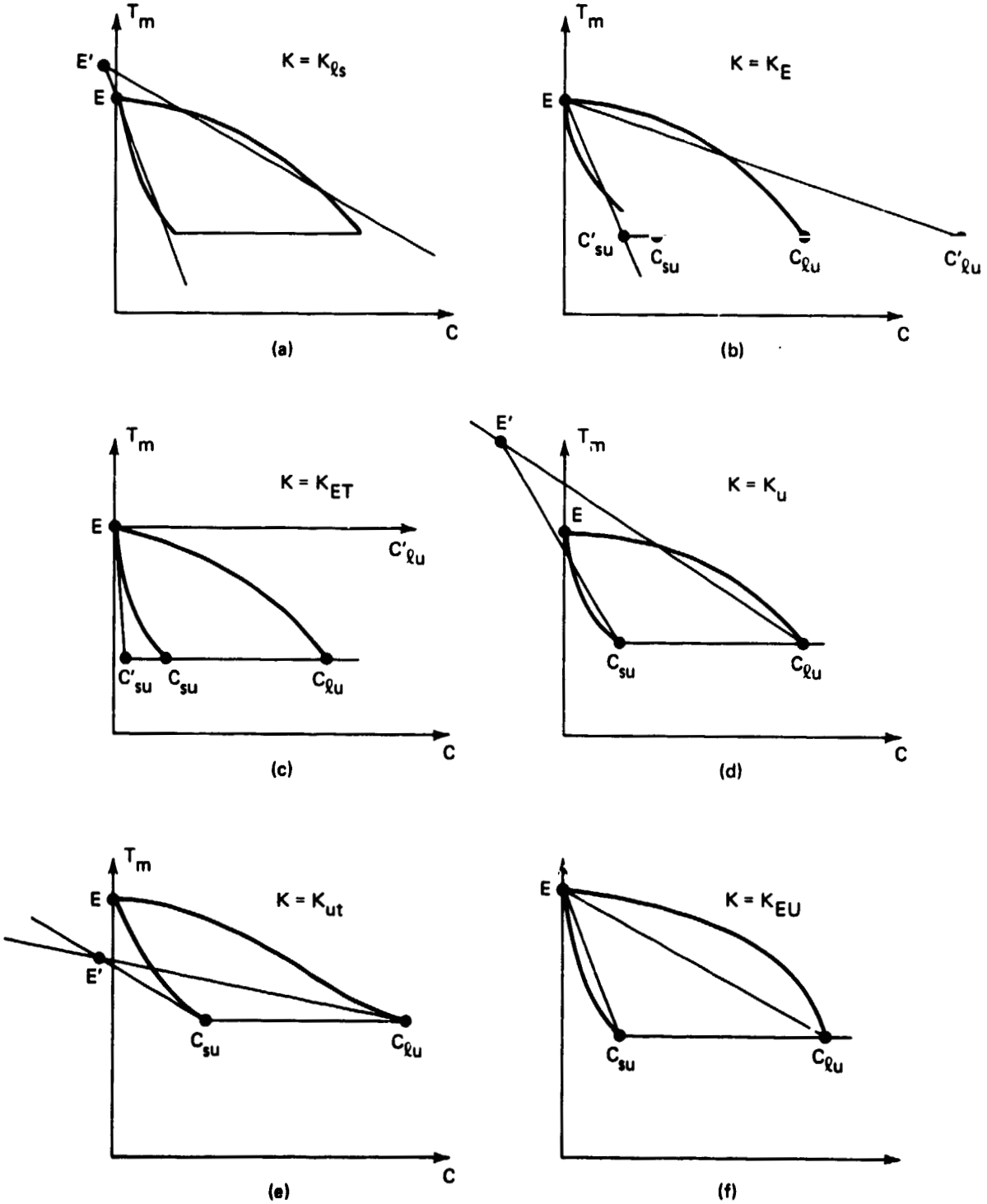

Fig. 2-3 Methods of Fitting Straight Lines to Curved Liquidus and Solidus and Their Associated Segregation Coefficients

all-important segregation coefficient k is markedly off, particularly when one of the liquidus and solidus lines is convex upward while the other is convex downward. The estimated eutectic compositions may be erroneous and useless in eutectic solidification work or in estimating the eutectic thickness at the grain boundaries.

Another method, particularly useful for dilute solutions or pure materials, is to pass the straight lines through the point E and tangent to the liquidus or solidus curve (Fig. 2-3c). These fitted straight lines, however, generally give the greatest errors in the estimated eutectic compositions. Further, for many liquidus curves, particularly those for intermetallic compounds, the liquidus is often nearly horizontal at the terminal region. The segregation coefficient $k=k_{ET}$ must then be zero or nearly so. The constant-k, normal freezing equation, Eq (27), then reduces to the meaningless form $c_s = 0$.

In Fig. 2-3d, the two straight lines pass respectively through the c_{su} and c_{lu} points while minimizing the sum of squares of the residual errors. While this set of lines is sometimes sufficient for eutectic solidification work, it is evidently inadequate for work on pure materials or dilute solutions.

Figure 2-3e shows a set of fitted, straight liquidus and solidus lines that intersect the same c_{su} and c_{lu} points, as in Fig. 2-3d, but are tangent to the respective liquidus or solidus curves. For most eutectic solidification with initial melt compositions near the eutectics, this set of straight lines is superior to that of Fig. 2-3d.

Figure 2-3f shows a set of fitted straight lines that pass through the points E and c_{su} or c_{lu}. The segregation coefficient $k = k_{EU}$ is seen to be greatly overestimated here.

There are other methods of fitting straight lines. We could, for example, assign different weights to different temperature or concentration ranges. These methods are, however, too specialized to be discussed here.

2.4.2 The Meaning of Constant Segregation Coefficient

With a few exceptions, such as Tiller (1962), Wilcox (1964), and Rubenstein (1971), practically all researchers in solidification assume a constant segregation coefficient k and, hence, perfectly straight liquidus and solidus lines on the constitutional diagrams. This coefficient k is generally defined as the ratio of solute concentration in the just frozen solid to that in the remaining melt, i.e., $k = c_s/c_l$. The values of c_s and c_l may be obtained experimentally or from the constitutional diagram. When dealing with dilute solutions or pure materials such as Ge, Si, W, or Ti, we find that both c_s and c_l approach zero and, hence, $k = 0/0$ which is undefined. In this case, we define k as the ratio of the slope of the solidus at point E (Fig. 2-3) to the slope of the liquidus at the same point. Thus, k becomes $k_o = k_{ET}$ of Fig. 2-3c. If c_s and c_l are fitted by two n-degree polynomials of the melt temperature, i.e., $c_s = \sum_{i=1}^{n} f_i T^i$ and $c_l = \sum_{i=1}^{n} a_i T^i$, then $k_o = k_{ET}$ is the ratio of the first fitted coefficient in the solidus equation to that in the liquidus equation. Thus, $k_o = f_1/a_1$.

It has been shown that none of the several methods of fitting straight lines to curved liquidus and solidus generally give accurate results in solidification work. Basically, it is impossible to accurately fit straight lines to these curves. The six segregation coefficients, each given for a particular type of fitting in Fig. 2-3, usually differ widely in value. Each is useful only in its limited range of application. Given a specified solidification problem, it is often difficult to decide which constant k should be chosen. Even with a properly chosen k, when a specific initial melt composition is given, the beginning of solidification and, hence, the solidification range, cannot generally be correctly ascertained. The upper ends of the fitted straight lines in Fig. 2-3a, 2-3d, and 2-3e do not even intersect at the point E, as they should. Ridiculous, negative solute concentrations and, hence, negative segregation coefficients may therefore appear.

Each of the several types of fitted straight lines in Fig. 2-3 gives a unique type segregation constant valid only in certain solidification applications. None is generally useful, each being often greatly different from the others. This is easily seen, e.g. in the Ge-Sb system. The computed segregation constant from the constitutional diagram, i.e., $k_{CD} = c_s/c_l$, varies from 0.0276 at the melting point of germanium (i.e., 1209K or 936°C) to 0.0390 at the eutectic temperature of 863K or 590°C. This represents an increase of 41.3% (see Li 1966a). In a very dilute solution, e.g., in most semiconductor work including the growth of nondegenerate germanium crystals, a segregation constant $k = k_o = 0.0276$ should be used for constant-k freezing equations, such as Eq (27). In a Sb-rich melt near the eutectic composition, however, a $k = k_U = 0.0390$ should be chosen.

In the case of dilute Ge-Sb solution, if we use k_U instead of the correct k_o, then $\Delta k = k_U - k_o = +0.0114$, and the percentage error in k is $\Delta k/k_o = +0.413$. The percentage errors in c computed according to Eq (27), i.e., $\Delta c/c = (1 + \frac{\Delta k}{k})(1-p)^{\Delta k} - 1$, are 41.1%, 40.9%, 40.7%, 40.5%, 40.2%, 39.8%, 39.4%, 38.7%, 37.6% and 36.6% for p = 0.1, 0.2, 0.3, 0.4, 0.5, 0.6, 0.7, 0.8, 0.9, and 0.95, respectively. The percentage errors in p computed from Eq (27), i.e.,

$$\Delta p/p = p^{\Delta k/k - \Delta k} - 1$$

are -2.69%, -1.89%, -1.42%, -1.08%, -0.819%, -0.604%, -0.422%, -0.264%, -0.125%, and -0.00608%, respectively, for the same values of p.

If, in the case of melts of near-eutectic compositions, we use k_o instead of the correct k_U, then $\Delta k = k_o - k_U = -0.0114$ and the percentage error in k is now $\Delta k/k_U = -0.292$. The percentage errorsin the computed c's are then -29.1%, -29.1%, -28.9%, -28.8%, -28.7%, -28.5%, -28.3%, -27.9%, -27.3%, and 26.8%, respectively, for the same ten values of p. The corresponding percentage errors in the computed p's are now 2.74%, 1.90%, 1.42%, 1.08%, 0.816%, 0.601%, 0.419%, 0.262%, -.124%, and 0.00602%, respectively.

Yet, the Ge-Sb system should be considered as a fairly well-behaviored system. The possible errors in k and, hence, computed c's and p's using any constant-k freezing

equations, are even much worse with many other systems. Consider, for example, the Au-Ag system having a constitutional diagram of the type shown in Fig. 2-1b. Any Au-Ag alloy can, therefore, be treated either as an Au alloy containing Ag as the solute, or as an Ag alloy containing Au. Considering Au-Ag as an Ag alloy containing Au, we see that the $c_{s,Au}$ is always greater than $c_{l,Au}$ except at the end points, where they are equal. The segregation coefficient $k_{Au} = k_{Au\ in\ Ag}$ is thus always > 1. In fact, k_{Au} varies from 1.000 to over 2.080, for the temperature range of 1336K or 1063°C to 1234K or 960.5°C. Considering the same alloy as an Au alloy containing Ag, we see $c_{s,Ag}$ never exceeds $c_{l,Ag}$. Hence, $k_{Ag} = k_{Ag\ in\ Au}$ never exceeds unity. In fact, k_{Ag} varies from less than 0.1986 to 1.000 over the same temperature range, representing an increase, of over 600% (Li 1968).

Li (1968) has fitted, by least-square techniques, the Au-Ag liquidus and solidus curves using straight lines passing through the Au terminal point, and also by quadratic or cubic polynomials through both the Au and Ag terminal points. According to the best-fitting equations presented, the constant segregation coefficient at the Au terminal point varies from 0.8781 through 0.7015 to 0.7287 for the linear, quadratic, and cubic polynomials, respectively. Thus, even at the same Au terminal point, the $k = f_1/a_1$ can vary by as much as 25.2% depending pn the degree of the polynomials chosen. The order of these k values is also inconsistent with the degree of the polynomials.

Thus, we are often faced with a bewildering array of unique segregation constants including: k_{1s}, Fig. 2-3a; k_E, Fig. 2-3b K_{ET}, Fig. 2-3c; k_U, Fig. 2-3d; k_{UT}, Fig. 2-3e; k_{EU}, Fig. 2-3f; and k_{oT}'s such as $k_{oT,1}$, $k_{oT,2}$, and $k_{oT,3}$. Any indiscriminate use of unspecified k is likely to confuse and mislead, particularly with melts of medium high solute concentrations such as 4.5% by Cu in Al (a favorite alloy system for solidification study), for which the choice of k is the most abundent.

For any binary alloy system A-B in general, and the Au-Ag system in particular, the segregation coefficient of one component in the other, e.g., of Ag in Au, is:

$$k_{Ag} = c_{s,Ag}/c_{l,Ag}$$

The other segregation coefficient for Au in Ag in the same alloy is:

$$k_{Au} = c_{s,Au}\ c_{1,Au} = (1-c_{s,Ag})\ (1-c_{1,Ag}) = (1-k_{Ag}\ c_{1,Ag})\ (1-c_{1,Ag}) = \frac{\left[1-K_{Ag}L_{Ag}(T)\right]}{\left[1-L_{Ag}(T)\right]}$$

If $c_{s,Ag} \leq c_{1,Ag}$, then $K_{Ag} \leq 1$ and $1 - k_{Ag}\ c_{1,Ag} \geq 1 - c_{1,Ag}$. Hence, k_{Au} must be ≥ 1, as observed. Thus, if $k_{A \text{ in } B} < 1$, then $k_{B \text{ in } A}$ must be >1.

Further, since $c_{1,Ag} = L_{Ag}(T)$, k_{Au} cannot, from the last equation, be constant unless $k_{Ag} \equiv 1 \equiv k_{Au}$. This condition is true only when the liquidus and solidus are one and the same curve, in which case Eq (27) reduces to the meaningless form $c = c_s = c_o$.

Notice that all the above k's refer to a system of c_s's and c_1's on either the weight or the atomic scale. That is, the k's are either k_{wt}'s or k_{at}'s. It can be shown that k_{wt} cannot be the same as k_{at} for any two alloy components unless $c_s = c_1$ on both the weight and atomic basis, i.e., only when both the liquidus and solidus are, again, one and the same. Further, if k_{wt} is constant, k_{at} cannot be constant, and vice versa. Hence, both k_{Au} and k_{Ag} in the Au-Ag system or $k_{A \text{ in } B}$ and $k_{B \text{ in } A}$ in any binary system, whether on the weight basis or on the atomic basis cannot be constant but must vary with the melt temperature.

2.4.3 The Best Value of the Segregation Coefficient

The best value of constant segregation coefficient k_c depends, of course, on the alloy system. For a fixed alloy system, the best k_c varies, as shown above, with the selection of atomic or weight fractions for expressing the solute concentrations, the initial melt composition, and the degree and number of terminal restrictions in the polynomial fitting of the liquidus and solidus curves. A change in the least-square fitting method (to account, e.g., for the fact that errors occur in both the solute concentrations and melt temperatures rather than only in the concentrations or temperatures) also changes the value of k_c. The best k_c also depends on the use of the resultant solidified material. In the manufacture of critical electronic, optical, or mechanical devices, the objective may be to minimize either absolute or percentage errors in solute concentrations c, concentration gradients $c_p = dc/dp$, or other properties related

to c or c_p. The minimization is to be achieved either over a specified region (i.e., between two fractions solidified, p_1 or p_2) or at a critical location (i.e., at the fraction solidified, p). The best k_c depends not only on the magnitude of allowable error, but on whether the error is positive or negative for the same magnitude. Specifically, Li (1967) has shown that if overestimated c values cause more serious damage than underestimated c's, then a slightly inflated k_c should be used for safety, especially when k_c and p are large.

However, it is always possible to find the optimum k_c, for use in Eq (27) for example, to best fit any given normal or abnormal freezing data. This is true even with alloys having distinctly curved liquidus and solidus lines. Further, the errors due to the assumed constancy of k_c can usually be estimated either analytically or by numerical methods. In the very narrow melt temperature range around $T_m = T_e - T$, for example, the optimal k_c can be determined from Eq (27) and (28).

$$1 - p_1 = \left(\frac{C_\ell}{C_o}\right)^{\frac{1}{1-k}} = \left(\frac{T_\ell}{T_o}\right)^{\alpha_c} = \left(\frac{T_\ell}{T_o}\right)^{\alpha}\left(\frac{1+rT}{1+rT_o}\right)^{\beta} \tag{33}$$

where $\alpha_c = 1/(1-k_c)$, and α, β, and r are defined in connection with Eq (28). Hence the optimized constant k_c, i.e., k_c^{op}, is such that:

$$\frac{1}{1-K_c^{op}} = \alpha_c^{op} = \frac{\beta \ell n \frac{1+rT}{1+rT_o}}{\ell n \frac{T}{T_o}} + \alpha \tag{34}$$

$$\text{or } k_c^{op} = \frac{\alpha_c^{op} - 1}{\alpha_c^{op}} = 1 - \frac{\ell n \frac{T}{T_o}}{\alpha \ell n \frac{T}{T_o} + \beta \ell n \frac{1+rT_o}{1+rT_o}} \quad \text{for } T \simeq T \tag{35}$$

In the above derivation, the liquidus and solidus curves are assumed to be adequately representable by quadratic functions of the melt temperature. In the general case when the liquidus and solidus are representable only by nth degree polynomials, the optimized k_c is

$$k_c^{op} = \frac{\alpha_c^{op} - 1}{\alpha_c^{op}} = 1 + \frac{\ell n \frac{T}{T_o}}{q_1 \ell n \frac{T}{T_o} + \sum_{i=2}^{n} q_i \ell n \frac{T-T_i}{T-T_o}} \quad \text{for } T \simeq T \tag{36}$$

For a wide solidification range, the optimized k_c may be determined by least-square techniques for the general polynomial case, such that:

$$\Sigma\left[\ell n\left(\frac{T}{T_o}\right)\right]\left(\frac{T}{T_o}\right)^{\frac{2}{k_c^{op}-1}} = \Sigma\left[\ell n\left(\frac{T}{T_o}\right)\right]\left(\frac{T}{T_o}\right)^{\frac{1}{k_c^{op}-1} - q_1} \prod_{i=2}^{n}\left(\frac{T-T_i}{T_o-T_i}\right)^{-q_i} \tag{37}$$

In practice, the k_c^{op} may often be more easily obtained by numerical methods using a computer. Table 2-1 lists the numerically obtained values of k_c^{op} for the system of Sb in Ge. The k_c^{op} is seen to increase with initial melt concentration c_o and fraction solidified p, the increases being greater with larger values of c_o and p. The standard errors in the computed p, computed with these k_c^{op} according to Eq (27) and compared with corresponding p values from Eq (28), can be as small as 3×10^{-12} for c/o = 0.001 and p = 0.01 to 0.20.

TABLE 2-1 OPTIMIZED CONSTANT k, $k^{op}_{c_l}$ FOR Ge ALLOYS CONTAINING Sb AS SOLUTE

C_o	p	$k^{op}_{c_l}$	σ
0.1	.01-.20	0.028063733	3.60065×10^{-6}
	.01-.40	0.02815576	1.11772×10^{-5}
	.01-.60	0.028 492	3.21579×10^{-5}
	.01-.80	0.0290365	1.45726×10^{-4}
	.01-Tu	0.0306733	5.88936×10^{-4}
0.01	.01-.20	0.0276402	3.19533×10^{-8}
	.01-.40	0.0276481	9.68934×10^{-8}
	.01-.60	0.0276641	2.65315×10^{-7}
	.01-.80	0.0277130	1.00608×10^{-6}
	.01-Tu	0.0293844	7.56718×10^{-5}
0.001	.01-.20	0.1276022	3.19838×10^{-10}
	.01-.40	0.0276029	9.66827×10^{-10}
	.01-.60	0.0276046	2.62887×10^{-9}
	.01-.80	0.0276093	9.81624×10^{-9}
	.01-.99	0.0277335	5.30022×10^{-7}
0.0001	.01-.20	0.0275833	2.87215×10^{-12}
	.01-.40	0.0275833	6.24331×10^{-12}
	.01-.60	0.0275835	1.12754×10^{-11}
	.01-.80	0.0275837	6.09533×10^{-11}
	.01-.99	0.0276087	5.13106×10^{-9}

2.4.4 Errors Due to Curvature of the Liquidus and Solidus Lines

We consider here the errors involved in the use of the constant-k, normal freezing equation when, in fact, the liquidus and solidus curves are not straight lines. Three cases are considered: quadratic, high-degree polynomial, or exponential functions of the melt temperature T_m.

In the first case, the liquidus and solidus curves can be represented by quadratic function of T_m, i.e.,

$$L(T) = c_1(T) = aT + bT^2 = a(T_e - T_m) + b(T_e - Tm)^2$$

$$S(T) = c_s(T) = fT + gT^2 = f(T_e - T_m) + g(T_e - T_m)^2$$

The segregation coefficient k used in Eq (27) should, particularly for such dilute alloys as semiconductor germanium or silicon and pure Be or Ti, be:

$$k_o = S(T)/L(T)_{T=0} = f/a$$

Equation (27) then shows that the proportion of liquid remaining is:

$$p_1^1 = 1 - p_s^1 = (c/kc_o)^{1/(k-1)} = (c_1/c_o)^{1/(k-1)} = (T/T_o)^{a/(f-a)}$$

According to Eq (28), the proportion of liquid remaining is, however,

$$p_1^2 = 1 - p_s^2 = (T/T_o)^{a/(f-a)}\left[\frac{1+(b-g)T/(a-f)}{1+(b-g)T_o/(a-f)}\right] \overset{B}{\doteq} \left(\frac{T}{T_o}\right)^{\frac{a}{f-a}}\left[1 + \beta\frac{b-g}{a-f}(T-T_o)\right] = \left(\frac{T}{T_o}\right)^{\frac{a}{f-a}}\left[1-\Gamma(T-T_o)\right]$$

where $\beta = (ab+ag-2bf)/(f-a)/(b-g)$ and $\Gamma = (ab+ag-2bf)/(a-f)^2$

To estimate p_1^2 by means of p_1^1 of Eq (25) thus involves percentage errors amounting to:

$$e^{12} = (p_1^1 - p_1^2)/p_1^2 = \frac{\alpha(T-T_o)}{a + \alpha(T-T_o)} \simeq \alpha(T-T_o) = \frac{ab + ag - 2bf}{(a-f)^2} \Delta T \simeq \frac{b}{a} \Delta T \qquad (38)$$

This error is thus roughly proportional to the solidification range $\Delta T = T-T_o$. Estimating the amount of eutectics thus represents the worst-case condition for the use of the constant-k normal freezing equation, Eq (27), particularly when initial concentration c_o is small. Error e^{12} is also inversely proportional to the square of the slopes of the liquidus and solidus lines, i.e., $(a-f)^2$. When both a and f are small, i.e., when the constitutional diagram has very steep liquidus and solidus curves and, in particular, when a-f is small, $1/(a-f)^2$ is very large and, hence, very large errors may result.

Examination of Hansen's (1958) binary constitutional diagrams discloses many systems whose liquidus and solidus are very close at the melting point of the pure solvent (i.e., $k_o = 1.0$), or are very close at the eutectic temperature when eutectic growth is of prime interest. For example, binary alloys having $k_o \approx 1$ include silver alloys containing Cd, Li, and Zn; gold alloys containing Ag, Al, Cd, Co, Cu, Ga, Fe, Pd, and Zn; iron alloys containing Be, Co, Mn, Ni, Si, and V; and nickel alloys of Cr, Mn, Ta, Ti, and V. In addition to $k_o \approx 1$, many systems have liquidus and solidu adequately representable only by cubic or higher degree functions of the melt temperature. Such systems include Ga in Au, Cd in Mg, Mg in Cd, Co in Pd, Mo Cr, Cr in Pd, Cr in Ti, Cu in Pd or Pt, Mn or Ni in Fe, Cr, Cr, Fe, and Ni in Pt, and Ta, Ti, and V in Ni.

As an example, consider the case of Sb in Ge. Here, $a = 4.668 \times 10^{-3}$, $b = -6.047 \times 10^{-6}$, $f = 1.288 \times 10^{-4}$, and $g = -8.222 \times 10^{-8}$ (Li, 1967). Hence,

$$e^{12} = -0.00133 \times (T-T_o) = -0.133\ \Delta T\ \%$$

The maximum solidification range to be considered occurs when a semiconductor-grade germanium starts to solidify at about the melting point of pure germanium (i.e., 1209K or 936°C) but finishes the solidification at the end of a rod or at the boundaries between subcells or subgrains at the eutectic temperature of 863.1K or 590°C. In this

case, $T_o = 0$ and $\Delta T = (1209-863.1)K = 346.1K$. The maximum error in the growth of Sb-doped germanium crystals is thus

$$e^{12} = -0.00133\ T\ \% = -44.7\%$$

That is, the constant-k equation consistently underestimates the actual p_1 in the Ge-Sb system. This underestimation may reach a maximum of about 44.7%.

As another example, consider Co in Ti. According to Hansen's (1958) diagram, coefficients a, b, f, and g are 2.3552×10^{-2}, 4.3175×10^{-5}, 1.4624×10^{-2}, and 6.7989×10^{-6}, respectively. The value of α may then be computed to be -0.10764%. Since the maximum solidification range is T = 908.1K, the maximum error is

$$e^{12}_{max} = \alpha\ \Delta\ T_{max} = -68.35\%$$

Thus, the amount of the critical eutectics at the grain or cell boundaries in these alloys, estimated using the constant-k equation, is always lower than the true value by up to 68.35%.

Often, the liquidus and solidus can be represented only by nth-degree polynomials of the melt temperature, i.e.,

$$c_l = \sum_{i=1}^{n} a_i T^i = \sum_{i=1}^{n} a_i (T_e - T_m)^i$$

$$c_s = \sum_{i=1}^{n} f_i T^i = \sum_{i=1}^{n} f_i (T_e - T_m)^i$$

The proportion of the remaining liquid is then given by Eq (29):

$$p_1^n = 1 - p_s^n = \prod_{i=1}^{n} \left(\frac{T-T_i}{T_o-T_i}\right)^{-q_i} = \left(\frac{T}{T_o}\right)^{a/(f-a)} \prod_{i=2}^{n} \left(\frac{1-\frac{T}{T_i}}{1-\frac{T}{T_o}}\right)^{-q} \simeq \left(\frac{T}{T_o}\right)^{a/(f-a)} \left[1 + (T-T_i) \sum_{i=2}^{n} \frac{q_i}{T_i}\right]$$

where T_i and q_i have been previously defined in connection with Eq (29).

Hence, the percentage error involved in the estimate of p_1 by means of the constant-k equation (Eq 27) when the liquidus and solidus are high-degree polynomials is:

$$e^{1n} = (p_1^1 - p_1^n)/p_1^n = \frac{-\sum_{i=2}^{n} \frac{q_i}{T_i}}{1 + (T-T_o)\sum_{i=2}^{n} \frac{q_i}{T_i}} (T-T_o) \simeq -\left(\sum_{n=2}^{n} \frac{q_i}{T_i}\right)(T-T_o) = -\left(\sum_{n=2}^{n} \frac{q_i}{T_i}\right)\Delta T \quad (39)$$

which is again proportional to solidification range $\Delta T = T - T_o$.

For ideal solutions, the molar concentration for the solvent A atoms is

$$1n\, x_A = -\frac{\Delta H_A}{R}\left(\frac{1}{T} - \frac{1}{T_A}\right) = -\frac{\Delta H_A}{RT_A^2} T \left(1 - \frac{T}{T_A}\right)^{-1} \simeq \frac{-\Delta H_A}{RT_A^2} T\left(1 + \frac{T}{T_A} + \frac{T^2}{2T_A^2} + \ldots\right)$$

The molar concentration for the solute species is

$$x_B = 1 - x_A \simeq \frac{\Delta H_A}{RT_A^2} T + \frac{\Delta H_A}{RT_A^3} T^2 + \ldots = \sum_{n=i}^{n} a_i T^i \text{ or } \sum_{i=1}^{n} f_i T^i,$$

for the liquidus or solidus lines, respectively.

Hence, an exponential function of the melt temperature in the liquidus and solidus equations can be approximated by appropriate polynomial functions of the melt temperature. The percentage errors involved in the use of the constant-k equation can, therefore, be similarly estimated or computed.

2.4.5 The Last Portion of Freezing Melt

Chalmers (1969) discussed the fact that normal freezing of an alloy melt results in the last material solidifying at concentrations higher, sometimes considerably so, than that of the original liquid. In 1939, Hayes and Chipman stated without proof that the last portion to freeze may be a eutectic.

To understand why the last portion of a melt to solidify under nonequilibrium conditions always takes place at eutectic temperature T_u (Fig. 1-13) yielding, invariably, the eutectic, we can intuitively reason as follows. We consider only the extreme case of a very dilute melt whose initial solute concentration is $c_o \simeq 0$. During one step of the freezing process the melt temperature decreases by perhaps $\Delta T_m = -\Delta T = 10K$ or $1K$, with an always incomplete or <u>fractional</u> loss by solidification, i.e., Δp or $\Delta p/(1-p)$ respectively, of the melt. Simultaneously, both the freezing solid and remaining melt are solute-enriched according to the solidus and liquidus curves (for the usual case when $k < 1$, as shown in Fig. 2-2). This stepwise nonequilibrium freezing process may be repeated many times, but eventually the melt temperature T_m must come down to T_u. At T_u, there must still be a finite but perhaps very small amount of the liquid melt left (since a fraction of a small fraction is still a finite fraction). This liquid, being at T_u, has the eutectic composition $c_u = c_{\ell u}$.

One can also obtain a proof of this conclusion from the normal freezing equations. Since at $T_m = T_u$, $c_s = c_{su}$, the proportion of the normally-frozen eutectic P_u is from Eq (27), for the constant-k case with linear liquidus and solidus lines.

$$p_u = \left\{1-p\right\}_{T_m=T_u} = \left(\frac{c_{su}}{kc_o}\right)^{\frac{1}{k-1}} \tag{40}$$

When the liquidus and solidus curves are quadratic functions of the melt temperature T_m, i.e., $c_\ell = a\,(T_e-T_m) + (T_e-T_m)^2$ and $c_s = f(T_e-T_m) + g_1\,(T_e-T_m)^2$, the appropriate normal freezing equation gives

$$p_u = \left\{1-p\right\}_{T_m=T_u} = \left(\frac{T_e-T_u}{T_e-T_i}\right)^r \cdot \left[\frac{(a-f) + (b-g)\,(T_e-T_u)}{(a-f) + (b-g)\,(T_e-T_i)}\right]^q \tag{41}$$

where r and q are constants for a given alloy system, as defined by Li (1067a); and a, b, f, and g correspond, respectively, to A_ℓ, b_ℓ, a_s, and b_s.

Since c_{su}, c_o, k, T_e, T_u, and T_i all have real, positive values, and since a,

f, b, g, r, and q are all real constants for a given alloy system (with $a > f \gg |b| \simeq |g|$), P_u must therefore be real, positive, nonzero, and calculable.

Similar mathematical proofs can be obtained for cases where the liquidus and solidus curves are cubic and higher-degree functions of the melt temperature (Li, 1968); are exponential functions of the reciprocal absolute melt temperature, i.e., ideal solutions (Li, 1971); or are portions of a ternary constitutional diagram of the pseudo-binary type (Li, 1972).

It should be emphasized that determining p_u from Eq (27), particularly when c_o is small, represents its worst-case usage. As will be pointed out, such a usage is not only pedagogically incorrect but may yield erroneous and completely misleading results. Such not uncommon usages (see, e.g., Flemings and Mehrabian, 1971) are, therefore, to be discouraged.

Mathematical proofs with the aid of the non-constant-k, normal freezing equations are, therefore, necessary for most cases where the liquidus and solidus lines are curves rather than straight lines. The intuitive proof given above is particularly desirable because it is universally true and applies to all normal freezing conditions, regardless of the types and shapes of the constitutional diagrams. All these proofs are, however, based on the assumptions of zero solid diffusion and infinite liquid diffusion. While solid diffusion is negligible in most freezing studies, as will be more full discussed, the liquid diffusion in actual freezing processes is never infinite. This condition results in a solute-enriched layer next to the solid-liquid interface (Tiller et al, 1953). The higher solute concentration in this layer, rather than the lower concentration in the main body of melt, now determines the concentration of the freezing solid. That is, the effective (variable) segregation coefficient k_e is now increased toward unity. However, k_e never reaches unity at finite growth velocity (that is, solute rejection by the freezing solid into the remaining liquid is unavoidable) and, above all, there is always a final solidifying portion in which the freezing conditions are nearly normal (Tiller et al, 1953). Hence the last solidifying eutectic weight or volume is never completely eliminated.

The above discussion thus shows that nonequilibrium freezing always results in the formation of a finite amount of eutectic at the eutectic temperature no matter how small the initial solute concentration.

2.4.6 Numerical Computation of Normal Freezing

The array of normal freezing equations presented above does not cover all conceivable types of constitutional diagrams. Often, the liquidus and solidus lines are not simple polynomial functions of the melt temperature. Computations, using closed-form equations, of the normal freezing behavior directly from basic thermodynamic constants are impossible for cases where the liquidus and solidus lines are not simple, logarithmic, or exponential functions of the melt temperature. For example, Thurmond and Kowalchik (1960) has shown that, when the heat capacity of the pure supercooled liquid solvent is constant but that of the pure solid solvent is linearly related to the melt temperature, the logarithm of the solute concentration in the liquid has three additive terms in addition to the one previously given for the ideal binary solution case. Here, the normal freezing differential equation cannot be solved exactly. Reisman (1970) has presented a large number of complicated equations for the liquidus lines, the normal freezing differential equation of which cannot be solved exactly and numerical methods must be used.

In most cases, the liquidus and solidus lines can be adequately represented by polynomial functions of the melt temperature. Yet, determination of the roots of the polynomial functions for insertion into the closed-form, general normal freezing equation, Eq (30), must be accomplished numerically if the polynomial functions are of quatic or higher degrees. Hence, there is a definite need for a reliable numerical methods of known accuracy that can be applied to any type of constitutional diagram.

A literature search failed to reveal such a numerical method. Gulliver in 1922 and Brody and Flemings in 1966 presented the same numerical method for variable-k, normal freezing computations. This is a combined graphic and finite-difference (Butler and Kerr 1962) method that approximates the liquidus and solidus curves by a series of straight-line segments. Pfann's equation, Eq (25), is repeatedly used, once for each pair of the segments between two consecutive isotherms. This method is simple and convenient, but its accuracy is limited by the large (at least 5 or 10%)

errors introduced when graphically estimating the local liquidus and solidus slopes and by the repeated error accumulation or buildup through the many computation steps. The accuracy, therefore, cannot be high or even satisfactory for critical solidification work, no matter how small the size of each computation step. Further, the accuracy has never been compared with closed-form, normal freezing solutions, other refined numerical methods, or even the same method with reduced computation step sizes. Note that Gulliver (1922) did disclose a useful method for metallurgists at a time when numerical methodology was not advanced and when modern computers or even calculators were not available.

Two numerical computation methods are briefly described below. These are the Runge-Kutta method and a finite-difference method.

2.4.6.1 The Runge Kutta Method

The Runge-Kutta method (Kunz, 1957) can be used to numerically integrate the normal freezing differential equation and to produce the final, computed value of fraction solidified p at any melt temperature T. This method is stable and self-starting; that is, only the functional values at the initial, or a single previous, point are required to obtain subsequent functional values (i.e., p and T). For this reason, we can easily change the step size h at any step in the computations. This is particularly desirable when the computed results must be more accurate in some solidificat on ranges than in others.

The ordinary differential equation for normal freezing, given as Eq (25), can be written:

$$\frac{dp}{dT} = \frac{(1-p)\,L'(T)}{L(T) - S(T)} = f(T,p)$$

where L'(T) is the temperature derivative of L(T), L'(T) is the temperature derivative of the fraction solidified p(T), i.e., dp/dT, and f(T,p) is a new function of both T and p.

For the case with quadratic liquidus and solidus lines, for example, the above equation becomes:

$$dp/dT = f(T,p) = \frac{(1-p)\,(a+2bT)}{(a-f)T + (b-g)T^2} \tag{42}$$

The initial conditions are $p_o = 0$, $T = T_o$, $L(T_o) = c_o$, and $S(T_o) = c_{so}$ (Fig. 2-2). The above normal freezing equation is solved numerically by using a single-step, fourth-order Runge-Kutta integration process (Kunz, 1957). In this process, the value of $f(T,p)$ at $T = T_n$ is used to compute $f_{n+1}(T,p)$; earlier values f_{n-1}, f_{n-2}, etc., are not used.

The relevant equation is:

$$f_{n+1} = f_n + (k_1 + 2K_2 + 2k_3 + k_4)/6 \tag{43}$$

where, for step size h;

$$k_1 = h\, f\,(T_n, p_n)$$

$$k_2 = h\, f\,(T_n + h/2,\ p_n + k_1/2)$$

$$k_3 = h\, f\,(T_n + h/2,\ p_n + k_2/2)$$

$$k_4 = h\, f\,(T_n + h,\ p_n + k_3)$$

2.4.6.2 The Finite-Difference Method

The basic differential equation for normal freezing, Eq (25), is

$$\frac{dp}{1-p} = -d\ln(1-p) = \frac{L'(T)}{L(T) - S(T)}\, dT$$

where $C_l = L(T)$ and $c_s = S(T)$ are function of the modified melt temperature for the liquidus and solidus, respectively. $L'(T)$ is the first derivative of $L(T)$ with respect to the modified temperature T and can be found from $L(T) = c_l$.

During a short time interval Δt, T, $c_l = L(T)$, and $c_s = S(T)$ are all fairly constant, and usually both c_l and c_s are increasing. Their difference, $Q(T) = L(T) - S(T)$, can also be considered as constant, which is the essence of the finite-difference method.

Hence,

$$\ln (1-p)\Big|_{p_i}^{p_{i+1}} = \ln \frac{1-p_{i+1}}{1-p_i} = -\int_{T_i}^{T_{i+1}} \frac{L'(T)}{Q(T)}\, dT = -\frac{1}{Q(T_i)} L(T)\Big|_{T_i}^{T_{i+1}}$$

$$= \frac{1}{Q(T_i)} \left[L(T_i) - L(T_{i+1}) \right] = Z_i - \frac{L(T_{i+1})}{Q(T_i)} , \tag{44}$$

where

$$Z_i = \frac{L(T_i)}{Q(T_i)} \tag{44a}$$

Knowing p_i at $T = T_i$, we can estimate p_{i+1} at $T = T_{i+1}$ (so that $\Delta T = T_{i+1} - T_{i1}$), as follows:

$$p_{i+1} = 1 - (1-p_i) \exp \left[Z_i - \frac{L(T_{i+1})}{Q(T_i)} \right] \tag{45}$$

Equations (44) and (45) allow us to compute the complete normal freezing behavior of an alloy having an initial solute concentration in the melt $c_o = c_{\ell o}$. The starting point for this computation is the point at which the liquid begins to greeze, i.e., $p_o = 0$, $T = T_o$, $c_l = c_{lo} = c_o$, $c_s = c_{so}$, and $Q(T_o) = L(T_o) - S(T_o)$. From these known values of parameters, Z_o can be computed by Eq (44a), from which

$$Z_o = L(T_o)/Q(T_o) = \frac{c_l}{c_{lo} - c_{so})}$$

We can then specify a constant (or variable) value of incremental temperature $\Delta T = T_{i+1} - T_i$, and find the successive values of T. From these T's, we can compute the values of L(T), S(T), and Q(T) = L(T) - S(T) for substitution and use in Eq (45).

Note that, in deriving Eq (45), the value of L(T), S(T), and Q(T) = L(T) - S(T) are assumed constant during the very short time interval Δt or temperature interval $\Delta T = T_{i+1} - T_i$. This represents the zero-th order approximation of polynomials L(T) and S(T). This approximation is selected to integrate the basic normal freezing equation, Eq (25), for use in the finite-difference method. As will be shown, this method gives useful results when compared with exact solutions from Eq (28) - (30).

Another way to integrate Eq (25) for use in the finite-difference method is to consider S(T) constant during the very short time or temperature interval. We then have

$$\frac{dp}{1-p} = -d\ell n\,(1-p) \qquad \frac{'(T)}{\ } - S(T)\ dT = d\ell n\,[L(T)-S(T)] \tag{46}$$

The results, computed according to Eq (46) are, however, no better than those obtained from Eq (44) - (45); they are therefore omitted from further discussion.

Added accuracy in the computed results may be achieved if we replace $Q(T_i)$ in Eq (44) and (45) by $Q(T_{i,\ i+1})$, the average of the two values of Q(T) at $T = T_i$ and $T = T_{i+1}$, respectively. We therefore have a choice of the following two computation schemes, which are arranged in the general order of decreasing accuracy in results but increasing ease in usage:

I. Equations 44 and 45, together with $Q(T_{i,\ i+1})$ and $Q(T_{i+1,\ i+2})$

II. Equations 44 and 45, together with $Q(T_i)$ and $Q(T_{i+1})$.

2.4.7 Computation Example

The following computations illustrate the above procedures. The alloy melt considered here consists of 10% Sb in Ge, i.e., $c_o = 0.10$.

The liquidus and solidus curves, L(T) and S(T) respectively, for the Ge-rich portion of the Ge-Sb system have been determined and represented by second-order equations, from which we find:

$$T_o = 22.05K$$

$$c_{s_o} = G(T_o) = 0.00280$$

$$Z_o = \frac{c_o}{c_o - c_{s_o}} \quad 1.03$$

Table 2-2 gives the computed values of the fraction, p, of solidified melt at 17 different melt or interface temperatures, for 10% Sb in Ge. Both computation schemes were used, together with a ΔT of from 10K down to 0.0001K in five decades. The number of sets of computed results thus varied from 32 (for ΔT = 10K) to 324,104 (for ΔT = 0.001K). Only a small fraction of these results are tabulated. Table 2-2 also includes the corresponding values of p computed with a closed-form equation derived for cases where both the liquidus and solidus curves can be expressed as quadratic equations of T, Eq (27), such as those given above for the Ge-Sb system.

In comparing the p values at a particular T, we notice that:

- The two computation schemes gave results close to the corresponding values obtained from the closed-form solution. This indicates that the numerical method is useful, at least for 10% Sb in Ge
- Scheme I gave much better results than scheme II. Thus, the value of averaging L(T), S(T), and Q(T) during the computations is substantial, and averaging procedures should generally be used.
- Decreasing ΔT generally improved accuracy or decreased deviation from the closed-form solution values, as would be expected
- For a given scheme with a specified ΔT, accuracy consistently improved with the decreasing melt temperature, Tm.

These conclusions are quantitatively disclosed in Table 2-3, which gives the average and standard deviations from the p's by the closed-form solution, for the different schemes. This table shows that for 10% Sb in Ge:

TABLE 2-2. VALUES OF p AT DIFFERENT MELT TEMPERATURES AS COMPUTED BY DIFFERENT METHODS, TOGETHER WITH VARIOUS VALUES OF ΔT FOR 1% Sb IN Ge

ΔT, K / scheme / T, K	ΔT 10K		ΔT 1K		ΔT 0.1K		ΔT = 0.01K		ΔT = 0.001K		Closed-Form Solution
	I	II	I	II	I	II	I	II	I	II	
1187.1	0	0	0	0	0	0	0	0	0	0	0
1167.1	0.46792	0.52733	0.47076	0.47623	0.47201	0.47255	0.47091	0.47097	0.47082	0.47083	0.47079
1147.1	0.63279	0.68569	0.63513	0.64014	0.63570	0.63620	0.63521	0.63526	0.63519	0.63519	0.63515
1127.1	0.71628	0.76132	0.71818	0.72251	0.71851	0.71894	0.71823	0.71827	0.71824	0.71825	0.71820
1107.1	0.76638	0.80535	0.76798	0.77175	0.76820	0.76857	0.76801	0.76805	0.76804	0.76805	0.76800
1087.1	0.79956	0.83398	0.80095	0.80429	0.80110	0.80143	0.80097	0.80101	0.80101	0.80101	0.80096
1067.1	0.82298	0.85394	0.82421	0.82723	0.82432	0.82462	0.82423	0.82426	0.82427	0.82427	0.82422
1047.1	0.84024	0.86853	0.84136	0.84412	0.84144	0.84172	0.84138	0.84141	0.84142	0.84142	0.84137
1027.1	0.85337	0.87955	0.85439	0.85696	0.85446	0.85472	0.85441	0.85444	0.85446	0.85446	0.85440
1007.1	0.86356	0.88806	0.86452	0.86692	0.86457	0.86481	0.86453	0.86456	0.86458	0.86458	0.86453
987.1	0.87159	0.89474	0.87249	0.87476	0.87253	0.87276	0.87251	0.87253	0.87256	0.87256	0.87250
967.1	0.87797	0.90003	0.87882	0.88098	0.87885	0.87907	0.87883	0.87886	0.87889	0.87889	0.87883
947.1	0.88303	0.90422	0.88385	0.88593	0.88388	0.88408	0.88386	0.88388	0.88391	0.88391	0.88385
927.1	0.88702	0.90752	0.88781	0.88983	0.88784	0.88804	0.88783	0.88785	0.88788	0.88788	0.88782
907.1	0.89012	0.91007	0.89089	0.89285	0.89091	0.89111	0.89091	0.89093	0.89097	0.89097	0.89090
897.1	0.89245	0.91199	0.89320	0.89512	0.89322	0.89341	0.89322	0.89324	0.89328	0.89329	0.89321
877.1	0.89409	0.91333	0.89483	0.89672	0.89485	0.89504	0.89485	0.89487	0.89492	0.89492	0.89484

TABLE 2-3. AVERAGE AND STANDARD DEVIATIONS FROM THE p's, OBTAINED BY THE CLOSED-FORM SOLUTION, FOR DIFFERENT COMPUTATION SCHEMES TOGETHER WITH VARIOUS VALUES OF ΔT FOR 10% Sb IN Ge

ΔT, K	10	1.0	0.1	0.01	0.001
No. of Results per Set, n	32	324	3239	32,398	324,104
• Computation Scheme I					
- Average Deviation	-1.274×10^{-3}	-1.342×10^{-5}	1.594×10^{-7}	4.675×10^{-6}	5.175×10^{-5}
- Standard Deviation	6.326×10^{-4}	6.497×10^{-6}	2.507×10^{-7}	1.728×10^{-6}	1.494×10^{-5}
• Computation Scheme II					
- Average Deviation	2.919×10^{-2}	2.940×10^{-3}	2.938×10^{-4}	3.415×10^{-5}	5.415×10^{-5}
- Standard Deviation	1.171×10^{-2}	1.093×10^{-3}	1.087×10^{-4}	9.582×10^{-6}	1.390×10^{-5}

- Minimum discrepancy from the closed-form results for each scheme was reached with a medium ΔT. Scheme I reached minimum standard deviations of about 3×10^{-7} with a ΔT of 0.1K, while scheme II had minimum standard deviations of about 1×10^{-5} with a ΔT of 0.01K
- Except with a ΔT of 0.001K, scheme I generally gave results one to over two orders of magnitude more accurate than corresponding values obtained from scheme II
- The average deviations of the results from p (from Eq (27) computed with scheme II were consistently positive; that is, this scheme usually overestimated p. Scheme I, on the other hand, changed from underestimation to overestimation as ΔT decreased from 10K to 0.001K
- Average deviations were as low as 1.6×10^{-7} for scheme I with $\Delta T = 0.1K$. Even with $\Delta T = 10K$, the same scheme had an average deviation of only -1.3×10^{-3}.

Knowing the standard deviations and number, n, of results per set, one can easily compute the maximum probable deviations for any single result. Thus since scheme I had an average deviation from p of -1.34×10^{-5} and a standard deviation of 6.50×10^{-6} with a ΔT of 1.0K and n of 324, 95% of the time one would expect any single numerically computed result to be accurate within the range $-1.34 \times 10^{-5} \pm 2.0 \times 6.50 \times 10^{-6}$ or -4.0×10^{-7} and -2.64×10^{-5}; that is, under these conditions the numerically computed result is almost always underestimated, by from 0.40 to 26.4 ppm in 95 times out of 100.

The above finite-difference procedures are well-adapted to rapid, automatic machine computations. Further, all these procedures apply for any liquidus or solidus curves that can be represented by reasonable mathematical functions, F(T) and G(T), respectively. These functions may be power series of T and include, as special cases, the simple straight-line (constant k) or quadratic equations shown above. These functions may also be exponential, logarithmic, or other types. Even several different functions for the same liquidus or solidus curve, but in different freezing ranges, can be handled with nearly equal facility and computational speed.

PART III

NUMERICAL PROGRAM

Section 1. INTRODUCTION

To understand solute segregation and defect formation in single crystal growth thoroughly, one requires a complete characterization of the (mass) diffusion and temperature fields in the solid and remaining melt. The zero-gravity effect on solidification appears to be subtle and may be overshadowed by other effects invariably in any such growth process, a condition necessitating that such characterization be accurately defined. Unfortunately, the coupled partial differential equations for the diffusion and temperature fields are generally not solvable. Although special-case solutions have been given for some types of physically nonsatisfying two-phase Stefan problems, we must resort to numerical computations for the general case solution. Existing numerical methods are always subject to such unrealistic assumptions as constancy of interfacial temperature, segregation coefficients, diffusion constants, and other material thermophysical properties.

A program for the numerical solution of unidirectional solidification (or crystal growth) from a semi-infinite binary alloy (with nonconstant segregation coefficient) has therefore been initiated. We numerically determine the interphase temperature, and temperatures and concentrations of the mesh points, for the interphase point after each time interval. The interphase temperatures and the temperatures and concentrations for the two adjacent mesh points are solved, iteratively, only after convergence has been obtained. The temperatures and concentrations of the remaining mesh points are determined by solving two tridiagonal systems of linear equations. The semi-infinite nature of the problem is handled by admitting as mesh points enough points, so that conditions at the penultimate (next to last) point have not changed significantly from the original ones. A scheme with variable time intervals is adopted to achieve convergence within reasonable computing time.

We have checked out the program for a binary alloy. The results compare favorably with those of the exact analytic solution, differing mainly in that the interphase temperature is not constant as assumed by the analytic solution.

Section 2. MATHEMATICAL DEFINITION OF THE SOLIDIFICATION PROBLEM

We consider here a liquid binary alloy directionally solidified into two phases, liquid and solid. We consider the liquid alloy to be semi-infinite with original (at t = 0) temperature T_o and concentration C_o. Solidification occurs when the temperature at x = 0 is changed from T_o to a lower value T_1, either instantaneously or gradually, such that T_1 is below the temperature T_2 at which the liquid mixture at concentration C_o can be in equilibrium with a solid phase. As solidification occurs, the solid phase grows and its boundary is given by x = y(t), the interface point, and the interface temperature at this point is $T_i(t)$. The partial differential equations describing the solidification process are:

$$a_s^2 \frac{\partial^2 T_s}{\partial x^2} = \frac{\partial T_s}{\partial t} ; D_s \frac{\partial^2 C_s}{\partial x^2} = \frac{\partial C_s}{\partial t} \text{ for } o < x < y(t) \tag{47}$$

$$a_\ell^2 \frac{\partial^2 T_\ell}{\partial x^2} = \frac{\partial T_\ell}{\partial t} ; D_\ell \frac{\partial^2 C_\ell}{\partial x^2} = \frac{\partial C_\ell}{\partial t} \text{ for } y(t) < x < \infty \tag{48}$$

The variables T and C represent the temperature and concentration (of solute in solvent) and the subscripts ℓ and s denote the liquid and solid phases, respectively. The quantities A_s, A_ℓ, D_s, and D_ℓ are assumed constant. The following conditions are assumed throughout:

$$T_\ell (x, 0) = T_o \text{ and } C_\ell (x, 0) = C_o \tag{49a}$$

$$T_\ell (\infty, t) = T_o \text{ and } C_\ell (\infty, t) = C_o \tag{49b}$$

$$T_s\,[y(t),\ t] = T_\ell\,[y(t),\ t] = T_i(t) \tag{49c}$$

$$C_s\,[y(t),\ t] = f_s\,[T_i(t)] \tag{49d}$$

$$C_\ell\,[y(t),\ t] = f_1\,[T_i(t)] \tag{49e}$$

$$\rho\gamma\dot{y}(t) = k_s \frac{\partial T_s}{\partial x} - k_\ell \frac{\partial T_\ell}{\partial x} \quad \text{for } x = y(t) \tag{49f}$$

$$\left\{f_s\,[T_i(t)] - f_\ell\,[T_i(t)]\right\} y(t) = D_\ell \frac{\partial C_\ell}{\partial x} - D_s \frac{\partial C_s}{\partial x} \quad \text{for } x = y(t) \tag{49g}$$

Equation (49a) specifies that the original mixture is all liquid at temperature T_o and concentration C_o. Equation (49b) is a consequence of the semi-infinite nature of the mixture so that, at any time t, the portion near infinity is unchanged. Equation (49c) assumes that there is an interface temperature $T_i(t)$ at the solid-liquid interface plane and that both the solid and liquid phases at $x = y(t)$ have this temperature; there is no jump in temperature. Equations (49d) and (49e) state that the concentrations of solid and liquid at the interface are given by the solidus and liquidus curves, respectively, of the constitutional diagram for the alloy. Equation (49f) connects the derivative of the moving boundary with the redistribution of temperature, and Eq (49g) connects the same boundary with that of the concentration.

The conditions on $T_s(o,\ t)$ and $C_s\ (o,\ t)$ are not fixed in our discussion and a number of alternatives are considered:

- $T_s\ (o,\ t) = T_1(t)$, with $T_1(t)$ equal to a constant for all t,
- Linear, $T_1(t) = T_o + t(T_1 - T_o)/s$ for $t < s$ and $T_1(t) = T_1$ for $t \geq s$,
- Exponential, $T_1(t) = T_1 + (T_o - T_1)\, e^{-t/s}$, so $T_1(0) = T_o$ and $T_1\ (\infty) = T_1$.

For $C_s(o, t)$ the conditions considered are $C_c(o, t) = c_1$, usually taken $C_s(T_2)$, or at times a condition conserving mass between 0 and ∞.

Our two approaches may be designated as analytic and numerical. The numerical approach can be applied to all three conditions on temperature, whereas the analytic approach holds only the case of constant temperature instantaneously applied. A variant of the analytic method, i.e., applying linearly varying temperature, should be investigated.

Section 3. THE ANALYTIC SOLUTION

A similiarity solution can be written in the form

$$y(t) = 2\beta\sqrt{t} \tag{50a}$$

$$T_s = T_1 + (T_i - T_1)\,\mathrm{erf}\,(x/2a_s\sqrt{t})/\mathrm{erf}\left[y(t)/2a_s\sqrt{t}\right] \tag{50b}$$

$$T_\ell = T_o + (T_i - T_o)\,\mathrm{erfc}\,(x/2a_\ell\sqrt{t})/\mathrm{erfc}\left[y(t)/2a_\ell\sqrt{t}\right] \tag{50c}$$

$$C_s = C_1 + \left[f_s(T_i) - C_1\right]\mathrm{erf}\,(x/2\sqrt{D_s t})/\mathrm{erf}\left[y(t)/2\sqrt{D_s t}\right] \tag{50d}$$

$$C_\ell = C_o + \left[f_\ell(T_i) - C_o\right]\mathrm{erfc}\,(x/2\sqrt{D_\ell t})/\mathrm{erfc}\left[y(t)/2\sqrt{D_\ell t}\right] \tag{50e}$$

The quantities T_i and β are determined from the boundary conditions. It is clear that, if $T_1 \geq T_2 = f_\ell^{-1}(C_o)$, then there is no solidification, $C_1(x, t) = C_o$, and $T_1(x, t) = T_o + (T_1 - T_o)\,\mathrm{erfc}\,(x/2a_\ell\sqrt{t})$. The solution given above satisfies boundary conditions (49a, b, c), and equations (49f) and (49g) are employed to determine β and T_i as follows (Rubenstein, 1971):

$$y = \beta\sqrt{t} \tag{51a}$$

$$\frac{\partial T_s}{\partial x} = (T_i - T_1)\frac{2}{\sqrt{\pi}}e^{-\frac{x^2}{4a_s^2 t}} \cdot \frac{1}{2a_s\sqrt{t}}/\mathrm{erf}\left[y(t)/2a_s\sqrt{t}\right] \tag{51b}$$

$$\frac{\partial T_\ell}{\partial x} = (T_i - T_o) \cdot \frac{2}{\sqrt{\pi}} e^{-\frac{x^2}{4a_\ell^2 t}} \cdot \frac{1}{2a_\ell\sqrt{t}} / \operatorname{erfc}\left[y(t)/2a_\ell\sqrt{t}\right] \tag{51c}$$

$$\frac{\partial C_s}{\partial x} = \left[f_s(T_i) - C_1\right]\frac{2}{\sqrt{\pi}} e^{-\frac{x^2}{4D_s t}} \frac{1}{2\sqrt{D_s t}} / \operatorname{erf}\left[y(t)/2\sqrt{D_s t}\right] \tag{51d}$$

$$\frac{\partial C_\ell}{\partial x} = \left[f_\ell(T_i) - C_o\right] \cdot -\frac{2}{\sqrt{\pi}} e^{-\frac{x^2}{4D_\ell t}} \frac{1}{2\sqrt{D_\ell t}} / \operatorname{erfc}\left[y(t)/2\sqrt{D_\ell t}\right] \tag{51e}$$

Substituting in Eq (49f) and (49g), eliminating the factor $\frac{1}{\sqrt{t}}$, and replacing x by y(t) and y(t) by $2\beta\sqrt{t}$, we get

$$\rho\gamma\beta = \frac{k_s (T_i - T_1) e^{-\frac{\beta^2}{a_s^2}}}{a_s\sqrt{\pi}\operatorname{erf}(\beta/a_s)} + \frac{k_\ell (T_i - T_o) e^{-\frac{\beta^2}{a_\ell^2}}}{a_\ell\sqrt{\pi}\operatorname{erfc}(\beta/a_2)} \tag{51f}$$

$$\left[f_s(T_i) - f_\ell(Ti)\right]\beta = \frac{-\sqrt{D_\ell}\left[(f_\ell(T_i) - C_o\right] e^{-\frac{\beta^2}{D_\ell}}}{\sqrt{\pi}\operatorname{erfc}(\beta/\sqrt{D_\ell})} - \frac{\sqrt{D_s}\left[f_s(T_i) - C_1\right] e^{\frac{\beta^2}{D_s}}}{\sqrt{\pi}\operatorname{erf}(\beta/\sqrt{D_s})} \tag{51g}$$

By rewriting Eq (51f) solving for T_i, we get

$$T_i = \frac{\left[\sqrt{\pi}\rho\gamma\beta e^{\frac{\beta^2}{a_\ell^2}} \operatorname{erfc}\left(\frac{\beta}{a_\ell}\right) a_s a_\ell \operatorname{erf}(\beta/a_s) + T_1 k_s a_\ell e^{\frac{\beta^2}{a_\ell^2} - \frac{\beta^2}{a_s^2}} \operatorname{erfc}(\beta/a_\ell) + T_o k_\ell a_s \operatorname{erf}(\beta/a_s)\right]}{\left[k_s a_\ell e^{\frac{\beta^2}{a_\ell^2} - \frac{\beta^2}{a_s^2}} \operatorname{erf}\left(\beta/a_\ell\right) + k_\ell a_s \operatorname{erf}\left(\beta/a_s\right)\right]} \tag{51h}$$

3.1 NUMERICAL METHOD FOR THE ANALYTIC SOLUTION

The successful method for solving the pair of equations (51g) and (51h) involved starting with an arbitrary (usual small) value for β. Substituting in Eq (51h) gave a value for T_i, and using the values for β and T_i in the right-hand side of Eq (51h) and in the multiplier of β gave a new value for β. This value was checked against the previous value, and if they agreed to a desired accuracy the solution was accepted. Otherwise, the two values were averaged and the procedure repeated. Failure of the procedure to converge after a reasonable number of iterations suggested that a different starting value be tried. Sometimes, iterates which failed to converge suggest a better starting value: if they diverge immediately try a smaller value, and if they oscillate try a value close to the point about which they seem to oscillate.

A modification of the analytic method, based upon the assumption that β need not be constant and that T_i also varies, has been included in the program. The assumption is that $y(t) = 2\beta(t)\sqrt{t}$, where $\beta(t) = \beta_o + \beta_1 t + \beta_2 t^2 + \ldots \beta_j t^j$ and

$$T_i(t) = T_{io} + tT_{i1} + . + t^j T_{ij} \tag{52}$$

This procedure was originally used to determine whether solutions of this more complex form existed, but was inconclusive because the values of the higher-term coefficients were sufficiently small to be explained away by computation error. However, this procedure may be useful in connection with a solution to the more realistic problem where $T_1(t)$ is variable. This is yet to be investigated.

The method of solution follows lines similar to those given above.

$$\dot{y}(t) = \frac{\beta_o}{\sqrt{t}} + 3\beta_1\sqrt{t} + \ldots + (2j+1)\beta_j t^{j-\frac{1}{2}} = \frac{\beta_d}{\sqrt{t}} \tag{53}$$

where

$$\beta_d = \beta_o + 3\beta_1, t + \quad + (2j+1)\beta_j t^j$$

First, assume initial estimates of β_0, β_1, ..., β_j and values of t = 0, Δt, ..., $j\,\Delta t$. Next, determine values of $T_i(t)$ and $\beta(t)$ by substituting into (51g) and (51h), taking care to replace β by β_d in those terms obtained from the derivative. Using the values of $\beta(t)$, we can find the coefficients by solving a linear system; these coefficients can then be compared with the previous estimates. If they agree, we can find the values of $T_i(t)$ for the coefficients T_{io}, ..., T_{ij}. If they do not agree to the required accuracy, the coefficients of $\beta(t)$ are averaged and the process repeated. To find estimates for the starting values β_o, β_1, ...β_j, we first solve for j-1 and use the coefficients so obtained as a first estimate for j, with β_j set equal to $-\beta_{j-1}{}^* .001$. Thus, we solve a sequence of problems j = 0, 1, ..., up to the desired value of j. The numerical results using this technique has been good, although its application to the case of constant T_1 has not been fruitful.

The only boundary condition for $C_s(o,t)$, discussed above, has been $C_s(o,t) = C_1$, a constant for all t. A variant condition is one based upon conservation of solute:

$$\int_o^{y(t)} (C_s - C_o)\,d\,x + \int_{y(t)}^{\infty} (C_\ell - C_o)\,d\,x = 0 \tag{54}$$

Using the expressions for C_s and C_ℓ in the analytic solution (Eq 50 c, d), we have

$$(C_1 - C_o)y(t) + \frac{f_s(T_i) - C_1}{\text{erf}\,(y/2\sqrt{D_s t})} \int_{\infty}^{y(t)} \text{erf}\,(x/2\sqrt{D_s t})dx + \frac{f_\ell(T_i) - C_o}{\text{erfc}\,(y/2\sqrt{D_\ell t})}$$

$$\int_{y(t)}^{\infty} \text{erfc}\,(x/2\sqrt{D_{it}})dx = 0 \tag{55}$$

$$\left.\begin{aligned} \int_o^u \text{erf}\,v\,d\,V &= u\,\text{erf}\,u + \frac{1}{\sqrt{\pi}}\,(e^{-u^2} - 1) \\ \text{and}\ \int_u^{\infty} \text{erfc}\,v\,d\,v &= -u\,\text{erfc}\,u + \frac{1}{\sqrt{\pi}}\,e^{-u^2} \end{aligned}\right\} \tag{56}$$

we obtain the relation

$$\left[f_s(T_i) - f_\ell(T_i)\right] y(t) + \frac{f_s(T_i) - C_1}{\text{erf}\,(y/2\sqrt{D_s t})} \cdot 2\sqrt{D_s t} + \frac{1}{\sqrt{\pi}}\left(e^{-\left[\frac{y(t)}{2\sqrt{D_s t}}\right]^2} - 1\right)$$

$$+ \frac{f_\ell(T_i) - C_o}{\text{erfc}\,(y/2\sqrt{D_\ell t})} \cdot 2\sqrt{D_\ell t}\,\frac{1}{\sqrt{\pi}}\, e^{-\left[\frac{y(t)}{2\sqrt{D_s t}}\right]^2} = 0 \qquad (57)$$

By comparing this condition with Eq (49g), we have

$$\left[f_s(T_i) - f_\ell(T_i)\right]\left[y(t) - 2t\dot{y}(t)\right] = \frac{1}{\sqrt{\pi}} \frac{f_s(T_i) - C_1}{\text{erf}\,(y/2\sqrt{D_s t})} \cdot 2\sqrt{D_s t} \qquad (58)$$

For the case where $y(t) = 2\beta\sqrt{t}$, $y(t) = 2t\dot{y}(t)$ and the condition is $f_s(T_1) - C_1 = 0$. This means that the concentration of the solid solute at $x = 0$ is the same as the concentration at the interface, and hence the concentration of the solute in the solid is constant everywhere. This is equivalent to the condition given by Rubinstein (1971): $\frac{\partial C_s}{\partial x} = 0$ at $x = 0$, which implies that $C_1 = f_s(T_i)$. However, if $(y(t) - 2t\dot{y}(t)$ is not zero, $f_s(T_i) - C_1$ can be computed to determine C_1 at every time interval.

The program for computing temperature and concentrations for the solidification of a binary alloy system is named BISCL. BISCL employs a subroutine BETTI to determine the values of β and T_i. The main program computes, for each instant of time t, $y(t)$, $\dot{y}(t)$, T_i, $f_s(T_i)$, and $f_\ell(T_i)$ and then, for each (x,t), $T(x,t)$ and $c(x,t)$. The spacing for x may be equal; $j\,\Delta x$ for $j = 0, 1, \ldots$ Ix-1 given by IAM = 0, or $0, 2^{j-1}\Delta x$ for $j = 1, \ldots$, Ix-1 where Δx given by DELX and IAM = 1. To compute $f_s(T_i)$ and $f_1(T_i)$, the points on the solidus and liquidus curve are input as a table of triplets (T, f_s, f_i), and Lagrangian interpolation is used to interpolate between tabular points. The number of interpolating points L is less than or equal to the number of triplets IF. The time intervals are equal, given by DELP, and are terminated when time exceeds TF. The number of iterations permitted before the program was stopped for further iteration is given by

NIT. The number of coefficients of $\beta(t) = \beta_0 + \beta_1 t + \ldots . \beta_j t^j$ is given by KT = j + 1. In the ordinary case, KT = 1. To determine the first approximation of β, the quantity FRX is multiplied by DELX. In the case of a failure to converge, an error indicator is set in BETTI and tested in the main program permitting a change in FRX. If FRX is set to zero, the program will stop. As a boundary condition at $C_s(o,t)$ if $C_1 > 0$ is input, this is held constant. If $C_1 = 0$, then it will assume a conservation of solute concentration and compute C_1 in the program as required (see above). a_s is designated by AS, a_ℓ by AL, D_s by DS, D_ℓ by GL, T_o by TO, T_1 by T1, C_o by CO, K_s by KXS, k_ℓ by XKL, ρ by RHO, and γ by GAMMA. Quantities needed by BETTI and BISCL are transmitted by a common statement.

3.2 GLOSSARY

The following is a glossary of additional terms used by the program.

SQDS - $\sqrt{D_s}$

SQDL - $\sqrt{D_\ell}$

SQT - $\sqrt{t}$

BETA - β

BETH - θ_d

TMIN - T_i

YT - $\dot{y}(t)$

DYDT - $y(t)$

AST - $2 D_s \sqrt{t}$

ALT - $2 a_\ell \sqrt{t}$

DST - $2\sqrt{D_s t}$

DLT - $2\sqrt{D_\ell t}$

YAST - Y T /AST

FAST - erf (YAST)

YDST - YT/DST

FDST - erf (YOST)

YALT - YT/ALT

FALT - erfc (YALT)

YDLT - YT/DLT

FDLT - erfc (YDLT)

FLT - f_ℓ(TMIN)

FST - f_s (TMIN)

FLTC - FLT-CO

FSTC - FST-C1

TEMP - T(x, t)

CN - C(x, t)

Section 4. THE NUMERICAL APPROACH TO SOLIDIFICATION

In order to solve the solidification problem numerically, we devised a technique for separating the two major aspects of the computation. One aspect involves the determination of the moving interface boundary, $x = y(t)$, and also the interface temperature, T_i; the other aspect concerns the determination of the temperatures, T, and concentrations, C_s and C_ℓ, on both sides of the interface. Although it is clear that the two are interconnected for computation purposes, we first extrapolated for a new set of temperatures and concentrations at the mesh points, then determined the interface point and temperature, and finally recomputed the temperature and concentrations based upon the interface point and temperature. In case of a failure to converge quickly to the interface point and temperature, we interposed new values of the temperatures and concentrations at the mesh points to help expedite the process. With this general strategy in mind, we shall explain in detail the various aspects of the program.

4.1 THE INTERFACE PROCEDURE

At time t, we computed the values of $T(x,t)$ and $c(x,t)$ at the mesh points and the values of $y(t)$, $\dot{y}(t)$, and $T_i(t)$. In addition, we obtained the values of $T(x, t + \Delta t)$ and $c(x, t + \Delta t)$ for all mesh points by extrapolation, and approximated $y(t + \Delta t)$, $\dot{y}(t + \Delta t)$, and $T_i(t + \Delta t)$. We next computed $f_s[T_i(t + \Delta t)]$ and $f_1(t + \Delta t)]$ from a Lagrangian interpolation on the solidus and liquidus curves. Recognizing that the interface point and temperature are crucially linked with the values of temperatures and concentrations of the adjoining mesh points, we recomputed the values of C and T at these points using a difference form of the partial differential equations.

Based upon the values of the concentrations at the interface and the adjoining mesh points, we computed the partial derivatives $\frac{\partial C_s}{\partial x}$ and $\frac{\partial C_\ell}{\partial x}$ and determined $\dot{y}(t + \Delta t)$ from the boundary condition Eq (49f). Substituting in Eq (49g), we determined a new value for the interface temperature. When the values of the interface derivative and temperature agreed sufficiently with the previous estimates, these values were accepted and $y(t + \Delta t)$ is determined from $y(t + \Delta t) = y(t) + \frac{1}{2}[\dot{y}(t) + \dot{y}(t + \Delta t)]\Delta t$. With $y(t + \Delta t)$, $T_i(t + \Delta t)$,

and the values of concentrations and temperatures at the adjoining points determined, we computed $f_s\left[T_i(t + \Delta t)\right]$ and $f_1\left[T_i(t + \Delta t)\right]$ and solved for the temperature and concentrations at the other mesh points. If $y(t + \Delta t)$ and $T_i(t + \Delta t)$ did not agree sufficiently, we averaged them and the iteration repeated. If conversion was not achieved after a designated number of iterations, new values for the mesh points are determined. If convergence was not achieved after a similar number of iterations, we halved interval Δt and determined values for $T(x, t + \frac{\Delta t}{2})$, $C(x, t + \frac{\Delta t}{2})$, $y(t + \frac{\Delta t}{2})$, $\dot{y}(t + \frac{\Delta t}{2})$, and $T_i(t + \frac{\Delta t}{2})$ by interpolation. The process was repeated until convergence was attained or the time interval cut down below an acceptable level. In the latter case, the program either accepts the values attained or is stopped. An additional device which aided in inducing convergence was based on a check of montonicity. The temperature must monotonically increase from $x = 0$ to $x = \infty$, as must the interface temperature. Thus, if values that violated this monotonicity appeared, they were replaced by those found by linear interpolation. Similarly, the concentrations in the liquid will decrease from $x = y(t)$ to $x = \infty$. A monotonic behavior, either nonincreasing or nondecreasing in the solid phase depending upon the condition upon $C_s(o, t)$, can also be expected.

The values of the concentrations and temperatures for the mesh points adjoining the interface point were also determined using this iteration process. Although convergence checks were not made on concentration and temperature values it is clear that, since these values ultimately involved in the expressions for computing the interface derivative and temperature, their failure to converge would have prevented the convergence of the derivative and interface temperature.

4.2 NUMERICAL APPROXIMATIONS

In order to determine the values of $\dot{y}(t + \Delta t)$ and $T_i(t + \Delta t)$ from the boundary conditions at the interface, one must have a means for approximating partial derivatives of the form $\frac{\partial u}{\partial x}$, where u is a function of x and t. In addition, computation of the concentrations and temperatures at the adjoining mesh points require approximations for expressions of the form $\frac{\partial u}{\partial t}$ and $\frac{\partial^2 u}{\partial x^2}$. We have already indicated that $y(t + \Delta t)$ is found

from $y(t + \Delta t) = y(t) + \frac{1}{2} \dot{y}(t) + \dot{y}(t + \Delta t)\ \Delta t$, sometimes called the modified Euler equation. Although this is a lower-order method than the usual Runge-Kutta employed by other researchers in similar situations, it is preferable here because $\dot{y}(t)$ is computed by an elaborate iterative scheme. Runge-Kutta involves the use of intermediate values of $\dot{y}(t)$, which would have to be computed in the same complicated manner. Only when explicit expressions are available for $\dot{y}(t)$ can Runge-Kutta be recommended.

The expressions for the partial derivatives are base upon difference expressions, assuming unequal spacing, because the presence of a varying interface point requires approximations involving the values at this point. Although economies in computing are available if the subdivisions of the mesh are equispaced, they must be sacrificed because of the varying interface point. To require that the interface points be at mesh points would necessitate a variable time step and a very small space interval in order that convergence on $\dot{y}$ and T_i be reached after reasonable number of iterations. In addition, the semi-infinite character of the problem, with little change in variables away from the origin, suggests that the space intervals increase in size. To accommodate such a situation, the key expression for the partial derivative $\left(\frac{\partial u}{\partial x}\right)$ at $x = x_1$ is given by $\frac{u(x_1 + \Delta x, t) - u(x_1 - \Delta x, t)}{2\Delta x}$, i.e., by a second order approximation. Thus, $\frac{u(x_2, t) - u(x_1, t)}{x_2 - x_1}$ is an approximation for $\frac{\partial u}{\partial x}$ at $x = \frac{x_1 + x_2}{2}$. Similarly, the expressions for $\frac{\partial^2 u}{\partial x^2}$ based upon the values of $u(x_1, t)$, $u(x_2, t)$, and $u(x_3, t)$ is given by

$$\left[\frac{u(x_3, t) - U(x_2, t)}{x_3 - x_2} - \frac{U(x_2 t) - U(x_1, t)}{x_2 - x_1}\right] \div (x_3 - x_1)/2$$

As a consequence, if the partial $\frac{\partial u}{\partial x}$ at $x = x_1$ is required for given values at x_1, x_2, and x_3, the formula $\left(\frac{\partial u}{\partial x}\right)_{x_1}, = \frac{u(x_2, t) - u(x_1, t)}{x_2 - x_1} + \frac{x_1 - x_2}{2} \frac{\partial^2 u}{\partial x^2}$ is used, where

$\frac{\partial^2 u}{\partial x^2}$ is computed as above and gives second-order accurate results. An arithmetic function statement of the form D2(X, F, Y, G, Z, H) = ((H-G)/(Z-Y)-(G-F)/(Y-X))/(Z-X)/2) is used to compute $\frac{\partial^2 u}{\partial x^2}$ using the six quantities x_1, $u(x_1, t)$, x_2, $u(x_2, t)$, x_3 and $u(x_3, t)$.

We use a similar approach to interpret $\frac{\partial u}{\partial t}$. $\frac{\partial u}{\partial t}$ is approximated by $\frac{u(s, t+\Delta t) - u(x, t)}{\Delta t}$, evaluated at $t + \frac{\Delta t}{2}$. Thus, the equation $\frac{\partial u}{\partial t} = q \frac{\partial^2 u}{\partial x^2}$ is approximated by

$$\frac{u(x,\ t + \Delta t) - u(x,\ t)}{\Delta t} = \tfrac{1}{2} q \left[\left(\frac{\partial^2 u}{\partial x^2} \right)_t + \left(\frac{\partial^2 u}{\partial x^2} \right)_{t + \Delta t} \right]$$

Here $\frac{\partial^2 u}{\partial x^2}$ at $t + \frac{\Delta t}{2}$ has been replaced by the average of the values at t and $t + \Delta t$. This is called the Crank-Nicholson method (Ref. 81). Since the evaluation of $\frac{\partial^2 u}{\partial x^2}$ at $t + \Delta t$ involves the values of $u(x,\ t + \Delta t)$ at three values of x, this equation has three unknowns. However, as an iterative method, one can assume the values needed for $\frac{\partial^2 u}{\partial x^2}$ are known and use the equation to find an improved value for $u(x, t + \Delta t)$. In this way the values of the concentrations and temperatures at the interface-adjoining mesh points are determined. This is a reasonable approach since many iterations may be required to compute $\dot{y}(t + \Delta t)$ and $T_i(t + \Delta t)$.

Evaluation of $\dot{y}(t + \Delta t)$ is obtained from

$$\dot{y}(t) = \left(D_\ell \frac{\partial C_\ell}{\partial x} - D_s \frac{\partial C_s}{\partial_x} \right) \div \left[f_s(T_i) - f_\ell(T_i) \right]$$

The partials are evaluated from the formula for $\frac{\partial u}{\partial x}$. To find an iterate of $T_i(t + \Delta t)$ in

the equation $\rho\gamma\,\dot{y}(t+\Delta t) = K_s \frac{\partial T_s}{\partial x} - K \frac{\partial T_\ell}{\partial x}$ with partials at $t+\Delta t$, we replace

$\frac{\partial T_s}{\partial x}$ by $\frac{T_i - T_s}{y(t+\Delta t) - x_j} + \frac{x_j - y(t+\Delta t)}{2} \frac{\partial^2 T}{\partial x^2}$; and $\frac{\partial T_\ell}{\partial x}$ by $\frac{T_{j-1} - T_i}{x_{j-1} - y(t+\Delta t)}$

$+ \frac{y(t+\Delta t) - x_{j-1}}{2} \left(\frac{\partial^2 T}{\partial x^2}\right)^2_{j-1}$, where the subscripts j and j-1 indicate the mesh point after and before the interface point, respectively. We can solve for T_i, excepting the T_i terms involved in $\left(\frac{\partial^2 T}{\partial x^2}\right)_j$ and $\left(\frac{\partial^2 T}{\partial x^2}\right)_{j-1}$. This gives an iterative formula for $T_i(t+\Delta t)$. We see that the values of concentrations and temperatures at the j and j-1 points play an important role in determining $\dot{y}(t+\Delta t)$ and $T_i(t+\Delta t)$, and their convergence presumes the convergence of the four other values.

4.3 THE SOLUTION FOR REMAINING MESH POINTS

When the values of interface derivative and temperature converged, we determined the interface point and concentrations of liquid and solid at the interface. The values for the concentrations and temperatures must then be computed for the remaining mesh points. To determine these values, four systems of equations, one each for concentrations and temperatures for each side of the interface point, must be solved. Since the values on the infinite side of the interface point change gradually, one need not consider too many mesh points. By starting with a small number of points, chosen so that the last few show no change from the initial values of C_o and T_o, the number of points is increased whenever the values at the pentultimate point shows some nontrivial change. The new points again have values C_o and T_o. The values $C_s(o,t)$ and $T_s(o,t)$ are determined from the initial conditions so that they, too, are already known. The values of $C_s(x_{j-1}, t)$ and $T_s(x_{j-1}, t)$, where j-1 indicates the mesh point before the interface point, and the values of $C_\ell(x_j, t)$ and $T_\ell(x_j, t)$, where j indicates the mesh point after the interface, are also known from the iterative process. At each of the interior points, the Crank-Nicholson equation involves the values at three mesh points: before, at, and after the point for which the

equation is given. Each system of equations is not only linear (since the coefficient of $\frac{\partial^2 u}{\partial x^2}$ is assumed constant), but also tridiagonal. A subroutine (TRIST) is used to set up the coefficients of each of the systems and calls upon a standard Grumman subroutine (TRIDI) to solve them.

The same procedure is used when convergence has not been achieved and an updated set of values for concentrations and temperatures are desired for continuing the iterations. This need results because the expressions for $\frac{\partial^2 u}{\partial x^2}$ at j-1 or j depend not only on the points subscripted by j-1 and j but also on those whose subscripts are j-2 and j+1.

4.4 STARTING PROCEDURES

The previous discussion assumes that $y(t)$, $\dot{y}(t)$, $T(t)$, and all values of $C(x,t)$ and $T(x,t)$ at the mesh points are known, and that first approximations are available for time $t+\Delta t$. However, all we know at time $t = 0$ is that $y(0) = 0$, but we have no knowledge of $\dot{y}(0)$ and $T_i(0)$. Indeed, it may even be ture that no solidification begins at time $t = 0$, because the temperature at $x = 0$ may be above the temperature T_2 at which solidification can begin for the given initial concentration C_o. In the latter case, until the surface temperature reaches T_2 the problem is that of pure heat conduction, and for each time interval one solves a single tridiagonal system. After each interval, we ascertain whether the temperature at the pentultimate point has changed nontrivally so that points should be added to the mesh.

However, when the temperature at the surface is below T_2 solidification occurs and, hence, a need arises for a starting procedure to determine $\dot{y}(t)$ and $T_i(t)$. An appreciation of the problems involved can be gained from the analytic solution for the case of constant surface temperature. In this case, as was discussed earlier, $y=2\beta\sqrt{t}$, $\dot{y} = \frac{\beta}{\sqrt{t}}$, and the interface temperature is constant at T_i. Then $\dot{y}(0)$ is infinite and, hence, no value that will give useful results can be assigned to $\dot{y}(0)$. One way to begin the numerical problem is to assume that the analytic solution holds at least for the first time interval. This would only be useful for the case of constant surface temperature. In addition, the purpose of the analytic solution, i.e., to check the accuracy of the numerical

solution, would lose some of its validity. As an alternative, we may use some aspects of the analytic solution to assist in starting the solution. One such aspect is that $y(t) = 2\dot{y}(t) \cdot t$. This enables us to estimate y(t) if an approximation of $\frac{dy}{dt}$ is given. However, having no value to T_i and y at $t = \Delta t$ to begin with, we have no means of computing $\frac{dy}{dt}$ using boundary equation (49f). As a variant, we may begin with an initial estimate of Δy, determine T_i by assuming a linear law for temperature from $x = 0$ to $x = 2\Delta x$, and determine Δt from $\frac{\Delta y}{\Delta t} = \frac{dy}{dt} = (K_s \frac{\partial C_s}{\partial x} - K_\ell \frac{\partial C_\ell}{\partial x}) \div \left[f_s(T_i) - f_\ell(T_i)\right]$. From this Δt, one finds another which is of the form $DELT/2^n$ and less than previous Δt, where DELT is an input to the program. A corresponding value for $y(\Delta t)$, $T(\Delta x, \Delta t)$ is estimated linearly. From then on, the iteratives continue in the usual manner, except that y is computed as $2\dot{y}\,\Delta t$. Convergence occurs, or else Δt is cut back. The next time step no longer requires a special starting procedure. It is useful to choose the original Δy somewhere between $\frac{1}{4}$ and $\frac{1}{2}$ of the length of the first space interval ΔX. This removes y far enough from the mesh points to make the differences meaningful.

4.5 PROBLEMS CAUSED BY INTERFACE APPROACHING MESH POINT

One of the greatest obstacles in the development of the program occurred when the interface point approached a mesh point. The time interval was halved, down to the limit, until it failed to converge for the smallest interval allowable. Relaxing the minimum time interval resulted in the use of an inordinate amount of computer time, nor did it always succeed in breaking through this mesh point barrier. In addition, discontinuities in interface derivative and interface temperature appeared after the mesh point was passed. There was a tendency to correct itself, however. Hence the discontinuity due to the definition of the partial derivatives with respect to different points was an unavoidable but self-disappearing evil.

The first solution to the mesh point approach problem was the development of an extrapolation procedure whenever the interface point neared the mesh point. For example, when the interface traversed 9/10 of the mesh width, the results of the last two points were extrapolated linearly to the mesh point. This carried the program through the difficulty with only a small error due to linear extrapolation.

Another solution to the approach problem was to change those points adjoining the interface point. Whenever the interface point came within an input fraction (1-S) of the mesh width, the adjoining point on the infinite side was shifted to the next point for all iteration considerations and the values of concentration and temperature at the skipped point were determined by a linear interpolation from the interface point to the assumed adjoining point. On the other hand, the adjoining point on the zero-side of the interface was not shifted until the interface point had passed a distance a ratio S of the mesh width. For example, if S = .15 and the interface point was .85 Δx, the adjoining point on the infinite side was shifted; and when it was 1.15 Δx. the adjoining point on the zero side was shifted. With this strategy, extrapolation was replaced by linear interpolation for the skipped point. Of course, a change in reference points made for discontinuities in derivative and interface temperature, but they seemed less severe and were quickly corrected as the interface moved away from the critical region around the mesh point.

4.6 TIME INTERVAL CONTROL

As indicated in the program, the time interval is subject to variation. The program allows for large time intervals when convergence occurs quickly, and smaller intervals when convergence is slow. The two factors are the initial DELT and the number of iterations NIT. DELT represents the largest allowable time interval, and DELT/128 is the smallest. If the number of iterations to convergence is less than or equal to NIT/4 then, for the next time interval, a time step twice as large is permitted. If, on the other hand, after NIT/2 iterations no convergence has been achieved, then the time interval for the current step is halved, if allowable, and maintained for the next step. If after NIT iterations no convergence has occurred, then the step size is halved again, if allowable, and iteration count restored to NIT/2 + 1. If it is not allowable, the program may stop or accept nonconvergent results as set by input. Another situation leading to step halving is the occurrance of a negative $\frac{dy}{dt}$. Since this is not physically realizable, it is assumed that the time step being used is too large, and a smaller one substituted for accurate results.

Another option that may affect time interval control is the desire to print results at fixed intervals. Thus, if results are required at an instant of time of t + Δt exceeds

that time, then Δt is adjusted so that $t + \Delta t$ will be exactly as required. Also, for the programs where the surface temperature is variable and no solidification takes place until temperature T_2 is reached, then the solidification time is used by the program for computation. If this is not the desired time for printout, the user will not be aware of these results.

Section 5. COMPUTER PROGRAMS FOR NUMERICAL SOLUTIONS

Four main programs have been developed in accordance with the ideas described above. Two programs solve the constant surface temperature problem, one (B INCR 3) using extrapolation to the mesh point and the other (B INCR 2) using the shifting of adjoining point method. The other two programs both use the shifting of adjoining points to solve for the linear surface temperature (B INCR) and the experimental surface temperature (B INCR 4). These four main programs use the same subroutines: MOTON to preserve monotomicity, and TRIST to set up and solve tridiagonal systems. In all four programs, the solidus and liquidus curves are input in the table manner as discussed in BISCL. Also, the mesh points are set up in the same way as in BISCL.

The results in Tables 3-1 through 3-3 were obtained using BISCL for the analytic solution of the solidification of 12% Sn in Ni, with an instantaneous change of surface temperature from 1800°K to 1400°K at time t = 0. The Ni-Sn phase diagram is from Hansen (1958), while material property data was from Smithells (1968). The coefficient of $\beta(t) = \beta_o + \beta_1 t + \beta_2 t^2 + \beta_3 t^3$ and $T_i(t) = T_{io} + T_{i1} t + T_{i2} t^2 + T_{i3} t^3$ are given. The values of interface point, interface derivative, and interface temperature are given for times t = .03125 sec to 1 sec, at intervals of .03125 sec. The values of T(x,t) and C(x,t) are given for t = .03126 sec, .0625 sec, and 1 sec.

TABLE 3-1 COMPUTED SOLIDIFICATION OF 12% Sn IN Ni, ACCORDING TO THE ANALYTIC SOLUTION (Sheet 1 of 2)

β_o	β_1	β_2	β_3
0.540109E-01	-0.888091E-04	0.897718E-04	-0.425002E-04
T_{io}	T_{i1}	T_{i2}	T_{i3}
0.157333E-04	-0.168538E-00	0.134766E-00	-0.559896E-01
TIME-t	y(t)	$\dot{y}(t)$	$T_i(t)$
0.312500E-01	0.190948E-01	0.305487E-00	0.157332E-04

X	T	C
0.0	0.140000E 04	0.333330E-01
0.100000E-01	0.149360E 04	0.598702E-01
0.200000E-01	0.157956E 04	0.195808E 00
0.400000E-01	0.169378E 04	0.139609E 00
0.800000E-01	0.178779E 04	0.120246E 00
0.160000E 00	0.179999E 04	0.120000E 00
0.320000E 00	0.180000E 04	0.120000E 00
0.640000E 00	0.180000E 04	0.120000E 00
0.128000E 01	0.180000E 04	0.120000E 00
0.256000E 01	0.180000E 04	0.120000E 00
0.512000E 01	0.180000E 04	0.120000E 00
0.102400E 02	0.180000E 04	0.120000E 00
0.204800E 02	0.180000E 04	0.120000E 00
0.409600E 02	0.180000E 04	0.120000E 00

TIME-t	y(t)	$\dot{y}(t)$	$T_i(t)$
0.6250000E-01	0.270028E-01	0.215984E 00	0.157332E 04

X	T	C
0.0	0.140000E 04	0.333330E-01
0.100000E-01	0.146657E 04	0.597497E-01
0.200000E-01	0.153083E 04	0.598738E-01
0.400000E-01	0.163269E 04	0.166143E 00
0.800000E-01	0.175121E 04	0.124121E 00
0.160000E 00	0.179905E 04	0.120001E 00
0.320000E 00	0.180000E 04	0.120000E 00
0.640000E 00	0.180000E 04	0.120000E 00
0.128000E 01	0.180000E 04	0.120000E 00
0.256000E 01	0.180000E 04	0.120000E 00
0.512000E 01	0.180000E 04	0.120000E 00
0.102400E 02	0.180000E 04	0.120000E 00
0.204800E 02	0.180000E 04	0.120000E 00
0.409600E 02	0.180000E 04	0.120000E 00

TABLE 3-1 COMPUTED SOLIDIFICATION OF 12% Sn IN Ni, ACCORDING TO THE ANALYTICAL SOLUTION (Continued) (Sheet 2 of 2)

TIME-t	y(t)	$\dot{y}(t)$	$T_i(t)$
0.937500E-01	0.330701E-01	0.176329E 00	0.157331E 04
0.125000E 00	0.381845E-01	0.152690E 00	0.157331E 04
0.156250E 00	0.426900E-01	0.136557E 00	0.157330E 04
0.187500E 00	0.467628E-01	0.124649E 00	0.157330E 04
0.218750E 00	0.505080E-01	0.115395E 00	0.157329E 04
0.250000E 00	0.539936E-01	0.107935E 00	0.157329E 04
0.281250E 00	0.572672E-01	0.101757E 00	0.157329E 04
0.312500E 00	0.603633E-01	0.965308E-01	0.157328E 04
0.343750E 00	0.633079E-01	0.920349E-01	0.157328E 04
0.375000E 00	0.661214E-01	0.881137E-01	0.157328E 04
0.406250E 00	0.688198E-01	0.846543E-01	0.157328E 04
0.437500E 00	0.714163E-01	0.815727E-01	0.157327E 04
0.468750E 00	0.739214E-01	0.788048E-01	0.157327E 04
0.500000E 00	0.763443E-01	0.763006E-01	0.157327E 04
0.531250E 00	0.786926E-01	0.740207E-01	0.157327E 04
0.562500E 00	0.809726E-01	0.719334E-01	0.157326E 04
0.593750E 00	0.831901E-01	0.700130E-01	0.157326E 04
0.625000E 00	0.853499E-01	0.682382E-01	0.157326E 04
0.656250E 00	0.874563E-01	0.665914E-01	0.157326E 04
0.687500E 00	0.895131E-01	0.650579E-01	0.157325E 04
0.718750E 00	0.915235E-01	0.636250E-01	0.157325E 04
0.750000E 00	0.934905E-01	0.622823E-01	0.157325E 04
0.781250E 00	0.954170E-01	0.610203E-01	0.157325E 04
0.812500E 00	0.973051E-01	0.598312E-01	0.157325E 04
0.843750E 00	0.991571E-01	0.587082E-01	0.157325E 04
0.875000E 00	0.100975E 00	0.576451E-01	0.157324E 04
0.906250E 00	0.102760E 00	0.566368E-01	0.157324E 04
0.937500E 00	0.104515E 00	0.556785E-01	0.157324E 04
0.968750E 00	0.106241E 00	0.547660E-01	0.157324E 04
0.100000E 01	0.107939E 00	0.538958E-01	0.157324E 04

X	T	C
0.0	0.140000E 04	0.333330E-01
0.100000E-01	0.141674E 04	0.471641E-01
0.200000E-01	0.143344E 04	0.557259E-01
0.400000E-01	0.146658E 04	0.597815E-01
0.800000E-01	0.153085E 04	0.599058E-01
0.160000E 00	0.163269E 04	0.166167E 00
0.320000E 00	0.175121E 04	0.124234E 00
0.640000E 00	0.179905E 04	0.120001E 00
0.128000E 01	0.180000E 04	0.120000E 00
0.256000E 01	0.180000E 04	0.120000E 00
0.512000E 01	0.180000E 04	0.120000E 00
0.102400E 02	0.180000E 04	0.120000E 00
0.204800E 02	0.180000E 04	0.120000E 00
0.409600E 02	0.180000E 04	0.120000E 00

These results in Table 3-2 and Table 3-3 are to be compared with those obtained by the numerical solution, B INCR 3, described above. The times are from .0625 sec to 1 sec in intervals of .0625 sec. The values of T(x, t) and C(x, t) are given at t = .00097653 sec, .0625 sec and 1 sec.

TABLE 3-2 COMPUTED SOLIDIFICATION OF 12% Sn IN Ni, ACCORDING TO THE NUMERICAL PROGRAM

TIME, t	y(t)	$\dot{y}(t)$	$T_i(t)$
0.976563E-03	0.262523E-02	0.134412E 01	0.153064E 04

X	0.00	0.100000E-01	0.200000E-01	0.400000E-01	0.800000E-01
T	0.140000E 04	0.176418E 04	0.179763E 04	0.179996E 04	0.180000E 04
C	0.333333E-01	0.128821E 00	0.120274E 00	0.120002E 00	0.120000E 00

TIME, t	y(t)	$\dot{y}(t)$	$T_i(t)$
0.625000E-01	0.272345E-01	0.233351E 00	0.157701E 04

X	0.0	0.100000E-01	0.200000E-01	0.400000E-01	0.800000E-01
T	0.140000E 04	0.146771E 04	0.153287E 04	0.163831E 04	0.176099E 04
C	0.333333E-01	0.553996E-01	0.578464E-01	0.160132E 00	0.124030E 00

TIME, t	y(t)	$\dot{y}(t)$	$T_i(t)$
0.127307E 00	0.400000E-01	0.163057E 00	0.157687E 04
0.187500E 00	0.476896E-01	0.123216E 00	0.158008E 04
0.250000E 00	0.552284E-01	0.117407E 00	0.157892E 04
0.312500E 00	0.623012E-01	0.108731E 00	0.157872E 04
0.375000E 00	0.687872E-01	0.989489E-01	0.157869E 04
0.437500E 00	0.746791E-01	0.899257E-01	0.157852E 04
0.500000E 00	0.800672E-01	0.690561E-01	0.157848E 04
0.562500E 00	0.841858E-01	0.636305E-01	0.158206E 04
0.625000E 00	0.881141E-01	0.614704E-01	0.158280E 04
0.687500E 00	0.919827E-01	0.619815E-01	0.158148E 04
0.812500E 00	0.996864E-01	0.611697E-01	0.158031E 04
0.875000E 00	0.103489E 00	0.605048E-01	0.157999E 04
0.937500E 00	0.107246E 00	0.597120E-01	0.157973E 04
0.100000E 01	0.110950E 00	0.588031E-01	0.157957E 04

X	0.0	0.100000E-01	0.200000E-01	0.400000E-01	0.800000E-01
T	0.140000E 04	0.141692E 04	0.143380E 04	0.146732E 04	0.153247E 04
C	0.333333E-01	0.461461E-01	0.541801E-01	0.572740E-01	0.573063E-01

X	0.160000E 00	0.320000E 00	0.640000E 00	0.128000E 01	0.256000E 01
T	0.163849E 04	0.176112E 04	0.179812E 04	0.179999E 04	0.180000E 04
C	0.158612E 00	0.123817E 00	0.120118E 00	0.120000E 00	0.120000E 00

TABLE 3-3 COMPUTED SOLIDIFICATION OF 12% Sn IN Ni, COMPARISON BETWEEN ANALYTIC SOLUTION AND NUMERICAL PROGRAM

Time, t, sec	Interface Position		Velocity of Solidification		Interface Temperature	
	$\Delta y(t)$	$\frac{\Delta y(t)}{y_a(t)}$	$\Delta \dot{y}(t)$	$\frac{\Delta \dot{y}(t)}{y_a(t)}$	$\Delta T_i^a(t)$	$\frac{\Delta T_i(t)}{T_i^a(t)}$
0.25	1.24×10^{-3}	2.30%	9.47×10^{-3}	8.78%	5.63	0.56%
0.50	3.73×10^{-3}	4.88%	-7.24×10^{-3}	-9.51%	5.21	0.33%
0.75	2.36×10^{-3}	2.53%	-6.20×10^{-4}	-1.00%	7.60	0.48%
1.00	3.01×10^{-3}	2.78%	5.01×10^{-3}	9.31%	6.33	0.40%
Average	2.58×10^{-3}	3.12%	0.26×10^{-3}	1.90%	6.19	0.39%

The average accuracy of the numerically computed results in this example (12% Sn in Ni) is only 3.12% off the analytic values on the interfacial position y(t); only 1.90% on the velocity of solidification $\dot{y}(t)$; and only 0.39% on the interfacial temperature $T_i(t)$.

Within the range of study, our numerical program is therefore considered to be adequate for some applications to the solidification problem.

PART IV

SUGGESTIONS FOR FUTURE WORK

Section 1. IMPROVEMENT OF MODEL OF SOLIDIFICATION

The present analytic model assumes all the material parameters to be constant. Such parameters include:

- Specific heats
- Conductivities
- Latent heat of fusion
- Diffusivities
- Densities.

In any real situation, these parameters are varying either as a function of concentration, or temperature, or both. By refining the program to account for such variations, we move toward a more accurate model. Even more significant, however, is the fact that we will have a tool for accurately weighing the role and significance of each of the parameters in the solidification process, both in one gravity and in zero gravity.

The second improvement in the model involves introduction of the evaporation effects which were so significant in work conducted during the first part of the contract. We have already briefly discussed evaporation and the role it plays in solidification. Only by accounting for this effect can we clearly define the initial conditions of the melt before solidification in order to ascertain zero gravity effects during solidification.

Finally, with the help of several fluids specialists in the Research Department at Grumman, we have begun to analyze the role of liquid metal fluid dynamics on solidification. Even in zero gravity, there is considerable fluid motion brought about by forces such as surface tension, field effects, etc., possibly resulting, again, from evaporative segregation. We want to account for, in some fashion, the effects of such fluid motion on solidification.

Section 2. EXPERIMENTAL CORRELATION

Analytical programs are a valuable part of the investigation and, for this reason, we want to use the programs at all stages of their development to aid in understanding solidification and segregation in zero gravity. Effects of initial and of boundary conditions, concentration range, etc., will also be systematically determined.

In addition, we want to correlate the program with a very real semi-conductor material. Certain III-V semiconductor compounds, such as GaAs and GaP, form ideal candidates for single crystal growth in space because of their technical importance, stringent demand for perfection, and high cost. GaAs, for example, is a high-mobility, temperature-stable material that has been widely used in lasers, light emitters, Gunn microwave oscillators, and the like. While these devices are already performing numerous unique and important functions, their lives, performances, and reliabilities are usually material-limited. That is, the GaAs starting materials invariably contain too many physical and chemical defects in the form of point, line, surface, massive, or spiral types. The origin and formative conditions of these defects have not been fully explained. A clear understanding of these defects is, therefore, an urgent requirement for material improvement.

Today, in manufacture, exact control of a compound's stoichiometric composition is required, but it may have a phase diagram which is distinctly nonlinear. In addition, elemental As and P are so evaporative relative to Ga as to make the required compositional control extremely difficult and nonreproducible. Yet, most conventional studies consider neither the differential evaporative behavior of the constituents nor the curvatures of the relevent phase boundaries. For this reason, we have placed major emphasis precisely on these two important areas.

GaAs is, therefore, an ideal candidate material; it is susceptible to improvement through use of analytical techniques. Our programs can begin to explain the formation of defects in such a material and, therefore, be used to ascertain the effectiveness of

the space environment in improving the material. Finally, the same programs will allow us to devise improved GaAs space growth procedures.

Continuing a relationship which was initiated on the current contract, Grumman will work in cooperation with the State University of New York at Stony Brook in an effort to correlate our analytical efforts with experimental results. Single crystals will be grown at SUNY-SB under highly controlled conditions and carefully prepared statistical plans. These materials will then be analyzed and results used to confirm findings obtained on the computer.

PART V

REFERENCES

1. Amelinckx, S., and Votaba, E., 1954, Naturwiseenschaften 31, 422.
2. Anderson, R. L., and Bancroft, T.A., 1952, Statical Theory in Research, McGraw-Hill, New York.
3. Belaya, A. D., 1970, Izv. Akad. Nauk. SSSR, Neorg. Mater. 6, 377.
4. Bikerman, J. J., 1958, Surface Chemistry, Academic Press, New York.
5. Brice, J. C., 1965, The Growth of Crystals from the Melt, North Holland Publishing Company, Amsterdam, p. 32.
6. Brody, H. D. and Flemings, M. C., 1966, T. M. 236, 615.
7. Bunshah, R. F., and Juntz, R. S., 1966, "Purification of Beryllium by Crucible-Free Vacuum Melting and Distillation" in Beryllium Technology, (edited by Schetky, L. M., and Johnson, H. A.), Vol. 1, p. 16, Gordon and Breach, New York.
8. Burton, W. K., Cabrera, N., and Frank, F. C., 1951, Phil. Trans. Roy. Soc. A243, 299.
9. Butler, R., and Kerr, E., 1962, An Introduction to Numerical Methods, Sir Isaac Ptiman & Sons, Ltd., London.
10. Cabrera, N., and Burton, W. K., 1949, Discussion in Faraday Society 5, 40.
11. Carruthers, J.R., and Grasso, M., 1970, J. Electrochem. Soc. 117, 1426.
12. Chalmers, B., 1969, Solidification, J. Wiley, New York.
13. Chalmers, B., 1964, Principles of Solidification, John Wiley & Sons, Inc.
14. Christian, J. W., 1965, The Theory of Transformations in Metals & Alloys, Pergamon Press, New York, p. 568.

15. Dippenaar, A., Bridgman, H. D. W., and Chadwick, G. A., 1971, J. Inst Metals 99, 137.

16. Dowd, J. J., and Rouse, R. L., 1953, Proc. Phys, Society, B66, 61.

17. Dushman, S., 1962, Scientific Foundations of Vacuum Techniques, John Wiley and Sons, New York.

18. Flemings, M. C., and Mehrabian, R., 1971, "Segregation in Castings and Ingots" in Solidification, ASM, Metals Park, Ohio, pp. 311-340.

19. Frank, F. C., 1949, Discussion in Faraday Society 5, 48.

20. Frenkel, 1946, Kinetic Theory of Liquids, Oxford University Press, London, p. 201.

21. Gorow, T. H., and Jentoft, R. E., 1967, Anal. Chim. Acta 39, 3383.

22. Gulliver, G. H., 1922, Metallic Alloys, Charles Griffin, London, pp. 391-425.

23. Hall, R. N., 1957, J. Phys, Chem. Solids 3, 63.

24. Hansen, M., 1958, Constitution of Binary Alloys, McGraw-Hill, New York.

25. Hayes, A., and Chipman, J., 1939, TM 135, 85.

26. Hildebrand, J. H., and Scott, R. L., 1950, Solubility of Nonelectrolytes, 3rd, Ed., Reinhold, N. Y., p. 300.

27. Hunt, J. D., and Chilton, J. P., 1966, J. Inst. Metals 94, 146.

28. Jain, R. K., and Trigunayat, G. C., 1968, Crystal Growth 2, 185.

29. Johnston, W. C., and Tiller, W. A., 1962, TM 224, 214.

30. Kunz, K. A., 1957, Numerical Analysis, McGraw-Hill, N. Y., pp. 183-189.

31. Kurgintsev, A. W., 1967, Fiz. Metallov. Metallovedenie 24, 282.

32. Lehovec, K., and Belmont, E., 1953, J. Appl. Phys. 24, 1482.

33. Li, C. H., 1966[a], Phys. Stat. Solidi 15, 3 & 419.

34. Li, C. H., 1966[b], "On Determining the Equations of Liquidus and Solidus by Least Squares Techniques with Terminal Restrictions, "Grumman Research Department Memorandum RM-330.

35. Li, C. H., 1967[a], Brit. J. Appl. Phys. 18, 359.

36. Li, C. H., 1967[b], "The Effect of Segregated Solutes on Fracturing Properties, "Discussion of Fracture of Metals, Polymers, and Glasses, ed. R. J. Bonis, J. J. Duga, and J. J. Gilman, Plenum Press, New York.

37. Li, C. H., 1967[c], J. Appl. Phys. 38, 2407.

38. Li, C. H., 1968, J. Appl. Phys. 39, 2094.

39. Li, C. H., 1971, J. Appl. Phys. 42, 4521.

40. Li, C. H., 1972, "Normal Freezing of Ideal Ternary Systems of the Pseudo-binary Type," Grumman Research Department Memorandum RM-557.

41. Li, C. H., 1972, "Normal Evaporation of Binary Alloys," Grumman Research Department Memorandum RM-558.

42. Luneau, M., 1942, Revue Metallurgie 39, 218.

43. Mathieu, K., and Neerfeld, H., 1942, Arch Eisenhuttenwessen 15, 389.

44. McFee, R. J., 1947, Chem Phys. 15, 856.

45. Mellor, J. W., 1924, A Comprehensive Treatise on Inorganic & Theoretical Chemistry 5, 879.

46. Menzies, A. W. C., and Sloat, C. A., 1929, Nature, Lond. 123, 348.

47. Mott, N. F., 1948, Prog. Phys. Soc. Lond. 60, 391.

48. Mullins, W. W., and Sekerka, R. F., 1964, J. Appl. Phys. 35, 444.

49. Obradovic, N. D., and Bennett, G. H. J., 1969, J. Inst. of Metals, 97, p. 186.

50. Orioni, R. A., and Hall, R. N., 1958, J. Phys. Chem. Solids 6, 97.

51. Pfann, W., 1952, TM 194, 747.

52. Pfann, W., 1954, TM 200, 294.

53. Pfann, W., 1966, Zone Melting, Second Ed., Wiley, New York.

54. Pfann, W., 1960, Solid State Physics, 1, Academic Press, N. Y., p. 17.

55. Pfann, W. G., 1962, J. Metals, 4, 747.

56. Pohl, R. G., 1954, J. Appl. Phys. 25, 668 and 1170.

57. Prigogine, I., and Defay, R., 1954, Chemical Thermodynamics, Longmans Green & Co., N. Y., pp. 357-358.

58. Rayleigh, Lord, 1902, Phil Mag 4, 521.

59. Reid, R. D., 1971, Private Communication.

60. Reisman, A,. 1970, Phase Equlilbria, Academic Press, N. Y.

61. Rubenstein, L. I., 1971, The Stefan Problem, Amer. Math. Soc., Providence, R. I., pp. 52-57.

62. Rutter, J., and Chalmers, B., 1953, Can. J. Physics 31, 15.

63. Scheil, E., 1940, Z. Metallk. 34, 70

64. Scheuer, E., 1931, Z. Metallk. 23, 237.

65. Scriven, L. E., and Sterling, C. V., 1960, Nature 187, 186.

66. Smithells, C. J., 1967, Metals Reference Book, 4th Ed., Plenum Press, N. Y.

67. Sterling, C. V., and Scriven, L. E., 1959, AIChE 5, 514.

68. Tefelske, T. and Chang, Y. A., 1972, "The Effect of Ag on the Activity of Zn in Dilute Liquid Sn Alloys by Torsion-Effusion Method, "AIME Annual Meeting, San Francisco.

69. Thurmond, C. D., and Scott, R. L., 1960, Bell Syst. Tech. J., 39, 169.

70. Thurmond, C. D., 1960, in Properties of Elemental & Compound Semiconductors, Gatos, H. C. Ed., Interscience, New York p. 121.

71. Thurmond, C. D., and Struthers, J. D., 1953, J. Phys, Chem. 57, 831.

72. Thurmond, C. D., and Kowalchik, M., 1960, Bell Syst. Tech. J. 39, 169.

73. Tiller, W., Jackson, K., Rutter, J., and Chalmers, B., 1953, Acta Met., 1, 428.

74. Voronkova, G. I., et al, 1969, Izv. Akad, Nauk. SSSR. Neorg. Mater. 5, 1691.

75. Votava, E., and Berghezan, A., 1959, Acta Meta 7, 6.

76. Walter, H. U., and Snyder, R. S., 1971, J. of the Less Common Metals 24, 467.

77. Wilcox, W. R., 1964, J. Appl. Phys. 35, 636.

78. Yen, James, 1972, Private Communication.

79. Zener, C., 1946, TM 167, 550.

80. Zinsmeister, G., 1964, Vakuum-Tech, no. 8, p. 223.

81. Crank, J. and Nicholson, P., 1947, Proc. Cambridge Phil. Soc. 43, 50.

PART VI

APPENDICES

These Appendices contain all of the papers pertaining to this contract that were either published or submitted for publication during the contract period. Two papers were presented at the American Association for Crystal Growth Second Symposium in Princeton, New Jersey, in July 1972.

APPENDIX A

EVAPORATIVE SEGREGATION IN 80% NI-20% Cr AND 60% Fe-40% Ni ALLOYS[†]

by

J. L. Mukherjee[‡]
K. P. Gupta[‡]

and

C. H. Li[‡]

October 1972

[†]Published as Grumman Research Department RM-552. Submitted for publication to the Journal of Vacuum Science

[‡]Department of Material Science, State University of New York at Stony Brook, New York 11790

[‡]Research Department, Grumman Aerospace Corporation, Bethpage, New York 11714

ACKNOWLEDGMENT

This work was carried out at Grumman Aerospace Corporation, Bethpage, New York, 11714, under partial support of NASA Contract No. NAS 8-27891.

ABSTRACT

The phenomenon of evaporative segregation in binary alloys has been investigated through a study of some experimental evaporation data relating to the Ni-Cr and Ni-Fe systems. In normal evaporation it is assumed that a) the evaporating alloy is always homogeneous, b) the vapor is instantly removed, and c) the alloy follows Raoult's law. The solutions of the evaporation equations for the two most important cases are presented and experimental data are analyzed with these equations. The difference between observed and calculated values of evaporation constants lies within one order of magnitude. This is surprising because of the major assumptions stated above. Experimental results have shown that the evaporation time t and final solute concentration m are logarithmically related, further supporting our evaporation equations. It is further shown that neglecting the nonlogarithmic term in these evaporation equations may introduce considerable errors in the analysis.

TABLE OF CONTENTS

DISCUSSION

The phenomenon of evaporative segregation in binary alloys has been quantitatively treated by Li (Refs. 1,2). By evaporative segregation, we mean solute enrichment or depletion in the evaporating alloy as a result of surface evaporation.

The formalism of evaporative segregation in alloys works surprisingly well for the several systems so far studied, notwithstanding the several major assumptions involved. In the present memorandum, we shall study only some experimental evaporation data relating to the Ni-Cr and Ni-Fe systems, as reported by N. D. Obradovic et al.(Ref. 3). Specifically, we shall compute the degree and rate of solute enrichment or depletion in the evaporating source at different temperatures and evaporation times.

In the treatment of the simple "normal" evaporation, it is assumed that a) the evaporating alloy is always homogeneous, b) the vapor is instantly removed, and c) the alloy follows Raoult's law. Such conditions exist or are nearly approached in an induction melt in vacuum or liquid in space. The solutions of the relevant differential equation for the following two important cases are (Ref. 2):

Case I: The solute is much more evaporative than solvent, i.e., $U \gg V$. Then the time to reach a final concentration m is

$$t_1 = G_1 \left[\ln \frac{(1 - m_o)m}{m_o(1 - m)} + \frac{m - m_o}{(1 - m_o)(1 - m)} \right] \qquad (1)$$

where

$G_1 = -N_o(1 - m_o)/AU$ (sec)

U = evaporation rate of the solute in $mol/cm^2/sec$

V = evaporation rate of the solvent in $mol/cm^2/sec$

m_o = initial molar fraction of solute

m = final molar fraction of solute after time t_1 (in sec)

N_o = total initial number of moles of both solvent and solute

A = evaporating area in cm^2

For nearly equal m and m_o (i.e., $m \simeq m_o$), or for small m and m_o (i.e., $m \simeq m_o \simeq 0$), Eq. (1) reduces to the following logarithmic expression:

$$t_1 = G_1 \ln\left|\frac{(1 - m_o)m}{m_o(1 - m)}\right| \tag{1a}$$

Case II: The solvent is much more evaporative than solute, i.e., $V \gg U$, then,

$$t_2 = G_2\left|\ln\frac{(1 - m_o)m}{(1 - m)m_o} + \frac{m - m_o}{mm_o}\right| \tag{2}$$

where $G_2 = m_oN_o/AV$. Again, for nearly equal m and m_o (i.e., $m \simeq m_o$), Eq. (2) reduces to a logarithmic expression very similar to (1a):

$$t_2 = G_2 \ln\left|\frac{(1 - m_o)m}{m_o(1 - m)}\right| \tag{2a}$$

G's are the time constants of evaporation. For the case when $U >> V$, solute depletion takes place, i.e., $m < m_o$ and, therefore, the logarithmic term in the parentheses is negative (the second term in the parentheses is often negligible by comparison with the logarithmic term). Since the evaporation time, t, must be positive, G_1 is negative, G_2 is always positive.

The evaporation rate in $mol/cm^2/sec$ for solute and solvent is given by (Ref. 4)

$$U = K\left(10^{A_u - B_u/T}\right) / \sqrt{M_u T} \tag{3}$$

$$V = K\left(10^{A_v - B_v/T}\right) / \sqrt{M_v T} \tag{4}$$

where

K = 5.833×10^{-5}, a constant for metals

M_u, M_v = molecular weights of solute and solvent, respectively

T = evaporating temperature in °K

A_u, B_u = evaporating constants for the solute

A_v, B_v = evaporating constants for the solvent.

Obradovic et al. (Ref. 3) give the final solute concentrations for Ni-Fe and Ni-Cr alloys after various evaporating times at 1600°C under various ambient pressures, as shown in Tables 1 and 2. These data have been analyzed by means of Eqs. (1) and (2), above. The solute and solvent evaporating constants, A_u, B_u, A_v, and B_v, are obtained from Ref. 4.

Table 1

CALCULATED AND OBSERVED VALUES OF G_2's FOR Fe-Ni

60% Fe-40% Ni Alloy

Log x = 1.7915 at t = 0, G_2 calc. ($\times 10^{-4}$) = 0.4369 sec

No.	Ambient Pressure ($\times 10^3$) Torr	Log x (x = wt % Fe) after 1800 secs	G_2 ($\times 10^{-4}$) Observed, secs: Two Terms	G_2 ($\times 10^{-4}$) Observed, secs: Logarithmic Term Only	$\frac{G_2(\text{logarithmic term})}{G_2(\text{two terms})}$	$\frac{G_2(\text{two terms})}{G_2(\text{calculated})}$
1	1	1.7787	1.4302	2.3923	1.67	3.27
2	5	1.7877	4.8355	8.0034	1.65	11.06
3	30	1.7812	1.7763	2.9627	1.67	4.06
4	50	1.7775	1.3034	2.1835	1.67	2.98
5	100	1.7710	0.8934	1.5080	1.68	2.04
6	200	1.7805	1.6942	2.8274	1.66	3.87
7	500	1.7862	3.4573	5.7324	1.67	7.91

Table 2

CALCULATED AND OBSERVED VALUES OF G_1's FOR Ni-Cr ALLOY

80% Ni-20% Cr Alloy

Log x = 1.2920 at t = 0, $-G_1$ calc. ($\times 10^{-4}$) = 0.1710 sec

No.	Ambient Pressure ($\times 1^{-3}$) Torr	Log x (x = wt % Fe) after 1800 secs	$-G_1$ ($\times 10^{-4}$) Observed, secs: Two Terms	$-G_1$ ($\times 10^{-4}$) Observed, secs: Logarithmic Term Only	$\frac{G_1 \text{ (logarithmic term)}}{G_1 \text{ (two terms)}}$	$\frac{G_1 \text{ (two terms)}}{G_1 \text{ (calculated)}}$
1	1	1.2600	1.5690	1.9815	1.26	9.17
2	5	1.2746	2.8730	3.6439	1.26	16.80
3	30	1.2663	1.9493	2.4663	1.26	11.39
4	50	1.2793	3.9210	4.9800	1.27	22.92
5	100	1.2773	3.3902	4.3033	1.26	19.82
6	200	1.2856	7.8135	9.9428	1.27	45.69
7	500	1.2826	5.3112	6.7525	1.27	31.05

Relevant data for computation of the G's are given below:

a) 60% Fe-40% Ni alloy:

U_{Ni} = 6.386 x 10^{-6} mol/cm^2/sec; N_o = 0.7478 mol; T = 1600°C;

V_{Fe} = 1.081 x 10^{-5} mol/cm^2/sec; A = 10.0 cm^2; Case II: U << V.

b) 80% Ni-20% Cr alloy:

U_{Cr} = 3.479 x 10^{-5} mol/cm^2/sec; N_o = 0.7582 mol; T = 1600°C;

V_{Ni} = 6.386 x 10^{-6} mol/cm^2/sec; A = 10.0 cm^2; Case I: U >> V.

It can be seen from Table 1 that for the Fe-Ni alloy, the values of G_2's are constant within one order of magnitude. The difference between observed and calculated values of G_2 is also within one order of magnitude. This is very surprising considering the fact that elemental evaporation rates generally differ by many orders of magnitude. Also, the above analysis is based on the assumptions of a) the evaporating alloy is always homogeneous; b) ideal solution behavior (and the solutions here are highly concentrated!); c) the vapor is instantly removed. The experimental data of Obradovic et al. (Ref. 3) on the Fe-Ni system shows no systematic dependence of evaporation kinetics on pressure as one would expect, and suggests large experimental errors, errors in measurements, or both.

Table 2 also shows the calculated and observed values of G_1's for the Ni-Cr alloy. Here, also, the values of G_1's are almost constant, and the differences between the observed and calculated values of G_1's are small. The data on the Ni-Cr system show some positive correlation between ambient pressure and the weight percent of chromium in the melt after 30 minutes.

The values of computed G's are constant within one order of magnitude. In particular, for the Fe-Ni system, at ambient pressures of 1, 30, 50, 200 ($\times 10^3$) torr, these same values are accurate to within 25 percent. Therefore, in some cases it is desirable to know these values to within 20 percent of their real values.

In Tables 1 and 2 the time constants G's have been calculated in two ways. First, G's were calculated by using only the logarithmic term. Next, the complete equation (1) or (2) involving both the logarithmic and nonlogarithmic terms was used. It is interesting to note that the ratio of G's calculated in two cases is constant and has an average value of 1.67 ± 0.01 for Fe-Ni alloy and 1.26 ± 0.005 for the Ni-Cr alloy. Mathematically, this means that for the case $U \gg V$ (in Ni-Cr alloy)

$$\frac{\ln\left[\frac{(1 - m_o)m}{m_o(1 - m)}\right] + \frac{m - m_o}{(1 - m_o)(1 - m)}}{\ln\left[\frac{(1 - m_o)m}{m_o(1 - m)}\right]} = 1.26 , \qquad (5)$$

or

$$\frac{\frac{m - m_o}{(1 - m_o)(1 - m)}}{\ln\left[\frac{(1 - m_o)m}{m_o(1 - m)}\right]} = 0.26 , \qquad (6)$$

and for the case $V \gg U$, i.e., in Fe-Ni alloy

$$\frac{\dfrac{m - m_o}{m_o m}}{\ln\left[\dfrac{(1 - m_o)m}{m_o(1 - m)}\right]} = 0.67 \ . \tag{7}$$

Experimental results have shown that the evaporation time t and the final solute concentration m are logarithmically related (Refs. 3,5), supporting our Eqs. (1) and (2). However, these same equations indicate that such relations are true only for vastly different solvent and solute evaporating rates, and, in addition, for small initial and final concentrations, m_o and m. These same equations also allow one to compute, e.g., the effective evaporating area, A, the solute or solvent evaporating rates U or V, or the evaporating temperature T. Further, neglecting the nonlogarithmic second terms in Eqs. (1) and (2) may introduce errors in T, A, U, or V by 26 percent in the 80% Ni-20% Cr case and 67 percent in the 60% Fe-40% Ni case.

The equations of normal evaporation can be made more realistic by introducing the concept of solvent-solute interaction. If one considers only first-order correction, then it can be shown that the ideal evaporation rates of solutes and solvents will be changed by a new factor related to the activity coefficient of the element in question. In other words,

$$\begin{aligned} U' &= \gamma_u U \\ V' &= \gamma_v V \ , \end{aligned} \tag{8}$$

where γ_u, γ_v are activity coefficients of solute and solvent, respectively, assumed constant in the vicinity of m_o; and U', V' are effective evaporating rates of solutes and solvents. Using the activity data of Fe-Ni alloy (Ref. 6) at 1600°C, we have recalculated the values of G_2. Now

$$G_2' = \frac{m_o n_o}{AV'} \tag{9}$$

where

$$V' = \gamma_v V$$

$$\gamma_v = \gamma_{Fe} = 0.977 \quad \text{for} \quad 60 \text{ mol \% Fe alloy.}$$

$$G_2' \text{ (cal)} = 0.4471 \times 10^{+4} \text{ sec.}$$

On applying similar first-order correction for Ni-Cr system (Ref. 7), the revised value of G_1 becomes,

$$G_1' \text{ (cal)} = 0.2138 \times 10^{+4} \text{ sec.}$$

These corrections, while not very large, do make a little better agreement between calculated and experimentally observed G values.

In conclusion, the simple normal evaporation approach seems to give fairly accurate and useful predictions, even for the highly concentrated Ni-Cr and Fe-Ni alloys.

REFERENCES

1. Li, C. H., Phys. Stat. Sol., Vol. 15, pp. 3 and 419, 1966.

2. Li, C. H., "Normal Evaporation of Binary Alloys," ro be published.

3. Obradovic, N. D. and Bennett, G. H. J., J. Inst. of Metals, Vol. 97, p. 186, 1969.

4. Dushman, S., Scientific Foundations of Vacuum Techniques, Wiley, New York, pp. 68 and 691, 1962.

5. Chang, Y. A. and Miller, R., "The Effect of Ag on the Activity Coefficient of Zn in Dilute Liquid Sn Alloys by Torsion Effusion Method," 1972 AIME Annual Meeting, San Francisco.

6. Hultgren, C. et al., Selected Values of Thermodynamic Properties of Metals and Alloys, Wiley, New York, p. 732, 1963.

7. Fruhan, R. J., "The Activity of Cr in Liquid Ni-Cr Alloys," Trans. Met. Soc. AIME, 1968, Vol. 242, p. 2007.

APPENDIX B

PURIFICATION KINETICS OF BERYLLIUM DURING VACUUM INDUCTION MELTING[†]

by

J. L. Mukherjee[‡]
K. P. Gupta[‡]

and

C. H. Li[‡]

October 1972

[†]Published as Grumman Research Department RM-553. Submitted for publication to the Metallurgical Transactions of AIME

[‡]Department of Material Science, State University of New York at Stony Brook, New York 11790

[‡]Research Department, Grumman Aerospace Corporation, Bethpage, New York 11714

ACKNOWLEDGMENT

This work was done under NASA Contract No. NAS 8-27891.

ABSTRACT

The kinetics of evaporation in binary alloys have been quantitatively treated. The formalism so developed works surprisingly well for several systems so far studied, notwithstanding the several major assumptions involved. In this memorandum, we have studied the kinetics of purification of beryllium through evaporation data actually acquired during vacuum induction melting. This study shows that normal evaporation equations are generally valid and useful for understanding the kinetics of beryllium purification. The normal evaporation analysis has been extended to cover cases of limited liquid diffusion. It has been shown that under steady-state evaporation, the solute concentration near the surface may be up to six orders of magnitude different from the bulk concentration. Corrections for limited liquid diffusion are definitely needed for the highly evaporative solute elements, such as Zn, Mg, and Na, for which the computed evaporation times are improved by five orders of magnitude. The commonly observed logarithmic relation between evaporation time and final concentration further supports the validity of our normal evaporation equations.

TABLE OF CONTENTS

INTRODUCTION

The kinetics of evaporation in binary alloys have been quantitatively treated by C. H. Li (Refs. 1,2). The formalism so developed works surprisingly well for the several systems so far studied, notwithstanding the several major assumptions involved. Specifically, in this normal evaporation approach, it is assumed that a) the evaporating alloy is always homogeneous in composition, b) the alloy follows Raoult's law, and c) the vapor is instantly removed. In this work, we have studied the kinetics of purification of beryllium through evaporation data actually acquired during vacuum induction melting by R. F. Bunshah and R. S. Juntz (Ref. 3).

EXPERIMENTAL DATA

The details of the vacuum induction melting procedure are as follows. Beryllium (SR grade flakes) in the form of a cylindrical compact was crucible-free induction melted under an ambient pressure of 10^{-6} torr. The cylindrical compact was 1-3/4 inches in diameter and 4 inches high, and weighed about 100-130 g. Since the actual temperature of the melt was not known, for the purpose of our computations, the temperature was assumed, for the sake of comparison, to be 1500°C, a temperature commonly used in Be melting (Ref. 3).

EQUATION OF NORMAL EVAPORATION

The solutions of the kinetic equations for two important cases are given in papers by Li and Mukherjee et al. (Refs. 2,4). In Case I, the solute evaporating rate, U, is much greater than the solvent evaporating rate, V, i.e., $U >> V$. The equation relating the evaporating time t_1 to final concentration, m, is, for this case,

$$t_1 = G_1\left[\ln\frac{(1 - m_o)m}{m_o(1 - m)} + \frac{m - m_o}{(1 - m_o)(1 - m)}\right] \qquad (1)$$

and in Case II when $U << V$, the evaporation time is given as follows:

$$t_2 = G_2\left[\ln\frac{(1 - m_o)m}{m_o(1 - m)} + \frac{m - m_o}{mm_o}\right], \qquad (2)$$

where

$G_1 = -N_o(1 - m_o)/AU$

$G_2 = +N_o m_o/AV$, and

m, m_o = mole fractions of solute at $t = t$ and $t = 0$, respectively.

G's are the time constants of evaporation. For Case I when $U >> V$, solute depletion takes place (or $m < m_o$) and, therefore, the logarithmic term in the parentheses is negative (the second term in the parentheses is, for small values of m and m_o, negligible by comparison with the logarithmic term). Since the evaporating time t_1 must be positive, G_1 must be negative. G_2, on the other hand, is always positive.

In Table 1 the times t_i, to reach the final concentrations m from initial concentration m_o (through evaporation from area A and with an initial total of N_o moles of both solute and solvent) for each element in the melt have been compiled using Eqs. (1) and (2) above. In the table, the ideal evaporation rates at temperature T°K of each element have been computed using the formula given in Ref. 5, viz.,

for the solute:

$$U = K\ 10^{A_u - B_u/T} \Big/ \sqrt{M_u T}$$

and (3)

for the solvent:

$$V = K\ 10^{A_v - B_v/T} \Big/ \sqrt{M_v T}\ ,$$

where $K = 5.833 \times 10^{-5}$ for metals; A_u, B_u, A_v, and B_v are elemental evaporation constants given in Ref. 5; and the M's are molecular weights.

Table 1

PURIFICATION KINETICS OF BERYLLIUM DURING CRUCIBLE-FREE VACUUM INDUCTION MELTING

Solute Element	Initial Conc., m_o, ppm Atomic	Final Conc. m, ppm Atomic	Ideal Evap. Rate at 1500°C, U_i, moles/cm²/sec	Time to Reach Final Conc., t_i, secs	$P = t_i U_i^*$ or $= t_i V_i^{**}$ moles/cm²	Surface Conc., m_s, Atomic	m_s/m_o	Effective Time to Reach Final Conc., t_e, secs	$\frac{t_e,\ 1400°C}{t_e,\ 1500°C}$
Fe	1.55	< 5	2.7885×10^{-6}	2.69×10^{3}	0.655	1.34×10^{-4}	8.60×10^{1}	2.69×10^{3}	3.49
Cr	0.65	2.1	8.7887×10^{-6}	2.84×10^{3}	0.690	1.79×10^{-5}	2.75×10^{1}	2.84×10^{3}	3.48
Ni	4.95	7.5	1.5353×10^{-6}	1.39×10^{3}	0.340	7.82×10^{-4}	1.57×10^{2}	1.40×10^{3}	3.48
Si	4.50	5.0	1.3320×10^{-6}	0.41×10^{3}	0.10	8.19×10^{-4}	1.82×10^{2}	0.41×10^{3}	3.48
Cu	1.50	1.55	4.2039×10^{-5}	0.13×10^{3}	0.032	8.66×10^{-6}	5.77	0.13×10^{3}	3.53
Al	6.50	4.0	1.6834×10^{-4}	-2.57×10^{3}	-0.625	9.37×10^{-6}	1.44	-2.57×10^{3}	3.49
Mg	4.0	0.03	5.9444	0.82	4.892	1.63×10^{-10}	4.00×10^{-5}	20.14×10^{3}	3.48
Zn	4.10	0.2	14.5917	0.20	3.020	6.82×10^{-11}	1.66×10^{-5}	12.43×10^{3}	3.48
Na	59.0	8.0	12.1483	0.16	1.998	1.17×10^{-9}	1.00×10^{-5}	8.22×10^{3}	3.49
Average					1.465			5.64×10^{3}	3.48

*for $U \gg V$

**for $U \ll V$

$V_i(Be) = 2.4287 \times 10^{-4}$ moles/cm²/sec

T = 1500 C

Ambient Pressure = 10^{-6} torr

TYPES OF IMPURITIES

Three types of impurities can be distinguished:

Type I. - The impurities that have much higher evaporating rates U than the solvent Be. For these impurities, such as Zn, Na, and Mg, evaporation Eq. (1) should be used.

Type II. - The impurities that have much lower evaporating rates U than the solvent Be. For these impurities, such as Fe, Cr, Ni, Cu, Ti, and Si, Eq. (2) should be used.

Type III. - The impurity that evaporates at about the same rate as the solvent Be, i.e., $U \simeq V$. Only a single element, Al, is in this group. For this impurity, a different evaporation equation in infinite series form should be used (Ref. 2).

PRELIMINARY DATA ANALYSIS

Since the exact temperature of the melt was not known, the exact evaporation rates could not be computed. However, since all the solute and solvent elements were evaporating from the same liquid-gas interface of a fixed area A for the same length of time, we can compute, from the measured m_o's and m's, the values of P, which is the product of the evaporating time and evaporation rate for a given solute with the help of Eqs. (1) and (2). The value of P should be constant for all the solutes.

$$t_1^i = t_1^{ideal} = \frac{-N_o(1 - m_o)}{AU_i}\left[\ln \frac{(1 - m_o)m}{m_o(1 - m)} + \frac{m - m_o}{(1 - m)(1 - m_o)}\right], \qquad (4a)$$

or

$$t_1^i U_i = t_1^{ideal} U_i = \frac{-N_o(1 - m_o)}{A}\left[\ln \frac{(1 - m_o)}{m_o(1 - m)} + \frac{m - m_o}{(1 - m)(1 - m_o)}\right] = P , \qquad (4)$$

where t_i is the estimated evaporation time computed separately for each element at the assumed temperature of 1500 C. Similarly, from Eq. (2) and the ideal evaporation rate of the solvent V_i at the same temperature, we have:

$$t_2^{ideal} V_{ideal} = P .$$

In Table 1 are listed the value of P's for each element. P is defined, as shown, such that

$$P = t_i \times U_i \quad \text{when} \quad V_i < U_i$$

$$P = t_i \times V_i \quad \text{when} \quad V_i > U_i .$$

It can be seen from Table 1 that P is almost constant for the low vapor pressure (Type II) impurities except for copper.

Because of our three assumptions of normal evaporation, and because of the assumed evaporating temperature of 1500° C, the computed values of t_i vary from element to element, even though they should be identically the same. The variations in t_i, however, are not very large so that the equations presented here are still useful.

The high vapor pressure (Type I) impurities (Mg, Na, Zn) also have uniform P values, which are roughly one order of magnitude higher than those for the low vapor pressure (Type II) elements. The negative value of P for aluminum shows that aluminum cannot be treated by Eqs. (1) and (2) because for this element $U \simeq V$ and a different evaporation equation in infinite series form should be used.

STEADY-STATE EVAPORATION

To explain the large variation in P values among different types of impurity elements, one should consider limited liquid diffusion. The concept of effective evaporation rates, U_e and V_e upon reaching a steady-state condition is now introduced.

$$P = t_e V_e = \text{constant} \tag{1a}$$

or

$$t_i V_i = P = \text{constant} \cong t_e V_e \ , \tag{2a}$$

where the subscripts i refer to ideal or normal evaporation values, while the subscripts e refer to effective or nonnormal values.

In the following paragraphs, the concept of U_e will be developed.

In normal evaporation, we assume that the evaporating alloy is always homogeneous, i.e., the liquid diffusion constant $D_\ell = \infty$. But because of the large (orders of magnitude) differences in evaporation rates of elements, the surface concentration of the solute m_s in the melt is not the same as the bulk concentration m_o due to the limited liquid diffusion. Figure 1 depicts the situation (at $t = 0$) (i.e., initial), and after reaching steady states, for the case $U >> V$.

For $U >> V$, the evaporating surface region soon becomes depleted of solute, and the surface concentration of the solute, m_s, will be different from the bulk concentration, m_o, specifically, $m_s << m_o$. After the initial transients, a steady-state for the alloy system and evaporating conditions will be reached. The steady-

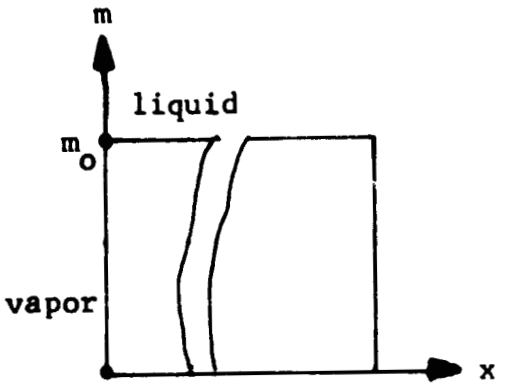

Fig. 1a Initial State, $t = 0$

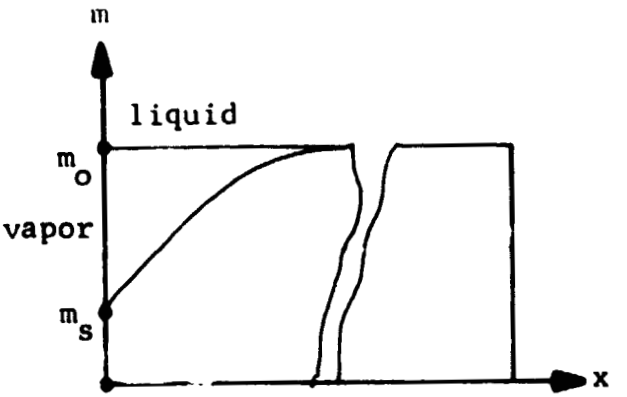

Fig. 1b Steady State, $t \geq t_s$

state concentration profile is shown in Fig. 1b. The equation of the profile, i.e., m versus x, can be derived according to a procedure used by Tiller et al. (Ref. 6) in their study of freezing with limited liquid diffusion, i.e.,

$$m = m_o \left\{1 + \frac{m_s - m_o}{m_o} \exp\left(\frac{-R}{D_e} x\right)\right\} , \tag{5}$$

where the receding rate R of the evaporating surface can be computed from U_i, V_i, m_s, M_u, M_v, and material densities.

In steady-state,

$$m_s U_i = m_o U_e , \tag{6a}$$

and

$$(1 - m_s) V_i = (1 - m_o) U_e , \tag{6b}$$

or

$$\frac{m_s U_i}{(1 - m_s) V_i} = \frac{m_o}{1 - m_o} . \tag{6c}$$

Solving for m_s,

$$m_s = \frac{m_o V_i}{(1 - m_o)U_i + m_o V_i} \quad . \tag{7}$$

Since

$$m_s U_i = m_o U_e, \tag{8}$$

where U_e is the effective evaporation rate of the solute due to the change in surface concentration. Substituting the m_s from Eq. (7) in Eq. (8) gives

$$U_e = \frac{m_s}{m_o} U_i = \frac{U_i V_i}{(1 - m_o)U_i + m_o V_i} \quad . \tag{9}$$

Similarly, for the case $V \gg U$,

$$(1 - m_s)V_i = (1 - m_o)V_e \tag{10}$$

or

$$V_e = \frac{1 - m_s}{1 - m_o} V_i = \frac{V_i U_i}{(1 - m_o)U_i + m_o V_i} = U_e \quad . \tag{11}$$

Thus, it can be seen mathematically that $V_e = U_e$. This means that in both cases, $U \gg V$, or $V \ll U$, the effective value of U or V is the same. This equality means that in the steady-state, the surface concentration m_s does not change with time, as expected.

Now consider Eq. (7) in some detail. Several cases can be distinguished; these are:

I. — $U \gg V$ and $m_o \simeq m \simeq 0$

$$m_s = \frac{m_o V_i}{(1 - m_o) U_i} = \frac{m_o V_i}{U_i}$$

or (11a)

$$\frac{m_s}{m_o} = \frac{V_i}{U_i} .$$

II. — $V \gg U$

a) $$m_o V_i \gg U_i \quad \text{or} \quad \frac{U_i}{V_i} \ll m_o \tag{11b}$$

then

$$m_s = 1 .$$

b)

$$m_o V_i \ll U_i \quad \text{or} \quad \frac{U_i}{V_i} \gg m_o \tag{11c}$$

then

$$m_s = \frac{m_o V_i}{(1 - m_o) U_i} = \frac{m_o V_i}{U_i}$$

when

$$m_o \simeq 0 .$$

c)

$$m_o V_i \simeq U_i \quad \text{or} \quad \frac{U_i}{V_i} \simeq m_o \ .$$

then

$$m_s = \frac{1}{2 - m_o} \simeq \frac{1}{2} \tag{11d}$$

when

$$m_o \simeq 0 \ .$$

The effective evaporation rate of the solutes, U_e, can be computed by Eq. (9). The effective evaporation rates have been variably raised or lowered to equal the ideal evaporation rate of the solvent (Be). In the case of high vapor pressure impurities like Mg, Zn, Na, this means a lowering of evaporating rates by about five orders of magnitude.

The surface concentration, m_s, and the ratio of surface to bulk concentration have been computed in Table 1 by Eq. (7). These ratios must also equal V_i/U_i. Now we have

$$P = t_e U_e = t_i U_i \ .$$

The effective time t_e, to reach the final concentrations m have been computed for all the impurities in Table 1; t_e should be a constant. It can be seen that for the low vapor pressure impurities, t_e is almost constant. Again, the t_e for Cu is one order of magnitude less than others in the low vapor pressure impurity group. Among the high vapor pressure impurities, the t_e is almost constant. It can be seen that t_e for the high vapor pressure impurities is one order of magnitude larger than that of low vapor pressure impurities.

NONIDEAL SOLUTIONS

The normal evaporation equations can be further modified by introducing the concept of solvent-solute interactions. If one considers deviation from the Raoult's law, it can be shown that the evaporation rates of solvent and solute will be changed by a new factor, the activity coefficient. For very dilute solutions, which we are considering, evaporation rates for solute and solvent can be given by $U' = \gamma_u U_e$ and $V' = V_e$, respectively, where γ_u is the activity coefficient of the solute (Henry constant, in this case).

In general, such consideration should not affect the estimated time, t_e, for the type I impurities (Fe, Ni, Cr, Ti, etc.), except in the case of copper. From the available phase diagram, it is evident that Be and Cu atoms have significant interactions with each other and form many compounds (Refs. 7,8). Thus the excess free energy for the system should be negative, resulting in a lower value of γ_{Cu} compared to the ideal solution case $\left(\gamma_{Cu}^{ideal} = 1.0\right)$. In such a situation, V'_{Be} is not very much higher than U'_{Cu}, and this leads to a greater effective time, $t_{e,Cu}$ to reach the final concentration. The exact value of γ_{Cu} is difficult to evaluate because of the lack of data in this composition range.

In the cases of Zn and Mg, the solubility in beryllium is negligible (Ref. 8) and so γ_{Zn} and γ_{Mg} should be greater than one. This would lower the estimated time, t_e, meaning a better agreement with the other elements.

It is important to note that exact calculation for the deviation from the ideal solution case is difficult because of the lack of data, and such estimations are purely qualitative.

CONCLUSIONS

1. Normal evaporation Eqs. (1) and (2) are generally valid and useful for the study of beryllium purification. This agrees with a previous study on the results of Ni-Fe and Ni-Cr systems (Ref. 4).

2. The computed values of $P = t_i U_i$ or $t_i V_i$ are essentially constant for the same type of solute elements, although differing by one order of magnitude between different types of elements.

3. The normal evaporation analysis has been extended to cover cases of limited liquid diffusion. It is shown that under steady-state conditions, the solute concentration near the surface, i.e., m_s, may be up to five orders of magnitude different from the bulk concentration, m_o.

4. Corrections for limited liquid diffusion are definitely needed for the highly evaporative solute elements Mg, Zn, and Na, for which the computed evaporation times, t_e, are improved by three or four orders of magnitude.

5. After these corrections, the computed times are comparable, even between different types of solute elements.

6. The agreement among the computed times can be further improved by considering the deviation from the ideal solution condition. Because of lack of data, it is difficult to give any quantitative calculation.

7. Estimations of solute evaporation behavior are now well within one order of magnitude.

8. The commonly observed logarithmic relation between evaporation time t and final concentration m further supports the validity of our normal evaporation equations. Such relations are, however, true only for widely different solute and solvent evaporating rates and for dilute solutions, as can be seen from Eqs. (1) and (2).

REFERENCES

1. Li, C. H., Phys. Stat. Sol., Vol. 15, p. 3 and p. 419, 1966.

2. Li, C. H., "Normal Evaporation of Binary Alloys," to be published.

3. Beryllium Technology, Vol. 1, p. 16, Gordon and Breach, New York, 1966.

4. Mukherjee, J. L., Gupta, K. P., and Li, C. H. "Evaporative Segregation in 80% Ni-20% Cr and 60% Fe-40% Ni Alloys" (to be published).

5. Dushman, S., Scientific Foundations of Vacuum Techniques, pp. 68 and 691, Wiley, New York, 1962.

6. Tiller, W. A. et al., Acta Met 1, 428, 1953.

7. Elliott, R. P., Constitution of Binary Alloys, First Supplement, McGraw-Hill, New York, 1965.

8. Shunk, F. A., Constitution of Binary Alloys, Second Supplement, McGraw-Hill, New York, 1969.

APPENDIX C

MOMENTUM GAIN BY EVAPORATING SURFACES

by

James T. Yen
Grumman Aerospace Corporation
Research Department
Bethpage, New York 11714

In this appendix, we evaluate the rate of momentum acquired by a liquid surface when its molecules are evaporating into a vacuum.

First, let us evaluate the evaporating rate and evaporating pressure by considering the equilibrium case. When the surface is at equilibrium with its surroundings, the rate of molecules leaving the surface by evaporation will equilibrate the rate of condensation, resulting in zero gain or less by the surface. These rates will be called the equilibrium rates of evaporation and condensation, and an evaluation of one will yield the value for the other. The condensing rate is readily given by

$$\frac{1}{4}\rho\bar{v} = \rho\left(\frac{RT}{2\pi}\right)^{\frac{1}{2}} = \frac{p}{(2\pi RT)^{\frac{1}{2}}} \tag{1}$$

At equilibrium, the rate of molecules impinging on a unit surface area is $\frac{1}{4}n\bar{v}$. Here, n is the number density, ρ the mass density, T the absolute temperature, and R the gas constant of the molecules in equilibrium with the liquid. The equilibrium evaporating rate is also given by Eq (1); this is the maximum rate at which molecules can escape from a liquid surface which is kept at a temperature T. Thus, the evaporating rate into a vacuum from this liquid surface is also given by Eq (1).

The pressure p in Eq (1) is the vapor pressure at saturation. Since pressure is a scalar quantity, it represents the sum of the pressures acting on the surface by the evaporating and the condensing molecules. At equilibrium, these two contributions equilibrate with each other. Hence, the equilibrium evaporating pressure is equal to

half of the saturation vapor pressure. When the surface is surrounded by a perfect vacuum, the condensing pressure vanishes and the pressure due to the evaporating molecules is just given by the equilibrium evaporating pressure, or half of the saturation vapor pressure. Consequently, we can expect that the rate of momentum acquired by a liquid surface when its molecules are evaporating into a vacuum is equal to half of the saturation vapor pressure. This is verified analytically below.

The molecules evaporating from a liquid surface kept at temperature T have a Maxwellian distribution function $n(2\pi RT)^{-\frac{3}{2}} e^{-v^2/2RT}$. Each beam of molecules emanating with a velocity v from a unit surface area and at an angle θ inclined from the normal to the area carries a flux rate of $nv\cos\theta$ and a momentum rate of $mnv^2\cos\theta = \rho v^2\cos^2\theta$. Hence the total momentum rate in question is given by $\rho(2\pi RT)^{-\frac{3}{2}} \iiint v^2\cos^2\theta\, e^{-\frac{v^2}{2RT}} v^2\sin\theta\, dv\, d\theta$. Integrating v from 0 to ∞, θ from 0 to $\frac{\pi}{2}$, and φ from 0 to 2π readily yields $\frac{1}{2}\rho RT = \frac{1}{2}p$ and completes the verification. If the surrounding vacuum is imperfect, then the rate is given by

$$\tfrac{1}{2}\alpha\rho \text{ with } \alpha \leq 1$$

α can be determined either from the given degree of imperfection or experimentally.

APPENDIX D

NORMAL FREEZING OF IDEAL TERNARY SYSTEMS OF THE PSEUDOBINARY TYPE[†]

by

C. H. Li[‡]

November 1972

[†]Published as Grumman Research Department RM-557. Submitted for publication to the Journal of Applied Physics

[‡]Research Department, Grumman Aerospace Corporation, Bethpage, New York 11714

ABSTRACT

Perfect liquid mixing but no solid diffusion is assumed in normal freezing. In addition, the molar compositions of the freezing solid and remaining liquid, respectively, follow the solidus and liquidus curves of the constitutional diagram. For the linear case, in which both the liquidus and solidus are perfectly straight lines, the normal freezing equation giving the fraction solidified at each melt temperature and the solute concentration profile in the frozen solid was determined as early as 1902, and has since been repeatedly published. Corresponding equations for quadratic, cubic, or higher-degree liquidus and solidus lines have also been obtained. This paper gives the equation of normal freezing for ideal ternary liquid solutions solidified into ideal solid solutions of the pseudobinary type. Sample computations with the use of this new equation were made and are given for the Ga-Al-As system.

TABLE OF CONTENTS

INTRODUCTION

Perfect liquid mixing but no solid diffusion is assumed in normal freezing. In addition, the molar compositions of the freezing solid and remaining liquid, respectively, follow the solidus and liquidus curves of the constitutional diagram.

For the linear case, in which both the liquidus and solidus are perfectly straight lines, the normal freezing equation giving the fraction solidified at each melt temperature and the solute concentration profile in the frozen solid was determined as early as 1902 (Ref. 1), and has since been repeatedly published (Refs. 2-9). Corresponding equations for quadratic, cubic, or higher-degree liquidus and solidus lines have also been obtained (Refs. 10-12). A recent publication presents the normal freezing equation for ideal dilute solutions or alloys in which the liquidus and solidus are exponential functions of the reciprocal absolute melt temperature (Ref. 13). The logarithm of the mole fraction segregation coefficient k_m for the dilute component is, therefore, also a linear function of the reciprocal of the absolute temperature. Further, in such ideal solutions, the ratio of partial pressure of each component, p_A, to that of the pure component, p_A^o, equals the atomic fraction x_A, i.e., $x_A = p_A/p_A^o$. This last equation permits the computation of the solidification behavior

of such solutions or alloys and the resultant solid concentration profiles from basic thermodynamic quantities without the use of phase diagrams.

THE PSEUDOBINARY SYSTEM

This memorandum gives the equation of normal freezing for ideal ternary liquid solutions of A, B, and C atoms (Fig. 1) solidified into ideal solid solutions of AB-AC compounds with A atoms on one sublattice and B or C atoms on the other. Such systems can be treated as pseudobinary systems. Account is taken of the entropy of mixing of the three atomic species to form the ideal liquid solutions along the pseudobinary.

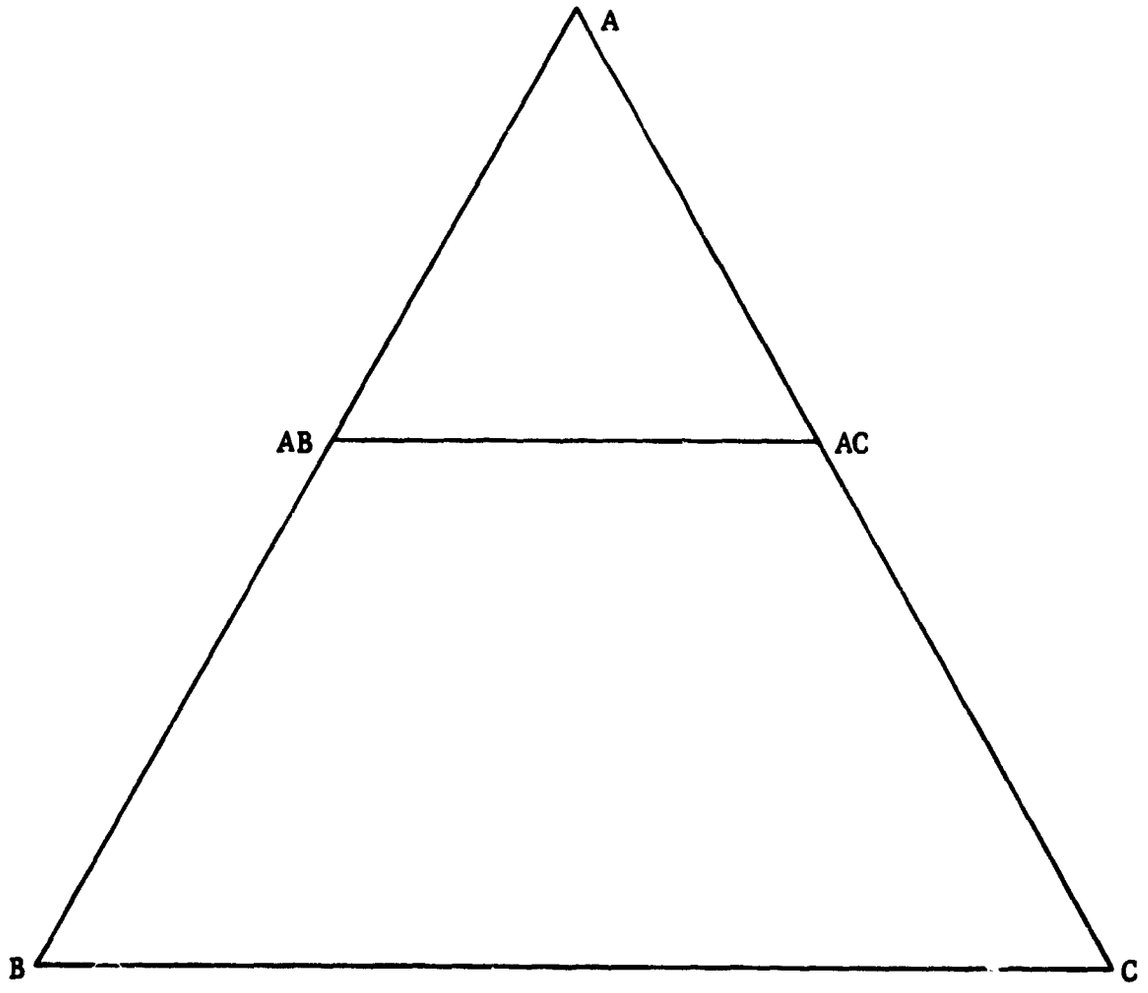

Fig. 1 Constitutional Diagram for a Ternary System of the Pseudobinary Type

For the compound AB, we have

$$AB(s) = A(l) + B(l) \quad . \tag{1}$$

The equilibrium constant for the reaction is

$$K = \frac{x_A^l \cdot x_B^l}{x_{AB}^s} \tag{2}$$

and the standard free energy ΔF_{AB}^o and the free energy of formation ΔF_{AB}^f are related to K at temperature T by

$$-\Delta F_{AB}^o + \Delta F_{AB}^f = RT \ln K \quad . \tag{3}$$

For the compound AB, the free energy of formation, ΔF_{AB}^f, is related to the free energy of melting, ΔF_{AB}^m, and the heat of melting, ΔH_{AB}^m, at the melting point T_{AB}^m by

$$\Delta F_{AB}^m = \Delta H_{AB}^m (1 - T/T_{AB}^m) = -\Delta F_{AB}^f - RT \ln 4 \quad . \tag{4}$$

It has been assumed that the difference in heat capacity between the liquid and solid is negligible. The $-RT \cdot \ln 4$ term is the ideal entropy of mixing to form the stoichiometric liquid phase. Hence,

$$-RT \ln 4 \cdot \frac{x_A^l \cdot x_B^l}{x_{AB}^s} = \Delta H_{AB}^m (1 - T/T_{AB}^m) \quad . \tag{5}$$

Similarly, for the compound AC, we have

$$-RT \ln 4 \cdot \frac{x_A^l \cdot x_C^l}{x_{AC}^s} = \Delta H_{AC}^m \left(1 - T/T_{AC}^m\right) \quad , \tag{6}$$

where ΔH_{AC}^m is the heat of formation of the compound AC, assumed constant; and T_{AC}^m is the melting point of AC.

For the ternary liquid phase of the pseudobinary,

$$\begin{aligned} x_A^l &= \tfrac{1}{2} \quad , \\ x_B^l + x_C^l &= \tfrac{1}{2} \quad . \end{aligned} \tag{7}$$

Hence,

$$-RT \ln 4 \cdot \tfrac{1}{2} \cdot x_B^l / x_{AB}^s = \Delta H_{AB}^m \left(1 - T/T_{AB}^m\right) \quad , \tag{8}$$

and

$$-RT \ln 4 \cdot \tfrac{1}{2} \cdot \left(\tfrac{1}{2} - x_B^l\right)/\left(1 - x_{AB}^s\right) = \Delta H_{AC}^m \left(1 - T/T_{AC}^m\right) \quad . \tag{9}$$

Equations (8) and (9) are essentially the same as those previously given (Refs. 14,15). From these equations,

$$\begin{aligned} 2 \cdot x_B^l &= x_{AB}^s \cdot \exp\left(-\frac{\Delta H_{AB}^m}{R}\left[1/T - 1/T_{AC}^m\right]\right) \\ &= x_{AB}^s \cdot \exp(a + b/T) = x_{AB}^s \cdot U \end{aligned} \tag{10}$$

$$\begin{aligned} 1 - 2 \cdot x_B^l &= \left(1 - x_{AB}^s\right) \cdot \exp\left(-\frac{\Delta H_{AC}^m}{R}\left[1/T - 1/T_{AC}^m\right]\right) \\ &= \left(1 - x_{AB}^s\right) \cdot \exp(f + g/T) = \left(1 - x_{AB}^s\right) \cdot V \end{aligned} \tag{11}$$

where

$$b = -\Delta H^m_{AB}/R \quad , \quad a = -b/T^m_{AB} \quad , \quad g = -\Delta H^m_{AC}/R \quad , \quad \text{and} \quad f = -g/T^m_{AC} \qquad (12)$$

are constants for a given ternary system of the type shown in Fig. 1, while the temperature-dependent variables

$$U = \exp(a + b/T) \quad \text{and} \quad V = \exp(f + g/T) \quad . \qquad (13)$$

Equations (10) and (11) yield the solidus equation for the compound AB

$$1 - x^s_{AB} \cdot U = (1 - x^s_{AB}) \cdot V \quad . \qquad (14)$$

Hence,

$$x^s_{AB} = (1 - V)/(U - V) \quad . \qquad (15)$$

The value of x^s_{AB} can be as small as zero when, according to Eqs. (15) and (13), $V = 1 = \exp(f + g/T)$, i.e., when $T = -g/f = T^m_{AC}$ and $x^l_B = x^s_{AB}/2 = 0$ [Eq. (11)], as expected. The value of x^s_{AB} can also be as large as 1 when $U = 1 = \exp(a + b/T)$ in accordance with Eqs. (15) and (13), i.e., when $T = -b/a = T^m_{AB}$ and $x^l_B = x^s_{AB}/2 = \frac{1}{2}$ [Eq. (10)], also as expected.

Notice that there are no AB or AC compounds in the melt, while in the solid there are only compounds AB and/or AC, but no individual elements A, B, and C. Hence, the thermodynamic molar concentrations x^s_{AB}, x^s_{AC}, x^l_A, x^l_B, x^l_C.

Considering the ternary liquid or solid solutions as a whole, and, without regard to crystallographic lattice arrangements, we

can define the chemical molar concentrations m_A, m_B, and m_C. Evidently,

$$\left.\begin{aligned} & m_A^s = m_A^l = \tfrac{1}{2} \quad , \\ & m_B^l + m_C^l = m_B^s + m_C^s = \tfrac{1}{2} \quad , \\ & m_B^l = x_B^l \quad , \text{ and} \\ & m_B^s = \tfrac{1}{2}\, x_{AB}^s \quad . \end{aligned}\right\} \qquad (16)$$

THE NORMAL FREEZING EQUATION

We can now balance the amount of component B in the remaining liquid by its chemical molar concentrations m_B^l and m_B^s, and then obtain the usual differential equation for normal freezing (Refs. 9, 11-13) as follows

$$\frac{dm_B^l}{m_B^l - m_B^s} = \frac{dp}{1 - p} \tag{17}$$

where p is the fraction solidified.

Substituting into the normal freezing differential equation results in

$$-d\ \ln(1 - p) = \frac{V(b[1 - v] - g[1 - U])}{(1 - U)(1 - V)(1 - V/U)} d(1/T)$$

$$= \left[\frac{\alpha}{(1 - U)} + \frac{\beta}{(1 - V)} + \frac{\gamma}{(1 - \cdot} \right. \quad d(\tfrac{1}{T})$$

where

$$\left.\begin{aligned} \alpha &= \frac{q}{q - 1} \\ \beta &= \frac{1}{1 - s} \\ \gamma &= \frac{r}{1 - r} \end{aligned}\right\} , \tag{18}$$

and

$$\left.\begin{aligned} q &= \exp(f - ga/b) \\ r &= \exp \frac{ag - bf}{g - b} \\ s &= \exp \frac{bf - ag}{g} \\ U_o &= \exp(f + g/T_o) \\ V_o &= \exp(a + b/T_o) \end{aligned}\right\} , \qquad (19)$$

and

$$p = 1 - \left[\frac{1 - U_o}{1 - U}\right]^{\alpha} \cdot \left[\frac{1 - V_o}{1 - V}\right]^{\beta} \cdot \left[\frac{1 - V_o/U_o}{1 - V/U}\right]^{\gamma} \qquad (20)$$

where T_o is the initial freezing temperature and can be determined from the pseudoliquidus line on substituting for x^1_{AB} the initial melt composition, $x^1_{AB,o} = 2 \cdot x^1_{B,o}$.

THE Ga-Al-As SYSTEM

This ternary system can be considered as a GaAs-AlAs pseudo-binary. In the liquid melt, we have

$$x_A^l = x_{As}^l = m_{As}^l = 0.5$$

$$x_B^l + x_C^l = x_{Ga}^l + x_{Al}^l = m_B^l + m_C^l = m_{Ga}^l + m_{Al}^l = 0.5 \quad .$$

In the GaAs-AlAs mixed crystal, we have

$$x_{GaAs}^s = 2m_{Ga}^s$$

$$x_{AlAs}^s = 2m_{Al}^s$$

$$x_{GaAs}^s + x_{AlAs}^s = 2(m_{Ga}^s + m_{Al}^s) = 1.0 \quad .$$

To determine the phase diagram [i.e., liquidus and solidus, Eqs. (8)-(15)] and, in addition, to compute the normal freezing behavior according to Eqs. (18)-(20), the following four thermodynamic constants are required (Ref. 14 gives the values of these constants):

- Melting point of GaAs 1511 K
- Melting point of AlAs 2013 K
- Heat of formation of GaAs 16.64 Kcal/mol
- Heat of formation of AlAs 22.8 Kcal/mol .

Hence, $a = 5.700$, $b = -11{,}470$, $f = 5.542$, $g = -8{,}374$, $q = 3.983$, $r = 0.1505$, $s = 166.5$, $\alpha = -1.335$, $\beta = 0.1772$, and $\gamma = 1.006$.

Table 1 summarizes the solidification behavior of the Ga-Al-As system, treated as a pseudobinary. The first three columns describe the phase diagram, i.e., the concentration of aluminum in the liquid melt x^l_{Al} and that of AlAs in the solid crystal x^s_{AlAs} at temperatures from 1720°C down to 1238°C at 20°C intervals. The next two columns, obtained from the first three, show that the segregation coefficient k for Al, i.e., $k_{Al} = x^s_{AlAs}/2x^l_{Al}$, always exceeds unity while that of Ga, i.e., $k_{Ga} = (1 - x^s_{AlAs})/(1 - 2x^l_{Al})$, never does so except at 1238°C. Both of these segregation coefficients, however, are widely variable, increasing with decreasing melt temperature, by factors of over 6.3 in the case of k_{Al} and of over 3.7 in the case of k_{Ga}. Thus, for this system, as well as for many others, the linear normal freezing equations (Refs. 1-9) involving constant segregation coefficients are generally not applicable.

These phase diagram data can, of course, be obtained also by means of the equations of Ilegems and Pearson (Ref. 14), or those of Steininger (Ref. 15). The direct computation of the normal freezing data from basic thermodynamic constants, however, appears to have never been attempted or published. By means of Eqs. (18) and (19) of this memorandum, these normal freezing data are calculated and given as the last nine columns. Here, the fraction

Table 1

SOLIDIFICATION OF Ga-Al-As SYSTEMS

T, °C	x^l_{Al}	x^s_{AlAs}	k_{Al}	k_{Ga}	$x^l_{Al,o}$ = 0.05	0.10	0.15	0.20	0.25	0.30	0.35	0.40	0.45
1720	0.4633	0.9808	1.058	0.2617									---
1700	0.4281	0.9607	1.122	0.2731								---	0.4156
1680	0.3946	0.9399	1.191	0.2852								0.0809	0.6776
1660	0.3627	0.9181	1.266	0.2982			Fraction Solidified, p				---	0.4072	0.7921
1640	0.3325	0.8955	1.346	0.3120							0.1805	0.5839	0.8541
1620	0.3038	0.8718	1.435	0.3267						---	0.3935	0.6921	0.8920
1600	0.2767	0.8470	1.530	0.3425						0.2029	0.5349	0.7638	0.9172
1580	0.2510	0.8210	1.635	0.3595					---	0.3728	0.6340	0.8142	0.9348
1560	0.2268	0.7937	1.749	0.3776					0.1904	0.4971	0.7066	0.8510	0.9477
1540	0.2040	0.7649	1.874	0.3972				---	0.3415	0.5910	0.7613	0.8788	0.9575
1520	0.1826	0.7345	2.012	0.4182				0.1470	0.4585	0.6637	0.8037	0.9004	0.9650
1500	0.1624	0.7024	2.162	0.4408			---	0.2926	0.5510	0.7211	0.8372	0.9174	0.9710
1480	0.1436	0.6684	2.328	0.4652			0.0604	0.4096	0.6252	0.7672	0.8642	0.9310	0.9758
1460	0.1259	0.6323	2.510	0.4915			0.2120	0.5049	0.6857	0.8048	0.8861	0.9422	0.9797
1440	0.1095	0.5938	2.712	0.5200		---	0.3369	0.5834	0.7355	0.8357	0.9041	0.9513	0.9829
1420	0.0942	0.5528	2.935	0.5510		0.0641	0.4408	0.6486	0.7769	0.8614	0.9192	0.9590	0.9856
1400	0.0799	0.5089	3.183	0.5845		0.2101	0.5280	0.7034	0.8117	0.8831	0.9318	0.9654	0.9878
1380	0.0668	0.4619	3.458	0.6210		0.3335	0.6018	0.7498	0.8411	0.9013	0.9424	0.9708	0.9897
1360	0.0546	0.4115	3.765	0.6607	---	0.4386	0.6646	0.7892	0.8662	0.9169	0.9515	0.9754	0.9914
1340	0.0435	0.3571	4.108	0.7041	0.0995	0.5289	0.7185	0.8231	0.8877	0.9302	0.9593	0.9793	0.9928
1320	0.0332	0.2985	4.492	0.7515	0.2489	0.6070	0.7652	0.8525	0.9063	0.9418	0.9660	0.9828	0.9940
1300	0.0239	0.2348	4.922	0.8034	0.3801	0.6757	0.8062	0.8782	0.9227	0.9520	0.9720	0.9858	0.9950
1280	0.0153	0.1660	5.407	0.8604	0.4982	0.7375	0.8431	0.9014	0.9374	0.9611	0.9773	0.9885	0.9960
1260	0.0076	0.0909	5.954	0.9232	0.6120	0.7970	0.8787	0.9238	0.9516	0.9699	0.9825	0.9911	0.9969
1240	0.0007	0.0091	6.573	0.9923	0.7782	0.8839	0.9306	0.9564	0.9723	0.9828	0.9900	0.9949	0.9982
1238	0.0000	0.0000	6.643	1.0000	1.0000	1.0000	1.0000	1.0000	1.0000	1.0000	1.0000	1.0000	1.0000

Basic thermodynamic constants used in the computation:

ΔH_{GaAs} = 16.64 Kcal/mol T_{GaAs} = 1511 K

ΔH_{AlAs} = 22.8 Kcal/mol T_{AlAs} = 2013 K

solidified, p, is given as a function of both the melt temperature, T, and the Al concentration in the original liquid melt, $x^{l}_{Al,o}$. The concentration profile can be obtained by plotting the concentration of AlAs in the solid crystal, x^{s}_{AlAs}, against the fraction solidified, p, for the appropriate initial Al concentration in the melt, $x^{l}_{Al,o}$.

OTHER SYSTEMS

Many other ternary systems can also be treated as pseudo-binaries. The necessary thermodynamic constants are usually available in the literature. Steininger (Ref. 15), for example, has examined a number of important systems and given the necessary thermodynamic constants required to compute the solidification behaviors and the phase diagrams. These systems include: InAs-GaAs, InSb-InAs, InSb-GaSb, GaSb-AlSb, InSb-AlSb, CdTe-ZnTe, CdTe-CdSe, HgTe-CdTe, GeTe-MnTe, $PbBr_2$-$PbCl_2$, InAs-InP, SnTe-PbTe, PbTe-PbSe, HgTe-HgSe, ZnTe-ZnSe, and HgTe-ZnTe. For the first 13 systems, his calculated solidus curves are in good to excellent agreement with the published experimental values. These systems can, therefore, be considered ideal. One can thus compute with some confidence their normal freezing behaviors according to Eqs. (18)-(20) of this memorandum.

REFERENCES

1. Lord Rayleigh, Phil. Mag., Vol. 4, 1902, p. 521.
2. Gulliver, G., Metallic Alloys, Chase Griffin, London, 1922, pp. 397-425.
3. Scheuer, E., Z. Metallk., Vol. 23, 1931, p. 237.
4. Hayes, A. and Chipman, J., Trans. AIME, Vol. 135, 1939, p. 85.
5. Luneau, M., Revue Métallurgie, Vol. 39, 1942, p. 218.
6. Mathieu, K. and Neerfeld, H., Arch. Eisenhüttenwesen, Vol. 15, 1942, p. 389.
7. Scheil, E., Z. Metallk., Vol. 34, 1942, p. 70.
8. McFee, R., "Foreign Ion Rejection in the Growth of Sodium Chloride Single Crystals from the Melt," J. Chem. Phys., Vol. 15, 1947, p. 856.
9. Pfann, W., Trans. AIME, Vol. 194, 1952, p. 747.
10. Li, C., "Epitaxial Growth of Silicon and Germanium," Phys. Stat. Solidi, Vol. 15, 1966, p. 3.
11. Li, C., "Normal Freezing with Variable Segregation Coefficients," Brit. J. Appl. Phys., Vol. 18, 1967, p. 359.
12. Li, C.,"Normal Freezing with Cubic Liquidus and Solidus Lines," J. Appl. Phys., Vol. 39, 1968, p. 2094.
13. Li, C., "Normal Freezing with Ideal Binary Solutions," J. Appl. Phys., Vol. 42, 1971, p. 4521.

14. Illegems, M. and Pearson, G., Proceedings of 1968 Symposium on GaAs, 1969; (London; The Institute of Physics and The Phys. Soc.) p. 3.

15. Steininger, J., J. Appl. Phys., Vol. 41, 1970, p. 2713.

APPENDIX E

NORMAL EVAPORATION OF BINARY ALLOYS[†]

by

C. H. Li[‡]

November 1972

[†]Published as Grumman Research Department RM-558. Submitted for publication to the Journal of Applied Physics

[‡]Research Department, Grumman Aerospace Corporation, Bethpage, New York 11714

ACKNOWLEDGMENT

The author wants to thank Prof. F. F. Y. Wang, Dr. J. L. Mukherjee, and Mr. K. P. Gupta, all of State University of New York, Stony Brook, our associate team members under NASA Contract NAS 8-27891, for stimulating discussions and help in data analyses.

ABSTRACT

In the study of normal evaporation, it is assumed that the evaporating alloy is homogeneous, that the vapor is instantly removed, and that the alloy follows Raoult's law. The differential equation of normal evaporation relating the evaporating time to the final solute concentration is given and solved for several important special cases. Uses of the derived equations are exemplified with a Ni-Al alloy and some binary iron alloys. The accuracy of the predicted results are checked by analyses of actual experimental data on Fe-Ni and Ni-Cr alloys evaporated at 1600°C, and also on the vacuum purification of beryllium. These analyses suggest that the normal evaporation equations presented here give satisfactory results that are accurate to within an order of magnitude of the correct values, even for some highly concentrated solutions. Limited diffusion and the resultant surface solute depletion or enrichment appear important in the extension of this normal evaporation approach.

TABLE OF CONTENTS

INTRODUCTION

In normal evaporation, we assume that the evaporating alloy is always homogeneous in composition, that the vapor is instantly removed, and that the alloy follows the Raoult's law (Ref. 1). Such conditions exist or are approached in an induction-stirred, melt-in-vacuum or liquid drop-in-space.

This memorandum deals with the normal evaporation of binary alloys. In particular, we study the evaporative segregation patterns, i.e., the type and degree of enrichment or depletion of solute in the evaporating source, at different evaporation temperatures and times.

DIFFERENTIAL EQUATION OF NORMAL EVAPORATION

The appendix of Ref. 2 gives the exact solution for the normal evaporation of binary alloys. This equation relates the concentration of the solute, m, at a time, t, when the mole fraction of the alloy remaining is F, as follows:

$$F = \frac{N}{N_o} = \left(\frac{m}{m_o}\right)^{\frac{V}{U-V}} \left(\frac{1 - m_o}{1 - m}\right)^{\frac{U}{U-V}} \tag{1}$$

where N and N_o are, respectively, the number of moles of both solvent and solute at evaporating times $t = t$ and $t = 0$; m_o is the initial molar concentration of the alloy; and U and V are, respectively, the evaporation rates of pure solute and solvent.

For pure solute and solvent, respectively, these evaporation rates in $mol/cm^2/sec$ are

$$U = K\, 10^{A_u - B_u/T} (M_u T)^{-\frac{1}{2}} \tag{2}$$

and

$$V = K\, 10^{A_v - B_v/T} (M_v T)^{-\frac{1}{2}} \tag{3}$$

where $K = 5.833 \times 10^{-5}\, \alpha$, $\alpha = 1$ for most metals (Ref. 1); M_u and M_v are, respectively, the molecular weights of the solute and solvent atoms; T is the evaporating temperature in degrees Kelvin; and A_u and B_u or A_v and B_v are evaporating constants for the solute or solvent given, for example, by Ref. 1.

Differentiating Eq. (1) yields

$$dm = \frac{(U - V)m(1 - m)}{[mU + (1 - m)V]N} dN \tag{4}$$

but

$$dN = - [mU + (1 - m)V]A \cdot dt \tag{5}$$

where A is the evaporating area of the alloy, assumed constant here.

Substituting Eq. (5) into Eq. (4) results in

$$dt = Gm^{\alpha}(1 - m)^{\beta}dm \tag{6}$$

where

$$G = - \frac{N_o(1 - m_o)^{\alpha+2}}{A(U - V)m_o^{\alpha+1}} \tag{7}$$

$$\alpha = (2V - U)/(U - V) \tag{8}$$

$$\beta = (V - 2U)/(U - V) \tag{9}$$

SPECIAL CASE SOLUTIONS OF THE NORMAL EVAPORATION EQUATION

Equations (6)-(9) allow us to determine the evaporating time, t, for an alloy to reach a specific solute concentration, m. Unfortunately, these equations are not exactly solvable in the general case. All of the following special and important cases, (except Case V), however, are solvable in closed forms.

Case I: The solute is much more evaporative than the solvent, i.e., $U >> V$; or $\alpha = -1$ and $\beta = -2$. In this case

$$dt_1 = \frac{G_1 dm}{m(1 - m)^2} \tag{10}$$

where

$$G_1 = - \frac{N_o(1 - m_o)}{AU}$$

and

$$t_1 = G_1 \left[\ell n \frac{(1 - m_o)m}{m_o(1 - m)} + \frac{m - m_o}{(1 - m_o)(1 - m)} \right] \tag{11}$$

When $m \simeq m_o$, the second term in the bracket is nearly 0. The evaporation time for this first case, t_1, is then a logarithmic function of m, as has been experimentally observed (see e.g., Ref. 3).

Also, when $m \simeq m_o \simeq 0$,

$$t_1 \simeq \frac{N_o}{AU} \ell n \frac{m_o}{m} \tag{12}$$

Case II: The solvent is much more evaporative than the solute, i.e., $V \gg U$; or $\alpha = -2$ and $\beta = -1$. In this case

$$dt_2 = \frac{G_2 dm}{(1 - m)m^2} \tag{13}$$

where

$$G_2 = \frac{m_o N_o}{AV}$$

and

$$t_2 = G_2\left[\ell n \frac{(1 - m_o)m}{m_o(1 - m)} + \frac{m - m_o}{m_o m}\right] \tag{14}$$

For dilute solutions (i.e., $m \simeq m_o \simeq 0$), t_2 also becomes a logarithmic function of m, as has been observed.

Case III: $\alpha = (2V - U)/(U - V) = 0$, i.e., $U = 2V$ and $\beta = -3$

$$t_3 = G_3\left[(1 - m)^{-2} - (1 - m_o)^{-2}\right] \tag{15}$$

where

$$G_3 = -\frac{N_o(1 - m_o)^2}{2AVm_o}$$

Case IV: $\beta = (V - 2U)/(U - V) = 0$, i.e., $V = 2U$ and $\alpha = -3$. In this case

$$t_4 = G_4\left(m^{-2} - m_o^{-2}\right) \tag{16}$$

where

$$G_4 = - \frac{N_o m_o^2}{2AU(1 - m_o)}$$

Equations (15) and (16) show that under some conditions, the evaporating time, t, is more adequately represented by linear functions of $(1 - m)^{-2}$ or m^{-2}, rather than by logarithmic functions of m.

Case V: For relatively dilute alloys, i.e., m and $\beta m << 1$, the following solution by series expansion can be obtained from Eq. (6):

$$dt_5 = Gm^{\alpha}\left[1 - \beta m + \frac{(\beta m)^2}{2!} + \cdots + (-1)^i \frac{(\beta m)^i}{i!} + \cdots\right] \qquad (17)$$

and

$$t_5 = G\left[\frac{m^{\alpha+1} - m_o^{\alpha+1}}{\alpha + 1} - \frac{m^{\alpha+2} - m_o^{\alpha+2}}{\alpha + 2}\beta + \cdots + (-1)\frac{m^{\alpha+i+1} - m_o^{\alpha+i+1}}{(\alpha + i + 1)i!}\beta^i \cdots\right] \qquad (18)$$

For computer calculations, it is desirable to know the ratio of the i^{th} term to the $(i - 1)^{th}$ term, thus

$$- \frac{T_i}{T_{i-1}} = \frac{\beta(\alpha + 1)\left(m^{\alpha+i+1} - m_o^{\alpha+i+1}\right)}{i(\alpha + i + 1)\left(m^{\alpha+i} - m_o^{\alpha+i}\right)} \qquad (19)$$

which is generally less than $\beta m/i$ or $\beta m_o/i$.

Because $\beta m \ll 1$ and i constantly increases with each additional term, this series converges rapidly unless β is very large, i.e., unless $U = V$, which leads to the following interesting case:

Case VI; The solute and solvent are evaporating at equal rates, i.e., $U = V$. In this case, we would expect

$$m = m_o \quad \text{for all} \quad t \,. \tag{20}$$

There is, then, no evaporative segregation, that is, there is neither solute enrichment nor depletion in the evaporating source.

For any pair of solvent and solute, there is a unique temperature, T_s, at which $U = V$ and, hence, the alloy concentration remains stable or constant. Equations (2) and (3) give:

$$T_s = \frac{B_u - B_v}{A_u - A_v - 0.5 \log(M_u/M_v)} \tag{21}$$

Case VII: With extremely dilute alloys, i.e., $m \simeq m_o \simeq 0$, we have (Ref. 2)

$$F = N/N_o = (m/m_o)^{\alpha+1} \tag{22}$$

Hence,

$$t_7 = \frac{N_o}{AV}\left[1 - (m/m_o)^{\alpha+1}\right] \tag{23}$$

EXAMPLES OF COMPUTATION

- The Ni-Al System:

As an example of the use of the various derived equations, the evaporation behavior of an alloy containing 8 percent by weight of Al in Ni at the melting point of pure Ni (i.e., 1453°C) is computed. Here, the solute element (Al) is comparatively highly evaporative relative to the solvent (Ni). Equation (11), therefore, applies, and the time, t_1, to reach a final solute concentration m from a specified initial concentration, m_o, is directly proportional to N_oA/U (in the G_1 constant). Table 1 gives the times to reach various final Al concentrations for one mole (53.66g) of the 8 percent Al in Ni alloy ($m_o = 0.159$) evaporating at 1453°C from its (supposedly constant) 10 cm^2 surface.

Table 1

NORMAL EVAPORATION OF 8% BY WEIGHT ALUMINUM IN NICKEL AT 1453°C

Final Solute Concentration		Alloy Remaining		Evaporation Time (sec)
Weight Fraction	Mole Fraction	Weight (g)	Mole	
0.080	0.1590	53.66	1.0000	0.00
0.079	0.1573	53.60	0.9977	14.08
0.078	0.1555	53.53	0.9955	28.29
0.077	0.1536	53.47	0.9932	42.64
0.076	0.1518	53.41	0.9910	57.12
0.075	0.1500	53.34	0.9887	71.75
0.074	0.1481	53.28	0.9865	86.54
0.073	0.1463	53.22	0.9842	101.46
0.072	0.1444	53.15	0.9820	116.55
0.071	0.1426	53.09	0.9798	131.80
0.070	0.1407	53.03	0.9775	147.22

- Iron Alloys:

The evaporation behavior of binary iron alloys containing 20 different solute elements has also been studied. Table 2, listing

Table 2

EQUI-EVAPORATIVE TEMPERATURES FOR TWENTY BINARY IRON ALLOYS

Solute	U/V at 1600°C	T_s, °C	Solute	U/V at 1600°C	T_s, °C
Cd	3.765×10^{6}	13,540	W	4.412×10^{-12}	-69,590
Zn	2.065×10^{6}	15,610	C	8.210×10^{-8}	5,263
Mg	9.074×10^{5}	19,610	Mo	1.879×10^{-7}	-12,130
Ca	5.503×10^{4}	9,335	Zr	1.950×10^{-6}	-47,790
Pb	3.333×10^{3}	4,976	B	6.832×10^{-5}	9,510
Mn	1.070×10^{3}	20,740	V	3.804×10^{-3}	8,574
Al	45.65	7,918	Ti	2.254×10^{-2}	34,650
Cu	12.25	5,613	Co	4.362×10^{-1}	4,318
Sn	9.978	2,686	Si	5.238×10^{-1}	2,825
Cr	3.158	-215	Ni	5.897×10^{-1}	3,036

the equi-evaporative temperatures for these 20 different alloy systems, also gives the ratios of the solute evaporating rate, U, at 1600°C, to that of the solvent iron, V. At 1600°C, 10 of these solute elements evaporate faster than the solvent (the three left columns) and 10 slower (the three right columns). Moreover, these ratios vary widely over 18 decades, from 4.41×10^{-12} for the slowest evaporating, W, to 3.76×10^{6} for the fastest evaporating, Cd. Because of this wide variation in evaporating rates,

and because of the extreme sensitivities of the evaporating surface to unsuspected contaminants, predicted or experimental evaporating results cannot generally be very accurate.

The equi-evaporative temperatures in iron alloys also vary widely. Binary iron alloys containing Cr, Zr, Mo, and W have no practical equi-evaporative temperatures. One can, therefore, always expect these alloys to change compositions continuously with the evaporating time.

Table 3 shows the effect of evaporating temperature on the U/V ratios for four different solute elements Mg, Ca, Mn, and Al. In the range of 1500°C to 1900°C and beyond, increasing

Table 3

EFFECT OF SOLUTE ELEMENTS AND EVAPORATING TEMPERATURES ON THE VALUES OF U/V (x 1000) IN IRON ALLOYS

	Solutes			
Temp (°C)	Mg	Ca	Mn	Al
1500	2132.0	118.2	1.649	0.06037
1600	907.4	55.03	1.070	0.04565
1700	421.2	27.68	0.7261	0.03552
1800	210.5	14.88	0.5110	0.02831
1900	112.1	8.466	0.3719	0.02304

the evaporating temperatures always decreases the U/V ratios. This can also be seen from Table 2, as the equi-evaporative temperatures shown for these four binary iron alloys are higher than 1600°C, at which temperature the four solute elements evaporate

much faster than the solvent iron. Table 3 also shows that for the same temperature variation, the more evaporative the solute element, the more percentage variation the U/V ratio. In the case of Mg, e.g., the U/V ratio decreases by about 20 times from 1500°C to 1900°C, whereas for Al, the same ratio decreases only by less than three times over the same temperature interval.

Figure 1 shows the effect of solute elements and evaporating temperature, T, on the evaporating time t, for a given set of initial and final solute concentrations (i.e., $m_o = 0.01$ and $m = 1$ ppm). For given m_o and m, the log t versus 1/T curves for these highly evaporative solute elements are approximately linear and have positive slopes. This can be expected from Eq. (11) since, for given m_o and m, log t is linearly related to B/T - 0.5 log T, and since 0.5 log T is small relative to B/T within the evaporating temperature range studied. Thus, one can determine, from Fig. 1, the value of the elemental evaporating constant B, or heat of evaporation $\Delta H = 4.574\ B$ (Ref. 1), for the solute elements by plotting log t versus 1/T and measuring the slope of the resultant, nearly straight lines.

In Fig. 2, the log t versus 1/T relationships also appear nearly linear for all the four different initial concentrations (i.e., $m_o = 10^{-1}$, 10^{-2}, 10^{-3}, and 10^{-4}) of Al in Fe. This can also be seen from Eqs. (11) and (12). All these nearly straight lines have identical slopes, from which the heat of evaporation of pure Al can be evaluated.

Figures 3 and 4 display the effect on the evaporating time, t, of final solute concentration, m, and either initial concentration m_o (in Fig. 3) or solute elements (in Fig. 4).

Figure 5 indicates that Mg, Ca, and Mn in Fe alloys are so evaporative at 1600°C that practically all of these elements

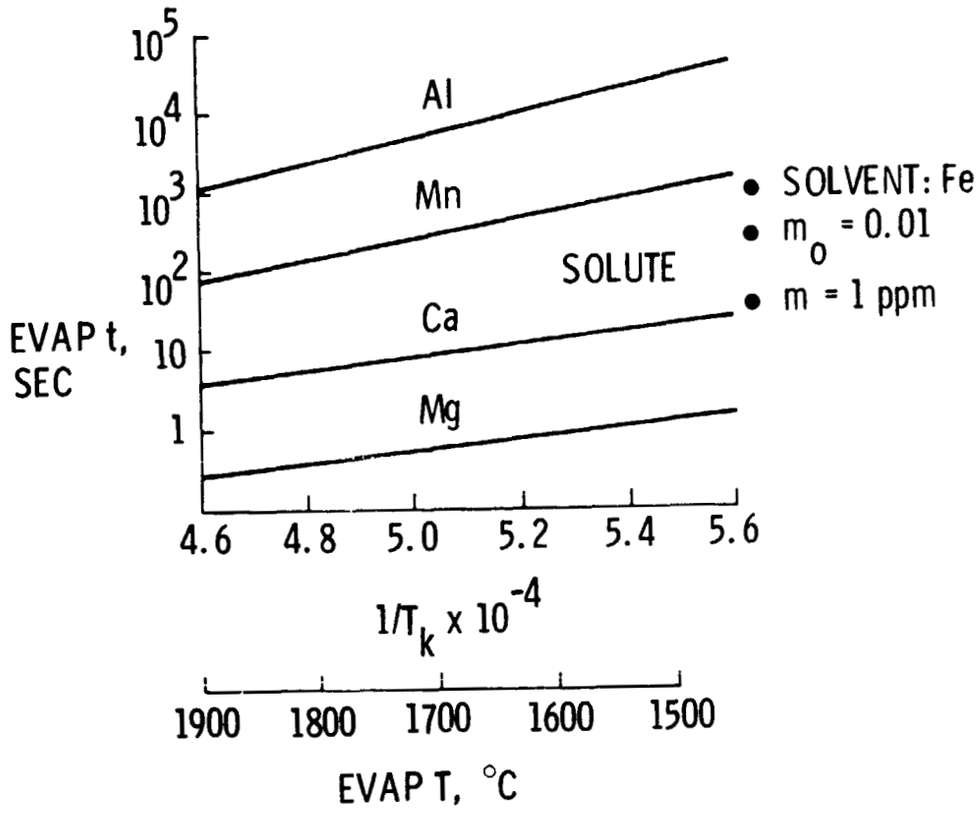

Fig. 1 Evaporating Times for Different Dilute Iron Alloys to Change Concentration from m_o = 0.01 to m = 1 ppm

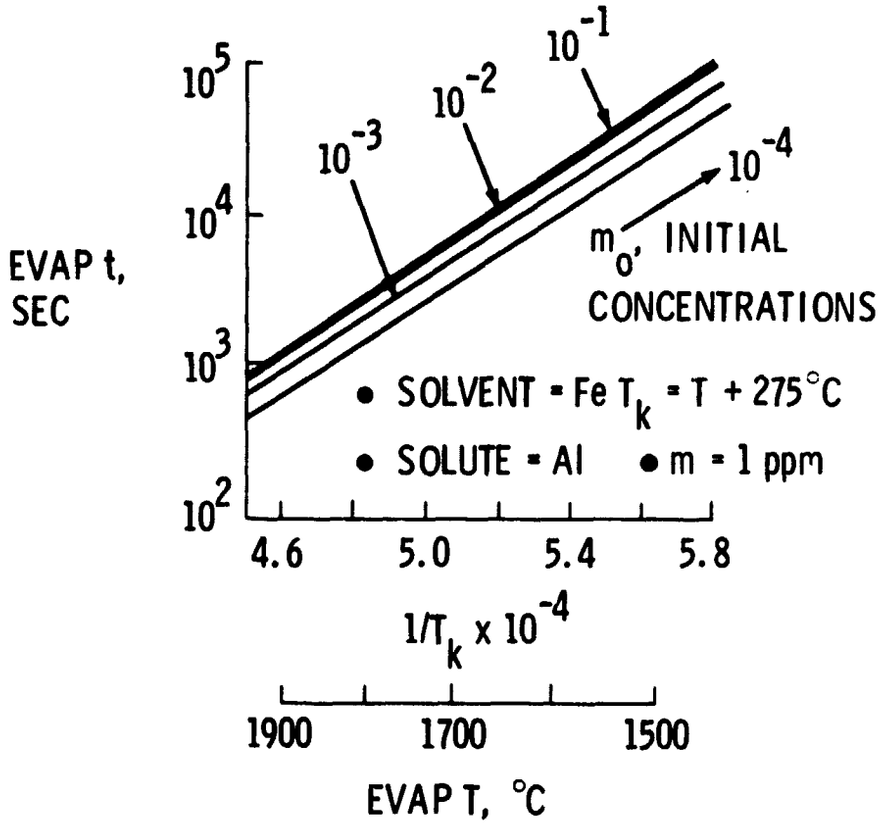

Fig. 2 Evaporating Times for Dilute Iron Alloys Containing Al and Starting at Four Different Initial Concentrations, to Reach a Final Concentration of m = 1 ppm

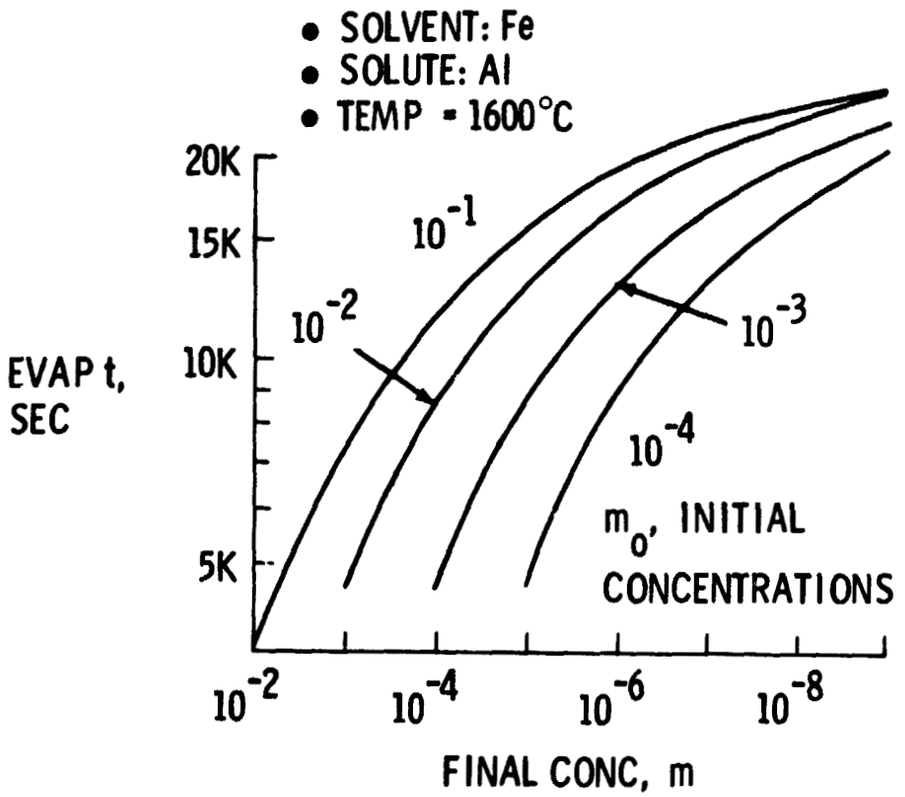

Fig. 3 Effect of Initial and Final Solute Concentrations on the Evaporating Times in Dilute Iron Alloys Containing Al at 1600°C

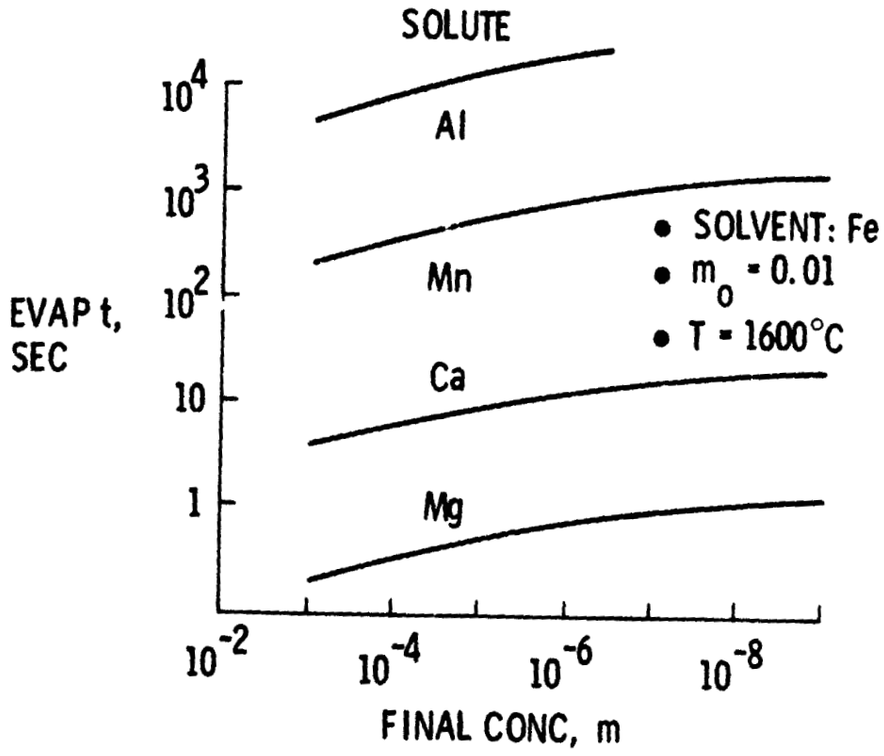

Fig. 4 Effect of Solute Elements and Final Concentration on the Evaporating Times in Dilute Iron Alloys at 1600°C

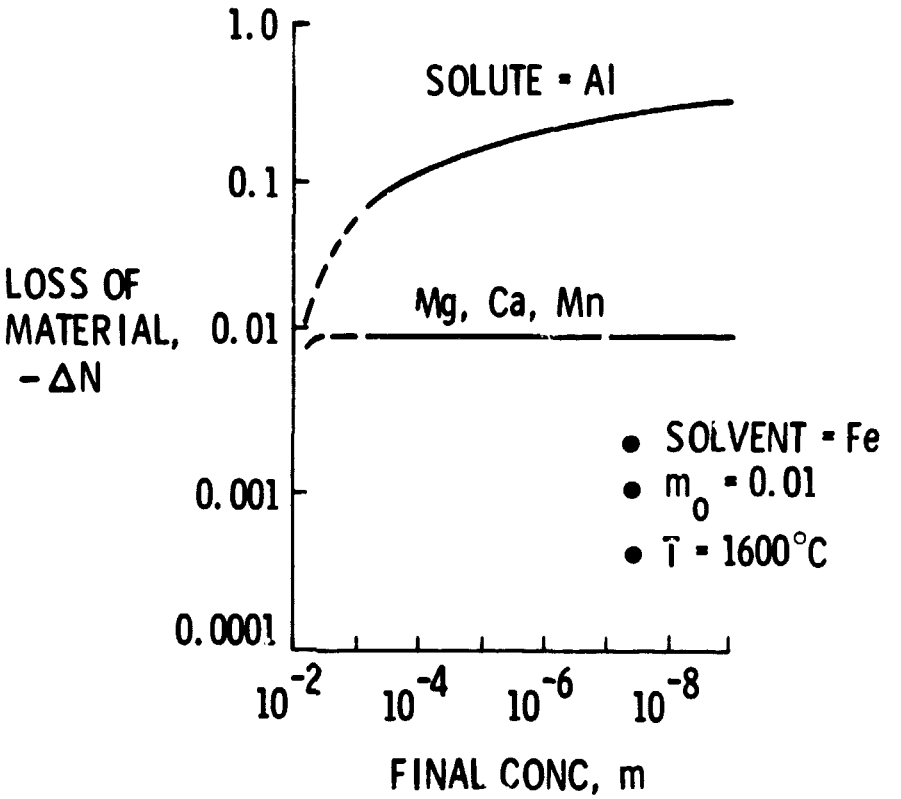

Fig. 5 Evaporation Loss of Dilute Iron Alloys at 1600°C As a Function of Solute Elements and Final Solute Concentrations

are removed by evaporation, without much evaporative loss of the solvent Fe atoms. On the other hand, Al is comparatively less evaporative so that much of the solvent Fe atoms are evaporated off together with Al. To achieve a purification factor of 10^7 (i.e., to $m = 10^{-9}$) from $m_o = 0.01$, for example, the initial evaporating alloy must lose over 30 percent of its material.

ACCURACY OF PREDICTED RESULTS

To check the validity of our derived equations for normal evaporation of binary alloys, the current literature has been searched. Several sets of alloy evaporation data have been found that are amenable to normal evaporation analysis. These sets include the following:

- The Fe-Ni and Ni-Cr Systems:

An analysis has been made of the data by Obradovi . et al. (Ref. 4) for Fe-Ni and Ni-Cr alloys evaporated at 1600 C for different times under various ambient pressures. In the 80% Ni-20% Cr case, evaporation started with $N_o = 0.7582$ moles of the alloy having an evaporating area $A = 10.0$ cm^2. The solute and solvent evaporating rates are, respectively, $U_{Cr} = 3.479 \times 10^{-5}$ and $V_{Ni} = 6.386 \times 10^{-6}$ mol/cm^2/sec. This is a case where the solute, Cr, is comparatively highly evaporative relative to the solvent, Ni. Hence, the evaporating time t_1 given in Eq. (11) applies, i.e.,

$$t_1 = G_1 \left[\ell n \frac{(1 - m_o)m}{m_o(1 - m)} + \frac{m - m_o}{(1 - m_o)(1 - m)} \right]$$

where $G_1 = -N_o (1 - m_o)/AU$, and m_o and m are the initial and final molar solute concentrations in the alloy.

Least square fits of the Obradovic data give nearly constant values of observed G_1: -1.785, -5.064, and -5.064 (x 10^4 sec) for ambient pressures of 1, 100, and 500 (x 10^{-3} torr). The calculated values of G_1, though also nearly constant, are, however, one order of magnitude smaller, indicating surface solute depletion. Similar analysis for the 60% Fe-40% Ni alloy evaporated with

N_o = 0.7478 moles and A = 10.0 cm^2 gives $U_{Ni} = 6.386 \times 10^{-6}$ and $V_{Fe} = 1.081 \times 10^{-5}$ $mol/cm^2/sec$. Here, the solvent Fe is much more evaporative than the solute Ni, and Eq. (14) applies. The values of observed evaporating coefficients $G_2 = m_o N_o/AV$ are 2.469, 1.369, and 8.386 (x 10^4 sec), for ambient pressures of 1, 100, and 500 (x 10^{-3} torr), respectively. The calculated G_2's are again nearly constant but also an order of magnitude smaller than the observed G_2's, again indicating solvent depletion (or solute enrichment) at the surface. Details of these analyses are given in Ref. 5.

- Beryllium Purification

The kinetics of normal evaporation for beryllium have been quantitatively checked with actual results of beryllium purification during vacuum induction melting. Details are given in Ref. 6. In these tests, beryllium was crucible-free, induction-melted under an ambient pressure of 10^{-6} torr. The actual temperature of the melt was not known, and the exact evaporating rates for the beryllium solvent and various solute elements cannot be computed. However, because all solute elements (i.e., Fe, Cr, Mn, Ni, Si, Al, Mg, Cu, Zn, and Na) and the solvent, Be, were evaporating from the same or common liquid-gas interface of a fixed area for the same length of time, we can compute the values of P, defined as the product of the evaporating time, t, and solvent evaporating rate, V (for V >> U), or solute evaporating rate, U (for U >> V); thus: P = tV or tU. Table 4 gives the initial concentrations and final concentrations (in ppm) of the various solutes, together with the value of P, actual surface concentrations, ratio of actual surface to bulk concentrations, and effective times to reach the final concentrations under the assumption that the evaporating temperature was 1250°C. The following conclusions can be drawn from Table 4:

1. The solute elements can be divided into three groups: Fe, Cr, Ni. Si, and Cu evaporate much more slowly than Be; Mg, Zn, and Na evaporate much more rapidly than Be; Al evaporates at about the same rate as Be.

2. The computed times to reach the final concentrations under normal evaporation conditions (complete liquid mixing) are fairly constant for the solute elements that evaporate much slower than Be (i.e., Fe, Cr, Ni, Si, and Cu), being about 4×10^4.

3. The computed times to reach the final concentrations for the highly evaporative Mg, Zn, and Na are also fairly constant, but about four orders of magnitude smaller.

4. After correction for limited liquid mixing (Ref. 7), the effective times to reach the final concentrations are much more constant, even between the groups of solute elements. In particular, the highly evaporative elements Mg, Zn, and Na have their results improved by several orders of magnitude.

5. Limited liquid diffusion must, therefore, be considered, particularly for the highly evaporative elements.

6. The surface solute concentrations can be changed by up to six orders of magnitude, so that the effective evaporating rates can be similarly changed.

Table 4

PURIFICATION KINETICS OF BERYLLIUM DURING CRUCIBLE-FREE VACUUM INDUCTION MELTING

Solute Element	Initial Conc., m_o, ppm Atomic	Final Conc. m, ppm Atomic	Ideal Evap. Rate at 1500°C, U_i, moles/cm^2/sec	Time to Reach Final Conc., t_i, secs	$P = t_i U_i$* or $= t_i V_i$** moles/cm^2	Surface Conc., m_s, Atomic	m_s/m_o	Effective Time to Reach Final Conc., t_e, secs	$\frac{t_e, 1400°C}{t_e, 1500°C}$
Fe	1.55	4.5	2.7885×10^{-6}	2.69×10^{3}	0.655	1.34×10^{-4}	8.60×10^{1}	2.69×10^{3}	3.49
Cr	0.65	2.1	8.7887×10^{-6}	2.84×10^{3}	0.690	1.79×10^{-5}	2.75×10^{1}	2.84×10^{3}	3.48
Ni	4.95	7.5	1.5353×10^{-6}	1.39×10^{3}	0.340	7.82×10^{-4}	1.57×10^{2}	1.40×10^{3}	3.48
Si	4.50	5.0	1.3320×10^{-6}	0.41×10^{3}	0.10	8.19×10^{-4}	1.82×10^{2}	0.41×10^{3}	3.48
Cu	1.50	1.55	4.2039×10^{-5}	0.13×10^{3}	0.032	8.66×10^{-6}	5.77	0.13×10^{3}	3.53
Al	6.50	4.0	1.6834×10^{-4}	-2.57×10^{3}	-0.625	9.37×10^{-6}	1.44	-2.57×10^{3}	3.49
Mg	4.0	0.03	5.9444	0.82	4.892	1.63×10^{-10}	4.00×10^{-5}	20.14×10^{3}	3.48
Zn	4.10	0.2	14 5917	0.20	3.020	6.82×10^{-11}	$1\ 66 \times 10^{-5}$	12.43×10^{3}	3.48
Na	59.0	8.0	12.1483	0.16	1.998	1.17×10^{-9}	1.00×10^{-5}	8.22×10^{3}	3.49
Average					1.465			5.64×10^{3}	3.48

*for U >> V

**for U << V

V_i (3e) = 2.4287×10^{-4} moles/cm^2/sec

T = 1500°C

Ambient Pressure = 10^{-6} torr

DISCUSSION AND CONCLUSION

These and other similar analyses suggest that the normal evaporation equations presented in this Memorandum work surprisingly well for the several alloy systems studied so far. These equations generally give results accurately to within an order of magnitude of the correct values, perhaps even for highly concentrated solutions (e.g., 20% Cr in Ni or 40% Ni in Fe). Such accuracies are usually sufficient for many evaporation studies.

In other more critical studies, however, refined evaporation analyses may be needed. In particular, the effect of limited diffusion and, hence, surface depletion or enrichment of the solute, must often be accounted for. This is true especially for the highly evaporative solutes such as, e.g., Mg, Zn, and Na in the solvent Be. We already have results that confirm this conclusion. Details of these results will be published in Ref. 7 and elsewhere.

REFERENCES

1. Dushman, S., Scientific Foundations of Vacuum Techniques, John Wiley and Sons, New York, 1962.

2. Li, C. H., Physica Status Solidi, Vol. 15, pp. 3 and 419, 1966.

3. Tefelske, T. and Chang, Y. A., "The Effect of Ag on the Activity of Zn in Dilute Liquid Sn Alloys by Torsion-Effusion Method," AIME Annual Meeting, San Francisco, January 1972.

4. Obradovic, N. D. and Bennett, G. H. J., J. Inst. of Metals, Vol. 97, p. 186, 1969.

5. Mukherjee, J. L., Gupta, K. P., and Li, C. H., "Evaporative Segregation in 80% Ni-20% Cr and 60% Fe-40% Ni Alloys," 1972, to be published.

6. Beryllium Technology, (edited by Schetky, L. M. and Johnson, H. A.), Vol. 1, p. 16, Gordon and Breach, New York, 1966.

7. Mukherjee, J. L., Gupta, K. P., and Li, C. H., "Purification Kinetics of Beryllium During Vacuum Induction Melting," 1972, to be published.

APPENDIX F

A NEW MECHANISM FOR THE FORMATION OF GROWTH SPIRAL[†]

Chou H. Li[‡]
Franklin F. Y. Wang[‡]
Kedar P. Gupta[‡]

ABSTRACT

A new mechanism is proposed to explain the formation of growth spirals in controlled melt-grown, crystalline samples of $Ba_4SrNb_{10}O_{30}$. Several distinguishing features of these spirals cannot be explained on the basis of the classical, core-first growth theory. These features are examined in detail, especially in comparison with the inherent or implied features of the classical spiral model. Characteristics of the spirals are predicted based on solidification theory, and are found to be in agreement with the observed results.

[†]Presented at American Association for Crystal Growth, 2nd Symposium, Princeton University, July 1972. Submitted for publication to the J. Applied Physics

[‡]Research Department, Grumman Aerospace Corporation, Bethpage, New York 11714

[‡]Materials Science Department, State University of New York at Stony Brook, New York 11790

Introduction

The spiral growth mechanism was first proposed by Frank (Ref. 1) in 1949 and has been developed into the classical BCF model (Refs. 1-3). Spiral markings had, however, long been observed on silicon carbide crystals (Refs. 4-5). Since 1949, many more spirals have been observed during evaporation-condensation (Refs. 6-7) and solidification (Refs. 8-10). Some of these spirals are rounded (Refs. 9) while others are segmented (Refs. 8-9).

The BCF model has been able to explain many of the observed effects and growth features. However, in our controlled crystal growth experiments on Barium Strontium Niobates (BSN), we observed some new phenomena that cannot be easily explained by the classical BCF model. In fact, some of these observed phenomena contradict the same model. This paper briefly describes the implications of the classical BCF model and some experimental results recently observed on these niobates in our laboratory. From these results we propose a new spiral growth model which seems to explain better the observed effects on the niobate materials.

Existing Theory

According to the BCF model of spiral formation, a nucleus is formed at a favorable spot on the solid substrate surface, and additional atoms then solidify or condense from the liquid or vapor

phase to spiral around this nucleus, i.e., to form the spiral. The distinguishing features of this theory are:

1. The spiral starts at its center or core region in the form of a screw dislocation and spirals out.
2. Adjacent or successive turns of the spiral should be separated by a thin boundary no thicker than a subgrain boundary, i.e., angstroms thick, since even the grain boundary in a polycrystalline material is generally believed to be only 10Å or less thick (Ref. 11).
3. The primary temperature gradient is perpendicular to the plane of the spiral (Ref. 10).
4. The step height in spirals, at least according to the BCF model, should be only one atomic layer thick.

Experimental Procedures

By using standard sintering techniques, polycrystalline samples of hypoeutectic composition ($4BaNb_2O_6$: $SrNb_2O_6$) were prepared (Ref. 12). The raw materials used in preparing these ceramic samples were: barium carbonate, from J. T. Baker, reagent grade; strontium carbonate, from J. T. Baker, reagent grade; and niobium pentoxide, from A. D. Mackay, 99.9 percent. The

sintering was done at 1350°C for more than 80 hours in air and the sintered material was checked for the completion of chemical reaction by using an IRD-Guinier camera.

Directional solidification of the sintered compacts was carried out in a 4 in. long, ½ in. diameter alumina crucible heated in a vertical tube-type platinum furnace. The temperature gradient was varied from 20-40°C/cm by changing the tapping of the resistance wire of the furnace, and the temperature was monitored by using three thermocouples placed at three different places. After heating the material to about 30-40°C above its melting temperature, the alumina crucible was withdrawn from the furnace at a constant rate of from 1-40 μm/sec. The longitudinal and transverse sections on the resultant, elongated samples were then examined on the solidified specimens.

New Experimental Results

The following observations have been made on these melt-grown, crystalline niobate samples prepared at 40 μm/sec:

1. The spirals consist of linear oriented segments, typically 150 μm or shorter.
2. Many spirals have only 1, 1½, 2, 3, ..., outer linear segments (see Fig. 1 at a).
3. The linear segments have been identified by electron microprobing as proeutectic crystals.

4. The spacings (Figs. 1-3 at b) between adjacent linear segments of the spirals are as wide as, or wider than, the thickness of the proeutectic crystals, i.e., tens or hundreds of μm rather than angstroms thick.
5. By probing, the materials in these spacings are identified as being of eutectic composition (Figs. 1-3 at b).
6. Both single spiral (Fig. 2, top) and paired spirals (Fig. 3, right) occur.
7. Clockwise and counterclockwise paired spirals exist, even only 70 μm apart on the same sample cross section (Fig. 3 at c).
8. The two adjacent, clockwise and counterclockwise spirals (Fig. 3) share the same single crystalline, outermost linear segment (Fig. 3 at d).
9. During spiral formation, there was a longitudinal temperature gradient of about 40°C/cm perpendicular to the axis of growth spirals.
10. The growth directions of the linear segments were often independent of the externally applied, longitudinal temperature gradient (see Figs. 2-3 at a).

Discussion

Many spirals are near ideal helices, each containing a single smooth spiraling segment with no discontinuities in the change of its slope (Ref. 9). Many other spirals are segmented (Refs. 8-9), similar to those noted in Observation 1. These segments apparently follow the preferred crystallographic orientations which probably coincide with the directions of fastest crystal growth or high thermal conductivities.

The spirals with only 1, 1½, 2, 3, ..., outer linear segments (Fig. 1) appear to represent different stages of growth, from the outermost points toward the center or core regions. The hypothesis of complete spiral formation first with subsequent core dissolution or homogenization is untenable, because the core would be solid, according to the classical theory, and, hence, have limited material diffusivities. Solid diffusion coefficients at near the melting point or crystal growth temperatures is typically only about 10^{-8} cm^2/sec, and the time to grow a 100 μm segment at a rate of 40 μm/sec is only 2.5 seconds. The diffusion length in this particular case is of the order of $\sqrt{Dt} = \sqrt{10^{-8} \times 2.5} =$ 1.6 μm, that is two orders of magnitude smaller than the segmental length.

The fact that linear segments are proeutectic crystals (Obs. 3) is in accordance with the relevant phase diagram (Ref. 12).

Observation 4, i.e., the wide spacings between adjacent segments, is in sharp contrast with prediction or implication of the conventional theory.

Observation 5, i.e., the materials in the spacing between spiral segments are eutectics, indicates that the linear segments froze first, protruding into the melt (somewhat like dendrites) and rejecting high-solute materials ahead of the liquid-solid interface, and also on one or both sides of the protruding segments, to be subsequently frozen as eutectics.

The interesting fact that adjacent clockwise and counterclockwise spirals share the same single crystalline, outermost linear segment (Obs. 8) also appears to defy satisfactory explanations according to the classical, core-first BCF growth model. The statistical probability is almost nil for two independent, separated nuclei in the melt to form the two segmented, clockwise and counterclockwise spirals that grew to reach perfect alignment and matching widths in the last and common, outermost linear segment. We would have to hypothesize that one nucleus must be transmitting complicated signals on growth characteristics, such as growth rates, growth directions, ... through the intervening liquid. This liquid is probably in a disordered state, so that at best, the signals are transmitted through with great distortion and absorption. The other nucleus must simultaneously receive and decode the

signal and, furthermore, take instantaneous, exact corrective action to achieve perfectly matched growth conditions. Even if we assume that somehow the two nuclei grew from opposite directions in an identically and instantaneously matching manner, we still expect the two approaching crystal segments to be separated by a solute-enriched layer, due to the limited liquid diffusion and solute pile-up in front of the growth interface. A loss of epitaxial relations must occur, i.e., two crystalline segments must form, one on each side of a distinct, solute-rich laye Such was not observed.

It is also interesting to note that the external or primary temperature gradient is transverse to the axis of the spiral (Obs. 9), rather than longitudinal thereto, in disagreement with the normal, spiral growth predictions. Some segments must, therefore, grow in the direction of this primary temperature gradient (at fast growth rates), some must grow against the temperature gradient (at 40°C/cm, or over 0.6°C over 150 μm), and some others must grow essentially isothermally.

A New Mechanism

It is, therefore, proposed that at least on the samples reported here, the spirals were formed from outside toward the center or core region. Such a mechanism has been suggested (Refs. 13-14).

All the above observations and discussions, including the formation of eutectics between the spiral spacings, can now be readily explained by the solidification theory (Ref. 15). Even the growth against a temperature of over 0.6°C can be ascribed to solute pile-up in front of the liquid-solid interface, and the resultant constitutional supercooling phenomenon (Ref. 16).

The two adjacent clockwise and counterclockwise spirals, such as those in Fig. 3, most likely shared the same nucleus, which was probably located in the middle of the outermost segment and grew in opposite directions to form the common outermost linear segment for the two spirals.

According to our core-last spiral growth mechanism, the combined effect of temperature and solute concentration fields makes it less likely for nucleation to occur at the center or core regions. Only under a special combination of phase diagram, material thermophysical properties, and external temperature fields (such as when the material in the core region has the highest melting point) can core nucleation become possible.

When nucleation does occur at an outer corner, the growth appears to follow the outline of some kind of local concentration cell, often only slightly influenced by the externally applied temperature gradient (Figs. 2-3). This can be seen from the fact that in our crystal growth experiment, the external temperature gradient

was 40°C/cm, or a maximum of 0.6°C over the 150 μm outer segments. According to the liquidus of the $SrNb_2O_6$ - $BaNb_2O_6$ pseudobinary phase diagram (Ref. 12), such a temperature difference corresponds to a change in liquid-solute concentration of only about 0.3 mole percent. On the other hand, the concentration effect from solute segregation and pile-up ahead of the solid-liquid interface is, according to the separation between liquidus and solidus on the same phase diagram, over 30 times greater.

The proeutectic crystals or linear segments, thus, appear to grow mainly along the isoconcentration lines generally following the cell boundaries, with rejection of solute (segregation coefficient being less than unity here) both longitudinally ahead of the grown segments and laterally at least toward the center of the spirals. We could thus predict that for these core-last grown spirals, the solute concentration of spiral segments should generally increase along the segments toward the last-freezing core region. Notice, also, that the differently oriented segments should have different growth rates and concentration profiles. The centers of the spirals must, in particular, have much higher solute concentrations approaching the eutectics.

Hence, at least in the BSN samples, the spiral growth seems to start from the outside inward.

References

1. F. C. Frank, Discussion in Faraday Society 5, 48, 1949.
2. W. K. Burton, N. Cabrera, and F. C. Frank, Phil. Trans. Roy. Soc. A243, 299, 1951.
3. N. Cabrera and W. K. Burton, Discussion in Faraday Society 5, 40, 1949.
4. J. W. Mellor, A Comprehensive Treatise on Inorganic & Theoretical Chemistry 5, 879, 1924.
5. A. W. C. Menzies and C. A. Sloat, Nature, Lond. 123, 348, 1929.
6. S. Amelinckx and E. Votaba, Naturwiseenschaften 31, 422, 1954.
7. E. Votava and A. Berghezan, Acta Meta 7, 6, 1959.
8. R. K. Jain and G. C. Trigunayat, Crystal Growth 2, 185, 1968.
9. A. Dippenaar, H. D. W. Bridgman, and G. A. Chadwick, J. Inst. Metals 99, 137, 1971.
10. J. D. Hunt and J. P. Chilton, J. Inst. Metals 94, 146, 1966.
11. N. F. Mott, Prog. Phys. Soc. Lond. 60, 391, 1948.
12. J. R. Carruthers and M. Grasso, J. Electrochem. Soc. 117, 1426, 1970.
13. C. B. Sclar and C. M. Schwartz, in Crystal Growth, ed. H. S. Peiser (Pergamon Press, New York, 1969), pp. 399-403.
14. G. G. Lemmlein, M. O. Kliya, and A. A. Chernov, Sov. Phys.-Crystallography 9, No. 2, 1964.
15. B. Chalmers, Solidification (Wiley, New York, 1969).
16. J. Rutter and B. Chalmers, Can. J. Phys. 31, 15, 1953.

Captions

Fig. 1 Broken Spiral Segments on $Ba_4Sr\ Nb_{10}O_{30}$ Melt-Grown Sample Formed at 40 μm/sec under Temperature Gradient of 40°C/cm. Magnification 220X

Fig. 2 Segmented Spirals on $Ba_4Sr\ Nb_{10}O_{30}$ Melt-Grown at 40 μm/sec under Temperature Gradient of 40°C/cm. Magnification 220X

Fig. 3 Segmented Paired Spiral on $Ba_4Sr\ Nb_{10}O_{30}$ Melt-Grown at 40 μm/sec under Temperature Gradient of 40°C/cm. Magnification 220X

a
b
100μm
Growth Direction
Cold
Hot
Temperature Gradient

a
b
d
c
100μm
Temperature Gradient


a
b
a
b
a
a
b
a
b
a
a
Temperature Gradient
100μm

APPENDIX G

STEADY-STATE SOLIDIFICATION IN THE Ni-Sn SYSTEM

INTRODUCTION

It is well known that solute redistributes as an alloy solidifies from its molten state. Pfann (1962) and several other authors have expressed the instantaneous solute concentration c as a function of the fraction solidified, g, i.e.,

$$c = k C_o (1-g)^{k-1}, \tag{1}$$

where C_o is the initial concentration of solute in the melt, $k = c_s/c_1$ is the segregation constant, and c_s and c_ℓ are the solute concentrations in the solid and liquid, respectively. Equation (1) is based on the following assumptions:

1. Diffusion in the solid is negligible.
2. The mixing in the liquid is complete.
3. k is constant.

Frenkel (1946) pointed out that assumption (2) is hardly true because the diffusion coefficient is too small to assume completely mixing. In addition to assumptions one and three, Chalmers (1964) assumed that convection in the liquid is negligible and that solute is transported by diffusion instead of being completely mixed. Then the concentration of solute in the liquid, c_1, is, under steady state conditions, a function of distance from the solid-liquid interface, x:

$$c_\ell = C_o \left[1 + \frac{1-k}{k} e^{-\frac{R}{D} x} \right] \tag{2}$$

where D is the diffusion coefficient in the liquid and R is the constant growth rate.

There is always an equilibrium temperature which corresponds to a certain solute concentration in the liquid phase. Chalmers (1964) pointed out that supercooling can occur if the temperature gradient, G, is controlled in such a way that the actual temperature in the liquid phase is lower than the equilibrium temperature. Figure G-1 shows that no supercooling can occur if G is larger than the critical temperature gradient of supercooling G_C. If G is smaller than G_c, however, a distance of supercooling, x, exists.

The constant value of k in Eq (1) and (2) is only a simplified assumption, since we know that the solidus and liquidus curves in most phase diagrams are not linear. In this appendix we will investigate the errors involved in calculating the critical temperature gradient G_c and distance of supercooling x when a constant k is assumed. For convenience in comparison, three models are assumed. The first is a linear model in which both the solidus and liquidus curves are linear functions of the melt temperature. This model corresponds to constant k. Both the solidus and liquidus curves should, of course, pass through the point representing the temperature of solid-liquid equilibrium of the pure solvent, and the slopes should be obtained by a least-square fitting of the experimental data over the entire solidification range. The second model is a pseudo-linear model. This model is the same as the first one, except that the slopes of solidus and liquidus curves are the slopes, or tangents, at the melting temperature of pure solvent. The third model is a quadratic model for both the solidus and liquidus curves, with the same terminal restrictions that they precisely pass through the solid-liquid equilibrium points for the pure solvent and eutectic. The shapes of the curves are also determined by least-square fitting of the experimental data.

THEORETICAL BACKGROUND

To express the liquidus and solidus curves, C_l and C_s, in terms of the melt temperature, we choose T_E, the equilibrium temperature of pure solvent, as the origin of the coordinate, so that the constant terms in both liquidus and solidus drop out automatically. Then the relation between the new coordinate or modified temperature T and old coordinate T' is $T = T_E - T'$.

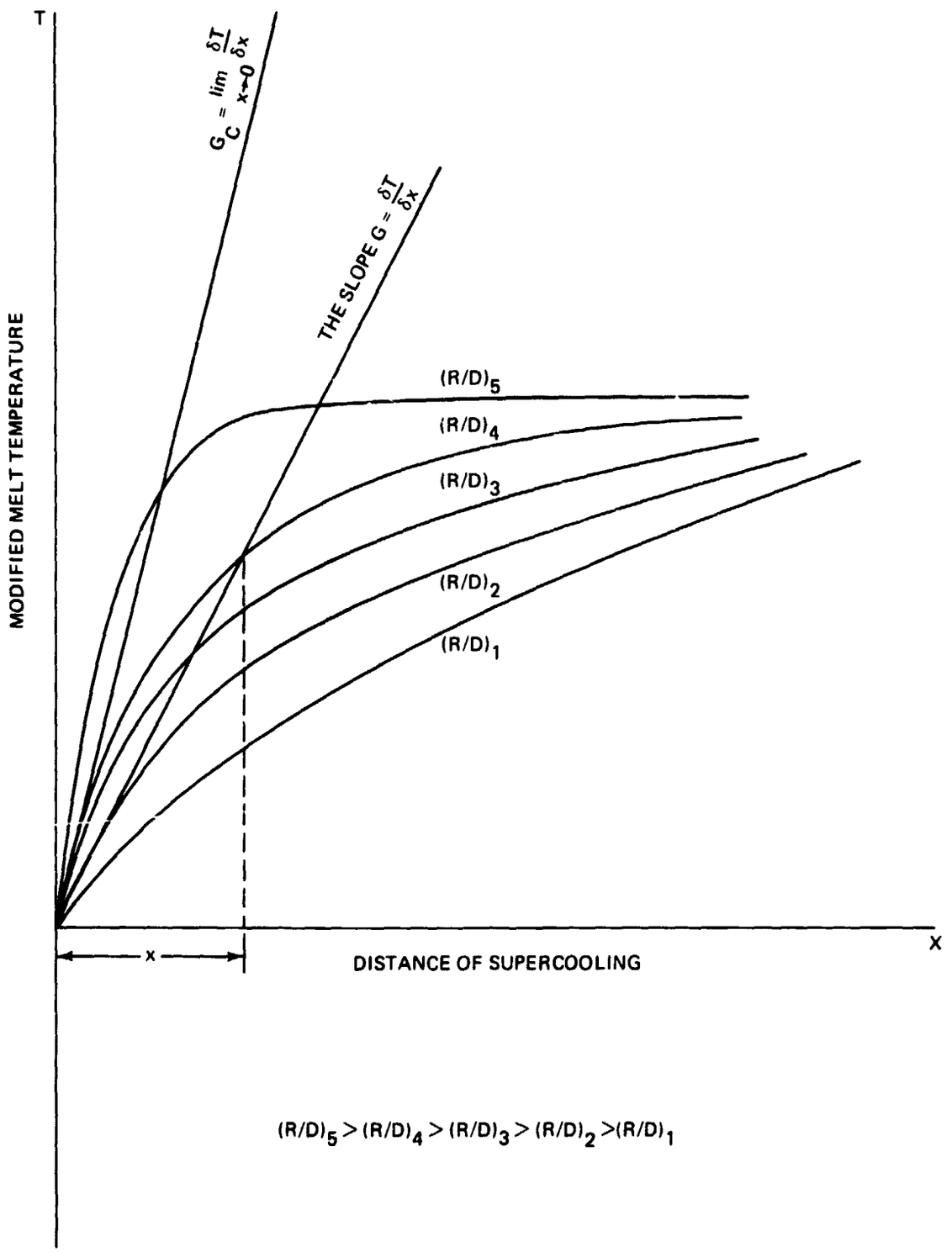

$$(R/D)_5 > (R/D)_4 > (R/D)_3 > (R/D)_2 > (R/D)_1$$

Fig. G-1 The Effect of R/D on x

For the linear model, the liquidus curve and the solidus curves can be expressed as

$$C_1 = A_1 T \tag{3}$$

$$C_s = B_1 T \tag{4}$$

and

$$k_1 = \frac{C_s}{C_1} = \frac{B_1}{A_1} = \text{constant} \tag{5}$$

For the quadratic model:

$$C_\ell = A_{12} T + A_{22} T^2 \tag{6}$$

$$C_s = B_{12} T + B_{22} T^2 \tag{7}$$

and

$$k_3 = \frac{C_s}{C_\ell} = \frac{B_{12} + B_{22} T}{A_{12} + A_{22} T} \tag{8}$$

which is a function of the temperature, T. If the temperature T is small, i.e., if the concentrations of solute c_s and c_1 are small, then the higher-degree terms of temperature in both C_ℓ and C_s are negligible, we thus obtain a new constant for k, i.e.,

$$k_2 = \frac{B_{12}}{A_{12}} \tag{9}$$

which is the pseudo-linear model.

G_c can be found by the chain rule relationship:

$$\frac{\partial C_\ell}{\partial x} = \frac{\partial C_\ell}{\partial T} \cdot \frac{\partial T}{\partial x}$$

$$G_c = \lim_{x \to o} \frac{\partial T}{\partial x} = \frac{\partial C_\ell}{\partial x} \Big/ \frac{\partial C_\ell}{\partial T}$$

Both $\partial C_\ell / \partial x$ and $\partial C_\ell / \partial T$ can be found from Eq (2), (3), and (6). Thus:

- For the linear case, $$G_{c1} = \frac{RT_o}{D}(1-k_1) \tag{10}$$
- For the pseudo-linear case, $$G_{c2} = \frac{RT_o}{D}(1-k_2) \tag{11}$$
- For the quadratic case, $$G_{c3} = \frac{RT_o}{D}(1-k_3)\frac{A_{12} + A_{22}T_o}{A_{12} + 2A_{22}T_o} \tag{12}$$

$$\simeq \frac{RT_o}{D}(1-k_2)\left[1 - \frac{A_{12}(A_{22}-B_{22}) - 2A_{22}B_{12}}{A_{12}(A_{12}-B_{12})}T_o\right]$$

where T_o is the equilibrium temperature of solid-liquid interface expressed in the new coordinate system. The real temperature is $T' = T_E - T_o$.

The distance of supercooling can be found by introducing the equation for the actual temperature in the liquid phase, after transformation into the new coordinate system:

$$T = T_o - Gx \tag{13}$$

Thus:

- From Eq (3), $$C_\ell = A_1 (T_o - Gx) \tag{14}$$
- From Eq (6), $$C_\ell = A_{12}(T_o - Gx) \tag{15}$$
- From Eq (6), $$C_\ell = A_{12}(T_o - Gx) + A_{22}(T_o - Gx)^2 \tag{16}$$

Then x can be found by equating Eq (14), (15), and (16) to Eq (2) for any model, and any given R/D and T_o.

COMPUTATION SCHEME

To find the values of A_1, B_1, A_{12}, A_{22}, B_{12}, and B_{22}, least-square computer programs were used which minimized the total error $y = \Sigma \left[1-A_{12} \frac{T}{C_\ell} - A_{22} \frac{T}{C_\ell}^2\right]^2$. Since we want both end points to be precise, we solve the following simultaneous equations for A_{12} and A_{22}:

$$\frac{\partial y}{\partial A_{12}} = -2 \quad 1-A_{12} \frac{T}{C_\ell} - A_{22} \frac{T}{C_\ell}^2 \quad \frac{T}{C_\ell} + \frac{T^2}{C_\ell} \frac{\partial A_{22}}{\partial A_{12}} = 0$$

and

$$1 = \frac{A_{12} Tu}{C_{\ell u}} + A22 \frac{Tu^2}{C_{\ell u}} \tag{17}$$

where $C_{\ell u}$ and T_u are the liquid concentration and temperature at the eutectic point respectively. The same procedure can be used to compute A_1, B_1, and B_{12}, B_{22} and the required data sets obtained from the phase diagrams.

To find k's and Gc's. Once we have obtained those coefficients, we can compute k's and Gc's from Eq (5) and (8), and (10), (11), and (12), respectively.

To compute the distance of supercooling, x. From equations (7), (16), and (2), we solve for x, for the quadratic case, as follows:

$$A_{12}(T_o-Gx) + A_{22}(T_o-Gx)^2 - (B_{12}T_o+B_{22}T_o^2)\left(1+\frac{1-k_o}{k_o} e^{-\frac{R}{D}x}\right) = 0 \tag{18}$$

Since the above equation is nonlinear, Newtons method can be used to find x by minimizing y, where

$$y = A_{12}(T_o - Gx) + A_{22}(T_o - Gx)^2 - (B_{12}T_o + B_{22}T_o^2)\left(1 + \frac{1-k_o}{k_o} e^{-\frac{R}{D}x}\right) \quad (19)$$

For the linear case:

$$y = A_1(T_o - Gx) - B_1 T_o\left[1 + \frac{1-k_o}{k_o} e^{-\frac{R}{D}x}\right] \quad (20)$$

and for the pseudo-linear case:

$$y = A_{12}(T_o - Gx) - B_{12}T_o\left(1 + \frac{1-k_o}{k_o} e^{-\frac{R}{D}x}\right) \quad (21)$$

where k_o is the segregation coefficient at a given solid-liquid equilibrium temperature.

COMPUTATION RESULT

A Ni-Sn System, in which both the solidus and liquidus curves are parabolas, was chosen for the study. Sn is the solute and Ni is the solvent in this system. Ten equilibrium data points, as tabulated below, were obtained from the phase equilibrium diagram given by Hansen (Ref. 4):

TABLE G-1 THE Ni-Sn PHASE DIAGRAM

T, K	C_s	C_ℓ
273.1	0.0	0.0
283.1	0.2000E 01	0.2000E 01
298.1	0.8500E 00	0.4000E 01
323.1	0.1800E 01	0.6900E 01
373.1	0.3700E 01	0.1220E 02
423.1	0.5900E 01	0.1700E 02
473.1	0.8600E 01	0.2150E 02
523.1	0.1200E 02	0.2600E 02
573.1	0.1700E 02	0.3000E 02
604.1	0.2000E 02	0.3230E 02

From these data, the required coefficients can be obtained by a least-square method:

A12	A22	B12	B22	A1	B1
0.1495	-1.568×10^{-2}	0.02337	1.120×10^{-2}	0.1157	0.03364

The segregation constants k's for the three different cases, i.e., k(1), k(2), and k(3) corresponding to the linear, pseudo-linear, and quadratic models, respectively, were computed for a given T and are listed in Table G-2.

TABLE G-2 VARIATION OF THE SEGREGATION COEFFICIENTS WITH TEMPERATURE FOR THE Ni-Sn SYSTEM

T', K	K(1)	K(2)	K(3)
1728	0.2908E 00	0.1563E 00	0.1563E 00
1718	0.2908E 00	0.1563E 00	0.1655E 00
1703	0.2908E 00	0.1563E 00	0.1797E 00
1678	0.2908E 00	0.1563E 00	0.2045E 00
1628	0.2908E 00	0.1563E 00	0.2583E 00
1578	0.2908E 00	0.1563E 00	0.3188E 00
1528	0.2908E 00	0.1563E 00	0.3873E 00
1478	0.2908E 00	0.1563E 00	0.4656E 00
1428	0.2908E 00	0.1563E 00	0.5559E 00
1397	0.2908E 00	0.1563E 00	0.6192E 00

The deviations of segregation constant k for the linear models from that of the quadratic model are given in Table G-3.

TABLE G-3 DEVIATIONS OF THE SEGREGATION COEFFICIENTS IN THE Ni-Sn SYSTEM

T, K	(K(L)-K(3))/K(3)	(K(2)-K(3))/K(3)
273.1	0.8604E 00	0.0
283.1	0.7567E 00	-0.5574E-01
298.1	0.6178E 00	-0.1304E 00
323.1	0.4221E 00	-0.2356E 00
373.1	0.1258E 00	-0.3949E 00
423.1	-0.8790E-01	-0.5097E 00
473.1	-0.2493E 00	-0.5965E 00
523.1	-0.3755E 00	-0.6643E 00
573.1	-0.4770E 00	-0.7189E 00
604.1	-0.5304E 00	-0.7476E 00

The critical temperature gradients, G_c, were computed by Eq (10), (11), and (12) for any given R/D and T and are listed in Table G-4. Computed distances of supercooling, x, are given in Table 5.

TABLE G-4 COMPUTED CRITICAL TEMPERATURE GRADIENTS IN THE Ni-Sn SYSTEM FOR THE THREE MODELS

T, K	R/D	$G_c(1)$	$G_c(2)$	$G_c(3)$
273.1	0.1000E 01	0.0	0.0	0.0
283.1	0.1000E 01	0.7092E 01	0.8437E 01	0.8434E 01
298.1	0.1000E 01	0.1773E 02	0.2109E 02	0.2107E 02
323.1	0.1000E 01	0.3546E 02	0.4219E 02	0.4211E 02
373.1	0.1000E 01	0.7092E 02	0.8437E 02	0.8402E 02
423.1	0.1000E 01	0.1064E 03	0.1266E 03	0.1256E 03
473.1	0.1000E 01	0.1418E 03	0.1687E 03	0.1668E 03
523.1	0.1000E 01	0.1773E 03	0.2109E 03	0.2073E 03
573.1	0.1000E 01	0.2128E 03	0.2531E 03	0.2464E 03
604.1	0.1000E 01	0.2348E 03	0.2793E 03	0.2693E 03
273.1	0.2500E 01	0.0	0.0	0.0
283.1	0.2500E 01	0.1773E 02	0.2109E 02	0.2109E 02
298.1	0.2500E 01	0.4433E 02	0.5273E 02	0.5269E 02
323.1	0.2500E 01	0.8865E 02	0.1055E 03	0.1053E 03
373.1	0.2500E 01	0.1773E 03	0.2109E 03	0.2100E 03
423.1	0.2500E 01	0.2660E 03	0.3164E 03	0.3141E 03
473.1	0.2500E 01	0.3546E 03	0.4219E 03	0.4171E 03
523.1	0.2500E 01	0.4433E 03	0.5273E 03	0.5182E 03
573.1	0.2500E 01	0.5319E 03	0.632RE 03	0.6159E 03
604.1	0.2500E 01	0.5869E 03	0.6982E 03	0.6733E 03
273.1	0.5000E 01	0.0	0.0	0.0
283.1	0.5000E 01	0.3546E 02	0.4219E 02	0.4217E 02
298.1	0.5000E 01	0.8865E 02	0.1055E 03	0.1054E 03
323.1	0.5000E 01	0.1773E 03	0.2109E 03	0.2105E 03
373.1	0.5000E 01	0.3546E 03	0.4219E 03	0.4201E 03
423.1	0.5000E 01	0.5319E 03	0.632RE 03	0.6282E 03
473.1	0.5000E 01	0.7092E 03	0.8437E 03	0.8341E 03
523.1	0.5000E 01	0.8865E 03	0.1055E 04	0.1036E 04
573.1	0.5000E 01	0.1064E 04	0.1266E 04	0.1232E 04
604.1	0.5000E 01	0.1174E 04	0.13J6E 04	0.1347E 04
273.1	0.1000E 03	0.0	0.0	0.0
283.1	0.1000E 03	0.7092E 03	0.8437E 03	0.8434E 03
298.1	0.1000E 03	0.1773E 04	0.2109E 04	0.2107E 04
323.1	0.1000E 03	0.3546E 04	0.4219E 04	0.4211E 04
373.1	0.1000E 03	0.7092E 04	0.8437E 04	0.8402E 04
423.1	0.1000E 03	0.1064E 05	0.1266E 05	0.1256E 05
473.1	0.1000E 03	0.1418E 05	0.1687E 05	0.1668E 05
523.1	0.1000E 03	0.1773E 05	0.2109E 05	0.2073E 05
573.1	0.1000E 03	0.2128E 05	0.2531E 05	0.2464E 05
604.1	0.1000E 03	0.2348E 05	0.2793E 05	0.2693E 05

The distances of supercooling, x, were computed by Eq (18), (19), and (20) for given values of R/D and T_o.

TABLE G-5 COMPUTED DISTANCES OF SUPERCOOLING IN THE Ni-Sn SYSTEM FOR THE THREE MODELS (Sheet 1 of 3)

G	R/D	K=273.1	K=283.1	K=298.1	K=323.1	K=373.1	K=423.1	K=473.1	K=523.1	K=573.1	K=604.1
5.0	0.1	0.0	0.0	0.0	0.0	7.4519	-0.0000	-0.0000	0.0000	-0.0000	-0.0000
5.0	0.5	0.0	0.0	2.5603	6.8629	14.1726	21.2762	0.0000	0.0000	-0.0000	-0.0000
5.0	1.0	0.0	0.7452	3.4314	7.0863	14.1845	21.2767	28.3690	35.4612	42.5535	46.9507
5.0	2.5	0.0	1.3726	3.5456	7.0922	14.1845	21.2767	28.3690	35.4612	42.5535	46.9507
5.0	5.0	0.0	1.4173	3.5461	7.0922	14.1845	21.2767	28.3690	35.4612	42.5535	46.9507
5.0	10.0	0.0	1.4184	3.5461	7.0922	14.1845	21.2767	28.3690	35.4612	42.5535	46.9507
5.0	25.0	0.0	1.4184	3.5461	7.0922	14.1845	21.2767	28.3690	35.4612	42.5535	46.9507
5.0	50.0	0.0	1.4184	3.5461	7.0922	14.1845	21.2767	28.3690	35.4612	42.5535	46.9507
5.0	100.0	0.0	1.4184	3.5461	7.0922	14.1845	21.2767	28.3690	35.4612	42.5535	46.9507
5.0	250.0	0.0	1.4184	3.5461	7.0922	14.1845	21.2767	28.3690	35.4612	42.5535	46.9507
10.0	0.1	0.0	0.0	0.0	0.0	0.0	1.2507	7.4519	-0.0000	-0.0000	0.0000
10.0	0.5	0.0	0.0	0.0	2.5603	6.8629	10.5849	14.1726	17.7281	21.2762	23.4751
10.0	1.0	0.0	0.0	1.2802	3.4314	7.0863	10.6381	14.1845	17.7306	21.2767	23.4753
10.0	2.5	0.0	0.5121	1.7508	3.5456	7.0922	10.6384	14.1845	17.7306	21.2767	23.4753
10.0	5.0	0.0	0.6863	1.7728	3.5461	7.0922	10.6384	14.1845	17.7306	21.2767	23.4753
10.0	10.0	0.0	0.7086	1.7731	3.5461	7.0922	10.6384	14.1845	17.7306	21.2767	23.4753
10.0	25.0	0.0	0.7092	1.7731	3.5461	7.0922	10.6384	14.1845	17.7306	21.2767	23.4753
10.0	50.0	0.0	0.7092	1.7731	3.5461	7.0922	10.6384	14.1845	17.7306	21.2767	23.4753
10.0	100.0	0.0	0.7092	1.7731	3.5461	7.0922	10.6384	14.1845	17.7306	21.2767	23.4753
10.0	250.0	0.0	0.7092	1.7731	3.5461	7.0922	10.6384	14.1845	17.7306	21.2767	23.4753
25.0	0.1	0.0	0.0	0.0	0.0	0.0	0.0	0.0	0.0	0.0	0.0
25.0	0.5	0.0	0.0	0.0	0.0	1.4904	3.5251	5.2661	6.8629	8.3819	9.3004
25.0	1.0	0.0	0.0	0.0	0.7452	2.6330	4.1910	5.6539	7.0863	8.5090	9.3893
25.0	2.5	0.0	0.0	0.5121	1.3726	2.8345	4.2552	5.6738	7.0922	8.5107	9.3901
25.0	5.0	0.0	0.1490	0.6863	1.4173	2.8369	4.2553	5.6738	7.0922	8.5107	9.3901
25.0	10.0	0.0	0.2633	0.7086	1.4184	2.8369	4.2553	5.6738	7.0922	8.5107	9.3901
25.0	25.0	0.0	0.2835	0.7092	1.4184	2.8369	4.2553	5.6738	7.0922	8.5107	9.3901
25.0	50.0	0.0	0.2837	0.7092	1.4184	2.8369	4.2553	5.6738	7.0922	8.5107	9.3901
25.0	100.0	0.0	0.2837	0.7092	1.4184	2.8369	4.2553	5.6738	7.0922	8.5107	9.3901
25.0	250.0	0.0	0.2837	0.7092	1.4184	2.8369	4.2553	5.6738	7.0922	8.5107	9.3901
50.0	0.1	0.0	0.0	0.0	0.0	0.0	0.0	0.0	0.0	0.0	0.0
50.0	0.5	0.0	0.0	0.0	0.0	0.0	0.2501	1.4904	2.5603	3.5251	4.0866
50.0	1.0	0.0	0.0	0.0	0.0	0.7452	1.7626	2.6330	3.4313	4.1910	4.6502
50.0	2.5	0.0	0.0	0.0	0.5121	1.3725	2.1170	2.8345	3.5456	4.2552	4.6950
50.0	5.0	0.0	0.0	0.2560	0.6863	1.4173	2.1276	2.8369	3.5461	4.2553	4.6951
50.0	10.0	0.0	0.0745	0.3431	0.7086	1.4184	2.1277	2.8369	3.5461	4.2553	4.6951
50.0	25.0	0.0	0.1373	0.3546	0.7092	1.4184	2.1277	2.8369	3.5461	4.2553	4.6951
50.0	50.0	0.0	0.1417	0.3546	0.7092	1.4184	2.1277	2.8369	3.5461	4.2553	4.6951
50.0	100.0	0.0	0.1418	0.3546	0.7092	1.4184	2.1277	2.8369	3.5461	4.2553	4.6951
50.0	250.0	0.0	0.1418	0.3546	0.7092	1.4184	2.1277	2.8369	3.5461	4.2553	4.6951
100.0	0.1	0.0	0.0	0.0	0.0	0.0	0.0	0.0	0.0	0.0	0.0
100.0	0.5	0.0	0.0	0.0	0.0	0.0	0.0	0.0	0.0	0.2501	0.6589
100.0	1.0	0.0	0.0	0.0	0.0	0.0	0.1251	0.7452	1.2802	1.7626	2.0433
100.0	2.5	0.0	0.0	0.0	0.0	0.5121	0.9696	1.3726	1.7508	2.1170	2.3408
100.0	5.0	0.0	0.0	0.0	0.2560	0.6863	1.0585	1.4173	1.7728	2.1276	2.3475
100.0	10.0	0.0	0.0	0.0	0.1280	0.3431	0.7086	1.0638	1.4184	1.7731	2.1277	2.3475
100.0	25.0	0.0	0.0512	0.1751	0.3546	0.7092	1.0638	1.4184	1.7731	2.1277	2.3475
100.0	50.0	0.0	0.0886	0.1773	0.3546	0.7092	1.0638	1.4184	1.7731	2.1277	2.3475
100.0	100.0	0.0	0.0709	0.1773	0.3546	0.7092	1.0638	1.4184	1.7731	2.1277	2.3475
100.0	250.0	0.0	0.0709	0.1773	0.3546	0.7092	1.0638	1.4184	1.7731	2.1277	2.3475

TABLE G-5 COMPUTED DISTANCES OF SUPERCOOLING IN THE Ni-Sn SYSTEM FOR THE THREE MODELS (Sheet 2 of 3)

G	R/D	K=273.1	K=283.1	K=293.1	K=323.1	K=373.1	K=423.1	K=473.1	K=523.1	K=573.1	K=604.1
5.0	0.1	0.0	0.0	0.0	0.0	11.5865	22.6948	32.4305	41.5216	50.2909	55.6391
5.0	0.5	0.0	0.0	3.4770	8.3043	16.8704	25.3110	33.7481	42.1852	50.6222	55.8532
5.0	1.0	0.0	1.1567	4.1522	8.4352	16.8741	25.3111	33.7481	42.1852	50.6222	55.8532
5.0	2.5	0.0	1.6609	4.2184	8.4370	16.8741	25.3111	33.7481	42.1852	50.6222	55.8532
5.0	5.0	0.0	1.6870	4.2185	8.4370	16.8741	25.3111	33.7481	42.1852	50.6222	55.8532
5.0	10.0	0.0	1.6874	4.2185	8.4370	16.8741	25.3111	33.7481	42.1852	50.6222	55.8532
5.0	25.0	0.0	1.6874	4.2185	8.4370	16.8741	25.3111	33.7481	42.1852	50.6222	55.8532
5.0	50.0	0.0	1.6874	4.2185	8.4370	16.8741	25.3111	33.7481	42.1852	50.6222	55.8532
5.0	100.0	0.0	1.6874	4.2185	8.4370	16.8741	25.3111	33.7481	42.1852	50.6222	55.8532
5.0	250.0	0.0	1.6874	4.2185	8.4370	16.8741	25.3111	33.7481	42.1852	50.6222	55.8532
10.0	0.1	0.0	0.0	0.0	0.0	0.0	4.9109	11.5665	17.3847	22.6948	25.8133
10.0	0.5	0.0	0.0	0.2269	3.4770	8.3043	12.6327	16.8704	21.0920	25.3110	27.9266
10.0	1.0	0.0	0.0	1.7385	4.1522	8.4352	12.6555	16.8741	21.0926	25.3111	27.9266
10.0	2.5	0.0	0.6954	2.0981	4.2184	8.4370	12.6556	16.8741	21.0926	25.3111	27.9266
10.0	5.0	0.0	0.8304	2.1092	4.2185	8.4370	12.6556	16.8741	21.0926	25.3111	27.9266
10.0	10.0	0.0	0.8435	2.1093	4.2185	8.4370	12.6556	16.8741	21.0926	25.3111	27.9266
10.0	25.0	0.0	0.8437	2.1093	4.2185	8.4370	12.6556	16.8741	21.0926	25.3111	27.9266
10.0	50.0	0.0	0.8437	2.1093	4.2185	8.4370	12.6556	16.8741	21.0926	25.3111	27.9266
10.0	100.0	0.0	0.8437	2.1093	4.2185	8.4370	12.6556	16.8741	21.0926	25.3111	27.9266
10.0	250.0	0.0	0.8437	2.1093	4.2185	8.4370	12.6556	16.8741	21.0926	25.3111	27.9266
25.0	0.1	0.0	0.0	0.0	0.0	0.0	0.0	0.0	0.0	0.4937	2.2596
25.0	0.5	0.0	0.0	0.0	0.0	2.3133	4.5390	6.4861	8.3043	10.0582	11.1278
25.0	1.0	0.0	0.0	0.0	1.1567	3.2430	5.0291	6.7417	8.4352	10.1240	11.1705
25.0	2.5	0.0	0.0	0.6954	1.6609	3.3741	5.0622	6.7496	8.4370	10.1244	11.1706
25.0	5.0	0.0	0.2314	0.8304	1.6870	3.3748	5.0622	6.7496	8.4370	10.1244	11.1706
25.0	10.0	0.0	0.3243	0.8435	1.6874	3.3748	5.0622	6.7496	8.4370	10.1244	11.1706
25.0	25.0	0.0	0.3374	0.8437	1.6874	3.3748	5.0622	6.7496	8.4370	10.1244	11.1706
25.0	50.0	0.0	0.3375	0.8437	1.6874	3.3748	5.0622	6.7496	8.4370	10.1244	11.1706
25.0	100.0	0.0	0.3375	0.8437	1.6874	3.3748	5.0622	6.7496	8.4370	10.1244	11.1706
25.0	250.0	0.0	0.3375	0.8437	1.6874	3.3748	5.0622	6.7496	8.4370	10.1244	11.1706
50.0	0.1	0.0	0.0	0.0	0.0	0.0	0.0	0.0	0.0	0.0	0.0
50.0	0.5	0.0	0.0	0.0	0.0	0.0	0.9822	2.3133	3.1770	4.5390	5.1627
50.0	1.0	0.0	0.0	0.0	0.0	1.1567	2.2695	3.2430	4.1522	5.0291	5.5639
50.0	2.5	0.0	0.0	0.0454	0.6954	1.6609	2.5265	3.3741	4.2184	5.0622	5.5853
50.0	5.0	0.0	0.0	0.3477	0.8304	1.6870	2.5311	3.3748	4.2185	5.0622	5.5853
50.0	10.0	0.0	0.1157	0.4152	0.8435	1.6874	2.5311	3.3748	4.2185	5.0622	5.5853
50.0	25.0	0.0	0.1661	0.4218	0.8437	1.6874	2.5311	3.3748	4.2185	5.0622	5.5853
50.0	50.0	0.0	0.1687	0.4219	0.8437	1.6874	2.5311	3.3748	4.2185	5.0622	5.5853
50.0	100.0	0.0	0.1687	0.4219	0.8437	1.6874	2.5311	3.3748	4.2185	5.0622	5.5853
50.0	250.0	0.0	0.1687	0.4219	0.8437	1.6874	2.5311	3.3748	4.2185	5.0622	5.5853
100.0	0.1	0.0	0.0	0.0	0.0	0.0	0.0	0.0	0.0	0.0	0.0
100.0	0.5	0.0	0.0	0.0	0.0	0.0	0.0	0.0	0.2269	0.9822	1.4190
100.0	1.0	0.0	0.0	0.0	0.0	0.0	0.4911	1.1567	1.7385	2.2695	2.5813
100.0	2.5	0.0	0.0	0.0	0.0454	0.6954	1.2030	1.6609	2.0981	2.5265	2.7901
100.0	5.0	0.0	0.0	0.0227	0.3477	0.8304	1.2633	1.6870	2.1092	2.5311	2.7927
100.0	10.0	0.0	0.0	0.1739	0.4152	0.8435	1.2656	1.6874	2.1093	2.5311	2.7927
100.0	25.0	0.0	0.0695	0.2098	0.4218	0.8437	1.2656	1.6874	2.1093	2.5311	2.7927
100.0	50.0	0.0	0.0830	0.2109	0.4219	0.8437	1.2656	1.6874	2.1093	2.5311	2.7927
100.0	100.0	0.0	0.0844	0.2109	0.4219	0.8437	1.2656	1.6874	2.1093	2.5311	2.7927
100.0	250.0	0.0	0.0844	0.2109	0.4219	0.8437	1.2656	1.6874	2.1093	2.5311	2.7927

TABLE G-5 COMPUTED DISTANCES OF SUPERCOOLING IN THE Ni-Sn SYSTEM FOR THE THREE MODELS (Sheet 3 of 3)

G	R/D	K=273.1	K=283.1	K=298.1	K=323.1	K=373.1	K=423.1	K=473.1	K=523.1	K=573.1	K=604.1
5.0	0.1	0.0	0.0	0.0	0.0	0.0000	0.0000	0.0000	-0.0000	0.0000	-0.0000
5.0	0.5	0.0	0.0	3.3706	7.8937	-0.0000	-0.0000	0.0000	0.0000	0.0000	0.0000
5.0	1.0	0.0	1.1408	4.0506	8.0400	15.2583	-0.0711	-0.0000	-0.0000	-0.0000	-0.0000
5.0	2.5	0.0	1.6447	4.1207	8.0425	15.2583	21.5681	26.8498	30.9128	33.4422	34.0065
5.0	5.0	0.0	1.6715	4.1208	8.0425	15.2583	21.5681	26.8498	30.9128	33.4422	34.0065
5.0	10.0	0.0	1.6719	4.1208	8.0425	15.2583	21.5681	26.8498	30.9128	33.4422	34.0065
5.0	25.0	0.0	1.6719	4.1208	8.0425	15.2583	21.5681	26.8498	30.9128	33.4422	34.0065
5.0	50.0	0.0	1.6719	4.1208	8.0425	15.2583	21.5681	26.8498	30.9128	33.4422	34.0065
5.0	100.0	0.0	1.6719	4.1208	8.0425	15.2583	21.5681	26.8498	30.9128	33.4422	34.0065
5.0	250.0	0.0	1.6719	4.1208	8.0425	15.2583	21.5681	26.8498	30.9128	33.4422	34.0065
10.0	0.1	0.0	0.0	0.0	0.0	0.0	3.6004	-0.0000	-0.0000	0.0000	-0.0000
10.0	0.5	0.0	0.0	0.2020	3.2618	7.4613	-0.0000	-0.0000	-0.0000	-0.0000	-0.0000
10.0	1.0	0.0	0.0	1.6853	3.9468	7.6257	10.7838	13.4249	15.4564	*******	*******
10.0	2.5	0.0	0.6869	2.0484	4.0211	7.6292	10.7840	13.4249	15.4564	16.7211	17.0033
10.0	5.0	0.0	0.8224	2.0604	4.0212	7.6292	10.7840	13.4249	15.4564	16.7211	17.0033
10.0	10.0	0.0	0.8357	2.0604	4.0212	7.6292	10.7840	13.4249	15.4564	16.7211	17.0033
10.0	25.0	0.0	0.8359	2.0604	4.0212	7.6292	10.7840	13.4249	15.4564	16.7211	17.0033
10.0	50.0	0.0	0.8359	2.0604	4.0212	7.6292	10.7840	13.4249	15.4564	16.7211	17.0033
10.0	100.0	0.0	0.8359	2.0604	4.0212	7.6292	10.7840	13.4249	15.4564	16.7211	17.0033
10.0	250.0	0.0	0.8359	2.0604	4.0212	7.6292	10.7840	13.4249	15.4564	16.7211	17.0033
25.0	0.1	0.0	0.0	0.0	0.0	0.0	0.0	0.0	0.0	0.0	0.5567
25.0	0.5	0.0	0.0	0.0	0.0	1.9837	3.7130	4.9962	5.9257	6.4897	6.6184
25.0	1.0	0.0	0.0	0.0	1.0762	2.8967	4.2602	5.3486	6.1723	6.6821	6.7957
25.0	2.5	0.0	0.0	0.6741	1.5787	3.0503	4.3135	5.3699	6.1826	6.6884	6.8013
25.0	5.0	0.0	0.2282	0.8101	1.6080	3.0517	4.3136	5.3700	6.1826	6.6884	6.8013
25.0	10.0	0.0	0.3210	0.8240	1.6085	3.0517	4.3136	5.3700	6.1826	6.6884	6.8013
25.0	25.0	0.0	0.3343	0.8242	1.6085	3.0517	4.3136	5.3700	6.1826	6.6884	6.8013
25.0	50.0	0.0	0.3344	0.8242	1.6085	3.0517	4.3136	5.3700	6.1826	6.6884	6.8013
25.0	100.0	0.0	0.3344	0.8242	1.6085	3.0517	4.3136	5.3700	6.1826	6.6884	6.8013
25.0	250.0	0.0	0.3344	0.8242	1.6085	3.0517	4.3136	5.3700	6.1826	6.6884	6.8013
50.0	0.1	0.0	0.0	0.0	0.0	0.0	0.0	0.0	0.0	0.0	0.0
50.0	0.5	0.0	0.0	0.0	0.0	0.	0.7201	1.6110	2.2392	2.6257	2.7308
50.0	1.0	0.0	0.0	0.0	0.0	0.	1.8565	2.4981	2.9629	3.2449	3.3092
50.0	2.5	0.0	0.0	0.0404	0.6524	1.	2.1489	2.6822	3.0902	3.3436	3.4001
50.0	5.0	0.0	0.0	0.3371	0.7894	1.52.	2.1568	2.6850	3.0913	3.3442	3.4007
50.0	10.0	0.0	0.1141	0.4051	0.8040	1.5258	2.1568	2.6850	3.0913	3.3442	3.4007
50.0	25.0	0.0	0.1645	0.4121	0.8043	1.5258	2.1568	2.6850	3.0913	3.3442	3.4007
50.0	50.0	0.0	0.1672	0.4121	0.8043	1.5258	2.1568	2.6850	3.0913	3.3442	3.4007
50.0	100.0	0.0	0.1672	0.4121	0.8043	1.5258	2.1568	2.6850	3.0913	3.3442	3.4007
50.0	250.0	0.0	0.1672	0.4121	0.8043	1.5258	2.1568	2.6850	3.0913	3.3442	3.4007
100.0	0.1	0.0	0.0	0.0	0.0	0.0	0.0	0.0	0.0	0.0	0.0
100.0	0.5	0.0	0.0	0.0	0.0	0.0	0.0	0.0	0.0764	0.4058	0.5314
100.0	1.0	0.0	0.0	0.0	0.0	0.0	0.3601	0.8055	1.1196	1.3129	1.3654
100.0	2.5	0.0	0.0	0.0	0.0378	0.6071	1.0002	1.2986	1.5178	1.6517	1.6817
100.0	5.0	0.0	0.0	0.0202	0.3262	0.7461	1.0740	1.3411	1.5451	1.6718	1.7001
100.0	10.0	0.0	0.0	0.1685	0.3947	0.7626	1.0784	1.3425	1.5456	1.6721	1.7003
100.0	25.0	0.0	0.0687	0.2048	0.4021	0.7629	1.0784	1.3425	1.5456	1.6721	1.7003
100.0	50.0	0.0	0.0822	0.2060	0.4021	0.7629	1.0784	1.3425	1.5456	1.6721	1.7003
100.0	100.0	0.0	0.0836	0.2060	0.4021	0.7629	1.0784	1.3425	1.5456	1.6721	1.7003
100.0	250.0	0.0	0.0836	0.2060	0.4021	0.7629	1.0784	1.3425	1.5456	1.6721	1.7003

The deviations of critical temperature gradients for the linear model, from the quadratic model for R/D = 100, are listed in Table G-6.

TABLE G-6 DEVIATIONS OF THE CRITICAL TEMPERATURE GRADIENTS IN THE Ni-Sn SYSTEM

T, K	GC(1)/GC(3)-1	GC(2)/GC(3)-1
273.1	0.0	0.0
283.1	-0.1591E 00	0.3376E-03
298.1	-0.1587E 00	0.8688E-03
323.1	-0.1578E 00	0.1842E-02
373.1	-0.1559E 00	0.4183E-02
423.1	-0.1533E 00	0.7259E-02
473.1	-0.1497E 00	0.1148E-01
523.1	-0.1446E 00	0.1762E-01
573.1	-0.1364E 00	0.2738E-01
604.1	-0.1283E 00	0.3699E-01

The deviations of the distances of supercooling for the linear models from the quadratic model are given in Tables G-7 and G-8.

TABLE G-7 DEVIATIONS OF THE DISTANCES OF THE SUPERCOOLING FOR MODEL 1 FROM THOSE OF MODEL 3 $(x_1-x_3)/x_3$ IN THE Ni-Sn SYSTEM

G	R/D	K=283.1	K=298.1	K=323.1	K=373.1	K=423.1	K=473.1	K=523.1	K=573.1	K=604.1
10.0	0.05	0.0	0.0	0.0	0.0	0.0	0.0	-1.000	-0.384	0.240
10.0	0.10	0.0	0.0	0.0	0.0	-0.653	-0.075	0.143	0.343	0.496
10.0	0.50	0.0	-1.000	-0.215	-0.080	-0.014	0.057	0.147	0.273	0.381
10.0	1.00	0.0	-0.240	-0.131	-0.071	-0.014	0.057	0.147	0.272	0.381
10.0	2.50	-0.255	-0.145	-0.118	-0.070	-0.014	0.057	0.147	0.272	0.381
10.0	5.00	-0.165	-0.140	-0.118	-0.070	-0.014	0.057	0.147	0.272	0.381
10.0	10.00	-0.152	-0.139	-0.118	-0.070	-0.014	0.057	0.147	0.272	0.381
10.0	25.00	-0.152	-0.139	-0.118	-0.070	-0.014	0.057	0.147	0.272	0.381
10.0	50.00	-0.152	-0.139	-0.118	-0.070	-0.014	0.057	0.147	0.272	0.381
10.0	100.00	-0.152	-0.139	-0.118	-0.070	-0.014	0.057	0.147	0.272	0.381
25.0	0.05	0.0	0.0	0.0	0.0	0.0	0.0	0.0	0.0	0.0
25.0	0.10	0.0	0.0	0.0	0.0	0.0	0.0	0.0	0.0	-1.000
25.0	0.50	0.0	0.0	0.0	-0.249	-0.051	0.054	0.158	0.292	0.405
25.0	1.00	0.0	0.0	-0.308	-0.091	-0.016	0.057	0.148	0.273	0.382
25.0	2.50	0.0	-0.240	-0.131	-0.071	-0.014	0.057	0.147	0.272	0.381
25.0	5.00	-0.347	-0.153	-0.119	-0.070	-0.014	0.057	0.147	0.272	0.381
25.0	10.00	-0.180	-0.140	-0.118	-0.070	-0.014	0.057	0.147	0.272	0.381
25.0	25.00	-0.152	-0.139	-0.118	-0.070	-0.014	0.057	0.147	0.272	0.381
25.0	50.00	-0.152	-0.139	-0.118	-0.070	-0.014	0.057	0.147	0.272	0.381
25.0	100.00	-0.152	-0.139	-0.118	-0.070	-0.014	0.057	0.147	0.272	0.381
50.0	0.05	0.0	0.0	0.0	0.0	0.0	0.0	0.0	0.0	0.0
50.0	0.10	0.0	0.0	0.0	0.0	0.0	0.0	0.0	0.0	0.0
50.0	0.50	0.0	0.0	0.0	0.0	-0.653	-0.075	0.143	0.343	0.496
50.0	1.00	0.0	0.0	0.0	-0.249	-0.051	0.054	0.158	0.292	0.405
50.0	2.50	0.0	-1.000	-0.215	-0.080	-0.014	0.057	0.147	0.273	0.381
50.0	5.00	0.0	-0.240	-0.131	-0.071	-0.014	0.057	0.147	0.272	0.381
50.0	10.00	-0.347	-0.153	-0.119	-0.070	-0.014	0.057	0.147	0.272	0.381
50.0	25.00	-0.165	-0.140	-0.118	-0.070	-0.014	0.057	0.147	0.272	0.381
50.0	50.00	-0.152	-0.139	-0.118	-0.070	-0.014	0.057	0.147	0.272	0.381
50.0	100.00	-0.152	-0.139	-0.118	-0.070	-0.014	0.057	0.147	0.272	0.381
100.0	0.05	0.0	0.0	0.0	0.0	0.0	0.0	0.0	0.0	0.0
100.0	0.10	0.0	0.0	0.0	0.0	0.0	0.0	0.0	0.0	0.0
100.0	0.50	0.0	0.0	0.0	0.0	0.0	0.0	-1.000	-0.384	0.240
100.0	1.00	0.0	0.0	0.0	0.0	-0.653	-0.075	0.143	0.343	0.496
100.0	2.50	0.0	0.0	-1.000	-0.157	-0.031	0.057	0.153	0.282	0.392
100.0	5.00	0.0	-1.000	-0.215	-0.080	-0.014	0.057	0.147	0.272	0.381
100.0	10.00	0.0	-0.240	-0.131	-0.071	-0.014	0.057	0.147	0.272	0.381
100.0	25.00	-0.255	-0.145	-0.118	-0.070	-0.014	0.057	0.147	0.272	0.381
100.0	50.00	-0.165	-0.140	-0.118	-0.070	-0.014	0.057	0.147	0.272	0.381
100.0	100.00	-0.152	-0.139	-0.118	-0.070	-0.014	0.057	0.147	0.272	0.381
250.0	0.05	0.0	0.0	0.0	0.0	0.0	0.0	0.0	0.0	0.0
250.0	0.10	0.0	0.0	0.0	0.0	0.0	0.0	0.0	0.0	0.0
250.0	0.50	0.0	0.0	0.0	0.0	0.0	0.0	0.0	0.0	0.0
250.0	1.00	0.0	0.0	0.0	0.0	0.0	0.0	0.0	0.0	-1.000
250.0	2.50	0.0	0.0	0.0	0.0	-0.653	-0.075	0.143	0.343	0.496
250.0	5.00	0.0	0.0	0.0	-0.249	-0.051	0.054	0.158	0.292	0.405
250.0	10.00	0.0	0.0	-0.308	-0.091	-0.016	0.057	0.148	0.273	0.382
250.0	25.00	0.0	-0.240	-0.131	-0.071	-0.014	0.057	0.147	0.272	0.381
250.0	50.00	-0.347	-0.153	-0.119	-0.070	-0.014	0.057	0.147	0.272	0.381
250.0	100.00	-0.180	-0.140	-0.118	-0.070	-0.014	0.057	0.147	0.272	0.381

TABLE G-8 DEVIATIONS OF THE DISTANCES OF THE SUPERCOOLING FOR MODEL 1 FROM THOSE OF MODEL 3 $(x_2-x_3)/x_3$ IN THE Ni-Sn SYSTEM

G	R/D	R=283.1	R=298.1	R=323.1	R=373.1	R=423.1	R=473.1	R=523.1	R=573.1	R=604.1
10.0	0.05	0.0	0.0	0.0	0.0	0.0	0.0	0.644	0.587	0.625
10.0	0.10	0.0	0.0	0.0	0.0	0.267	0.304	0.356	0.422	0.471
10.0	0.50	0.0	0.059	0.062	0.102	0.150	0.205	0.267	0.339	0.391
10.0	1.00	0.0	0.031	0.049	0.096	0.148	0.204	0.267	0.339	0.391
10.0	2.50	0.012	0.024	0.047	0.096	0.148	0.204	0.267	0.339	0.391
10.0	5.00	0.010	0.023	0.047	0.096	0.148	0.204	0.267	0.339	0.391
10.0	10.00	0.009	0.023	0.047	0.096	0.148	0.204	0.267	0.339	0.391
10.0	25.00	0.009	0.023	0.047	0.096	0.148	0.204	0.267	0.339	0.391
10.0	50.00	0.009	0.023	0.047	0.096	0.148	0.204	0.267	0.339	0.391
10.0	100.00	0.009	0.023	0.047	0.096	0.148	0.204	0.267	0.339	0.391
25.0	0.05	0.0	0.0	0.0	0.0	0.0	0.0	0.0	0.0	0.0
25.0	0.10	0.0	0.0	0.0	0.0	0.0	0.0	0.0	0.0	0.753
25.0	0.50	0.0	0.0	0.0	0.143	0.182	0.239	0.286	0.355	0.405
25.0	1.00	0.0	0.0	0.070	0.107	0.153	0.207	0.268	0.340	0.392
25.0	2.50	0.0	0.031	0.049	0.096	0.148	0.204	0.267	0.339	0.391
25.0	5.00	0.014	0.024	0.047	0.096	0.148	0.204	0.267	0.339	0.391
25.0	10.00	0.010	0.023	0.047	0.096	0.148	0.204	0.267	0.339	0.391
25.0	25.00	0.009	0.023	0.047	0.096	0.148	0.204	0.267	0.339	0.391
25.0	50.00	0.009	0.023	0.047	0.096	0.148	0.204	0.267	0.339	0.391
25.0	100.00	0.009	0.023	0.047	0.096	0.148	0.204	0.267	0.339	0.391
50.0	0.05	0.0	0.0	0.0	0.0	0.0	0.0	0.0	0.0	0.0
50.0	0.10	0.0	0.0	0.0	0.0	0.0	0.0	0.0	0.0	0.0
50.0	0.50	0.0	0.0	0.0	0.0	0.267	0.304	0.356	0.422	0.471
50.0	1.00	0.0	0.0	0.0	0.143	0.182	0.230	0.286	0.355	0.405
50.0	2.50	0.0	0.059	0.062	0.102	0.150	0.205	0.267	0.339	0.391
50.0	5.00	0.0	0.031	0.049	0.096	0.148	0.204	0.267	0.339	0.391
50.0	10.00	0.014	0.024	0.047	0.096	0.148	0.204	0.267	0.339	0.391
50.0	25.00	0.010	0.023	0.047	0.096	0.148	0.204	0.267	0.339	0.391
50.0	50.00	0.009	0.023	0.047	0.096	0.148	0.204	0.267	0.339	0.391
50.0	100.00	0.009	0.023	0.047	0.096	0.148	0.204	0.267	0.339	0.391
100.0	0.05	0.0	0.0	0.0	0.0	0.0	0.0	0.0	0.0	0.0
100.0	0.10	0.0	0.0	0.0	0.0	0.0	0.0	0.0	0.0	0.0
100.0	0.50	0.0	0.0	0.0	0.0	0.0	0.0	0.644	0.587	0.625
100.0	1.00	0.0	0.0	0.0	0.0	0.267	0.304	0.356	0.422	0.471
100.0	2.50	0.0	0.0	0.119	0.127	0.169	0.218	0.277	0.346	0.397
100.0	5.00	0.0	0.059	0.062	0.102	0.150	0.205	0.267	0.339	0.391
100.0	10.00	0.0	0.031	0.049	0.096	0.148	0.204	0.267	0.339	0.391
100.0	25.00	0.012	0.024	0.047	0.096	0.148	0.204	0.267	0.339	0.391
100.0	50.00	0.010	0.023	0.047	0.096	0.148	0.204	0.267	0.339	0.391
100.0	100.00	0.009	0.023	0.047	0.096	0.148	0.204	0.267	0.339	0.391
250.0	0.05	0.0	0.0	0.0	0.0	0.0	0.0	0.0	0.0	0.0
250.0	0.10	0.0	0.0	0.0	0.0	0.0	0.0	0.0	0.0	0.0
250.0	0.50	0.0	0.0	0.0	0.0	0.0	0.0	0.0	0.0	0.0
250.0	1.00	0.0	0.0	0.0	0.0	0.0	0.0	0.0	0.0	0.753
250.0	2.50	0.0	0.0	0.0	0.0	0.267	0.304	0.356	0.422	0.471
250.0	5.00	0.0	0.0	0.0	0.143	0.182	0.230	0.286	0.355	0.405
250.0	10.00	0.0	0.0	0.070	0.107	0.153	0.207	0.268	0.340	0.392
250.0	25.00	0.0	0.031	0.049	0.096	0.148	0.204	0.267	0.339	0.391
250.0	50.00	0.014	0.024	0.047	0.096	0.148	0.204	0.267	0.339	0.391
250.0	100.00	0.010	0.023	0.047	0.096	0.148	0.204	0.267	0.339	0.391

DISCUSSION

The segregation constant k. The solidus and the liquidus for the Ni-Sn system display moderate curvatures (Hansen 1958). The errors involved for linear model assumption are illustrated in Fig. G-2 through G-6.

Figures G-2 through G-6 show that, for the pseudo-linear model, the errors of k, G_c and x are always approximately proportional to T_o, which in turn is proportional to the concentration of solute and zero for pure solvent. For the segregation coefficient, k, the error is about 0.3%/degree K, with the rate of change slightly decreasing at higher T_o. For G_c, the error is about 0.08%/degree K, with the rate of change slightly increasing at higher T_o. For x, the error is about 0.11%/degree K, with the rate also slightly increasing at higher T_o. For the linear model, the error in k varies from +85% to -55%, the rate of change being about 0.4%/degree K. The error in G_c is always negative at about -16% to -13%, the average rate of increase being 0.01%/degree. The error of x varies from -25% to +38% for $T_o = 0$ to $T_o = 331$K, the average rate of change being about +0.19%/degree.

As expected, Table G-2 shows that k_1 and k_2 are independent of the melt temperature, while k_3 increases by over four times (from 0.156 to 0.6192) as the modified temperature T_o increases from 0 K to 331K. Table G-3 shows that, compared to k_3, k_1 is overestimated by 86% at small temperature difference and underestimated by 53% at $T_o = 331^o$ (eutectic point); and k_2 is always underestimated, the amount being proportional to the modified temperature, T_o. A relationship between $\frac{k_1 - k_3}{k_3}$ and $\frac{k_2 - k_3}{k_3}$ with T_o is shown in Fig. G-2.

The critical temperature gradient. From Eq (11), (12), and (13), we see that G_{c_1}, G_{c_2}, and G_{c_3} in Table G-4 should be linearly proportional to R/D and T_o, and G_{c_1} and G_{c_2} should also be proportional of (1-k). Table G-6 and Fig. G-3 show how

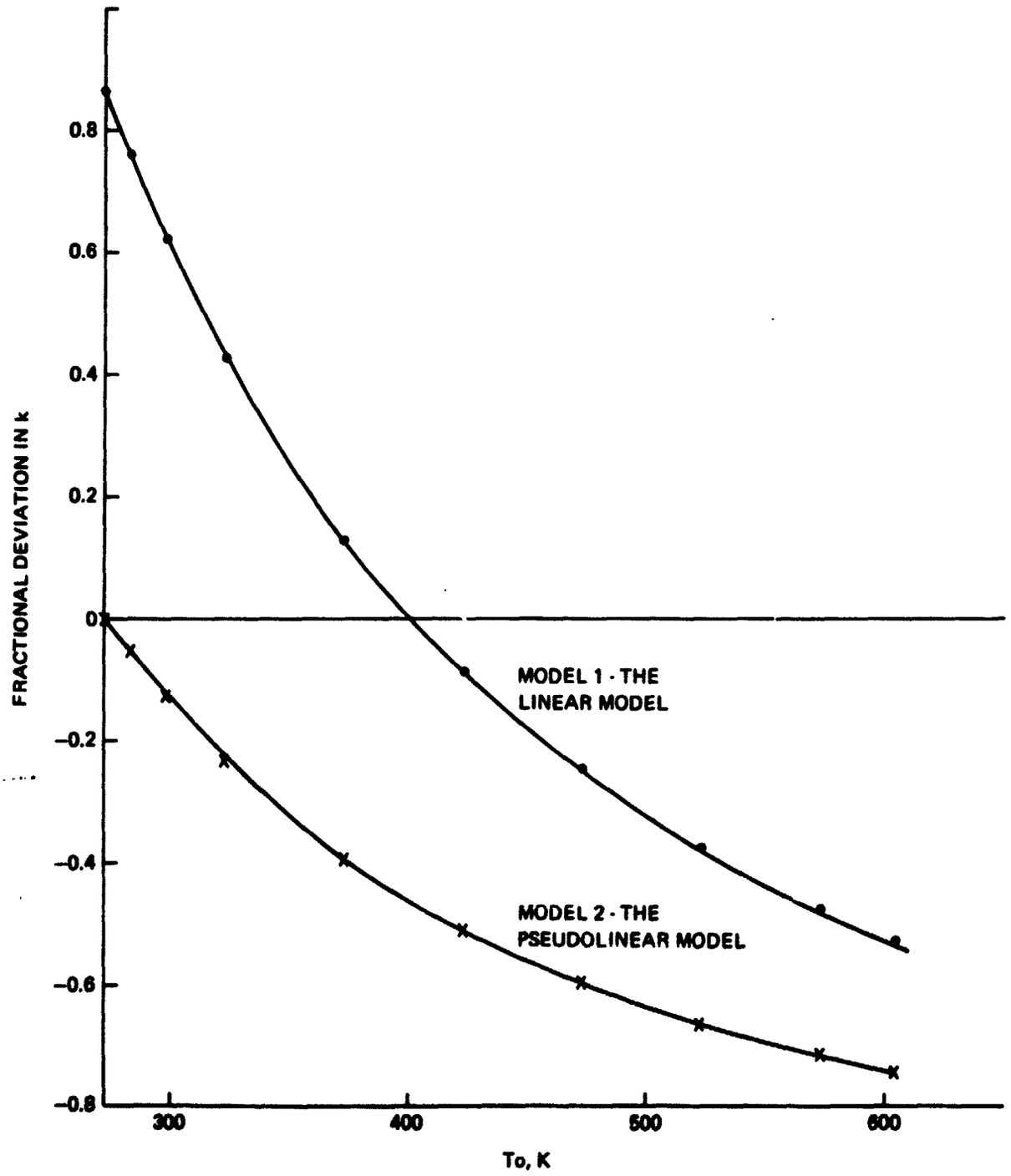

Fig. G-2 The Fractional Deviation of K vs To for Model 1 and Model 2 from Model 3

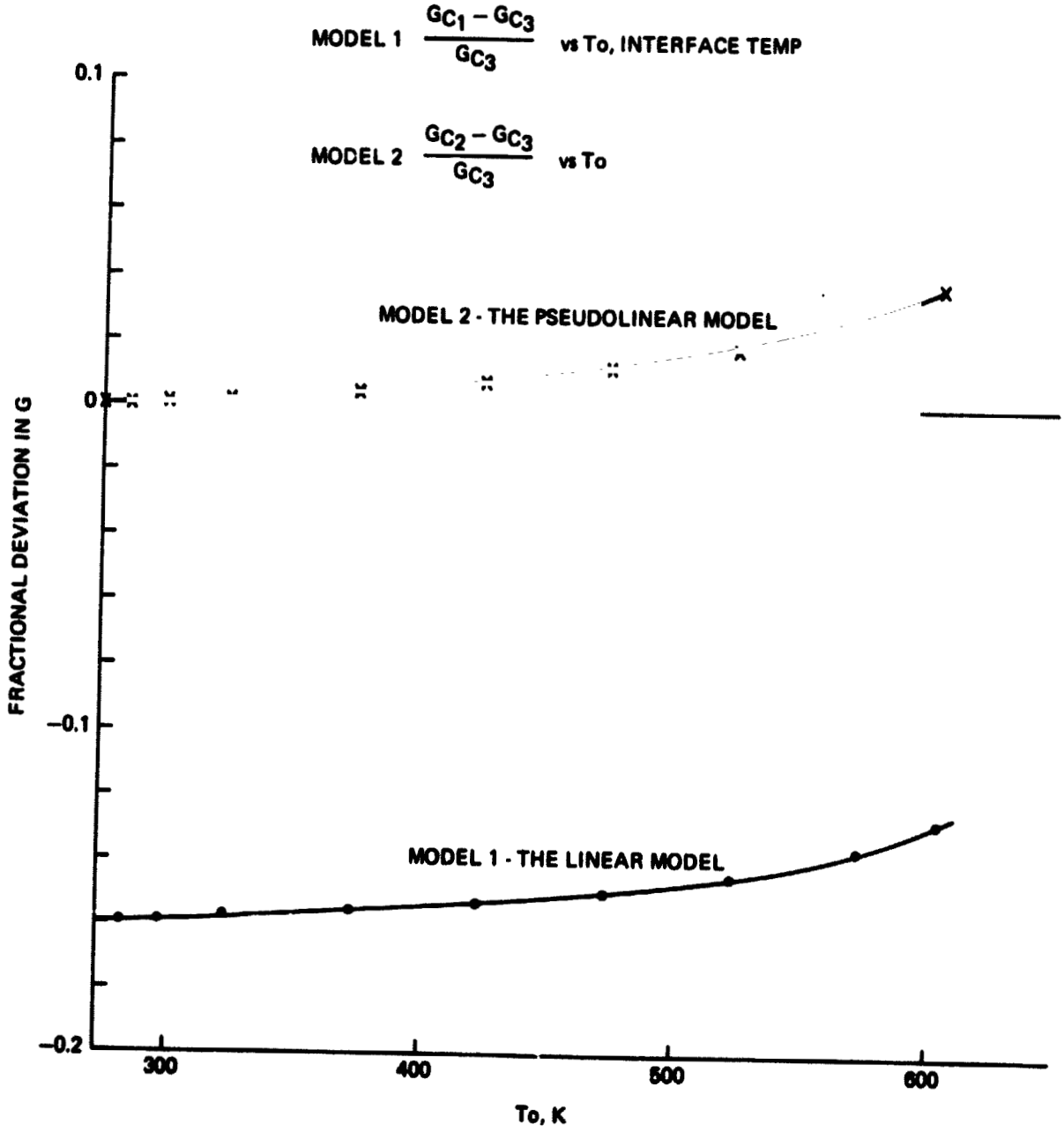

Fig. G-3 Fractional Deviation of G vs To for Model 1 and Model 2 from Model 3

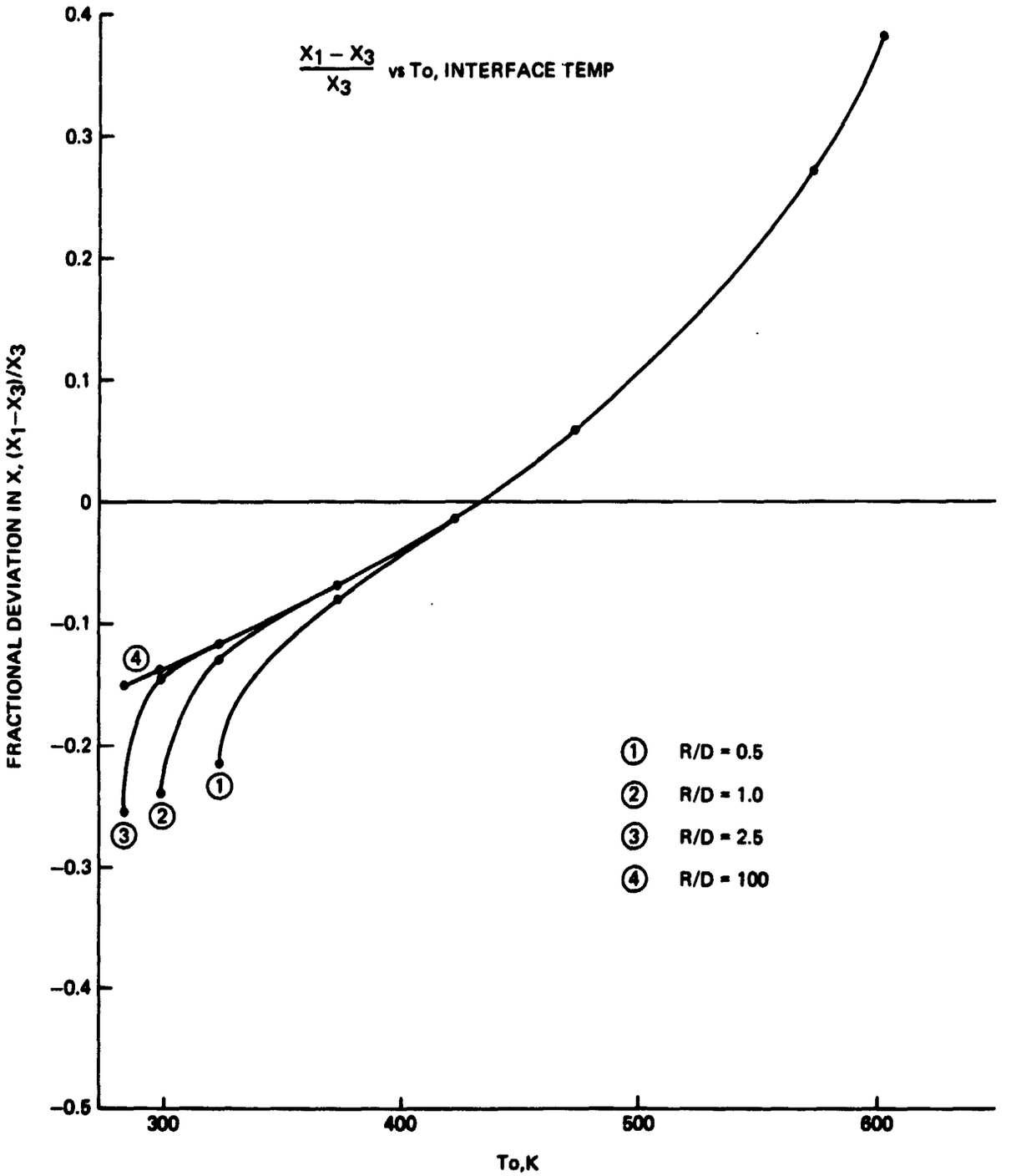

Fig. G-4 Fractional Deviation in x vs To, for Model 1

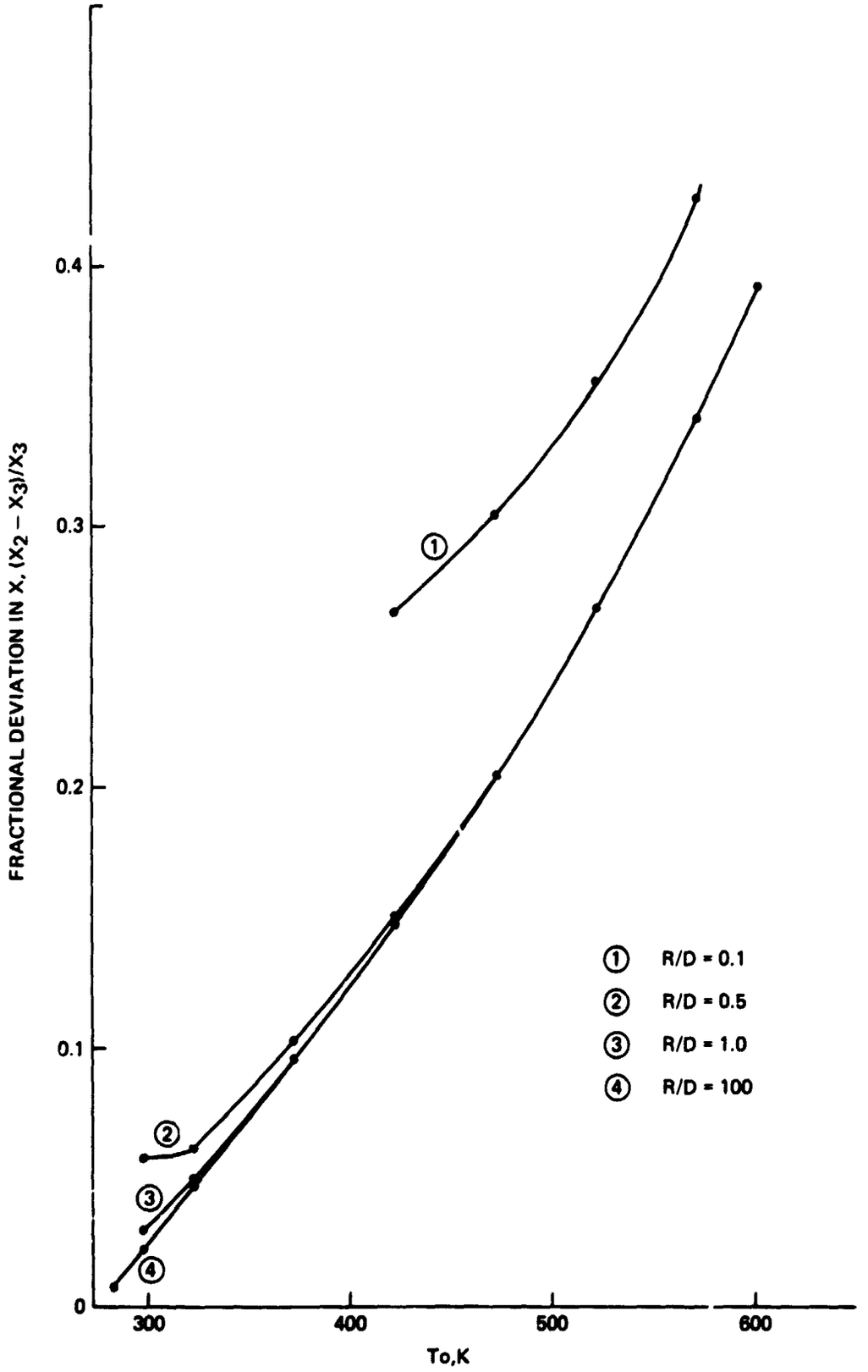

Fig. G-5 Fractional Deviation in x vs To, for Model 2

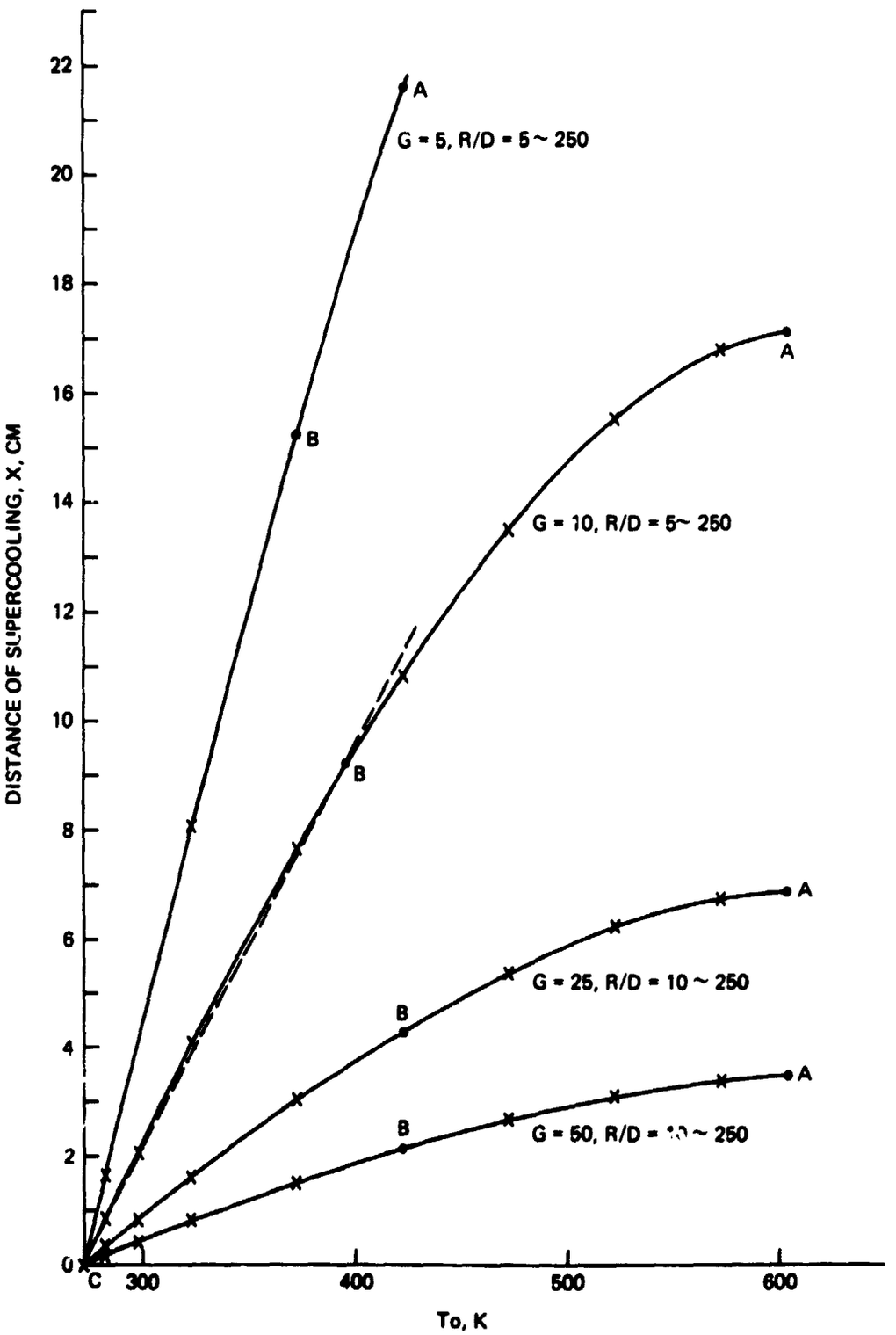

Fig. G-6 Distance of Supercooling vs To, for Various G and R/D, Model 1

much G_{c_1} and G_{c_2} can deviate from G_{c_3}. Specifically, G_{c_1}'s are always underestimated by about 15%; but G_{c_2}'s are always slightly overestimated from zero up to 3%.

The distance of supercooling. When $R/D\,x > 5$ in Eq (18), (19), and (20), then $e^{-R/D\,x} + 1 \approx 1$. Equations (18), (19), and (20) can then be solved for x.

- Linear model: $$x_1 = \frac{T_o}{G}(1-k_1) \tag{21}$$

- Pseudo-linear model: $$x_2 = \frac{T_o}{G}(1-k_2) \tag{22}$$

- Quadratic model: $$x_3 = \frac{T_o}{G}\left[1 - \frac{A_{12}}{2T_oA_{22}} - \sqrt{\frac{A_{12}}{2A_{22}T_o} - \frac{B_{12}}{T_oA_{22}} - \frac{B_{22}}{A_{22}}}\right] \tag{23}$$

The values of x's in Eq (21), (22), and (23) correspond to the BC section in Fig. G-6. In this section, x is proportional to T_o but inversely proportional to G. The portion of Fig. G-6 for $R/D\,x < 5$ corresponds to the AB section. If R/D is so small that $G > G_c$, which corresponds to curve (1) in Fig. G-1, then there is no supercooling. This condition of no supercooling continues as R/D increases, until $G = G_c$. If R/D increases again, then x continues to increase, which corresponds to curves (3) and (4) in Fig. G-1. Table G-7 and Fig. G-4 show that the fractional deviation of x_1, defined as $(x_1-x_3)/x_3$, is underestimated by about 30% at small values of modified melt temperatures T, but overestimated by about 40% at large values of T. Table G-8 and Fig. G-5 show that the fractional deviation of x_2, defined as $(x_2-x_3)/x_3$, is overestimated from 0 to 40% as the modified temperature increases from 0 to 331K, i.e., as the melt temperature decreases from the melting point of pure Ni (1726K or 1455°C) to the Ni-Sn eutectic temperature (1397K or 1124°C).